

https://dspace.org/

Late Triassic to Early Jurassic ecology: An insight into diet and trophic levels using non-traditional Ca isotopes

Davechand, Priyanka

2023-07

University of the Witwatersrand, Johannesburg

https://hdl.handle.net/10539/42917

Davechand, Priyanka. (2023). Late Triassic to Early Jurassic ecology: An insight into diet and trophic levels using non-traditional Ca isotopes. [PhD thesis, University of the Witwatersrand, Johannesburg]. https://hdl.handle.net/10539/42917

Downloaded from a DSpace repository. https://dspace.org/

UNIVERSITY OF THE WITWATERSRAND, JOHANNESBURG

Late Triassic to Early Jurassic ecology: An insight into diet and trophic levels using non-traditional Ca isotopes.

Priyanka Davechand

831772

Supervised by:

Prof. Grant Bybee and Prof. Jonah Choiniere

A thesis submitted in fulfilment of the requirements for the degree of Doctor of Philosophy in Geosciences in the Faculty of Science, University of the Witwatersrand, Johannesburg, South Africa.

DECLARATION

I, Priyanka Davechand (student number: 831772), declare that this thesis is my own, unaided work. It is being submitted for the Degree of Doctor of Philosophy at the University of the Witwatersrand, Johannesburg. It has not been submitted before for any degree or examination at any other University.



Priyanka Davechand (signature of candidate)

_____26_____ day of _____July 2023_____ at _University of the Witwatersrand__

ABSTRACT

The diet and trophic structuring of organisms in deep time is poorly understood, making comparison of ancient and modern ecosystems challenging. Proxy data (e.g., dental morphology, jaw muscle reconstruction) remain the most common mode of palaeodietary inference, but the correlative strength of these proxies remains untested due to a lack of direct evidence and an incomplete sampling of palaeobiodiversity. These major challenges in palaeodietary reconstruction can be overcome using novel geochemical markers in fossilised tooth enamel, which provide direct evidence of palaeodiet and trophic relationships.

Traditional stable isotopes of carbon, oxygen, and nitrogen have been used in the past to infer palaeodiets, but these elements are susceptible to diagenetic alteration during fossil preservation and require large sample amounts for assays. In contrast, non-traditional calcium ($\delta^{44/42}$Ca) isotopes are less susceptible to diagenesis and require significantly smaller sample amounts. This, together with the fractionation that Ca isotopes undergo as a bio-essential element, allows $\delta^{44/42}$Ca to be utilised on a broad range of palaeontological questions including assessing dietary range and trophic level.

The diverse ecosystems of the Elliot Formation (Karoo Supergroup) in South Africa are represented by abundant fossils of a variety of reptilian and mammalian stem lineages that co-existed during the latest Triassic–earliest Jurassic interval (218–190 Ma). The broad range of body sizes, inferred dietary preferences, and phylogenetic positions make the Elliot palaeoecosystems an ideal natural laboratory in which to apply palaeodietary isotopic tools. This dissertation aims to assess the palaeotrophic divisions of the Elliot Formation vertebrates using non-traditional $\delta^{44/42}$Ca isotopes.

This research uses ion-exchange chromatography on vertebrate tooth enamel to assess the palaeodietary preferences of Elliot Formation reptilian and mammalian lineages. To obtain these data, existing techniques for sample preparation of non-traditional $\delta^{44/42}$Ca isotopes were modified and optimised at the Wits Isotope Geoscience Laboratory (WIGL) at the University of the Witwatersrand. $\delta^{44/42}$Ca analysis was conducted on a variety of specimens across a broad range of amniote lineages, ranging from: dinosaurs such as presumed herbivorous sauropodomorphs *Massospondylus and Aardonyx*, the presumed omnivorous ornithischian (*Lesothosaurus* and *Heterodontosaurus*), and the presumed carnivorous theropod *Megapnosaurus*; to cynodont therapsids (*Tritylodon, Pachygenelus and Scalenodontoides)*; to pseudosuchians such as the crocodylomorphs *Protosuchus* and *Orthosuchus* and earlier branching taxa (‘rauisuchians’ and poposauroids). A leaching procedure was also tested to ensure that the results produced were not

influenced by diagenetic biases. Once consistent and reproducible methods were finalised, column chemistry and Multicollector-Inductively Coupled Plasma Mass Spectrometery (MC-ICPMS) analysis was conducted on the different Karoo-aged specimens.

There are various outcomes from this dissertation. One important outcome was the optimisation of time for Ca separation using ion-exchange chromatography. This allowed for a shorter chemical preparation time and increased the number of analyses completed per session. Another improvement of the method was that the leaching procedure can be used to control for any diagenetic biases by removing secondary calcite in samples as old as those from the Triassic–Jurassic period. Elliot taxa were then analysed, and significant differences were found between $\delta^{44/42}$Ca values of large carnivorous pseudosuchians ('rauisuchians'; -0.45 ‰ to -1.17 ‰) and co-occurring herbivorous sauropodomorph genera (-0.26 ‰ to -0.69 ‰). These results indicated that non-traditional $\delta^{44/42}$Ca isotopes can be used to understand trophic structures and palaeodiets in ecosystems at least 210 million years old. We also found that while some taxa had $\delta^{44/42}$Ca isotope values in-line with their presumed diets, other taxa had more diverse diets than initially presumed. $\delta^{44/42}$Ca-enriched values in this study provide evidence for herbivory in crocodylomorph and the oldest theropod. There is also a possibility of an omnivorous diet for presumed herbivorous *Lesothosaurus* as the $\delta^{44/42}$Ca values are relatively depleted to other herbivores.

In addition to diet, calcium plays a major role in the formation of reptilian eggs and there are documented changes in $\delta^{44/42}$Ca values during the reproductive cycle. To assess this in a living system, *Crocodylus niloticus*, was analysed to understand if $\delta^{44/42}$Ca could be used to identify the difference in sex based on the $\delta^{44/42}$Ca values. No isotopic differences were found between the juvenile male and female *Crocodylus niloticus* samples.

Testing these important ecological principles in temporally constrained formations allows us to understand the historical nature of biodiversity changes, especially across periods when environments on Earth were experiencing extreme conditions. The ability to determine factors such as palaeodiet and palaeotrophic range will enable the development and improvement of palaeoecological analysis. This research presents the first ever $\delta^{44/42}$Ca values on Karoo-aged vertebrate fossils and will have a large impact on how palaeoecological reconstruction is conducted in the future of palaeosciences.

ACKNOWLEDGEMENTS

I cannot express enough gratitude for all the people who have played an important role in supporting me during this research journey. To my supervisors, Prof. Grant Bybee and Prof. Jonah Choiniere, thank you for your continuous support, encouragement and guidance. Your supervision has gone beyond that of research and has added to my personal growth. Thank you for always lending an ear to listen and a brain to pick. Thank you for always pushing me to strive for my best, sharing your passion for science and for aiding me in becoming a better scientist.

My thanks go to my parents, sisters and family members that have played an important role in harnessing my curiosity and keeping me grounded during this time. Thank you for always cheering me on and being by my side when I needed it. To my fur-babies: Bruno, Max, Chelsea, Rocky†, Gabs, and my sweet Alaska, thank you for the unconditional love.

Thank you to Nompumelelo Maringa, Mandy-Jane Sebola, Lungelwa Ndevu, Kimberley Beaton, Caitlin Stewart, Peace Zowa and Shaeen Chetty for being the best type of friends a postgraduate student could ask for. Thank you for lifting me up when I was feeling down, cheering me on and helping in your unique ways, even if it was a cup of coffee. Thank you, Christine Steininger and Raksha Naidoo, for your words of wisdom during this PhD. I have treasured your golden nuggets of wisdom.

To the ENS Lyon team, thank you to Auguste Hassler, Jeremy Martin, Yohan Coutilloux-Pochat and Vincent Balter for your valuable contributions to this science. Your hospitality and knowledge in this field has added to the high-quality of my science.

To the ESI team, Sifelani Jirah and Bernard Zipfel, thank you for assisting me in hunting down fossils. Thank you to Marlin Patchappa for your assistance, patience and knowledge. To Linda Iaccheri, Loic LeBras and Andrew Logue, thank you for all your help in the Wits Isotope Geosciences Laboratory. Thank you to Trevor and Karen for their help and enthusiasm for my research. A note of appreciation must go to the individuals of ChemGeoDynamics and Stormberg Giants who make science fun and exciting. Lastly, thank you to all who have been part of my journey to PhD. Your words of encouragement, jokes and corridor chats are all much appreciated.

I would like to acknowledge the support of the following funding sources: Council for Geosciences, DST-NRF Centre of Excellence in Palaeosciences (CoE-Pal), GENUS, Geological Society of South Africa (GSSA) Research Education and Investment (REI) Fund, Palaeontological Scientific Trust (PAST).

CONTENTS

DECLARATION i

ABSTRACT ii

ACKNOWLEDGEMENTS iv

CONTENTS v

List of Figures viii

List of Tables xiv

1. Overview 1

1.1. Purpose of the study 3

1.1.1. Aims and Hypotheses 3

1.1.2. Objectives 3

1.2. Thesis format and author contributions 4

2. General literature review 7

2.1. Proxies for palaeodiet and palaeotrophic range determination 7

2.2. Geochemistry of Ca 8

2.3. Time period and geological setting 11

2.4. Dinosauria and other taxa 14

2.4.1. Pseudosuchia or 'crocodile-line' archosaurs: 'Rauisuchians' and crocodylomorphs 14

2.4.2. Dinosauria: Ornithischians, theropoda and sauropodomorphs 15

2.4.3. Therapsida: Gomphodonts (*Scalenodontoides macrodontes*), Trithelodontids (*Pachygenelus monus*), tritylodontids (*Tritylodon*). 17

3. Method setup and optimisation for Ca isotopes in the WIGL 19

3.1. Abstract 19

3.2. Introduction 19

3.3. Methods 22

3.3.1. Microdrilling and sample preparation 22
3.3.2. Sample digestion 23
3.3.3. Ion-exchange chromatography 26
3.4. Results 37
3.4.1. Microdrilling 37
3.4.2. Calibrations 38
3.5. General Discussion 47
3.6. Conclusion 48
4. Best practices for Ca isotope analysis on palaeontological samples 49
4.1. Abstract 49
4.2. Introduction 49
4.3. Methods 50
4.3.1. Sample leaching 51
4.3.2. Effect of maturation on Ca-fractionation 52
4.4. Results 53
4.4.1. Sample leaching 53
4.4.2. Effect of maturation on Ca-fractionation 56
4.5. Discussion 58
4.5.1. Sample leaching 58
4.5.2. Effect of maturation on Ca-fractionation 60
4.6. Conclusion 60
5. Characterising the diverse palaeoecosystem of the Elliot Formation, South Africa, using Ca isotopes to trace diet. 62
5.1. Abstract 62
5.2. Introduction 63
5.3. Methodology 65
5.4. Results 66

5.4.1. Isotopic determination of palaeotrophic positions 66
5.5. Discussion 73
5.5.1. Isotopic determination of palaeotrophic positions 73
5.5.2. Resource partitioning in sympatric herbivores 77
5.5.3. Differing $\delta^{44/42}$Ca values for presumed diets 79
5.6. Conclusion 82
6. Sex determination of *Crocodylus niloticus* using Ca isotopes. 83
6.1. Abstract 83
6.2. Introduction 83
6.3. Methodology 88
6.4. Results 90
6.5. Discussion 91
6.6. Conclusion 92
7. Generalised Conclusion 94
8. Reference list 96
Appendix 108
Appendix A. 109
Appendix B. 120
Appendix C. 129
Appendix D 139
Appendix E 139
Appendix F 140
Appendix G. 141

List of Figures

Figure 2.1: Photographs of archosaur and dinosaur teeth from the Elliot Formation **(a)** A 'rauisuchian' tooth (BP/1/5163) with the red circled area indicating the preserved serrations (adapted from Tolchard *et al*., 2019). **(b)** A holotype (BP/1/6235) of sauropodomorph *Arcusaurus pereirabdalorum* indicating leaf-shaped teeth (adapted from Yates *et al.*, 2011).……..……7

Figure 2.2: Locality map and stratigraphic section of Karoo cranial fossil study material (Appendix G). **(a)** A distribution map showing the geological overview and distribution of fossils in this study within the Karoo Supergroup **(b)** A schematic stratigraphic section of the Elliot Formation (Stormberg Group; Karoo Supergroup), from approximately 227 to 190.8 Ma, modified after Bordy *et al.* (2020) showing the position of each fossil analysed in this study. The BP number represents the different fossils, and the colours represent the different taxa as shown in (a). Specimens with poor provenance are not shown above……...13

Figure 2.3: Photograph of 'Rauisuchian' tooth specimen (BP/1/5163A) with the orange arrow indicating the fine-tooth serrations……..……..14

Figure 2.4: Image of a 'leaf shaped' *Pulanesaura* tooth specimen (BP/1/6204) (McPhee *et al.*, 2015)……..17

Figure 3.1: A generalised methodology for non-traditional $\delta^{44/42}$Ca isotopes from Martin *et al.* (2017) **(a)** The specimen was sampled. **(b)** Leaching and digestion of the powder sample in preparation for the ion-exchange chromatography. **(c)** The digested sample was loaded onto the column and various acids were added to move the different ions of interest through the column. **(d)** The sample was loaded onto the Neptune MC-ICPMS machine, and the target collectors counted the different intensities. **(e)** The intensities were then recorded, and isotopic ratios were calculated……...……21

Figure 3.2: The tungsten carbide Dremel drill bit used for microdrilling the samples……22

Figure 3.3: A simplified schematic diagram of the microdrilling method showing the general steps to obtain the required sample amount. **(a)** Photos of the sample and sample spot are taken. **(b)** The sample spot is cleaned with Milli-Q followed by Isopropanol. **(c)** The sample is secured in the Dremel vise, and a drop of Milli-Q is pipetted onto the sample spot. **(d)** Microdrilling is done using a tungsten carbide drill bit. **(e)** The droplet containing sample is collected. **(f)** The sample is pipetted into a beaker and put on a hotplate to dry down.……...……..23

Figure 3.4: A simplified schematic diagram of sample digestion before ion-exchange chromatography. **(a)** Weigh the dry down sample to ensure there is ≥ 400 µg**. (b)** Add HNO_3 and H_2O_2 to remove any organic matter. **(c)** Open the beaker lid every 10 minutes to release the gas from the organic material being broken down. **(d)** Cap and place the beaker on the hotplate for sample digestion. **(e)** Add H_2O_2 to remove any remaining organic matter and dry down. **(f)** Add HCl to prepare the sample for the first stage of ion-exchange chromatography. **(g)** Dry down the HCl. **(h)** Add the required calculated amount of 0.4 N HCl for the ion-exchange chromatography…….25

Figure 3.5: The different columns and the dimensions used for Calibration 1. **(a)** Smaller column (71 mm) similar to those used in the ENS, Lyon. **(b)** The Bio-Rad Poly-Prep ® chromatography column (90 mm) used for Stage 1 and 2 of the chemistry..……..……..30

Figure 3.6: Tungsten Dremel drill bit with the ~400 µg sampled bone fragment powder. This is sufficient for Ca isotope analysis...……37

Figure 3.7: Images of specimens drilled for Ca isotope analysis using the handheld Dremel microdrill with a tungsten drill bit. Magnification of x0.67 used **(a)** An example of a drilled proxy of a fossil bone fragment. **(b)** An example of a drilled baboon tooth..……37

Figure 3.8: An adult female *Crocodylus niloticus* tooth, sampled using the micro-drill to perform calcium ion-exchange chromatography at ENS, Lyon. The black arrow (sample spot 8b) indicates a sample spot ~500 µm in diameter.……38

Figure 3.9: Column 1 of calibration 1 for the WIGL Ca-Fe-Sr matrix separation from the juvenile crocodile tooth. The matrix was eluted using the 0.4 M and 1 N HCl. The Ca-Fe-Sr aliquot is eluted and collected when the 6 N HCl was introduced to the column. The wash was collected at the 22 mL mark.……...39

Figure 3.10: Column calibration 1 for the WIGL Ca-Fe-Sr matrix separation from the juvenile crocodile tooth using a Bio-Rad Poly-Prep® column. The matrix was eluted using the 0.4 M and 1 N HCl. The Ca-Fe-Sr aliquot is eluted and collected when the 6 N HCl was introduced to the column. The wash was collected at the 22 mL mark.....……...…….39

Figure 3.11: Column 1 of calibration 2 for the WIGL Ca-Fe-Sr matrix separation from the juvenile crocodile tooth using a Bio-Rad Poly-Prep® column. The matrix was eluted using the 0.4 M and 1 N HCl. The Ca-Fe-Sr aliquot is eluted and collected when the 6 N HCl was introduced to the column. The wash was collected at the 22 mL mark.……40

Figure 3.12: Column 2 of calibration 2 for the WIGL Ca-Fe-Sr matrix separation from the juvenile crocodile tooth using a Bio-Rad Poly-Prep® column. This chemistry included an additional 2 mL

of acid. This was 1 mL to the Mg elution stage and 1 mL to the Ca elution stage. The matrix was eluted using the 0.4 M and 1 N HCl. The Ca-Fe-Sr aliquot is eluted and collected when the 6 N HCl was introduced to the column. The wash was collected at the 24 mL mark……..…41

Figure 3.13: Column 3 of calibration 2 for the WIGL Ca-Sr separation from the juvenile crocodile tooth using a micro-column. The Ca was eluted using the 3 N HNO_3. The Sr aliquot was then eluted when the 0.5 N HNO_3 was introduced to the column at 6 mL.……...……...41

Figure 3.14: Column 3 of calibration 2 for the WIGL Ca-Sr separation from the juvenile crocodile tooth using a micro-column. The Ca was eluted using the 3 N HNO_3. The Sr aliquot was then eluted when the 0.5 N HNO_3 was introduced to the column..……...……...……42

Figure 3.15: Column 2 of calibration 2 for the WIGL Ca-Fe-Sr matrix separation from the juvenile crocodile tooth using a Bio-Rad Poly-Prep® column. The matrix was eluted using the 0.4 M and 1 N HCl. The Ca-Fe-Sr aliquot is eluted and collected when the 6 N HCl was introduced to the column. The wash was collected at the 24 mL mark. ……..……43

Figure 3.16: Calibration 5 for the WIGL Ca-Sr separation from the NIST-SRM1486 using a micro-column. The Ca was eluted using the 3 N HNO_3. The Sr aliquot was then eluted when the 0.5 N HNO_3 was introduced to the column……..……...43

Figure 3.17: The WIGL reference materials, represented by the points, and their standard deviations represented by the black error bars. The red line represents the mean literature value (Tacail *et al.*, 2015; Hassler *et al.*, 2018) for the different standards and the grey band (range) is the standard errors for these means. The standard errors for the different mean literature values are: NIST-SRM1486 (-1.0 ± 0.07 ‰) and NIST-SRM1400 (-1.0 ± 1.00 ‰). The error range for SRM1400 is not shown as it spans from -2 to 0 per mil (Appendix D).……...……44

Figure 3.18: Column 1 of calibration 7 for the WIGL Ca-Fe-Sr matrix separation from the juvenile crocodile tooth using a Bio-Rad Poly-Prep® column. This chemistry included an addition of 2 mL of acid. The matrix was eluted using the 0.4 M and 1 N HCl. The Ca-Fe-Sr aliquot is eluted and collected when the 6 N HCl was introduced to the column. ……..……..…45

Figure 3.19*:* Column 2 of calibration 7 for the WIGL Fe removal from the Ca-Sr from the NIST-SRM1486 using a Bio-Rad Poly-Prep® column.……....45

Figure 3.20: Column 3 of calibration 7 for the WIGL Ca-Sr separation from the NIST-SRM1486 using a micro-column. The Ca was eluted using the 3 N HNO_3. The Sr aliquot was then eluted when the 0.5 N HNO_3 was introduced to the column.……46

Figure 4.1: SRM1486 samples analysed in the WIGL. The WIGL standard sample that was leached (red) and unleached (black) samples are represented by the points, and their standard deviations represented by the error bars. The red line represents the mean unleached literature value for the standard, blue line represents the combined mean value for the unleached data analysed and the grey band (range) is the standard error for the mean. The standard error for the SRM1486 mean literature value is (0.1 ± 0.07 ‰).…….....55

Figure 4.2: Elliot Formation tooth enamel samples analysed that were unleached or leached prior to ion-exchange chromatography. **(a)** A box plot showing the $\delta^{44/42}$Ca (‰) values of the *Massospondylus, Aardonyx and* 'rauisuchian' samples that were unleached and analysed (orange) and resampled, leached and analysed (blue). Three samples per taxa were analysed. Image source: prehistoric-wildlife.com;.Bordy *et al.* (2020) **(b)** An ordinary least squares (OLS) regression showing the relationship between the unleached (x-axis) vs leached (y-axis) $\delta^{44/42}$Ca (‰) values of each sample analysed. The OLS regression has a slope (red line) of 0.81 and $R^2 = 0.9337$. A slope of 1 is represented by the solid black line.……..……56

Figure 4.3: Effect of maturation on Ca-fractionation for samples Ca1.6, Ca3.3, Ca3.5, Ca4.4 and Ca4.6 were analysed on different days and represented by the different points. The colour of the points corresponds to the batch number. It should be noted that two batches were analysed on day 1 separated by 6 hours (see methods). The black lines represent the standard errors.…….57

Figure 4.4: ICP Ca reference standard samples analysed for Ca isotope compositions. The ICP Ca samples are represented by the points (blue) with a trend line (blue) of 0.9949x – 0.0003…….57

Figure 5.1: The $\delta^{44/42}$Ca (‰) difference between presumed Elliot Formation herbivores and carnivores. **(a)** The box plots, displaying Quartiles 1, 2, and 3, of the presumed herbivorous sauropodomorph genera namely: *Massospondylus* and *Aardonyx* are represented in blue and the presumed carnivorous 'rauisuchians' are represented in red. There is a distinct variation in the $\delta^{44/42}$Ca (‰) values between the herbivores and carnivores. Silhouettes of *Massospondylus*, *Aardonyx* and 'rauisuchian' scaled relative to the mass of the animals. This is showing the variation in morphology, size and stature. Image sources: prehistoric-wildlife.com. **(b)** $\delta^{44/42}$Ca (‰) values of sauropodomorph specimens analysed. The juvenile specimens of *Massospondylus* (red) and the lower upper Elliot Formation (luEF) (triangle) are indicated above. The rest of the specimens are upper upper Elliot Formation (uuEF) (square) and range from sub-adult to adult (blue)……..…...70

Figure 5.2: The $\delta^{44/42}$Ca (‰) difference between presumed herbivores, carnivores and omnivores. The box plots, displaying Quartiles 1, 2, and 3, of the co-occurring presumed herbivorous taxa represented in green, presumed carnivorous represented in red and the presumed omnivorous taxa represented in blue. Silhouettes are not to scale. Image sources: prehistoric-wildlife.com...……71

Figure 5.3: The $\delta^{44/42}$Ca (‰) difference between the $\delta^{44/42}$Ca values and the estimated body mass of the a) herbivores, b) carnivores and c) omnivores. The box plots, displaying Quartiles 1, 2, and 3, of the co-occurring presumed herbivorous taxa represented in green, presumed carnivorous represented in red and the presumed omnivorous taxa represented in blue. Image sources: prehistoric-wildlife.com.……...72

Figure 5.4: Hypothetical Elliot Formation food web using the $\delta^{44/42}$Ca (‰) values. The dietary preferences are suggested based on the $\delta^{44/42}$Ca (‰) values obtained in this study. *uEF carnivore such as *Dracovenator* that could not be analysed. Silhouettes of all taxa are scaled relative to the mass of the animals. Image sources: prehistoric-wildlife.com……..……76

Figure 6.1: (a) Showing the position of the chevrons and pelvic bones in a *Tyrannosaurus rex.* **(b)** Female *Tyrannosaurus rex* caudal vertebrae and pelvic bones. Highlighted area indicating distance between first chevron and ischial **(c)** Male *Tyrannosaurus rex* caudal vertebrae and pelvic bones. Highlighted area indicating distance between first chevron and ischial. (Erickson *et al.*, 2005)…...85

Figure 6.2: (a) Showing the position of the chevrons and pelvic bones in an *Alligator mississipiensis.* **(b)** Female *Alligator mississipiensis* caudal vertebrae and pelvic bones. Highlighted in orange indicates the distance between first chevron and ischial **(c)** Male *Alligator mississipiensis* caudal vertebrae and pelvic bones. Highlighted in orange shows the distance between first chevron and ischial. (Erickson *et al*., 2005).……...85

Figure 6.3: An embryo of an *Alligator mississipiensis* on day 26 in the egg (Erickson *et al.*, 2005). ……...86

Figure 6.4: (a) Male *Agujaceratops* **(b)** Female *Agujaceratops*. Silhouettes modified from images on Dinosaurfact.net (2007). ……..86

Figure 6.5: (a) Pair of eggs highlighted by the yellow circle attached to fossilised pelvis **(b)** Eggshell texture preserved (Cheng, 2005). ……...87

Figure 6.6: Sampling of *Crocodylus niloticus* teeth. **(a)** A juvenile tooth prepared for microsampling using the handheld Dremel. **(b)** The MicroMill used to sample the adult tooth (Female E)…….89

Figure 6.7: Specimen Female E with the labels indicating the 9 sample spots 1b to 9b from the bottom of the tooth to the top of the crown. …….90

Figure 6.8: The $\delta^{44/42}$Ca (‰) difference between female and male *Crocodylus niloticus*. The scatter plots (red and blue points) display the $\delta^{44/42}$Ca (‰) values with the standard error (black lines) **(a)**

The consecutive cross section sampling points are in the same range for Female E. **(b)** The male and female juvenile *Crocodylus niloticus* samples have $\delta^{44/42}$Ca (‰) values in the same range…..91

List of Tables

Table 3.1: Table listing the specific reagents and materials used for the different stages of Ca ion-exchange chromatography……..……21

Table 3.2: Table briefly describing the different column calibrations conducted to setup and optimise the Ca separation procedures in the WIGL…….....28

Table 3.3: Ca ion-exchange chromatography method used for calibration 1……...31

Table 3.4: Ca ion-exchange chromatography method used for column 2 of calibration 2 with the addition of 1 mL of 1 N HCl (Mg elution) and 1 mL of 6 N HCl (Ca elution). Amended volume highlighted in red. …….32

Table 3.5: Ca-Sr ion-exchange chromatography separation method used for column 3 of calibration 2 after the Ca-Sr separation from the matrix. …….....33

Table 3.6: Ca ion-exchange chromatography method used for calibration 4. Amended volume highlighted in red……...34

Table 3.7: Ca-Sr ion-exchange chromatography method used for calibration 4. Amended volume highlighted in red. ……..……35

Table 3.8: Ion-exchange chromatography method for Fe removal from Ca-Sr used in calibration 7…….36

Table 3.9: Table showing percentage recovery (%) comparing before chemistry sample and after chemistry sample (Appendix E). KED represents kinetic energy discrimination and STD represents standard values……..……46

Table 4.1: Fossil tooth samples analysed in this study represent ESI fossil tooth enamel. This is to test the effect of sample leaching using leached vs unleached samples...…….51

Table 4.2: Fossil tooth samples analysed in this study. These samples were used to test the effect of maturation on Ca-fractionation…….52

Table 4.3: Summary of the mean, lowest and highest $\delta^{44/42}$Ca values for unleached vs leached Elliot Formation samples (listed in Table 4.1 herein) (Appendix G)……54

Table 5.1: Summary of the mean, lowest and highest $\delta^{44/42}$ Ca values. The mean, lowest, highest, 25th percentile (Quartile 1) and 75th percentile (Quartile 3) $\delta^{44/42}$ Ca values for the taxa mentioned

and selected in this study. 2 s.e.= 2 standard error from the values are represented in the $\delta^{44/42}$ Ca (‰) column…….……..…..….68

Table 6.1: *Crocodylus niloticus* specimens analysed in this study.……..…….88

1. Overview

The sparse nature of the fossil record and poor preservation of fossils result in many unanswered palaeoecological questions. Were they similar to modern ecosystems? How did past ecosystems change over geological time? What effects did disruptive events like mass extinctions have on ecosystem functionality? Did ecological factors like niche partitioning and predator-prey body mass relationships influence species diversity and population size in deep time as they do in modern ecosystems (Kartzinel *et al*., 2015; Nakazawa *et al*., 2013)? Little is known about continental ecosystems of the past, and the answers to many of these questions are still elusive.

Trophic structuring and food webs are fundamental features of ecosystems that provide insight into ecosystem functionality and the ecological principles that govern biological life forms on Earth that affect co-existence and survival of different species. Ecosystem reconstruction and characterisation depend on a thorough sampling of the biodiversity and can be challenging in deep time due to the lack of preservation, sparse fossil-bearing units or poor taxonomic classification. Understanding trophic structures and food webs provides insight into functional ecology and the roles and functions different species played within their ecosystem. It will enable the development and improvement of palaeoecological analysis.

When referring to past ecosystems, inferences of diet in the fossil record are generally based on a limited number of proxies like dental morphology, reconstruction of jaw muscles (and thereby jaw motion) and gut capacity (Tolchard *et al.,* 2019; Maclaren *et al*., 2017). The best direct evidence for palaeodiets is the gut contents of exceptionally well-preserved specimens, which are unfortunately rare and scattered (Salgado *et al.,* 2017). An example of this is a study by Salgado *et al.* (2017), where seeds of cycads and other seeds were found within an ornithischian dinosaur. The well-preserved gut content provided an insight into the diet of *Isaberrysaura mollensis.* The different dietary preferences and habits of vertebrates in modern ecosystems allow for predictable patterns in ecology. Examples of this are modern herbivorous bovids, which move in larger groups, are generally larger in size compared to predatory carnivores (Makin *et al.,* 2017).

Stable isotopes have been used as independent means of assessing palaeodiets, trophic levels and food webs in modern and ancient ecosystems (Martin *et al.,* 2018; Hassler *et al.,* 2018). Elements like carbon, oxygen and nitrogen are some of the isotopic systems used to address some aspects of these dietary dynamics and to assist in the reconstruction of early ecosystems (Higgins, 2018). These elements are essential in living organisms and can be found in bone, blood and tissue (Martin *et al.,* 2017). Unfortunately, isotopes of these elements have limitations as they can be influenced by secondary processes and external fluids (e.g., hydrothermal fluids) resulting in spurious isotope values

(Reynard and Balter, 2014). These elements can also be reset by diagenesis as bone material is porous and easily chemically altered (Reynard and Balter, 2014). These isotope systems require a relatively large amount of sample which is undesirable as it can cause damage to the fossils. Robust geochemical markers, preserved in tooth enamel, may indicate which animals served as top predators, how herbivores contributed to different niches and how different ecosystems could have been affected by events such as mass extinction (Martin *et al*., 2017; Tacail *et al.*, 2014).

Calcium (Ca), a bio-essential element, displays isotopic fractionation along the trophic chain and within and among plants and animals (Heuser *et al.,* 2011; Morgan *et al.,* 2012 and Martin *et al.,* 2017). This can assist in determining palaeodiet and palaeotrophic level as the uptake of food and water by plants and animals influence the Ca concentrations and isotopic fractionation in the body (Hindshaw *et al*., 2013; Martin *et al*., 2017). Ca is not easily diagenetically altered in tooth enamel compared to dentine and bones in the body (Martin *et al*., 2017). Recent studies have shown the utility of the non-traditional Ca isotope ($\delta^{44/42}$Ca) method to understand dietary preferences in modern and Cretaceous settings (i.e., 65 Ma) (Martin *et al*., 2018; Martin *et al.,* 2022).

A critical endeavour for palaeoecology is developing isotopic proxies to assist in understanding ancient population dynamics and dietary behaviours of terrestrial ecosystems in deep time. This Ph.D. research focuses on using non-traditional $\delta^{44/42}$Ca isotopes from fossilised tooth enamel on a variety of specimens across a broad range of amniote lineages, ranging from: dinosaurs such as presumed herbivorous sauropodomorphs *Massospondylus and Aardonyx*, the presumed omnivorous ornithischian (*Lesothosaurus*), and the presumed carnivorous theropod *Megapnosaurus*; to cynodont therapsids (*Tritylodon, Pachygenelus and Scalenodontoides)*; to pseudosuchians such as the crocodylomorphs *Protosuchus* and *Orthosuchus* and earlier branching taxa (‘rauisuchians’ and poposauroids). The samples in this Ph.D. study are from the Elliot Formation (Stormberg Group, Karoo Supergroup) in South Africa as it is palaeontologically-rich and highly diverse (Sciscio and Bordy, 2016), but also provides an opportunity to test palaeontological Ca isotope analysis on Karoo-aged ecosystems.

Ca is also essential in reproductive physiology and can influence $\delta^{44/42}$Ca values (Tacail *et al.,* 2017). Animals that are oviparous or experience lactation require Ca for eggshell development or milk production, respectively (Dacke *et al.,* 2015; Tacail *et al.,* 2017). This research tests the utility and application of $\delta^{44/42}$Ca isotopes in sex determination in male and female modern crocodilians, *Crocodylus niloticus*. Could possible $\delta^{44/42}$Ca isotope differences exist between the sexes and can this technique be applied to extinct species? Current sexing methods rely on large sample sizes and involve destructive methods such as osteohistology (Chapman *et al.,* 1997). Sex determination may provide a better understanding of sexual anatomical differences within different tetrapod groups and their population dynamics within groups.

1.1. Purpose of the study

The purpose of this study is to determine if non-traditional $\delta^{44/42}$Ca isotopes, as used in recent modern and Cretaceous studies (Martin *et al.*, 2018; Hassler *et al.*, 2018), can be applied to terrestrial ecosystems as old as the Triassic–Jurassic period. Developing metrics that can contribute to understanding population dynamics and dietary behaviour is therefore a critical endeavour for advancing palaeontological analysis of past ecosystems. This PhD research will also further extend and test the application of $\delta^{44/42}$Ca isotopes in determining the sex of extant taxa with the intention to apply it to ancient taxa.

1.1.1. Aims and Hypotheses

In the diverse ecosystems of the Elliot Formation, there are a variety of individuals that co-existed in the same time period, but little independent evidence exists identifying where they may be placed on the trophic spectrum. This provides an excellent opportunity to apply palaeodietary isotopic tools to a well-constrained scientific problem within vertebrate palaeontology. The main aim of this thesis will be to assess the trophic divisions of the Elliot Formation vertebrates using the non-traditional $\delta^{44/42}$Ca system.

This Ph.D. research will test four hypotheses:

1. We can test and control for minor diagenetic biases by leaching samples as old as those found in the Triassic–Jurassic period.
2. Ca isotope systematics can be used to identify herbivores and carnivores from the same palaeoecosystems in deep time.
3. Ca isotope systematics can identify and differentiate trophic levels in contemporaneous vertebrates from the extinct Elliot ecosystems.
4. $\delta^{44/42}$Ca values vary within the same species due to the difference in sex, i.e., male and female.

1.1.2. Objectives

To test these hypotheses, the following objectives and methods will be carried out:

Hypothesis 1

- Objectives**:** To optimise the current ion-exchange chromatography method for Ca ion-exchange separation outlined in Tacail *et al.* (2014) and to investigate the effectiveness of leaching samples to control for diagenetic biases in terrestrial samples.

Hypothesis 2

- Objectives: To distinguish the difference between presumed herbivorous sauropodomorphs and carnivorous 'rauisuchians' and poposauroids using Ca isotopic analysis.

Hypothesis 3

- Objectives: To distinguish between presumed herbivorous, carnivorous, and omnivorous diets and assess respective trophic levels and dietary range of Late Triassic–Early Jurassic dinosaurs and other co-existing taxa from the Elliot Formation.

Hypothesis 4

- Objectives: Ca isotopic analysis on *Crocodylus niloticus* tooth samples will be used to identify if there are any differences or trends in the $\delta^{44/42}$Ca isotope values for the different sexes and if so, could it be extended to identify the sex of extinct animals.

1.2. Thesis format and author contributions

This thesis is organised into seven chapters, several of which are currently or will shortly be submitted for international peer-review. A brief description and documentation of author contributions is summarised below.

General literature review (Chapter 2)

Chapter 2 provides general background information on the proxies of palaeodiet and palaeotrophic range determination, geochemistry of Ca, the time period, geological setting and presumed diets of the selected taxa in this PhD research.

Method optimisation, set up and best practices for $\delta^{44/42}$Ca isotopes (Chapters 3 and 4)

Chapter 3 focuses on the set up and optimisation of ion-exchange chromatography for Ca isotope analysis. Chapter 4 discusses the best practices required for sample preparation to ensure accurate $\delta^{44/42}$Ca values are produced. These chapters discuss and document different factors, such as leaching, that need to be implemented when trying to obtain the $\delta^{44/42}$Ca values of palaeontological samples.

Chapter 3 focuses on a description of the methodology used in this work, along with workflows used to optimise the Ca ion-exchange separation method setup in the Wits Isotope Geoscience Laboratory (WIGL) at Wits University. This chapter addresses further adaptation of the method to allow for a time-efficient separation of Ca ions. Priyanka Davechand has been trained at the École normale supérieure de Lyon (ENS; France) in ion-exchange chromatography and has successfully implemented and developed a time-efficient ion-exchange separation techniques in the WIGL. The

ion-exchange chromatography, data collection and interpretation were conducted by Priyanka Davechand.

Chapter 4 discusses the best practices required for Ca isotope analysis in palaeontological samples. This chapter highlights analytical conditions and an additional sample preparation method, known as leaching, that must be used when carrying out ion-exchange chromatography to obtain the $\delta^{44/42}$Ca values in fossils. It addresses different practices that are recommended to ensure high-quality data are produced. Leaching and avoiding sample ageing will produce accurate $\delta^{44/42}$Ca values and avoid any deviations due to diagenetic biases or incorrect practices left unaddressed. It is important to consider the length of time that samples are prepared for mass spectrometry to avoid any fractionation. The ion-exchange chromatography, data collection and interpretation were conducted by P. Davechand. Mass spectrometry on the Thermofisher Neptune MC-ICPMS in Lyon was conducted by Auguste Hassler and P. Davechand.

Characterisation of Elliot Formation palaeoecosystems (Chapter 5)

Chapter 5 discusses the application of Ca isotopes in characterising the diverse palaeoecosystem of the Elliot Formation in South Africa using Karoo-aged fossils. Varying $\delta^{44/42}$Ca values for herbivorous vs carnivorous diet is proof in concept for using Ca isotopes to understand palaeodiets and palaeotrophic range. The method is applied to a variety of taxa with the aim to determine the palaeodiets of presumed herbivores, carnivores and omnivores. Sample preparation which entails of: drilling, digestion and leaching; and ion-exchange chromatography was performed by P. Davechand. The Ca data, and processing and interpretation of the data was also conducted by P. Davechand. The mass spectrometry on the Ca aliquots was conducted by A. Hassler, P. Davechand and Yohan Coutilloux-Pochat at the ENS, Lyon. A subsection of this chapter has been submitted to *Biology Letters* by the *Royal Society Publishing* (Appendix A) and is currently being revised.

Sex determination (Chapter 6)

Chapter 6 is a further extension of the application of $\delta^{44/42}$Ca to determine sex for *Crocodylus niloticus*. This is to explore the utility of the analysis for other variables. The $\delta^{44/42}$Ca values for the female and male teeth were discussed, analysing any potential differences which could be attributed to sex differences. This study has the potential to expand sample size and further analyse the possibility of $\delta^{44/42}$Ca to understand the sex difference. The sample collection, preparation, all stages of the ion-exchange chromatography and interpretation were conducted by P. Davechand. The mass spectrometry was carried out by A. Hassler at the ENS, Lyon.

Journal articles enclosed in this PhD appendix.

a. Tracing diet in Mesozoic archosaurs and dinosaurs of the Elliot Formation, South Africa using Ca isotopes (Appendix A)

This paper focuses on the utility of $\delta^{44/42}$Ca in deep time and the varying $\delta^{44/42}$Ca values for herbivorous vs carnivorous diet. This is proof in concept of using $\delta^{44/42}$Ca isotopes to understand palaeodiets with the possibility to understand palaeotrophic range when applying this technique to taxa that once co-existed. Samples were drilled, digested and all the stages of ion-exchange chromatography to collect the Ca aliquots was performed by P. Davechand. The Ca aliquots analysed on the Thermofisher Neptune MC-ICPMS by A. Hassler and P. Davechand. Data interpretation was done by P. Davechand, Jonah Choiniere, Grant Bybee, A. Hassler, Jeremy Martin, Y. Coutilloux-Pochat and Vincent Balter. This paper has been submitted *Biology Letters* of *The Royal Publishing* and is currently being revised.

b. Absence of temperature effect on elution profiles on anionic and cationic ion-exchange resins from 4°C to 28°C (Appendix B)

This paper shows that this type of chemistry can allow for a 'greener chemistry' as controlled temperatures and air-conditioning is not required when conducting ion-exchange chromatography to collect Ca ions. This type of ion-exchange chromatography is not affected by temperature changes. The column chemistry using the AG50W-X12 resin and reference material standards NIST-SRM1486 and IAPSO were carried out by Aline Lamboux, A. Hassler and P. Davechand. Data collection and interpretation was done by A. Lamboux with assistance from A. Hassler, Vincent Balter and P. Davechand.

c. Simultaneous analysis of stable and radiogenic strontium isotopes in reference materials, plants, and modern tooth enamel (Appendix C)

Appendix C highlights the potential of future analysis and studies in utilising strontium isotopes ($\delta^{88/86}$Sr) alongside $\delta^{44/42}$Ca as these isotope systems follow the same ion separation techniques. The ion-exchange chromatography, data collection and interpretations were done by Danae Guiserix *et al*. P. Davechand assisted in the setup of the method and supervised the ion-exchange chromatography procedure conducted in the WIGL.

2. General literature review

2.1. Proxies for palaeodiet and palaeotrophic range determination

Dietary inference for long-extinct taxa for which no close living relatives exist is commonly done using morphological proxy data such as tooth morphology and dentary function (Tolchard *et al.*, 2019; Bakker, 1987). Tooth morphology is the most frequently used dietary proxy for extinct animals. Conspicuous features of the dentition, like crown height, cusp complexity, and enamel wear, have a long tradition of use for dietary inference in mammalian research (Cabreira *et al.*, 2016). Similar studies across amniotes are in their infancy e.g., crocodyliforms cusp complexity (Melstrom and Irmis, 2019). Among reptiles and stem mammals, other tooth features, such as ziphodont and serration density have often been cited as evidence for carnivory. While this has been used in past studies as diet indicators, they have seldom been tested among living animals. For example, all snakes are carnivorous but not all have serrated teeth, a characteristic typically used to be a definite indicator for carnivory (Lillywhite, 2014).

A definite distinction for a presumed carnivorous 'rauisuchian' tooth may be described to be large and pointed with frequent serrations as carnivores generally have ziphodont, finely serrated teeth (Fig. 2.1a) (Nesbitt *et al.*, 2013; Sander, 1997). Whereas a presumed herbivorous sauropodomorph may have leaf-shaped teeth with larger serrations (Fig. 2.1b) (Popowics and Fortelius, 1997; Sanders, 1997).

Unfortunately, there are also tooth morphologies for which there is no consensus as to what the animals may have used them for or morphologies which may show an overlap between herbivores and carnivores. An example is leaf-shaped teeth and small fleshy cheeks of the therizinosaurids that are presumed to be either herbivorous or omnivorous (Barrett, 2005). Troodontids are another example of species with serrated teeth but are presumed herbivorous (Zanno and Makovicky, 2011).

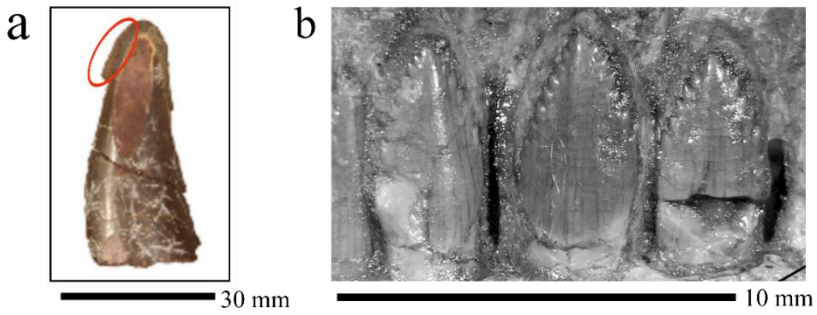


Figure 2.1: Photographs of archosaur and dinosaur teeth from the Elliot Formation **(a)** A 'rauisuchian' tooth (BP/1/5163) with the red circled area indicating the preserved serrations (adapted from Tolchard et al., 2019). **(b)** A holotype (BP/1/6235) of sauropodomorph Arcusaurus pereirabdalorum indicating leaf-shaped teeth (adapted from Yates et al., 2011).

The dentary function can also be studied by reconstructing possible jaw muscle attachments, wear in the teeth and tooth position. This is done to understand jaw motion and if mastication was vital when consuming food (Crompton *et al.,* 1963). Jaw motion allows for the comparison of possible mastication of extinct species with modern-day animals. Tooth wear is also used as a dietary proxy as herbivores are thought to have more worn teeth compared to carnivores whose teeth may have broken or fallen off while pulling at flesh (Popowics and Fortelius, 1997). Tooth position has also been used as a proxy. For example, if many teeth are closely packed in consecutive rows and have smooth surfaces, the teeth may have been used for tearing through vegetation. However, closely packed, highly serrated teeth are presumed to be in favour of a carnivorous diet (Barrett, 2005).

Gut content is the best evidence for palaeodiet but is exceedingly rare in the fossil record. In a paper by Salgado *et al.* (2017), a basal *Isaberrysaura mollensis* had well-preserved gut contents which consisted of seeds and fructifications. Coprolites, the fossilised faeces of ancient animals, can also infer dietary preferences but may not provide complete evidence of palaeodiet as it is quite difficult to identify the particular species that the coprolite may be produced by (Gee, 2011).

While tooth morphology and jaw functional anatomy are good proxies for diet in the close ancestors of living taxa, their predictive ability in the deep fossil record is essentially untested and limited by the lack of modern analogues and homology issues. Studying morphological characteristics like the jaw shape and jaw motion to understand the type of food consumed and jaw motion is conjectural. Preserved gut cavities are extremely rare to find and could even be contaminated with external material (Salgado *et al.,* 2017). While all these proxies may assist to distinguish between herbivores and carnivores, it may not be enough to understand their roles in an ecosystem and the other factors such as possible predator-prey relationship. Tooth shape, morphology and jaw motion can sometimes be non-specific evidence, but if used alongside isotopic proxies, it can provide thorough evidence for dietary dynamics. In contrast, $\delta^{44/42}$Ca analysis of tooth enamel is advantageous as it does not require a full skull or jaw to carry out the analysis (Martin *et al.,* 2017). The small amount of sample powder and crystalline apatite structure required for Ca analysis is less likely to be influenced by diagenesis opposed to the collagen used in recent carbon, oxygen and nitrogen studies.

2.2. Geochemistry of Ca

An element is defined by the number of protons and neutrons in the nucleus. While proton numbers are a constant, the number of neutrons in an element can vary. These elemental variations, with their varying neutron numbers, are called ‘isotopes’ and this results in variable atomic masses for the different isotopes of the element (Best, 2002). Isotopes occur in both radioactive and stable form where isotopes generally undergo fractionation (i.e., concentration of one isotope over another) during physiochemical processes or reactions which exploit mass differences between the isotopes (Hoefs,

2015). This fractionation affects the stable isotopic composition of rocks, waters, bones and teeth (Jaouen *et al*., 2012).

Ca is a bio-essential element with six naturally occurring stable isotopes (^{40}Ca, ^{42}Ca, ^{43}Ca, ^{44}Ca, ^{46}Ca, and ^{48}Ca) (Farkaš, 2018). ^{44}Ca isotopes are of particular importance because their fractionation ratio to ^{42}Ca isotopes (hereafter, $\delta^{44/42}$Ca) is influenced by a variety of biological processes, such as diet composition. Ca isotopes found in the body are commonly measured and reported as $\delta^{44/42}$Ca (Tacail *et al*., 2017). By calculating the $\delta^{44/42}$Ca, one can fingerprint the initial biological reactions and processes from bone and teeth as they are well-vascularised and porous (Russell *et al.*, 1978; Knudson *et al.*, 2010; Reynard and Balter, 2014).

Bio-essential elements like Ca are physiologically important for protein transport and interact structurally with bones and teeth as part of bioapatite ($Ca_5(PO_4, CO_3)_3(OH, F, Cl, CO_3)$) formation (Hoppert, 2011; Lucas *et al.,* 2015). Isotopes of Ca were initially used for analysing geological material until Skulan *et al.* (1997) identified Ca isotopic differences in biological material of aquatic and terrestrial organisms of the same trophic levels.

Ca isotopes in the body are influenced by the $\delta^{44/42}$Ca values of the food and waters consumed from the surrounding environment (Skulan *et al.*, 1997). As the plants and/or mineralised tissues and bones are consumed, the $\delta^{44/42}$Ca values are more depleted in ^{44}Ca due to biological fractionation resulting in relatively more ^{42}Ca than ^{44}Ca moving through the trophic chain (Morgan *et al.*, 2012; Martin *et al.*, 2017). Typically, a diet that includes more bone material will have lower Ca isotope ($\delta^{44/42}$Ca-depleted) values than the source, as bones are enriched in lighter Ca isotopes due to biological fractionation within the food source (Martin *et al*., 2017; Skulan and DePaolo, 1999). While the body can be influenced by the $\delta^{44/42}$Ca values obtained from the surrounding resources consumed, these values can be overprinted during the lifespan of an animal or diagenetically altered in its preserved tissues after death (e.g., during fossilisation) (Tacail *et al*., 2017). If a bone breaks, the Ca isotopes will be overprinted during the remodelling processes with a preference of ^{42}Ca over ^{44}Ca during fractionation as ^{42}Ca is incorporated easier into bone material (Morgan *et al*., 2012).

Fossilised bone material is highly porous and is more likely to be affected by diagenetic alteration when compared with teeth (Martin *et al*., 2017). The porous bone structure allows for more secondary and external minerals to easily infill and crystallise within the pore spaces (Reynard and Balter, 2014). In teeth, the dentine is more porous compared to the enamel as it is more vascularised (Enax *et al.*, 2013). Due to the porosity, dentine can be easily affected by diagenetic alteration whereas enamel has a solid crystalline structure that is difficult to alter because of low porosity, large crystal size and low organic content (Bocherens *et al.*, 1994). Even though tooth enamel is highly unlikely to be diagenetically altered, teeth and bone can have an infilling or precipitation of secondary calcite ($CaCO_3$) in the pore spaces (Martin *et al*., 2017). This calcite can influence the Ca isotopes as the

secondary calcite favours the heavy Ca isotope (^{44}Ca) and will obscure the ratios. Fortunately, removal of the secondary calcite can be achieved through leaching as outlined by Balter *et al.* (2002), revealing primary Ca isotopic values.

Ca isotopes can also be used to further understand and reconstruct extant ecosystems. In a case study by Hindshaw *et al.* (2013), the roots of trees had relatively negative $\delta^{44/42}$Ca values as there was a depletion of ^{44}Ca whereas the leaves had relatively positive values as there was an enrichment in ^{44}Ca. This is due to the heavy ^{44}Ca being deposited in the leaves while the lighter ^{42}Ca is enriched in the roots of the plant as ^{42}Ca passes through the soil to the roots easily (Hindshaw *et al.*, 2013). The isotopic fractionation of Ca can also be observed between plants and animals as well as within trophic levels. In a study by Martin *et al*. (2018), a range of modern taxa including Hyaenidae, Suidae, Bovidae and Felidae amongst others were analysed. The study displayed an offset between the carnivorous Felidae and Hyaenidae and the herbivorous Bovidae. The Bovidae had relatively $\delta^{44/42}$Ca-enriched values compared to the Felidae, which had relatively $\delta^{44/42}$Ca-depleted values compared to the Bovidae (Martin *et al*., 2018). This was due to the depletion in ^{44}Ca when moving through the trophic levels and experiencing fractionation in the body. Bone, blood and organs are depleted in ^{44}Ca compared to the food source (Morgan *et al.*, 2012).

Past ecosystems, trophic structure and diet could therefore also be reconstructed and inferred in palaeontological studies using $\delta^{44/42}$Ca (Martin *et al*., 2017, Dodat *et al.*, 2020). Isotopic analyses may also still be conducted on a broken tooth whereas comparative analyses may struggle if there is a lack of features such as tooth shape (Nesbitt *et al.*, 2013). A study by Hassler *et al.* (2018) showed that even though the studied assemblages shared the same ecosystem, the spinosaurids consumed marine resources whereas abelisaurid and carcharodontosaurid theropods consumed terrestrial resources. Dinosaurs presumed to be carnivorous displayed $\delta^{44/42}$Ca-depleted values compared to presumed herbivorous dinosaurs (Hassler *et al*., 2018). There is also a difference in the $\delta^{44/42}$Ca values of the food source, fish, which is reflected in the secondary consumers being abelisaurid and carcharodontosaurid. The difference in the $\delta^{44/42}$Ca values of the fish can be due to the surrounding environment e.g., water and food consumed by the fish (Hassler *et al.*, 2018).

The unique demands of reproductive physiology also perturb the Ca cycle of vertebrates and can lead to fluctuation of $\delta^{44/42}$Ca values. For example, the lactation process in mammals produces milk that is enriched in ^{42}Ca since it is secreted more easily through the mammary epithelium of the producer's body during breastfeeding. This results in $\delta^{44/42}$Ca-depleted milk (Reynard *et al.*, 2011; Tacail *et al*., 2017). The consumer's teeth will be more $\delta^{44/42}$Ca-depleted as a there is a larger intake of ^{42}Ca over ^{44}Ca ions (Tacail *et al*., 2017). Egg production requires a large influx of Ca for shell formation when an organism is about to lay the eggs (Skulan and DePaolo, 1999). The increase in Ca levels observed around the time of egg-laying is known as hypercalcemia (Wink *et al.*, 1987). Ca levels in the bodies

of female crocodiles increase when the ovarian follicles are developing (Wink *et al.*, 1987). There is an increase in osteoderm density due to higher Ca levels in female crocodiles during this period (Dacke *et al.*, 2015), but it is unknown how this effects the $\delta^{44/42}$Ca values in the producer's body.

2.3. Time period and geological setting

The Triassic period (251–201 Ma), the first stage of the Mesozoic era, was a time period when continental ecosystems recovered from one of the worst mass extinction events in Earth's history (McCarthy and Rubidge, 2005). This geological interval was an important time period in the development of modern biodiversity patterns as dinosaurs, squamates, and the earliest mammals radiated following the end-Permian extinction event (Benson, 2018). In the Triassic, these ecosystems were mixed, with dinosaurs, pseudosuchians, and non-mammalian therapsids filling a broad range across the body size spectrum and a wide variety of trophic roles. The Triassic ecosystems proved to be quite successful in allowing ancient animals to flourish and fulfil different ecological niches due to suggested factors like an increase in aridity and a decrease in species competition as a result of the end-Permian extinction (Irmis, 2010). It has been suggested that food webs dominated by large reptiles and mammal relatives seemed to remain more stable when compared to food webs that included smaller animals, but our ability to test this hypothesis is limited (Roopnarine and Angielczyk, 2015).

By the Jurassic Period, dinosaurs continued to diversify and fulfil herbivorous and carnivorous roles and niches, emerging as the ecosystem victors with medium to large body sizes within ecosystems (Hull, 2015). Early mammals remained small and rare through to the Jurassic Period (Hull, 2015). It was towards the end of this period that early mammals started to evolve from therapsids (Close *et al.*, 2015). This may be due to long-term stabilization of the food webs and trophic structuring, which is more properly sorted in these body size classes.

A mass extinction event occurred at the end of the Triassic period (ca. 200 Ma), hypothesised to be caused by volcanic eruptions of the Central Atlantic Magmatic Province (CAMP) activity (Irmis, 2010). This volcanic activity released large amounts of toxic gases (e.g., fluorine) into the atmosphere that led to sea-level change, climate change, aridification and anoxic seawater conditions which led to biodiversity loss due to inhabitable conditions (Hautmann, 2012; Kovács *et al.*, 2020; Fox *et al.*, 2022). Marine taxa were strongly affected by this event, but the effect on terrestrial taxa is poorly understood (Hautmann, 2012; Kovács *et al.*, 2020; Schoepfer *et al.*, 2022). Therefore, it is beneficial to understand how ecosystems were affected and how long it took for these ecosystems to stabilise following the end-Triassic extinction event. Functional palaeoecology and resource partitioning of the

ancient animals obtained from this study would provide important insight into the recovery patterns following the end-Triassic extinction event.

The Elliot Formation, part of the Stormberg Group from the Karoo Supergroup, formed between 218–190 Ma and preserves the Triassic–Jurassic boundary (Sciscio *et al.*, 2017; Bordy *et al.*, 2020). The samples analysed in this Ph.D. study are from the Elliot Formation in South Africa, spanning the latest Triassic–earliest Jurassic interval (Norian–Pliensbachian) (Bordy *et al.*, 2020) (Fig. 2.2). Fluvio-lacustrine-to-arid sediments in the Elliot Formation were favourable matrices to preserve the fossil specimens that existed close to the Triassic–Jurassic boundary (Catuneanu *et al.*, 2005; Sciscio and Bordy, 2016; Dollman *et al*., 2019). The Elliot Formation preserves abundant vertebrate fossils, particularly amniote lineages, and these fossil taxa are presumed to have diets ranging from herbivorous to carnivorous (Yates *et al.*, 2011; McPhee *et al.*, 2015; Sciscio and Bordy, 2016; Tolchard *et al.*, 2019; Bordy *et al.*, 2020). The morphological diversity of the fossils suggests that phylogenetically related taxa co-existed and had adapted to fill different niches (McPhee *et al.*, 2017).

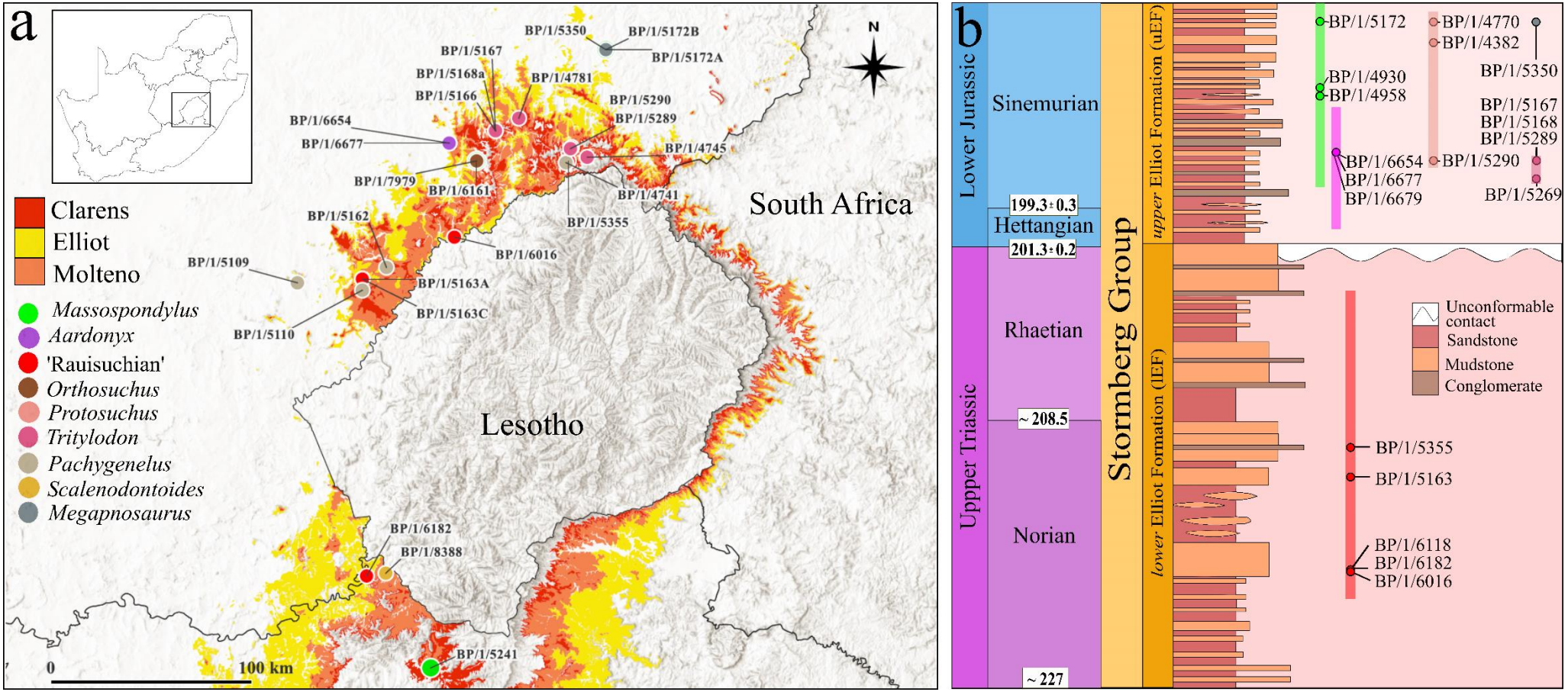


Figure 2.2: Locality map and stratigraphic section of Karoo cranial fossil study material (Appendix G). **(a)** A distribution map showing the geological overview and distribution of fossils in this study within the Karoo Supergroup **(b)** A schematic stratigraphic section of the Elliot Formation (Stormberg Group; Karoo Supergroup), from approximately 227 to 190.8 Ma, modified after Bordy *et al.* (2020) showing the position of each fossil analysed in this study. The BP number represents the different fossils, and the colours represent the different taxa as shown in (a). Specimens with poor provenance are not shown above.

2.4. Dinosauria and other taxa

The abundant fossils of the Elliot Formation include a wide range of vertebrate lineages and body sizes, making them ideal for understanding Triassic–Jurassic ecosystems. Specimens with dentition in this formation include pseudosuchian or 'crocodile-line' archosaurs, dinosauria and therapsida, which are some of the groups that existed during the Late Triassic to Early Jurassic Period (Knoll, 2004; Viglietti *et al*., 2020a, 2020b). These relatively abundant groups have been selected for this study and are documented below, as they co-existed temporally, spatially and provide a range of presumed dietary preferences, including carnivory and herbivory.

2.4.1. Pseudosuchia or 'crocodile-line' archosaurs: 'Rauisuchians' and crocodylomorphs

This group of archosaurs show characteristics which are 'crocodile-like' and led to the modern-day crocodilian lineage. Pseudosuchia are ancestrally carnivorous which later branched off to members of the group being large-bodied carnivores especially 'rauisuchids' and non-crocodylomorph loricatans (e.g., *Batrachotomus kupferzellensis*) (Knoll, 2004; Mujal *et al*., 2022).

'Rauisuchians'

'Rauisuchia' is a general term used for groups of non-crocodylomorph loricatans from the Triassic Period (Nesbitt *et al.,* 2013). 'Rauisuchians' were pre-eminent large-bodied carnivores of the Triassic Period and went extinct during the end-Triassic extinction (Tolchard *et al.,* 2019). Numerous large, ziphodont, finely serrated teeth (Fig. 2.3), attributed to 'rauisuchians', have been found in the lower Elliot Formation in South Africa (Nesbitt *et al.,* 2013), but body fossils are quite rare (Tolchard *et al.,* 2019). Although there is no direct evidence, 'rauisuchians' may have fed on co-existing fauna such as *Scalendontoides* (Tolchard *et al.*, 2019; Nesbitt *et al.,* 2013). The lack of other large-bodied predators suggests that 'rauisuchians' may have had a specialised diet and fed on larger herbivorous dinosaurian.

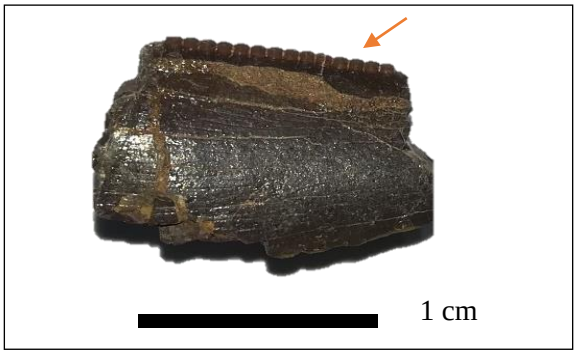


Figure 2.3: Photograph of 'Rauisuchian' tooth specimen (BP/1/5163A) with the orange arrow indicating the fine-tooth serrations.

Crocodylomorpha: *Orthosuchus stormbergi* and *Protosuchus richardsoni*

Crocodylomorphs are diverse and stratigraphically distributed close to the base of the Clarens Formation and in the uppermost part of the Elliot Formation (Dollman *et al.,* 2019; Viglietti *et al.,* 2020). *Orthosuchus stormbergi* is a Lower Jurassic armoured crocodylomorph which is found and confined to the uppermost section of the Elliot Formation (Nash, 1968; Dollman *et al.,* 2019). *Orthosuchus* is presumed to be carnivorous but appears to have a more complex palate construction and differing dentition which can infer a more specialised diet (Nesbitt *et al.,* 2013). Historical research presumed early branching taxa such as *Orthosuchus stormbergi* and *Protosuchus richardsoni* were carnivores hunting smaller prey, such as lizards and insects. However, a recent study of the complexity of their dentition and the construction of their palates suggests that some early crocodylomorph taxa may have been at least partially herbivorous (Nesbitt *et al.,* 2013; Dollman and Choiniere, 2022; Melstrom and Irmis, 2019).

2.4.2. Dinosauria: Ornithischians, theropoda and sauropodomorphs

Dinosauria is a group of late-branching archosaurs whose living descendants include all birds. To date, dinosaurs in the Elliot Formation were medium to gigantic in body size, with long necks and tails, bipedal and quadrupedal postures, and a range of hypothesised diets from hypercarnivory to bulk herbivory (Baron *et al.,* 2017; Barret, 2004). Dinosauria consists of two large clades: Ornithischia and Saurischia, where saurischians are further divided into the ancestrally carnivorous Theropoda and Sauropodomorpha (Benton, 2007).

Ornithischians: *Heterodontosaurus* and *Lesothosaurus diagnosticus*

Ornithischian dinosaurs are one of the two main herbivorous lineages of dinosaurs. Ornithischians appear in the fossil record in the earliest Jurassic, but their ancestry and origins remain obscure especially with the recent debate on major dinosaur relationships (Baron *et al.,* 2017; Müller and Garcia, 2020; Button *et al.,* 2023). The Elliot Formation has the best record of early branching ornithischians in the world (Radermacher *et al.,* 2021).

Heterodontosaurids are the earliest branching clade of ornithischians, with a global distribution that spans the Jurassic–early Cretaceous. In southern Africa, several species of heterodontosaurids are found in the Early Jurassic, upper Elliot and Clarens formations (Barrett *et al.,* 2016; Butler *et al.,* 2008). Some of these heterodontosaurid taxa include *Lycorhinus angustidens, Abrictosaurus consors, Pegomastax africanus* and *Heterodontosaurus tucki* (Porro *et al.,* 2011; Sereno, 2012; Radermacher *et al.,* 2021). *Heterodontosaurus* is large in size and is the most commonly found heterodontosaurid (Porro *et al.,* 2011). *Heterodontosaurus tucki* is presumed to be herbivorous as its posterior maxillary and dentary teeth show clear occlusal dental wear, probably from grinding tough plant material

(Norman *et al.,* 2011). However, its sharp canines and premaxillary beak indicate potential for omnivory (Sciscio *et al.,* 2017; Crompton and Attridge, 1986).

Lesothosaurus diagnosticus is an early branching ornithischian that is more closely related to the charismatic ceratopsians and duckbilled dinosaurs than it is to Heterodontosaurids. *Lesothosaurus* fossils were recovered from the Early Jurassic strata of the upper Elliot Formation (Barrett *et al.,* 2016). It is presumed to be omnivorous due to the dental wear, leaf-shaped teeth and the shape of the mandible (Fastovsky, 2000; Sciscio *et al.,* 2017). Dental wear suggests that this dinosaur could have been herbivorous and used its beak to feed on soft fructifications and shoots (Sciscio *et al*., 2017).

Theropoda: *Megapnosaurus rhodesiensis*

'Syntarsus' rhodesiensis, now referred to as *Megapnosaurus rhodesiensis,* lived in the Early Jurassic Period in Zimbabwe and South Africa (Munyikwa and Raath, 1999; Raath, 1969). *Megapnosaurus rhodesiensis* is one of the theropods present in the upper Elliot and Clarens Formations and Karoo-aged basins of Zimbabwe (Knoll, 2004; Bristowe and Raath, 2004). This dinosaur is considered a predator as it has ziphodont teeth that are strongly recurved with prominent serrations (Munyikwa and Raath, 1999). *Megapnosaurus rhodesiensis* lived alongside *Massospondylus carinatus, Aardonyx celestae, Pulanesaura eocollum* and the therapsid *Tritylodon* (Munyikwa and Raath, 1999).

Sauropodomorphs

Sauropodomorph dinosaurs are iconic for their elongate necks and tails, small skulls, and often gigantic body sizes (Kutty *et al.,* 2007; Rauhut *et al.,* 2011; Apaldetti *et al.,* 2021; Botha *et al.,* 2022). This group of dinosaurs were abundant during the Mesozoic Era and had a global distribution by the Early Jurassic (Apaldetti *et al.,* 2018).

Sauropodomorphs were the most successful herbivorous dinosaur group during the Triassic Period, occurring in large numbers and becoming taxonomically and morphologically diverse by the Norian (Mannion, 2009; McPhee *et al.,* 2017; Benson, 2018). Sauropodomorphs were relatively unaffected by the Early Triassic extinction, with most lineages crossing this boundary and a rapid rebound of maximum body size (McPhee *et al.,* 2017; McPhee *et al.,* 2018). South Africa has a variety and abundance of sauropodomorphs in the Early Jurassic Elliot Formation *Masspondylus* Assemblage biozone including *Massospondylus carinatus, Aardonyx celestae,* and *Pulanesaura eocollum* (McPhee *et al.,* 2017; Viglietti *et al.,* 2020). *Massospondylus carinatus* is the most abundant dinosaur fossil in the upper Elliot Formation of the Karoo Supergroup and comprises ~ 95% of the biomass in their fauna (Chapelle and Choiniere, 2018; Gow *et al.,* 1990). All known *Massospondylus* fossils are found in the Early Jurassic rocks, between the upper Elliot and lower Clarens Formations of the Karoo Supergroup (Kitching and Raath, 1984). *Massospondylus carinatus, Pulanesaura* and *Aardonyx*

celestae are all presumed to be herbivorous due to their leaf-shaped teeth (Fig. 2.4) (Yates *et al.*, 2010; McPhee *et al.*, 2015; Yates *et al.*, 2011).

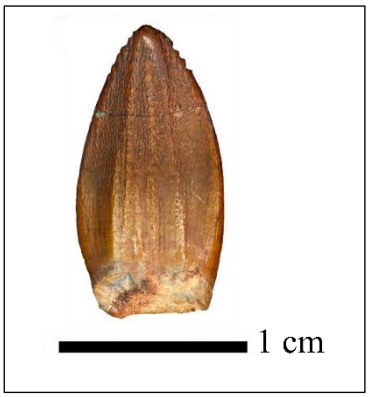


Figure 2.4: Image of a 'leaf shaped' *Pulanesaura* tooth specimen (BP/1/6204) (McPhee *et al.*, 2015).

Aardonyx celestae and *Pulanesaura eocollum* lived alongside *Massospondylus* and shared the same ecosystem (McPhee and Choiniere, 2016). These dinosaurs display a similar phylogenetic history but show adaptations in size, digestion, and foraging preferences to slightly different herbivorous niches just as modern grazers do in ecosystems such as the Kruger National Park (McPhee and Choiniere, 2016; Owen-Smith *et al.*, 2015). The size differences between the sauropodomorphs, differences in their gross anatomy, and potential postural differences (Yates *et al*., 2010) are possibly correlated with different foraging strategies. *Massospondylus* is suggested to be a selective browser feeding on high-quality forage and requiring less food (Chapelle *et al.*, 2021). Whereas *Pulanesaura* is much larger in size and is presumed to bulk browse on low quality vegetation requiring more food to meet its nutritional needs (Yates *et al.*, 2010). The varying body sizes between *Massospondylus, Aardonyx* and *Pulanesaura* affects the type of vegetation they consume, and their digestion processes required to process the amount and quality of food consumed (Owen-Smith, 1988). These feeding mechanisms are observed in modern ecosystems.

2.4.3. Therapsida: Gomphodonts (*Scalenodontoides macrodontes*), Trithelodontids (*Pachygenelus monus*), tritylodontids (*Tritylodon*).

Therapsida, commonly called 'mammal-like reptiles', is the lineage that ultimately gives rise to mammals. The main Karoo basin, including the Elliot Formation, is unquestionably the most time-extensive and complete record of therapsid evolution on Earth (Kemp, 2006). *Scalenodontoides macrodontes* is a gomphodont that was found in the lowermost part of the Elliot Formation during the Late Triassic (Crompton and Ellenberger, 1957; Battail, 2005; Abdala *et al.*, 2007, Viglietti *et al.*, 2020). It is presumed to be herbivorous due to dentary characteristics such as the distinctive gomphodont dentition, with large crushing surfaces on its postcanines (Gow and Hancox, 1993).

Tritylodon longaevus, found in the lowermost upper parts of the Elliot Formation, could have been a more specialised herbivore that broke down hard foods like roots in its oral cavity based on the precise dental occlusion of the upper and lower postcanines (Smith and Kitching, 1997; Gow *et al.*, 1990). *Pachygenelus monus* existed during the Lower Jurassic Period (Gow, 2001; Bonaparte and Crompton, 2017). This therapsid has a less specialised dentition and is presumed to be a small generalist herbivore (Bonaparte and Crompton, 2018).

3. Method setup and optimisation for Ca isotopes in the WIGL

3.1. Abstract

This chapter focuses on a description of the methodology used in this work, along with workflows used to optimise the Ca ion-exchange separation method in the WIGL. The ion-exchange chromatography mentioned in this chapter is modified from Tacail *et al.* (2014). It discusses the three stages of ion-exchange chromatography required to collect Ca ions: 1) matrix removal, 2) Fe removal, and 3) Ca and Sr separation. The result of method optimisation allowed for an adapted stage 1 matrix separation procedure using a Bio-Rad Poly-Prep® column with adjusted amounts of acid from Tacail *et al.* (2014). This modification has allowed for a time-efficient separation technique while still maintaining a clean chemistry and producing high quality data.

Reference materials such as bone meal (NIST-SRM1486) and bone ash (NIST-1400) were used alongside a modern juvenile *Crocodylus niloticus* (CN1) tooth sample, for the ion-exchange column calibrations. The *Crocodylus niloticus* tooth sample was only used for the column calibration and not for comparison of the $\delta^{44/42}$Ca values produced. However, the reference material produced $\delta^{44/42}$Ca values close to the means of NIST-SRM1486 (-0.98 ± 0.16 ‰) and NIST-SRM1400 (-1.11 ± 0.2 ‰). This is within the standard deviation of the literature values of NIST-SRM1486 (-1.0 ± 0.07 ‰) and NIST-SRM1400 (-1.0 ± 1.00 ‰) stated in Hassler *et al.* (2018) and Tacail *et al.* (2015).

3.2. Introduction

Ion-exchange chromatography is a method which separates different elemental ions depending on their affinity to the ion exchanger resin (Schönbächler and Fehr, 2013). The column chemistry uses commercial ion-exchange resin to separate inorganic anions and cations from the sample. This is an ultra-clean separation method that can be used to separate elements of interest from the matrix. Separation and removal of the matrix and any unwanted elements is done to avoid any interference and can result in precisions < 0.1‰ (Schönbächler and Fehr, 2014). In ion-exchange chromatography there is the stationary phase and the mobile phase. The mobile phase, the sample being carried in the acid medium, moves relative to the stationary phase, the ion-exchange resin (Schönbächler and Fehr, 2014).

This highly precise method of separating the ions is becoming one of the common methods of analysing isotopes from various samples in different fields like hydrogeology and biochemistry (Martin *et al.*, 2017). Non-traditional $\delta^{44/42}$Ca isotopes are being utilised in various fields such as geology, bioarchaeology, biomedical and palaeobiology (Skulan and DePaolo, 1999; Albarède, 2015;

Hassler *et al.*, 2018; Tacail *et al.*, 2020). A major advantage of the non-traditional $\delta^{44/42}$Ca isotope method is the extremely small mass of enamel/bone required, on the order of approximately 400 µg of powder. As the $\delta^{44/42}$Ca isotope system is becoming more widely used in ecosystem reconstruction and dietary studies (Martin *et al.*, 2018; Martin *et al.*, 2022), optimisation of this method would allow for time-efficient ion separation and increased throughput. The shortcomings of non-traditional $\delta^{44/42}$Ca isotopes are further discussed in Chapter 4 which highlights the importance of leaching and the effect of maturation on the Ca-fraction after ion-exchange chromatography.

In this research, various methods will be tested to optimise the separation of Ca ions as efficiently as possible. Microdrilling techniques will also be tested to ensure minimum damage during the sampling process. Tooth enamel is the sample material required for this research as enamel is not as highly susceptible to diagenetic alteration compared to dentine and/or bone material (Fisher, 1981). The small pore spaces and larger apatite crystals make tooth enamel more resistant to physical and chemical alteration during fossilisation (Botha *et al*., 2004).

The ion-exchange chromatography method used in this research is based on and adapted from methods first put forward by Tacail *et al.* (2014). As mentioned in Tacail *et al.* (2014), the separation techniques for Ca consists of three different procedures. The first separation procedure uses AG® 50W-X12 cation exchange resin in a Bio-Rad Poly-Prep® column to separate the Ca, Fe and Sr from the matrix using 6 N HCl (Table 3.1). The Ca and Sr aliquots are collected simultaneously as these ions behave similarly in organisms (Cuéllar-Cruz and Moreno, 2019). The second separation procedure uses AG® 50W-X8 resin in a Bio-Rad Poly-Prep® column to remove any Fe ions from the Ca and Sr aliquot using 0.5 N HCl (Table 3.1). The last procedure separates the Ca ions from the Sr ions using Sr-spec resin in a micro-column using 3 N nitric acid (HNO_3) (Table 3.1). Fig. 3.1 shows a generalized workflow for non-traditional $\delta^{44/42}$Ca isotopes, and this chapter focuses on Fig. 3.1a, b and c of the method (Martin *et al.*, 2017).

Table 3.1: Table listing the specific reagents and materials used for the different stages of Ca ion-exchange chromatography.

Chemistry stage	Column type		Resin used	
Stage 1: Matrix removal and collection of Ca-Sr	Bio-Rad Poly-Prep®	Purchased from the Bio-Rad website (https://www.bio-rad.com/)	AG® 50W-X12 Cation Exchange Resin, analytical grade, 100-200 mesh	Purchased from the Bio-Rad website (https://www.bio-rad.com/)
Stage 2: Fe removal from Ca-Sr	Bio-Rad Poly-Prep®	Purchased from the Bio-Rad website (https://www.bio-rad.com/)	AG® 50W-X8 Cation Exchange Resin, analytical grade, 20-50 mesh	Purchased from the Bio-Rad website (https://www.bio-rad.com/)
Stage 3: Removal of Sr and collection of Ca	Micro-columns	Made in-house	Sr spec™ resin	Purchased from fisher scientific (https://www.fishersci.com)

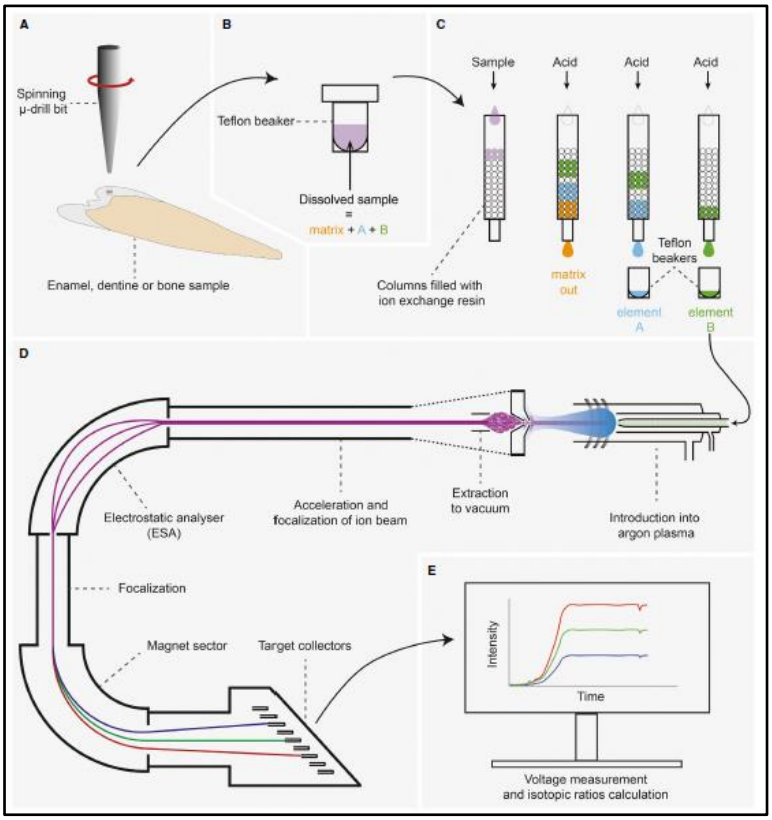


Figure 3.1: A generalised methodology for non-traditional $\delta^{44/42}$Ca isotopes from Martin *et al.* (2017). **(a)** The specimen was sampled. **(b)** Leaching and digestion of the powder sample in preparation for the ion-exchange chromatography. **(c)** The digested sample was loaded onto the column and various acids were added to move the different ions of interest through the column. **(d)** The sample was loaded onto the Neptune MC-ICPMS machine, and the target collectors counted the different intensities. **(e)** The intensities were then recorded, and isotopic ratios were calculated.

3.3. Methods

3.3.1. Microdrilling and sample preparation

Microdrilling of samples was done to obtain the required amount of enamel powder (~400 µg). A handheld 8200 Dremel and a specialist microdrill with non-contaminating tungsten-carbide drill bits (Fig. 3.2) was used to ensure minimal destruction and accurate sampling of the fossil specimens. A maximum of one or two drill spots were created on specimens. All articulated teeth were sampled in the WIGL.

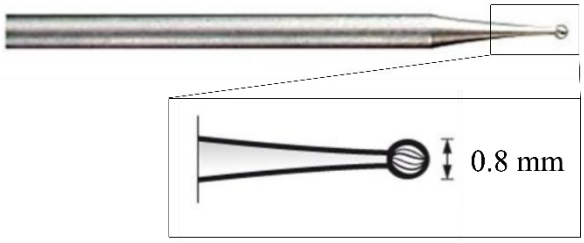


Figure 3.2: The tungsten carbide Dremel drill bit used for microdrilling the samples.

In preparation for the Ca ion-exchange chromatography of a bone/tooth enamel sample (Appendix G), the following detailed sampling protocol was carried out (Fig. 3.3):

1. High-resolution, scaled photographs were taken of the teeth and/or bones before sampling begins (Fig. 3.3a).
2. When sampling, it was vital to remain consistent in sampling the same location (i.e., the crown) and only the enamel of the tooth to avoid the dentine for the various specimens. Sampling the same location avoids sampling different parts of the tooth that may have a variation in isotopes due to processes involved in tooth development.
3. The sample spot was gently cleansed using minimal amounts of ultrapure water (Milli-Q) and isopropanol (Fig. 3.3b).
4. Once the sample was secured in a Dremel vise, <100 µL Milli-Q was pipetted onto the desired sample spot (Fig. 3.3c)
5. A small drill spot was created using tungsten carbide bits that were thoroughly cleaned prior to sampling. The drill spot produced a small amount of powder within the Milli-Q droplet (Fig. 3.3d).
6. The Milli-Q droplet was taken up into the pipette tip and then pipetted out into a weighed beaker (Fig. 3.3e, f).
7. The beaker was left to dry on the hot plate at approximately 90 °C. Once the sample dried down and the beaker was cool, the beaker was re-weighed to ensure the desired amount of sample has been collected.
8. Specimens were re-photographed to document the sampling spot.

9. Extensive cleaning of the drill and individual drill bits took place in between each specimen to avoid cross-specimen contamination using isopropanol and Milli-Q.

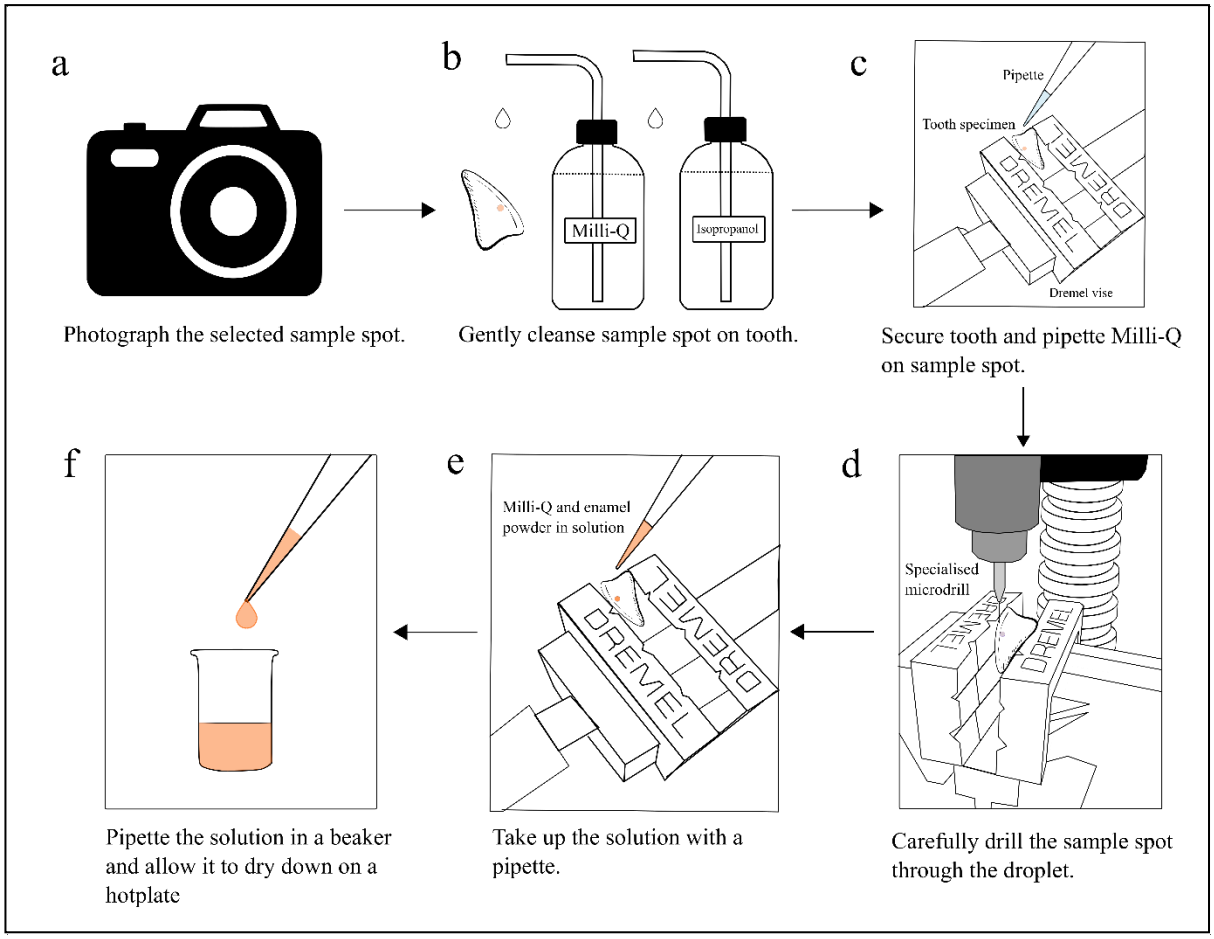


Figure 3.3: A simplified schematic diagram of the microdrilling method showing the general steps to obtain the required sample amount. **(a)** Photos of the sample and sample spot are taken. **(b)** The sample spot is cleaned with Milli-Q followed by Isopropanol. **(c)** The sample is secured in the Dremel vise, and a drop of Milli-Q is pipetted onto the sample spot. **(d)** Microdrilling is done using a tungsten carbide drill bit. **(e)** The droplet containing sample is collected. **(f)** The sample is pipetted into a beaker and put on a hotplate to dry down.

3.3.2. Sample digestion

To prepare the tooth enamel material and reference materials (NIST-SRM1486 and NIST-SRM1400) for ion-exchange chromatography, sample digestion was modified based on the method mentioned in Hassler *et al.* (2018) (Fig. 3.4). NIST-SRM1486 and NIST-SRM1400 reference materials were obtained from the National Institute of Standards and Technology. Prior to digestion, the samples were weighed to calculate the amount of 0.4 N HCl acid required as a loading medium for the sample to be introduced to the column (Fig. 3.4a). The ratio of sample powder to 0.4 N HCl acid was 400 µg of sample to 200 µL of 0.4 N HCl acid. Firstly, 2 mL of 12 M HNO_3 acid and 500 µL 9.85 M hydrogen peroxide (H_2O_2) were added to the sample powders and the beakers were capped and put on

a hotplate at 110 °C (Fig. 3.4b). The samples were regularly degassed at 10-minute intervals (Fig. 3.4c). Once degassing was complete, the beakers were capped and put on a hotplate at 110 °C for 48 hours (Fig. 3.4d). Thereafter another 500 µL of 9.85 M H_2O_2 was added to the samples and the samples were left uncapped on the hotplate between 90 – 100 °C to dry (Fig. 3.4e). Once the samples were dried down, just enough 6 N hydrochloric acid (HCl) acid was added to cover the sample in the beaker (Fig. 3.4f). The sample was again left to dry down at 90 °C (Fig. 3.4g). Once dried, the calculated amount of 0.4 N HCl acid was added as the loading medium onto the column (Fig. 3.4h).

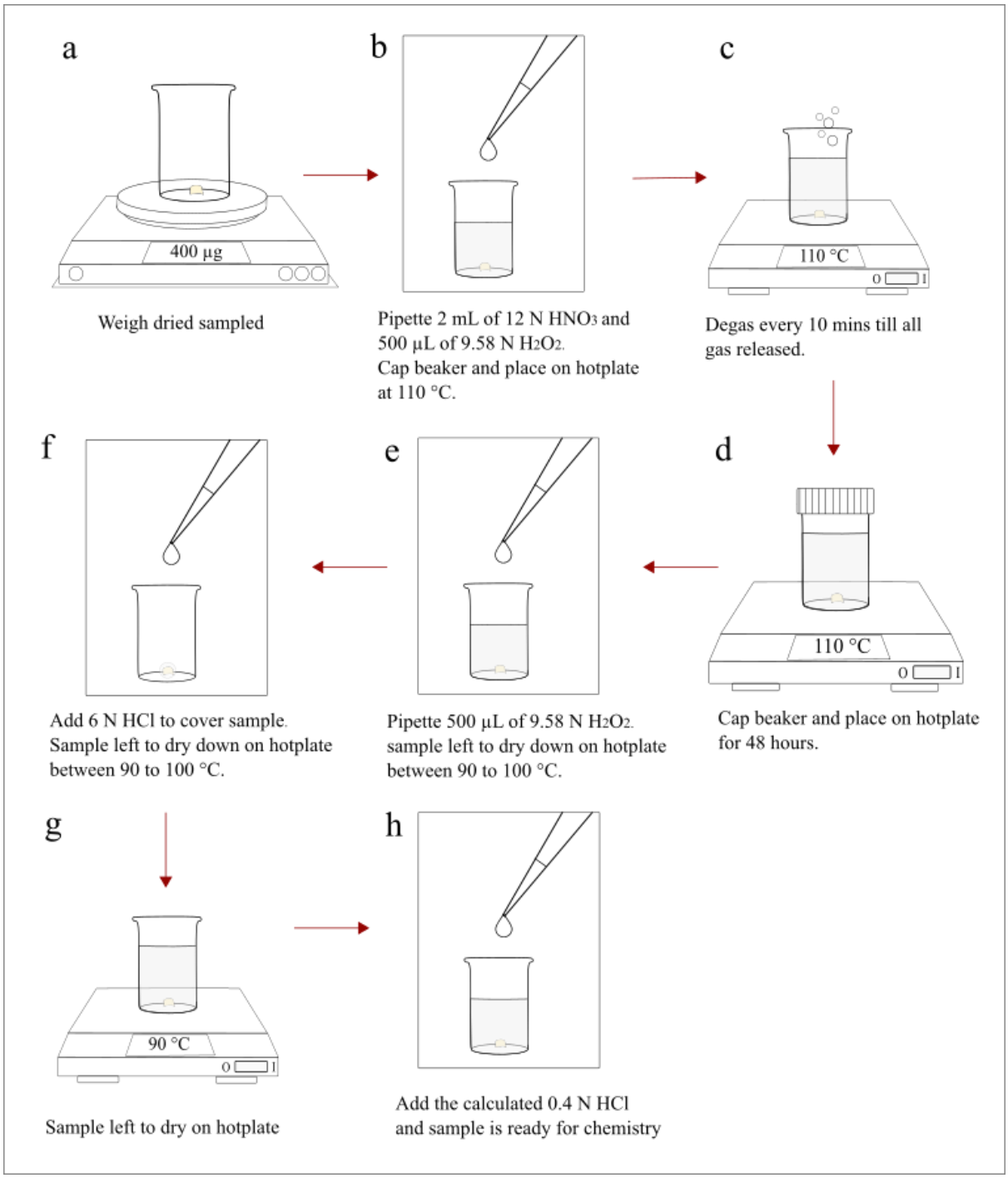


Figure 3.4: A simplified schematic diagram of sample digestion before ion-exchange chromatography. **(a)** Weigh the dry down sample to ensure there is ≥ 400 µg**. (b)** Add HNO_3 and H_2O_2 to remove any organic matter. **(c)** Open the beaker lid every 10 minutes to release the gas from the organic material being broken down. **(d)** Cap and place the beaker on the hotplate for sample digestion. **(e)** Add H_2O_2 to remove any remaining organic matter and dry down. **(f)** Add HCl to prepare the sample for the first stage of ion-exchange chromatography. **(g)** Dry down the HCl. **(h)** Add the required calculated amount of 0.4 N HCl for the ion-exchange chromatography.

3.3.3. Ion-exchange chromatography

3.3.3.1. Columns preparation

Before the ion-exchange chromatography could be performed, the columns underwent a rigorous washing process using the following steps:

1. The columns were submerged in a vessel, containing concentrated HCl, for an hour and then rinsed three times with Milli-Q. The columns were then placed in a vessel with 6 N HCl acid and left on the hotplate at 100 °C for 1 hour.
2. The columns were then taken off the hotplate, allowed to cool and rinsed with Milli-Q.
3. The columns were soaped and submerged in a vessel filled with Milli-Q water and placed on a 100 °C hotplate for two days. After two days, the vessel was removed from the hotplate and the columns were rinsed to remove soapy residue using Milli-Q water. The columns were each rinsed three times with Milli-Q water.
4. After rinsing, the columns were submerged in a vessel containing 6 N HNO_3 acid and 1% HF acid. The vessel was placed onto a hotplate at 100 °C for 2 days.
5. They were then removed and the 6 N HCl and 1% HF acid was discarded. The columns were rinsed and then air dried.

3.3.3.2. Resin preparation

To prepare the AG® 50W-X12 and AG® 50W-X8 cation exchange resins, the following procedure was followed:

1. Milli-Q was added to a bottle with some resin. The bottle was manually shaken for a few seconds, and then the Milli-Q was discarded. This was done three times.
2. 6 N HCl acid was then added to the resin in the bottle, enough to cover the resin, and the bottle was manually shaken. The 6 N HCl acid was then discarded. This was done minimum of three times and continued until the organic matter (visible as froth) was discarded.
3. Milli-Q was added to the resin and the bottle was stored until use.

To prepare the Sr-Specific resin, the following procedure was followed:

1. The dry resin was decanted into a beaker containing 0.5 N HNO_3. The beaker was placed in an ultrasonic bath for 1 to 2 mins.
2. Once the resin settled, the foamy float was discarded and more 0.5 N HNO_3 acid was added to the beaker. This was done two or three more times until there was little to no floatation.

Once the resins were cleaned and ready to be used, the required columns were filled with a specific amount of Milli-Q. This was dependant on the amount of resin needed in the column as mentioned in

methods by Tacail *et al*. (2014). For the first separation procedure, 210 µL of AG® 50W-X12 cation exchange resin was required. Therefore, 210 µL of Milli-Q was pipetted into the Bio-Rad Poly-Prep® column, the water level was marked (to indicate the amount of resin required), and the resin was then added to the column. Once the required resin amount was filled, 6 N HCl was added to the reservoir of the column to clean and remove any possible impurities.

3.3.3.3. Ion-exchange column calibrations

A variety of column calibrations were conducted in the WIGL to test the most efficient method to separate and collect the desired Ca aliquots from the samples as shown below in Table 3.2. To test the various columns and chemical procedures, a juvenile *Crocodylus niloticus* tooth specimen was prepared for calibrations 1 to 3. Ground-truthing of the isotopic systematics was performed on reference material: NIST-SRM1486, NIST-SRM1400 and the modern juvenile crocodile teeth, *Crocodylus niloticus*, as there is easier access to specimens of known sex, diet and age. Modern crocodilians were used as the presumed metabolic similarity between crocodilians and extinct reptilians such as dinosaurs (Brazaitis and Watanabe, 2011). The whole tooth of a juvenile *Crocodylus niloticus* was digested as enamel and dentine would not yield different elemental Ca values due to the specimen not being buried and exposed to any external processes or fluids. Reference material, NIST-SRM1486 and NIST-SRM1400, were selected, digested, and analysed in calibrations 3 to 8 as values produced from the ion-exchange chromatography should yield similar $\delta^{44/42}$Ca values to those produced in literature (Tacail *et al.*, 2015; Hassler *et al.*, 2018). The reference material NIST-SRM1486 was used more frequently as it has the most reliable reproduced isotopic composition.

Leaching was not carried out on any of the calibration reference material (NIST-SRM1486 and NIST-SRM1400) and the *Crocodylus niloticus* sample as the samples were not exposed to any diagenetic processes. All WIGL calibrations were then analysed using a ThermoFischer iCAP at the Wits Earthlab to obtain measured concentrations of major and trace elements.

Table 3.2: Table briefly describing the different column calibrations conducted to setup and optimise the Ca separation procedures in the WIGL.

Calibration run	Column no.	Separation stage being tested	Sample	Calibration details
Calibration 1 *Column 1 and 2:* Testing the type of column for matrix removal and collection of Ca, Sr	Column 1	*Stage 1:* - Matrix removal and collection of Ca-Sr) - AG® 50W-X12 cation exchange resin (Table 3.3)	*Crocodylus niloticus tooth* (enamel and dentine)	Using a standard smaller column (Fig. 3.5a) similar to those used at the ENS to test the efficient separation of Ca from the matrix. The eluted acid was collected in 1 mL increments.
	Column 2			Using a standard Bio-Rad Poly-Prep ® chromatography column (Fig. 3.5b) to test the efficient separation of Ca from the matrix. This followed the method outlined in Tacail *et al.* (2014). The eluted acid was collected in 1 mL increments.
Calibration 2 *Column 1 and 2:* Improvement of matrix elution *Column 3:* Testing the column for Sr purification	Column 1	*Stage 1* (Table 3.3)	*Crocodylus niloticus tooth* (enamel and dentine)	Re-run of Column 2 in Calibration 1 to ensure the calibration results were repeatable and reliable. The eluted acid was collected in 1 mL increments.
	Column 2	*Stage 1* (Table 3.4)		This calibration was based on Calibration 1 Column 2 results and was amended by adding 1 mL of 1 N HCl to the Mg elution step and 1 mL 6 N HCl to the Ca-Sr elution step. The eluted acid was collected in 1 mL increments.
	Column 3	*Stage 3* (Table 3.5)		This calibration collected bulk aliquots of Ca and Sr by using Table 3.3 followed by Table 3.5.
Calibration 3 *Column 1:* Improvement of Sr purification	Column 1	*Stage 3:* - Ca-Sr separation - Sr-Specific resin (Table 3.4 and 3.5)	*Crocodylus niloticus tooth* (enamel and dentine)	Using an inhouse microcolumn, this was to test the separation of Ca from Sr following the method outlined in Tacail *et al.* (2014). The eluted acid was collected in 1 mL increments.

Calibration 4 *Column 1:* Improvement of Sr purification	Column 1	*Stage 1 + 3* (Table 3.6 and 3.5)	NIST-SRM1486	The *Stage* 1 method of Calibration 2 Column 2 was further amended by an additional 3 mL of 0.4 N HCl to the matrix removal stage. The eluted acid was collected in 1 mL increments.
Calibration 5 *Column 1:* Improvement of Sr purification	Column 1	*Stage 3* (Table 3.7)	NIST-SRM1486	The method of Column 1 of Calibration 3 was further amended with an additional 10 mL of 0.5 N HNO_3 to ensure all Sr was removed off the column. The eluted acid was collected in 1 mL increments.
Calibration 6 *Column 1:* To test the separation and collection of Ca	Column 1	*Stage 1 + 3* (Table 3.6 and 3.7)	NIST-SRM1486 and NIST-SRM1400	The aim of this calibration was to obtain $\delta^{44/42}$Ca values. This was to ensure a clean chemistry with no contamination and fraction. Calibration 6 was for isotopic value reproduction using the reference materials. This calibration collected bulk aliquots of Ca and Sr.
Calibration 7 *Column 1:* Improvement of Sr purification *Column 2:* Testing Fe removal *Column 3:* Testing Sr purification	Column 1	*Stage 1* (Table 3.6)	NIST-SRM1486	Amended method used was from Column 1 of Calibration 4. The eluted acid was collected in 1 mL increments.
	Column 2	*Stage 2* - Fe removal from Ca-Sr - AG®1-X8 resin (Table 3.8)		Using a standard Bio-Rad Poly-Prep ® chromatography column (Fig. 3.5b) to test the efficient separation of Fe from the Ca-Sr. This followed the method outlined in Tacail *et al.* (2014). The eluted acid was collected in 1 mL increments.
	Column 3	*Stage 3* (Table 3.7)		This calibration was carried out to ensure the effective separation of Ca and Sr.
Calibration 8 *Column 1:* Testing the Ca collected after all three stages of chemistry	Column 1	*Stages 1, 2 and 3* Yield test (Table 3.6, 3.6 and 3.7)	NIST-SRM1486	This calibration was a yield test done to ensure all the Ca is being collected off the column after three stages of ion-exchange chemistry.

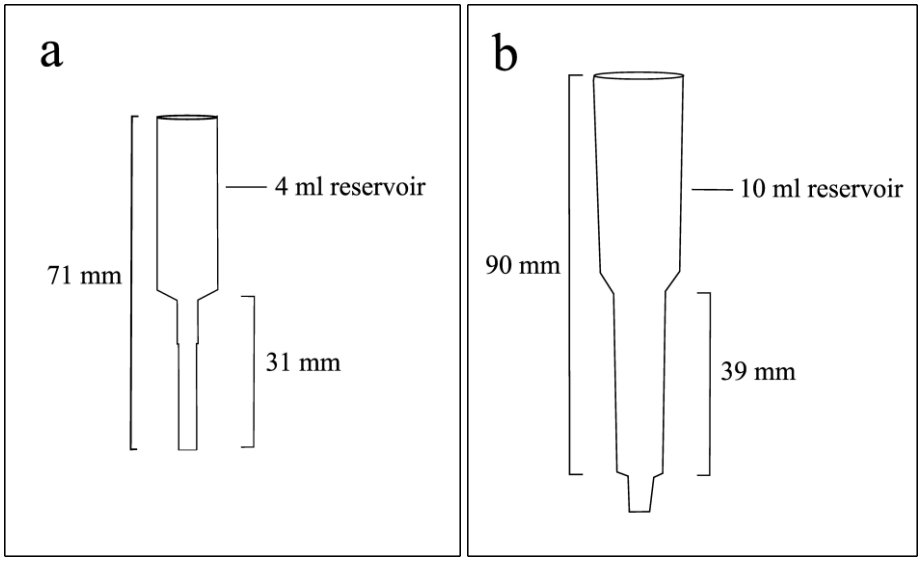


Figure 3.5: The different columns and the dimensions used for Calibration 1. **(a)** Smaller column (71 mm) similar to those used in the ENS, Lyon. **(b)** The Bio-Rad Poly-Prep ® chromatography column (90 mm) used for Stage 1 and 2 of the chemistry.

3.3.3.3.1. Calibration 1

The sample used in this calibration was a juvenile *Crocodylus niloticus* tooth. The first calibration was to test two different column types with different dimensions. This was done to understand which column separated the desired ions from the matrix effectively and efficiently. One column had dimensions close to those used at the ENS, Lyon (Column 1) (Fig. 3.5a) while the other was a standard Bio-Rad Poly-Prep® column (Column 2) (Fig. 3.5b). The ion-exchange method shown below in Table 3.3 was carried out to remove matrix and collect the Ca elution.

Table 3.3: Ca ion-exchange chromatography method used for calibration 1.

Step	**Acid**	**Volume (mL)**
Matrix removal		
AG50W-X12 resin (200-400 mesh) ~ 2mL		
Condition	0.4 N HCl	2.5 mL
Load	0.4 N HCl	0.2 mL
Elution (matrix – phosphorous (P), sodium (Na), potassium (K), sulphur (S))	0.4 N HCl	13.8 mL
Elution (matrix – magnesium (Mg))	1 N HCl	3.5 mL
Ca elution (Ca, strontium (Sr), iron (Fe))	6 N HCl	2.5 mL
Wash	N HCl	2 mL

3.3.3.3.2. Calibration 2

The following tests for calibration 2 were designed around the results of calibration 1. Three Bio-Rad Poly-Prep® columns of the same dimensions (Fig. 3.5b) were used during this calibration. Each column tested the following parameters:

Column 1: This column was run using the original matrix separation method from ENS based on Tacail *et al.* (2014) (Table 3.3). Each 1 mL increment of acid was collected separately. There was no change to this column calibration as it was done to duplicate the calibration 1 of column 1 to ensure repeatable results were being produced.

Column 2: This column was also incrementally run but there was an additional 1 mL of acid added to the Mg elution step and 1 mL of acid to the Ca elution step as indicated in Table 3.4 below. This was done to ensure all the Ca was eluted and collected at the right time.

Column 3: This column tested the separation of the Ca and Sr ions. The procedure indicated in Table 3.3 was used to separate and collect the bulk Ca-Sr aliquot from the matrix. The Ca and Sr aliquot in 6 N HCl was left to dry down at 90 °C. Once dried, a drop of 14 N HNO_3 was added to cover the sample. The sample was placed on the hotplate to dry down at 90 °C. Once the sample was dried, 300 µL of 3 N HNO_3 was added to the sample. The sample was ready to be loaded onto the Sr-Specific resin using Table 3.4 to separate the Ca and Sr ions.

Table 3.4: Ca ion-exchange chromatography method used for column 2 of calibration 2 with the addition of 1 mL of 1 N HCl (Mg elution) and 1 mL of 6 N HCl (Ca elution). Amended volume highlighted in red.

Step	**Acid**	**Volume (mL)**
Matrix removal		
AG50W-X12 resin (200-400 mesh) ~ 2mL		
Condition	0.4 N HCl	2.5 mL
Load	0.4 N HCl	0.2 mL
Elution (matrix – P, Na, K and S)	0.4 N HCl	9.8 mL
Elution (matrix –Mg)	1 N HCl	4.5 mL
Ca elution (Ca, Sr and Fe)	6 N HCl	3.5 mL
Wash	6 N HCl	2 mL

Table 3.5: Ca-Sr ion-exchange chromatography separation method used for column 3 of calibration 2 after the Ca-Sr separation from the matrix.

Sr removal	**Acid**	**Volume (mL)**
Sr-Specific resin (Eichrom) ~ 0.7mL		
Condition	3 N HNO_3	2.5 mL
Load	3 N HNO_3	0.3 mL
Elution (Ca)	3 N HNO_3	3.2 mL
Elution (Sr)	0.5 N HNO_3	2 mL

3.3.3.3.3. Calibration 3

After collecting the bulk aliquots for Ca and Sr with column 3 of calibration 2, calibration 3 was done to ensure that the Ca and Sr ions were successfully separated when carrying out the ion-exchange chromatography using the Sr-Specific resin. In calibration 3, the bulk Ca was collected following the procedure in Table 3.4. Table 3.5 was then used for the Ca and Sr separation procedure.

The Ca-Sr separation method was conducted using Sr-Specific resin and was done incrementally to ensure full recovery of the Ca and removal of Sr. The elution collection differed at the beginning of this calibration as the Sr was collected at the first 0.3 mL mark. This is when only the sample, diluted in 0.3 mL, was loaded onto the column and eluted. This was collected separately to the 0.7 mL of 3 N HNO_3 that followed to complete the first 1 mL at the beginning of the chemistry.

3.3.3.3.4. Calibration 4

Calibration 4 focused on analysing the reference material NIST-SRM1486 using the adjusted method shown in Table 3.6 below. The wash and P, Na, K, S phase was further extended to understand the volume of 6 N HCl acid required to elute and collect all the Ca-Sr ions during the matrix and Ca-Sr separation stage (Table 3.5). Between carrying out the methods in Table 3.6 and

Table 3.5, the Ca and Sr aliquot in 6 N HCl was left to dry down at 90 °C. Once dried, a drop of 14 N HNO_3 was added to cover the sample. The sample was put onto the hotplate to dry down at 90 °C. Once the sample was dried, 300 µL of 3 N HNO_3 was added to the sample. The sample was ready to be loaded for the Ca-Sr separation stage (Table 3.5).

Table 3.6: Ca ion-exchange chromatography method used for calibration 4. Amended volume highlighted in red.

Step	**Acid**	**Volume (mL)**
Matrix removal		
AG50W-X12 resin (200-400 mesh) ~ 2mL		
Condition	0.4 N HCl	2.5 mL
Load	0.4 N HCl	0.2 mL
Elution (matrix – P, Na, K and S)	0.4 N HCl	12.8 mL
Elution (matrix –Mg)	1 N HCl	4.5 mL
Ca elution (Ca, Sr and Fe)	6 N HCl	3.5 mL
Wash	6 N HCl	12 mL

3.3.3.3.5. Calibration 5

In this calibration, the Ca-Sr separation procedure was further amended to ensure all the Sr was removed off the column. Table 3.6 was first carried out to separate matrix from the Ca-Sr aliquot was then used for calibration 5. This resulted in adding 10 mL of 0.5 N HNO_3 acid to elute all the Sr off the column. Table 3.7 below is the method used for Ca and Sr ion separation.

Column 1: Collected the Ca aliquots for quantitative analysis and ensured that all the Sr was removed off the column.

Table 3.7: Ca-Sr ion-exchange chromatography method used for calibration 4. Amended volume highlighted in red.

Sr removal	**Acid**	**Volume (mL)**
Sr-Specific resin (Eichrom) ~ 0.7mL		
Condition	3 N HNO_3	2.5 mL
Load	3 N HNO_3	0.3 mL
Elution (Ca)	3 N HNO_3	3.2 mL
Elution (Sr)	0.5 N HNO_3	16 mL

3.3.3.3.6. Calibration 6

This calibration was designed to test isotopic value reproduction of NIST-SRM1486 and NIST-SRM1400. This was to ensure the Ca was properly separated and produced accurate $\delta^{44/42}$Ca values without any fractionation. The NIST-SRM1486 and NIST-SRM1400 reference material analysed had to have similar $\delta^{44/42}$Ca values as those stated in literature (Tacail *et al.*, 2015; Hassler *et al.*, 2018). Calibration 6 followed the separation procedures outlined in Table 3.6 and 3.7 above.

3.3.3.3.7. Calibration 7

This calibration was done to set up the Fe separation procedure in the WIGL using the reference material NIST-SRM1486. The acid for the three columns were collected in increments and tested the following procedures:

Column 1: The eluted acid was collected in increments to separate Ca-Fe-Sr and matrix using the resin AG50-X12 and the procedure outlined in Table 3.6.

Column 2: This column was to test the Fe separation method mentioned in Table 3.8 below. The procedure in Table 3.6 was carried out to remove the matrix and collect the Ca-Fe-Sr aliquot. This aliquot was then put to dry down at 90 °C. Once the sample was dried down, 200 µL of 6 N HCl was added to the sample. This was ready for the Fe separation (Table 3.8 below) the AG1-X8 resin.

Column 3: This column was to test the separation of Ca and Sr ions using the amended procedure mentioned in Table 3.7. First the Ca-Sr ions were separated from the matrix using the procedure in Table 3.6. Once the Ca-Sr ions were separated, the sample was put to dry down at 90 °C. Once the sample was dried, a drop of 14 N HNO_3 was added to cover the sample. The sample was then placed on the hotplate to dry down at 90 °C. 300 µL of 3 N HNO_3 was added to the sample to load onto the column for the next step. This was to ensure the effective separation of Ca and Sr using Sr Specific resin following the method mentioned in Table 3.7.

Table 3.8: Ion-exchange chromatography method for Fe removal from Ca-Sr used in calibration 7.

Fe removal	**Acid**	**Volume (mL)**
AG1-X8 resin (100-200 mesh) ~ 2mL		
Condition	6 N HCl	5 mL
Load	6 N HCl	4.5 mL
Elution (matrix)	0.5 N HCl	5 mL
Remaining on resin: Fe (Zn, Cu)		

3.3.3.3.8. Calibration 8

This calibration was a yield test to ensure all the Ca ions were being recovered after going through the various separation procedures: 1) Ca-Sr-Fe matrix separation; 2) Fe removal and 3) Ca-Sr separation. A yield test was done to test the Ca recovery after all three ion-exchange chromatography stages, as sample loss can occur during the different stages of chemistry. This yield test was done using the reference material NIST-SRM1486. To calculate this, the following equation was used: (Ca concentration after chemistry ÷ Ca concentration before chemistry) × 100. This calibration ran the methods mentioned in Table 3.6, Table 3.8 and Table 3.7, consecutively.

3.4. Results

3.4.1. Microdrilling

Producing the requisite enamel powder produced exceptionally small spots on the surface of the enamel/bone, on the order of ~500 µm in diameter (Fig. 3.6). Under normal lighting conditions, these marks can barely be seen. Magnified images (Magnification 0.67x) of fossil bone and teeth as shown in Fig. 3.7 and 3.8 illustrate the minimal damage that was created during the sampling process. The microdrilling techniques were successfully tested in the ultra-clean WIGL.



Figure 3.6: Tungsten Dremel drill bit with the ~400 µg sampled bone fragment powder. This is sufficient for Ca isotope analysis.

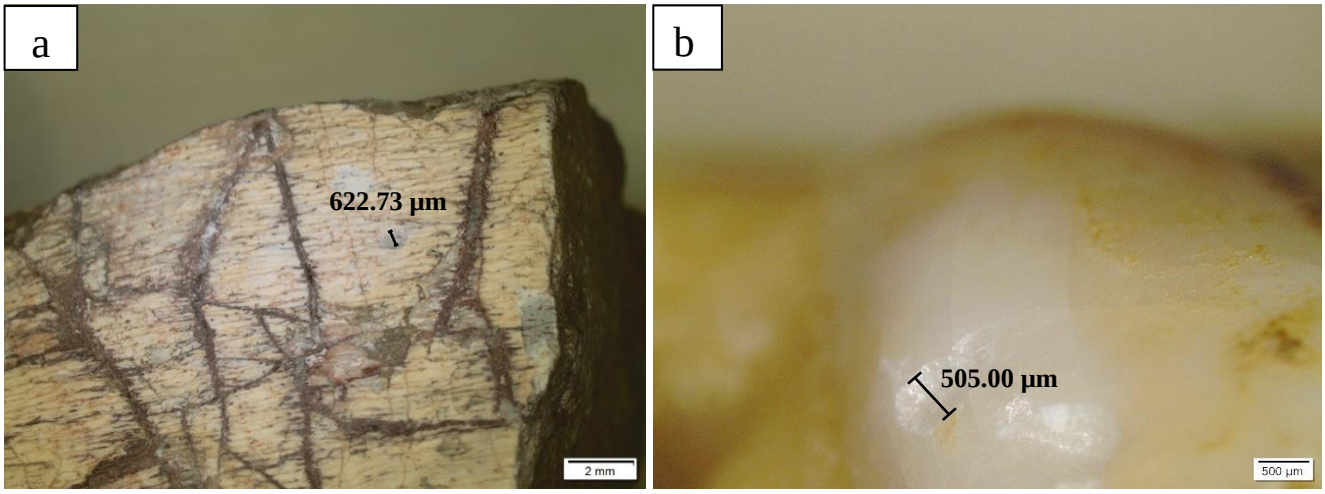


Figure 3.7: Images of specimens drilled for Ca isotope analysis using the handheld Dremel microdrill with a tungsten drill bit. Magnification of x0.67 used **(a)** An example of a drilled proxy of a fossil bone fragment. **(b)** An example of a drilled baboon tooth.

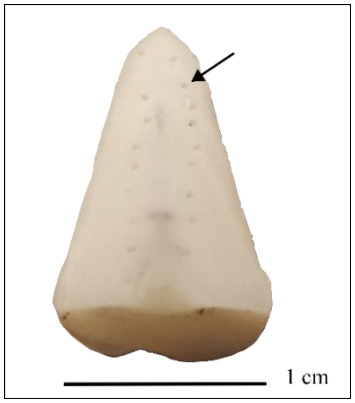


Figure 3.8: An adult female *Crocodylus niloticus* tooth, sampled using the micro-drill to perform calcium ion-exchange chromatography at ENS, Lyon. The black arrow (sample spot 8b) indicates a sample spot ~500 µm in diameter.

3.4.2. Calibrations

3.4.2.1. Calibration 1

Column 1 took approximately 10 hours to run the first separation for the ion-exchange chromatography whereas the Column 2 took approximately 3 hours in total. The elution curves for both columns are similar as shown below in Fig. 3.9 and 3.10. Column 2, the standard Bio-Rad Poly-Prep® column, did not fully elute all the Ca compared to Column 1 as the Ca concentration is still relatively high during the wash phase (Fig. 3.10).

Column 1 eluted Mg after 2 mL of 1 N HCl was added (Fig. 3.9) whereas column 2 eluted Mg after 1 mL of 1 N HCl (Fig. 3.10). Mg is removed by 19.5 mL for column 1 but continues to be eluted from the column till 21 mL for column 2. For column 1, the Ca is eluted between 19.5 mL to 22 mL (Fig. 3.9) whereas the Ca is eluted from 19.5 mL to 22.5 mL for column 2 (Fig. 3.10). The Ca is present in the wash phase of 6 N HCl for column 2 (Fig. 3.10).

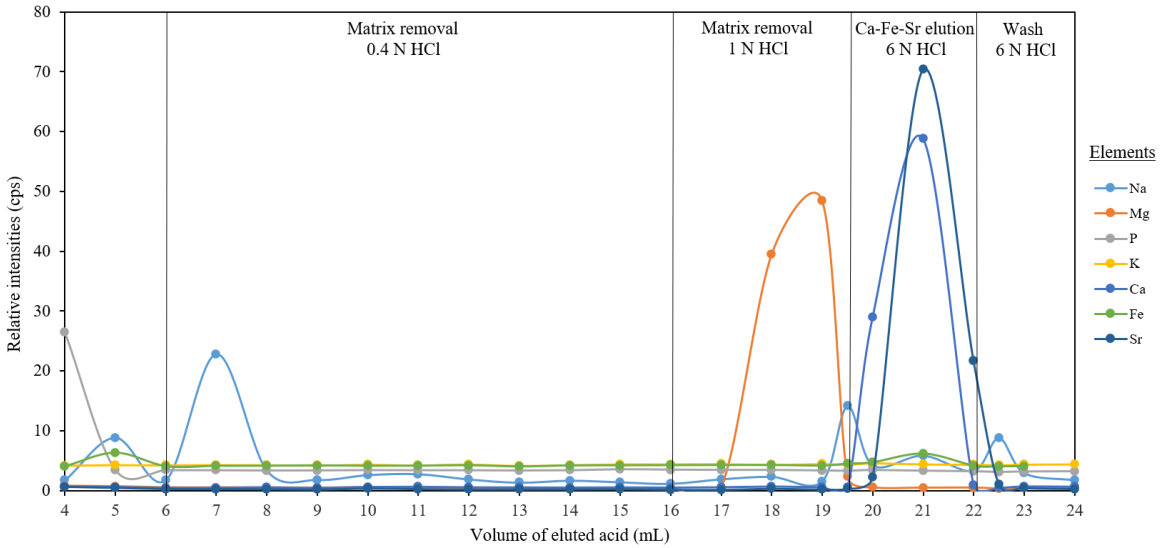


Figure 3.9: Column 1 of calibration 1 for the WIGL Ca-Fe-Sr matrix separation from the juvenile crocodile tooth. The matrix was eluted using the 0.4 M and 1 N HCl. The Ca-Fe-Sr aliquot is eluted and collected when the 6 N HCl was introduced to the column. The wash was collected at the 22 mL mark.

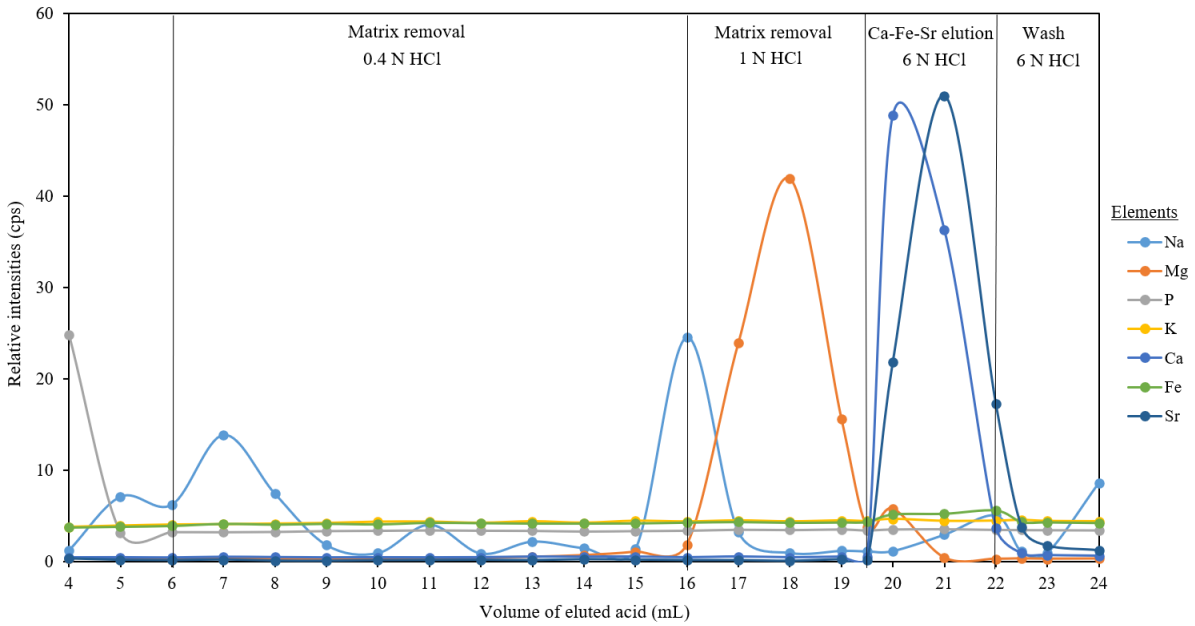


Figure 3.10: Column calibration 1 for the WIGL Ca-Fe-Sr matrix separation from the juvenile crocodile tooth using a Bio-Rad Poly-Prep® column. The matrix was eluted using the 0.4 M and 1 N HCl. The Ca-Fe-Sr aliquot is eluted and collected when the 6 N HCl was introduced to the column. The wash was collected at the 22 mL mark.

3.4.2.2. Calibration 2

Column 1 yielded the same results as column 2 of calibration 1 with a relatively high Ca concentration present during the column wash phase as no amendments were made to the procedure (Fig. 3.11). An additional 1 mL of 1 N HCl and 6 N HCl was added to the Mg and Ca-Sr elution stages, respectively. This extended the Mg and Ca-Sr separation stages for column 2 resulting into the elution of Mg to be from 16 mL to 20 mL and Ca elution from 20 mL to 24 mL (Fig. 3.12). Unfortunately, the Mg, Ca and Sr ions are still being eluted after the desired elution stages as we see the Mg ions present at 20.5 mL and the Ca-Sr ions present at 24.5 mL of acid which is the wash phase. Column 3 separated the Ca and Sr ions as the Ca ions are low after 4.5 mL of acid, but the Sr ions continue to be eluted off the column after 10 mL (Fig. 3.13).

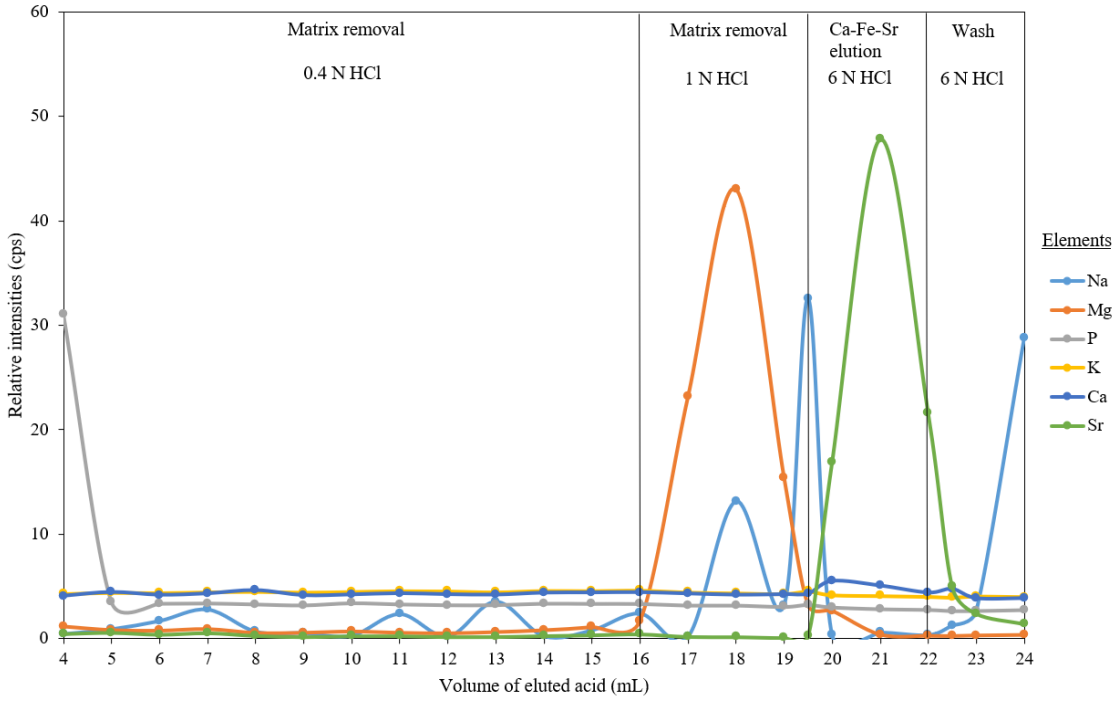


Figure 3.11: Column 1 of calibration 2 for the WIGL Ca-Fe-Sr matrix separation from the juvenile crocodile tooth using a Bio-Rad Poly-Prep® column. The matrix was eluted using the 0.4 M and 1 N HCl. The Ca-Fe-Sr aliquot is eluted and collected when the 6 N HCl was introduced to the column. The wash was collected at the 22 mL mark.

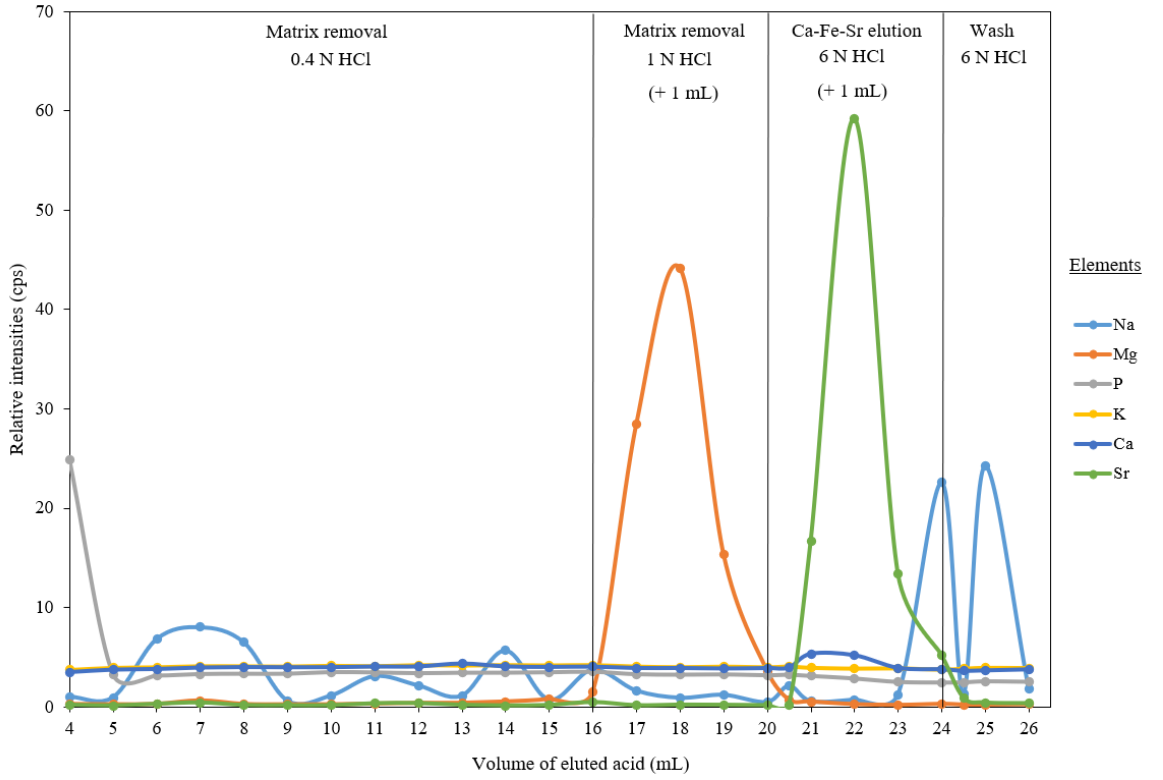


Figure 3.12: Column 2 of calibration 2 for the WIGL Ca-Fe-Sr matrix separation from the juvenile crocodile tooth using a Bio-Rad Poly-Prep® column. This chemistry included an additional 2 mL of acid. This was 1 mL to the Mg elution stage and 1 mL to the Ca elution stage. The matrix was eluted using the 0.4 M and 1 N HCl. The Ca-Fe-Sr aliquot is eluted and collected when the 6 N HCl was introduced to the column. The wash was collected at the 24 mL mark.

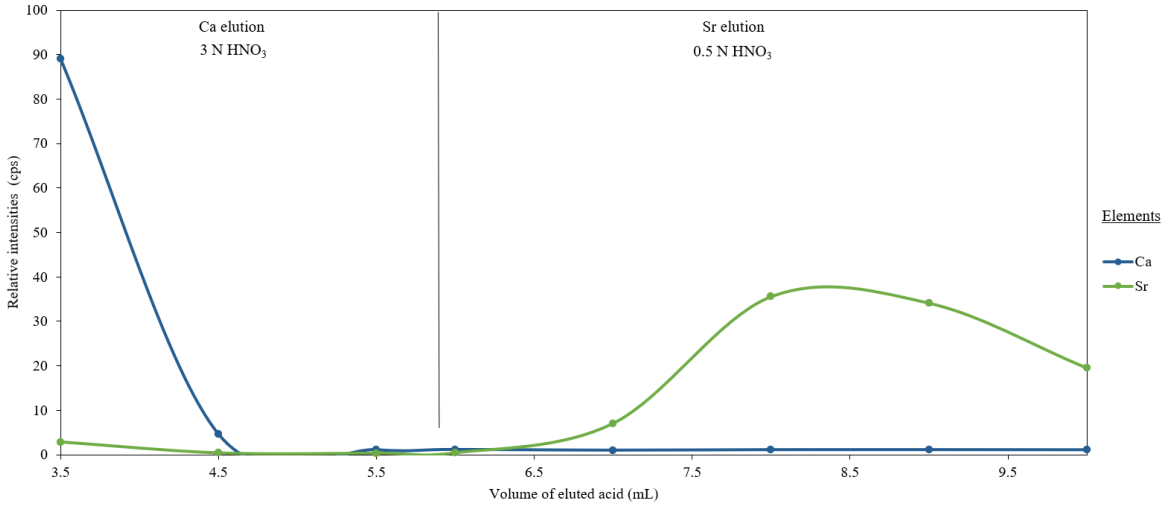


Figure 3.13: Column 3 of calibration 2 for the WIGL Ca-Sr separation from the juvenile crocodile tooth using a micro-column. The Ca was eluted using the 3 N HNO_3. The Sr aliquot was then eluted when the 0.5 N HNO_3 was introduced to the column at 6 mL.

3.4.2.3. Calibration 3

All the Ca ions are collected by 4.5 mL of acid but the Sr ions continue to be eluted off the column after 10 mL of 0.5 N HNO_3 as the relative intensity of Sr is still high at 10 mL of eluted acid (Fig. 3.14).

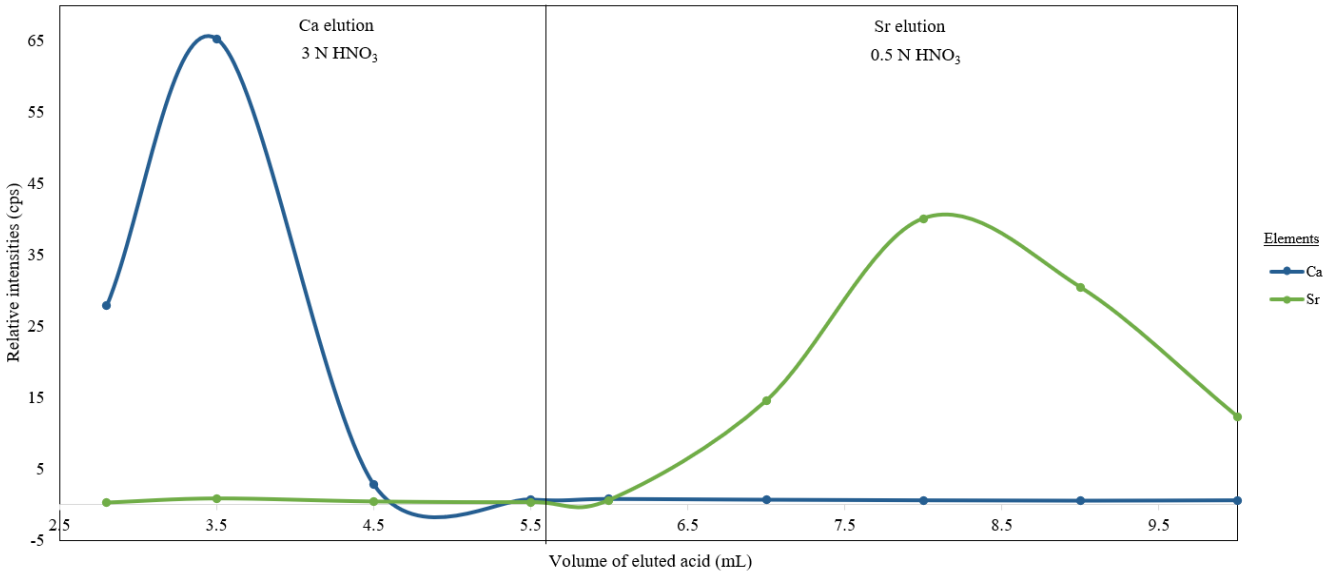


Figure 3.14: Column 3 of calibration 2 for the WIGL Ca-Sr separation from the juvenile crocodile tooth using a micro-column. The Ca was eluted using the 3 N HNO_3. The Sr aliquot was then eluted when the 0.5 N HNO_3 was introduced to the column.

3.4.2.4. Calibration 4

In this calibration, all the different ions are eluted during the desired stages as shown in Fig. 3.15 below. The Mg comes off the column during the 1 N HCl phase and the Ca is eluted off the column during the 6 N HCl. The Ca is not present during the 6 N HCl wash phase.

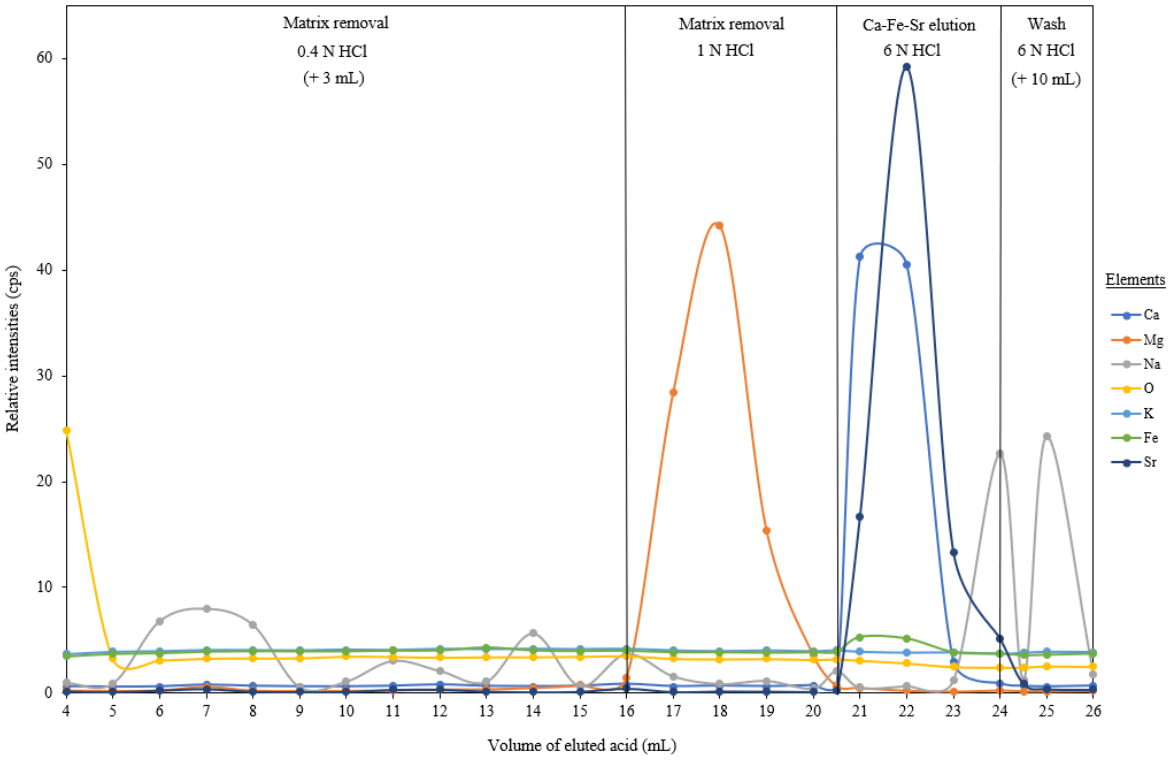


Figure 3.15: Column 2 of calibration 2 for the WIGL Ca-Fe-Sr matrix separation from the juvenile crocodile tooth using a Bio-Rad Poly-Prep® column. The matrix was eluted using the 0.4 M and 1 N HCl. The Ca-Fe-Sr aliquot is eluted and collected when the 6 N HCl was introduced to the column. The wash was collected at the 24 mL mark.

3.4.2.5. Calibration 5

The additional 10 mL of 0.5 N HNO_3 acid in calibration 5 allowed for all the Sr ions to be successfully eluted off the column as shown in Fig. 3.16. The Sr concentration approaches 0 cps at 21 mL. All the Ca is eluted at 5.5 mL.

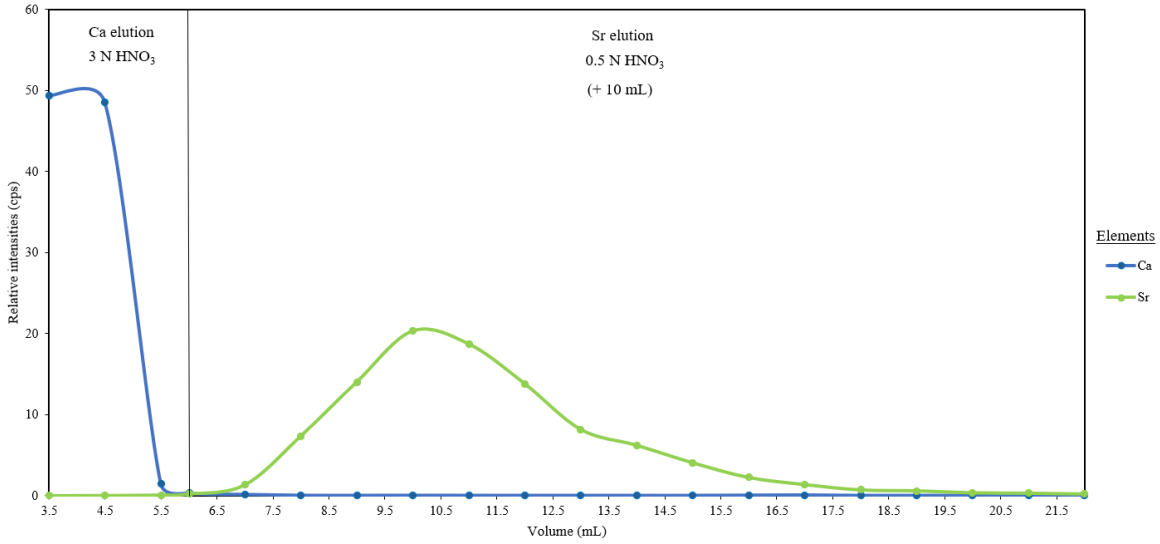


Figure 3.16: Calibration 5 for the WIGL Ca-Sr separation from the NIST-SRM1486 using a micro-column. The Ca was eluted using the 3 N HNO_3. The Sr aliquot was then eluted when the 0.5 N HNO_3 was introduced to the column.

3.4.2.6. Calibration 6

All the NIST-SRM1486 and NIST-SRM1400 reference materials analysed in this calibration are in-line with the literature values presented in Tacail *et al.* (2015) and Hassler *et al*. (2018) as shown below in Fig. 3.17. The $\delta^{44/42}$Ca values for the reference material samples processed in the WIGL fall within the accepted range of the literature values for the reference material (NIST-SRM1486 and NIST-SRM1400) compositions (Fig. 3.17). They all fall in the close range of the literature mean value or with the standard deviation of these values.

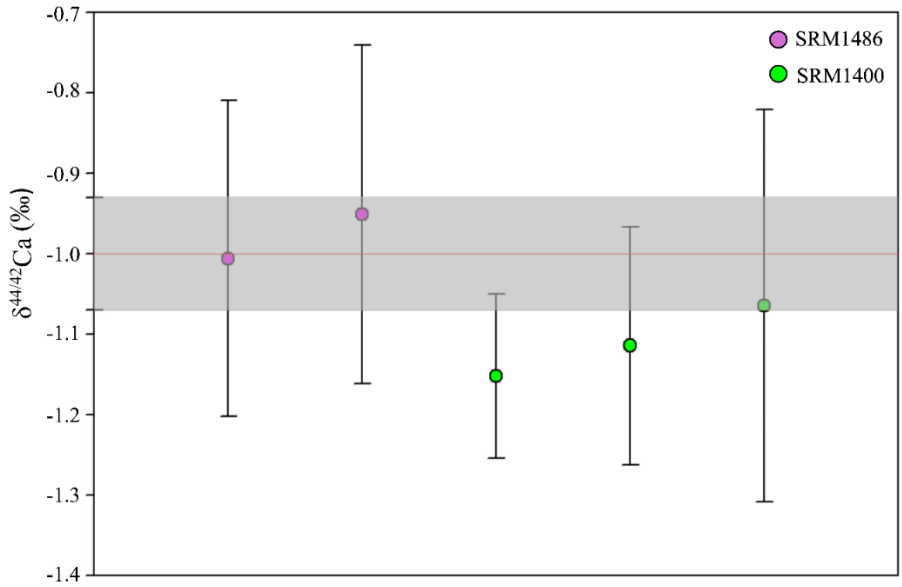


Figure 3.17: The WIGL reference materials, represented by the points, and their standard deviations represented by the black error bars. The red line represents the mean literature value (Tacail *et al.*, 2015; Hassler *et al.*, 2018) for the different standards and the grey band (range) is the standard errors for these means. The standard errors for the different mean literature values are: NIST-SRM1486 (-1.0 ± 0.07 ‰) and NIST-SRM1400 (-1.0 ± 1.00 ‰). The error range for SRM1400 is not shown as it spans from -2 to 0 per mil (Appendix D).

3.4.2.7. Calibration 7

Column 1 successfully eluted the matrix ions and the Ca-Sr-Fe (Fig. 3.18). The Ca ions are eluted from 17.5 mL to 21 mL of acid. This is the method which will be used for ion separation with the fossil samples. For Column 2, Fe removal procedure, the results do not show much of an Fe spike as there is a low concentration of Fe in the reference material NIST-SRM1486 (Fig. 3.19). The Fe intensity does not fluctuate throughout the procedure and shows a steady state. Column 3 for this calibration separated and eluted all the Ca and Sr ions off the column (Fig. 3.20).

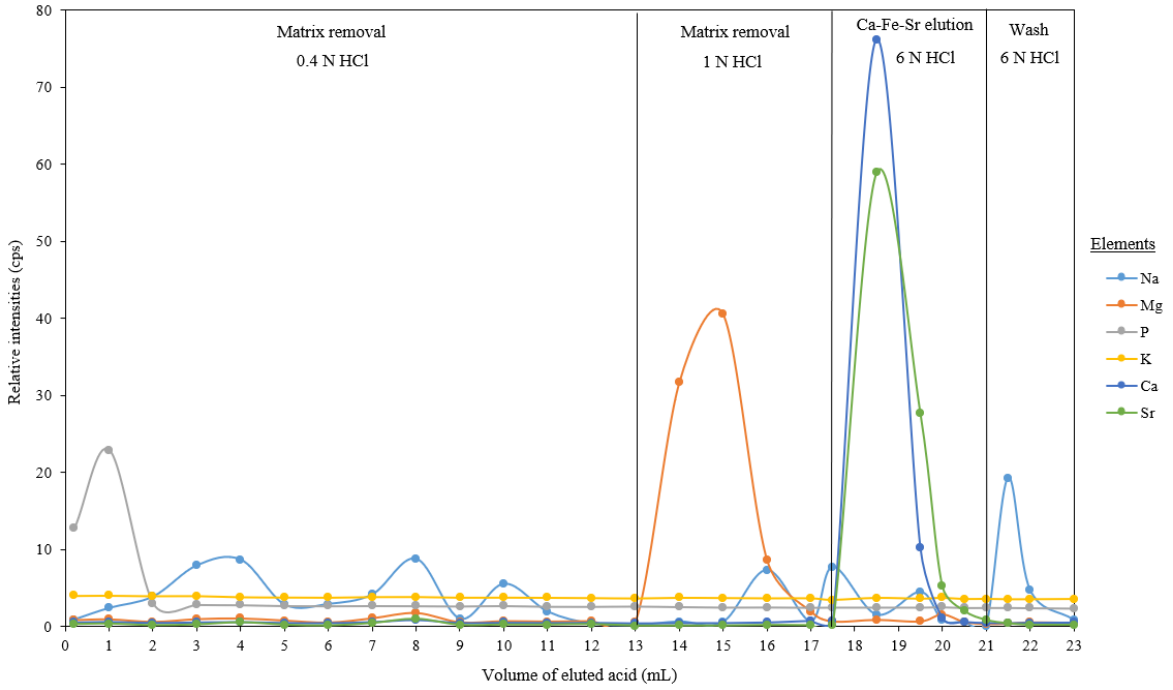


Figure 3.18: Column 1 of calibration 7 for the WIGL Ca-Fe-Sr matrix separation from the juvenile crocodile tooth using a Bio-Rad Poly-Prep® column. This chemistry included an addition of 2 mL of acid. The matrix was eluted using the 0.4 M and 1 N HCl. The Ca-Fe-Sr aliquot is eluted and collected when the 6 N HCl was introduced to the column.

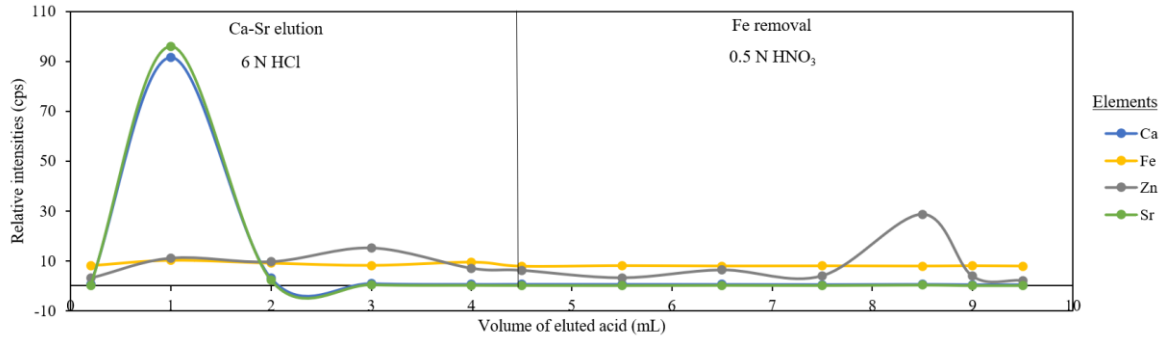


Figure 3.19*:* Column 2 of calibration 7 for the WIGL Fe removal from the Ca-Sr from the NIST-SRM1486 using a Bio-Rad Poly-Prep® column.

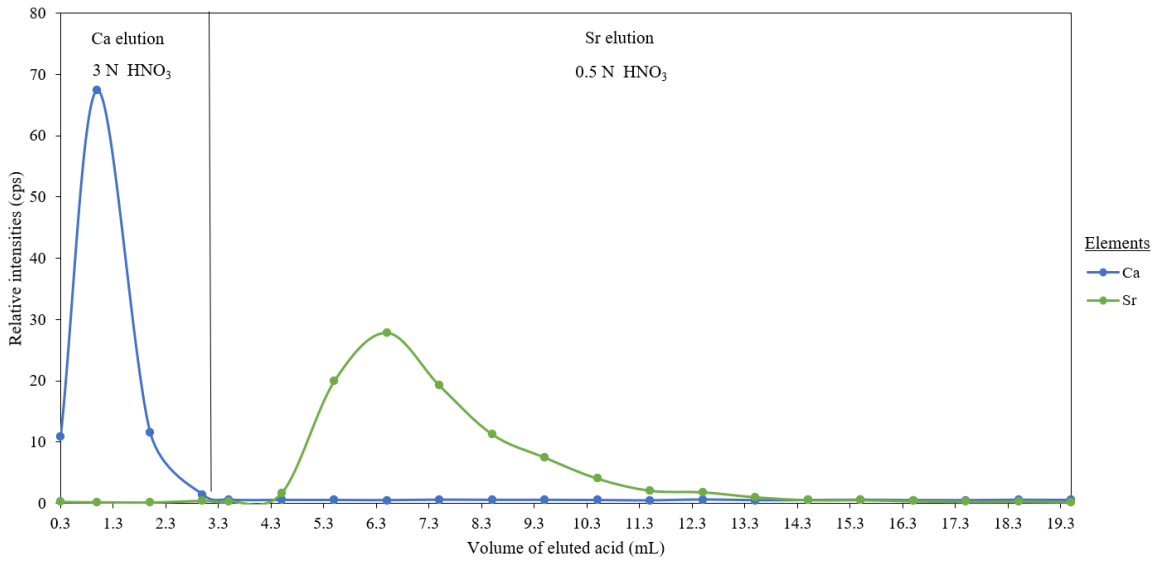


Figure 3.20: Column 3 of calibration 7 for the WIGL Ca-Sr separation from the NIST-SRM1486 using a micro-column. The Ca was eluted using the 3 N HNO_3. The Sr aliquot was then eluted when the 0.5 N HNO_3 was introduced to the column.

3.4.2.8. Calibration 8

The percentage recovery of Ca ions is relatively high after the three stages of ion-exchange chromatography across all ions as shown in Table 3.9 below. Additional ppm values can be found in the Appendix E. This indicates a good recovery of Ca, and the different procedures can be used to analyse the fossil samples.

Table 3.9: Table showing percentage recovery (%) comparing before chemistry sample and after chemistry sample (Appendix E). KED represents kinetic energy discrimination and STD represents standard values.

	^{44}Ca ppm (KED)	^{44}Ca ppm (STD)	^{48}Ca ppm (STD)	^{88}Sr ppm (KED)
Ca after chemistry sample (Y2.1C)	18750.32	123266.82	9060.15	0.31
Ca before chemistry sample (Y2.2)	22362.55	145983.85	9296.43	231.22
Percentage recovery	**83.85**	**84.44**	**97.46**	**0.13**

3.5. General Discussion

In calibration 1, the two columns with different dimensions (Fig. 3.5) produced similar calibration curves but had a large time difference to carry out the separation procedure. The Bio-Rad Poly-Prep® column produced similar separation results to column 1 of calibration 1, but it was much quicker to carry out the matrix separation stage as the Bio-Rad Poly-Prep® column is slightly broader in diameter and allows for more surface area of the resin to be exposed and easier flow of the acid.

When performing column chemistry during ion-exchange chromatography, different acids and acid concentrations elute the different ions from the column. In calibration 2 column 2, there are still Ca ions that are being eluted past the Ca collection step (Fig. 3.12). To avoid this and ensure all the ions are eluted at the desired time, additional amounts of acid was added to increase the elution and collection steps of the calibration. This is to avoid collecting ions that are still being eluted off the column and mixing with the desired Ca aliquot.

Calibration 2 is an example of a calibration that required amendments to ensure that the correct ions are being eluted, discarded or collected at the right time. In calibration 2, the stage 1 chemistry which is done to remove matrix and to collect the Ca-Sr aliquot had to be amended. The addition of the 1 mL of 1 N HCl and 1 mL of 6 N HCl acids extended the elution time for the different ions. Fig. 3.15 shows that the relative intensities were lower for Mg and Ca at the end of the desired elution step which means that most of those ions were eluted and collected from the column.

For the Fe stage, no amendments were made as the low concentration of Fe ions did not have a peak or spike in the elution curve (Fig. 3.19). Stage 3 using Sr spec resin needed adjustments as the Ca was continuing to come off with the Sr leading to contamination (Fig. 3.13). The Ca-Sr separation stage was further extended to ensure that all the Sr was also being eluted off the column.

The reference material, NIST-SRM1486 and NIST-SRM1400, analysed reproduced the $\delta^{44/42}$Ca values that are within the limits of international reference literature values (Fig. 3.17). Successful method setup and calibrations are quantified by comparing Ca isotopic values produced in the WIGL with accepted values for international reference standards. This shows that the results are not affected by fractionation and there is no other external influence that could obscure or influence the results.

The high recovery yield of Ca ions collected after going through three stages of ion-exchange chromatography shows that most of the Ca ions are being recovered and there is minimal amount of sample lost throughout the different chemistry stages (Table 3.9)

When comparing the method by Tacail *et al.* (2014) and the column chemistry of this chapter, it produces similar results, but the technique used here is more time efficient. The disadvantage to the method developed here is that the method uses slightly more acid than that of Tacail *et al.* (2014), but it cuts the duration of the method down by 6 hours allowing for a higher throughput.

3.6. Conclusion

Following multiple column calibrations, the Ca ion-exchange chromatography method has been successfully set up in the WIGL. All three stages of the chemistry can be carried out to ensure clean, reliable, and efficient separation and collection of Ca ions. The column chemistry of stage 1 has been adjusted to a third of the time taken for the original method developed in Tacail *et al.* (2014) by using the Bio-Rad Poly-Prep® columns and increasing the amounts of acid in the matrix separation and Ca-Fe-Sr concentration steps while still performing effective ion separation. The scientific standards and samples analysed during this process show that a clean and efficient chemistry for the separation of ions were achieved. This time-efficient method will allow for more analyses to be conducted.

4. Best practices for Ca isotope analysis on palaeontological samples

4.1. Abstract

Good sample practices are imperative for producing high-quality and accurate data. This is especially true when working with small sample quantities, such as the minimally invasive 400 µg used for $\delta^{44/42}$Ca isotope analysis when sampling fossil specimens. These ancient remains may have been exposed to different processes during fossilisation (e.g., hydrothermal fluid alteration) which can diagenetically alter preserved tissue resulting in misleading data. This chapter focuses on the best practices for conducting such analyses, including the analytical conditions, and leaching procedure required to produce high-quality and accurate $\delta^{44/42}$Ca data. The selected samples in this research include the oldest terrestrial specimens yet analysed for $\delta^{44/42}$Ca isotopes.

To ensure that the $\delta^{44/42}$Ca data produced are not obscured by diagenetic biases, a leaching methodology was tested prior to sample digestion. Here we show that leaching has a consistent effect on a range of fossil samples.

We also identified the fractionation of the Ca samples after the ion-exchange chromatography was performed and before MC-ICPMS analysis. The $\delta^{44/42}$Ca values of the selected samples appeared to drift towards more positive values when left in the loading acid, 0.05 N HNO_3, for MC-ICPMS analysis. It is important lab practice that samples are analysed as soon as they are prepared in the 0.05N HNO_3 to avoid fractionation resulting in inaccurate $\delta^{44/42}$Ca values. These results highlight the importance of good analytical practices to ensure that the most accurate and high-quality data is produced.

4.2. Introduction

Non-traditional $\delta^{44/42}$Ca isotopes are being utilised in a variety of studies to understand dietary preference (Martin *et al.*, 2022). While $\delta^{44/42}$Ca isotopes can provide an insight into dietary preferences and trophic positioning in ancient ecosystems, incorrect lab practices could produce inaccurate $\delta^{44/42}$Ca values and thus be positively misleading for trophic positioning of extinct animals. It is imperative that the correct lab practices and procedures are carried out to produce high-quality data as bone and tooth material are exposed to a variety of external environmental factors, e.g., groundwater flow during fossilisation. Exogenous ions may be carried through the hard tissue matrix, and be deposited either on the surface, in the interior cavities such as pore spaces, or by direct replacement of elements in the crystalline lattice (Heuser *et al.*, 2011). These

factors can alter the native concentration of elements in bone and tooth material with respect to their immediate post-mortem values. Fossilised bone material is more likely to be affected by diagenesis compared to fossil tooth enamel because it is highly porous (Martin *et al.,* 2017). The former's high porosity allows for precipitation of secondary minerals whereas the crystalline structure of tooth enamel is less likely to be diagenetically altered (Bocherens *et al.,* 1994). Precipitation of secondary calcite ($CaCO_3$) can influence the Ca isotopes as the calcite favours the heavy Ca isotope (^{44}Ca) and will obscure the resulting $\delta^{44/42}Ca$ ratios (Martin *et al.,* 2017; Martin *et al.,* 2022). Due to the densely packed solid crystalline structure of the hydroxyapatite in enamel, Ca is not as easily diagenetically altered in tooth enamel, when compared to dentine and bones in the body (Martin *et al.,* 2017). However, fossil tooth enamel can still be affected by diagenetic alteration and the reflected $\delta^{44/42}Ca$ values will be influenced by exogenous secondary calcite. $\delta^{44/42}Ca$ values can also be influenced by sample fractionation after the separation of Ca ions using ion-exchange chromatography. It is important to ensure that the Ca aliquots are measured without any fractionation and changes occurring to the sample after separation to avoid the incorrect or false $\delta^{44/42}Ca$ values being obtained.

While Ca isotopes are useful in modern and relatively younger palaeontological samples (Martin *et al.,* 2018; Martin *et al.,* 2022), a major outstanding question is whether the $\delta^{44/42}Ca$ isotopic method can be applied to ancient ecosystems in much deeper time, as fossilised bone and tooth material are more susceptible to diagenetic processes. Therefore, it is critical to test for the influence of diagenetic signatures in the ancient fossil record. Here, we test the efficacy of leaching procedures to ensure that the most accurate $\delta^{44/42}Ca$ data is obtained and is as close to true to post-mortem $\delta^{44/42}Ca$ values as possible. Sampled fossil tooth enamel powders (Table 4.1) was leached to minimise the effect of secondary calcite on the Ca isotope values, controlling for any diagenetic biases that could affect the $\delta^{44/42}Ca$ values. This chapter will also highlight the importance of analysing samples as soon as they are prepared for MC-ICPMS to avoid fractionation and inaccurate $\delta^{44/42}Ca$ determination.

4.3. Methods

Different samples were used to test sample leaching and the effect of maturation on Ca-fractionation as this limited the amount of sample powder required, minimising the sample spot on the fossil specimens.

4.3.1. Sample leaching

The leaching method used in this study was modified based on the method by Balter *et al.* (2002) to remove any diagenetic effects. Table 4.1 shows the unleached and leached samples used to test the effects of leaching. These specimens were chosen due to the difference in diet as there was the presumed herbivorous sauropodomorphs and the presumed carnivorous 'rauisuchians'. Two sauropodomorphs, *Massospondylus* and *Aardonyx*, were selected as these are co-occurring herbivorous sauropodomorphs subject to similar diets and the same environment. The standard reference material NIST-SRM1486 was also leached as a control.

Table 4.1: Fossil tooth samples analysed in this study represent ESI fossil tooth enamel. This is to test the effect of sample leaching using leached vs unleached samples.

Specimen no.	Sample no. (unleached)	Sample no. (leached)	Genus
BP/1/4930	Ca5.1	A1.1	*Massospondylus*
BP/1/4958	Ca2.3	A1.2	*Massospondylus* (juvenile)
BP/1/5231	Ca4.3	A1.3	*Massospondylus* (juvenile)
BP/1/6679	Ca1.1	A1.5	*Aardonyx*
BP/1/6677	Ca1.2	A1.6	*Aardonyx*
BP/1/6654	Ca2.1	A1.7	*Aardonyx*
BP/1/6016	Ca4.4	A2.1	'Rauisuchian'
BP/1/5163A	Ca3.2	A2.2	'Rauisuchian'
BP/1/5163C	Ca3.4	A2.3	'Rauisuchian'
SRM1486	A3.8	A1.8	-

The microdrilled sample powders, prepared in accordance with protocols outlined in Chapter 3, were transferred into 2 mL polypropylene (PP) microcentrifuge tubes and 500 µl of ultrapure acetic acid (0.1 N) was added to each sample. The microcentrifuge tubes were capped and manually shaken for 10 seconds to allow interaction between the sample powder and acetic acid. The centrifuge tubes were left for 25 minutes for the powder to settle and the acetic acid to dissolve any secondary calcite. The tubes were put into a microcentrifuge for 30 seconds with a power of 14.5 and 2000 revolutions per minute (rpm). The top liquid phase was then extracted using a clean pipette tip and discarded.

1 mL of ultrapure water (Milli-Q) was added to the sample in the tube and the tube was capped and manually shaken for 10 seconds. The samples were then centrifuged for 30 seconds (at 14.5 power

and 2000 rpm). The top liquid was extracted and discarded. This process was repeated again twice more to remove any secondary calcite and acetic acid.

The samples were transferred to a Perfluoroalkoxy (PFA) Savillex 7 mL beakers by rinsing the microcentrifuge tubes with 1.5 mL Milli-Q followed by a rinse with 0.5 mL concentrated nitric acid (HNO_3). 1.5 mL Milli-Q water was added again for the final rinse to transfer any sample remnants. The leached samples, mentioned in Table 4.1, were left to dry down at 90°C on a hotplate.

4.3.2. Effect of maturation on Ca-fractionation

The effect of maturation on Ca-fractionation is a different test to assess the length of time samples can sit in solution before being tested. It is important to consider as it can be a measure of isotope drift. The Karoo fossil specimens were microdrilled, digested and had undergone the three different stages of ion-exchange chromatography as explained in Chapter 3, Tables 3.6, 3.8 and 3.7 in the WIGL. The following samples were used in this study: Ca1.6, Ca3.3, Ca3.5, Ca4.4 and Ca4.6 (Table 4.2). Following the last step in Table 3.7, the samples were placed on a hotplate at 90 °C to dry down. Once the samples were dry, a drop of concentrated (14 M) HNO_3 was added to each beaker to cover the sample. The samples were then left to dry down on the hotplate at 90 °C. After the samples dried, the beakers were capped, sealed and carefully packaged to be transported to the ENS in Lyon, France.

Table 4.2: Fossil tooth samples analysed in this study. These samples were used to test the effect of maturation on Ca-fractionation.

Sample number	Specimen number	Taxa
Ca1.6	BP/1/6608	Theropod
Ca3.3	BP/1/5163B	‘Rauisuchian’
Ca3.5	BP/1/5163D	‘Rauisuchian’
Ca4.4	BP/1/6016	‘Rauisuchian’
Ca4.6	BP/1/8235	‘Rauisuchian’

The samples mentioned in Table 4.2 were carefully opened in the clean lab at the ENS and a small amount of concentrated (15 N) HNO_3 acid was added to each beaker to cover the sample spot. The sample beakers were capped and placed on the hotplate at 120 °C to 130 °C for an hour. The beakers were uncapped, and the samples were left to dry at 80 °C. Once the samples were dry, they

were then prepared for mass spectrometry on the ThermoScientific Neptune Plus MC-ICPMS MC-ICPMS analyses by adding a calculated amount of 0.05 N HNO_3 to dilute the samples to a desired concentration. The samples were diluted in 2 mL of 0.05 M HNO_3 acid and then diluted again with the 0.05 M HNO_3 to get a concentration on 1.25 mg/L.

The configuration and setup of the MC-ICPMS followed the protocol explained in Tacail *et al.* (2014). The variable multicollector detector array consisted of nine Faraday collectors, eight mobile collectors and one stable central detector, to collect ions of interest and were arranged to collect the following: $^{42}Ca^{+}$, $^{42.5}Ca^{+}$, $^{43}Ca^{+}$, $^{43.5}Ca^{+}$, $^{44}Ca^{+}$, $^{84}Sr^{2+}$, $^{86}Sr^{2+}$ $^{88}Sr^{2+}$ and $^{40}Ar^{1}H_2^{+}$. Argon and Sr were analysed to control and correct for possible interferences. After sample dilution, the samples (Table 4.2) were loaded into the instrument and introduced as a dry plasma using a Cetac Aridus II. Nitrogen was injected into the chamber with an Argon mixture to stabilise the Argon aerosol carrying sample (Chapter 3, Fig. 3.1) (Martin *et al.*, 2017). The in-house reference standard, ICP Ca Lyon, which is a Specpure Ca plasma standard solution (Alfa Aesar) purified of strontium traces, was used for standard-sample bracketing. Sample bracketing is performed before and after each sample measurement and is used to detect and correct for any instrumental biases and/or drift (Tacail *et al.*, 2014).

To test for fractionation, the batch of samples (Table 4.2) were analysed twice on day one with a 6-hour time difference and again after 48 hours (day 3). The samples followed identical MC-ICPMS analytical methodology to ensure comparability.

4.4. Results

4.4.1. Sample leaching

The reported NIST-SRM1486 reference material analysed in this study produced an average $\delta^{44/42}$Ca value of -0.96 ± 0.05 ‰ (2 s.e., n = 7) with an offset of approximately 0.05 ‰ compared to the mean literature value of 0.1 ± 0.07 ‰ (Fig. 4.1). The one leached reference material (plotted in red on Fig. 4.1) is very close to the literature mean value. The unleached mean $\delta^{44/42}$Ca values for the different taxa are as follows: *Massospondylus* (-0.23 ± 0.03 ‰ (2 s.e., n = 3)), *Aardonyx* (-0.31 ± 0.02 ‰ (2 s.e., n = 3)) and 'rauisuchian' (-0.52 ± 0.07 ‰ (2 s.e., n = 3)) (Table 4.3). Whereas the leached mean $\delta^{44/42}$Ca values are: *Massospondylus* (-0.47 ± 0.06 ‰ (2 s.e., n = 3)), *Aardonyx* (-0.62 ± 0.05 ‰ (2 s.e., n = 3)) and 'rauisuchian' (-0.72 ± 0.09 ‰ (2 s.e., n = 3)) (Table 4.3) (Fig. 4.2b).

Table 4.3: Summary of the mean, lowest and highest $\delta^{44/42}$Ca values for unleached vs leached Elliot Formation samples (listed in Table 4.1 herein) (Appendix G).

Taxa	Genus	Unleached		Leached		Presumed diet
Sauropodomorph		$\delta^{44/42}$Ca (‰)	2 s.e. (‰)	$\delta^{44/42}$Ca (‰)	2 s.e. (‰)	Herbivore
	Massospondylus (n = 3)					
	Mean	-0.2270	0.0314	-0.4652	0.0550	
	Lowest	-0.3074	0.0279	-0.5809	0.0855	
	Quartile 1 (25 percentile)		-	-0.5197	-	
	Quartile 3 (75 percentile)		-	-0.4073	-	
	Highest	-0.1289	0.0358	-0.3561	0.0539	
	Aardonyx (n = 3)					
	Mean	-0.3141	0.0172	-0.6219	0.0480	
	Lowest	-0.3490	0.0404	-0.6587	0.0350	
	Quartile 1 (25 percentile)	-0.3456	-	-0.6375	-	
	Quartile 3 (75 percentile)	-0.2966	-	-0.6034	-	
	Highest	-0.2509	0.0088	-0.5906	0.0512	
Crurotarsan	'Rauisuchian' (n = 3)					Carnivore
	Mean	-0.5161	0.0665	-0.7174	0.0932	
	Lowest	-0.8590	0.0114	-0.9861	0.0645	
	Quartile 1 (25 percentile)	-0.6787	-	-0.8526	-	
	Quartile 3 (75 percentile)	-0.3447	-	-0.5830	-	
	Highest	-0.1909	0.0825	-0.4471	0.0977	

The approximate $\delta^{44/42}$Ca mean shift of -0.25 ± 0.04 ‰ (2 s.e.) relative to the unleached samples is observed among samples with a broad range of $\delta^{44/42}$Ca values, presumed diets, body sizes, and stratigraphic positions (Fig 4.2a). The unleached samples are consistently enriched in heavier $\delta^{44/42}$Ca values.

The box plots representing the leached $\delta^{44/42}$Ca values for the *Aardonyx* and 'rauisuchian' show lower variance (Fig. 4.2a). The simple linear regression of the leached and unleached values using the standard major axis (SMA) (slope of 0.84 and a $R^2 = 0.9337$, *p*-value = 2.24×10^{-5}) with a y-axis intercept of -0.31 and ordinary least squares (OLS) (slope of 0.81 and $R^2 = 0.9337$, *p*-value = 2.24×10^{-5}) (Fig. 4.2b).

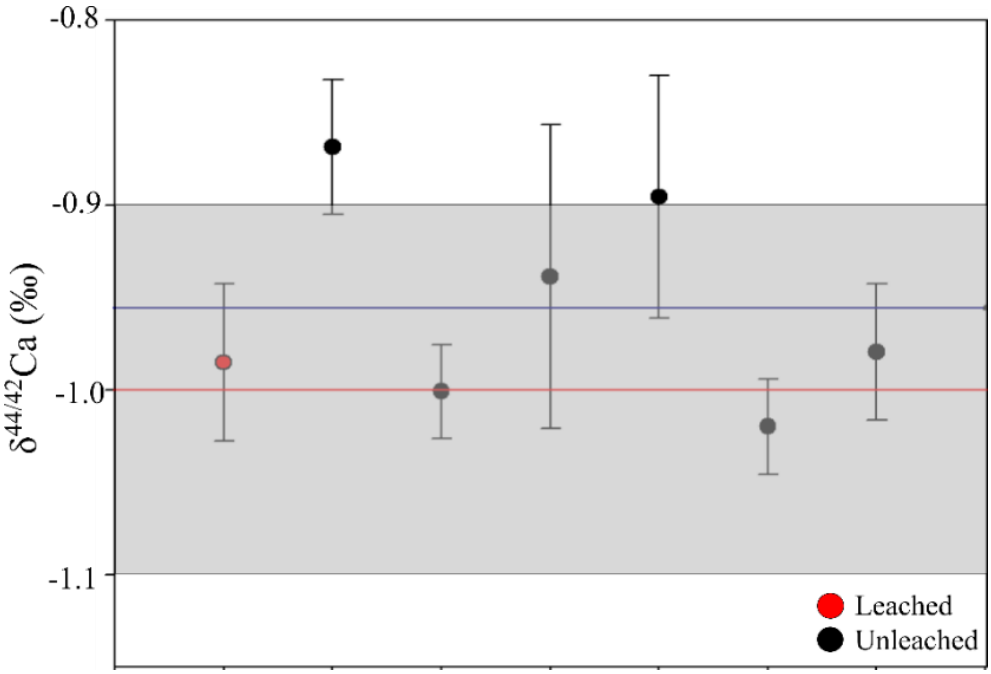


Figure 4.1: SRM1486 samples analysed in the WIGL. The WIGL standard sample that was leached (red) and unleached (black) samples are represented by the points, and their standard deviations represented by the error bars. The red line represents the mean unleached literature value for the standard, blue line represents the combined mean value for the unleached data analysed and the grey band (range) is the standard error for the mean. The standard error for the SRM1486 mean literature value is (0.1 ± 0.07 ‰).

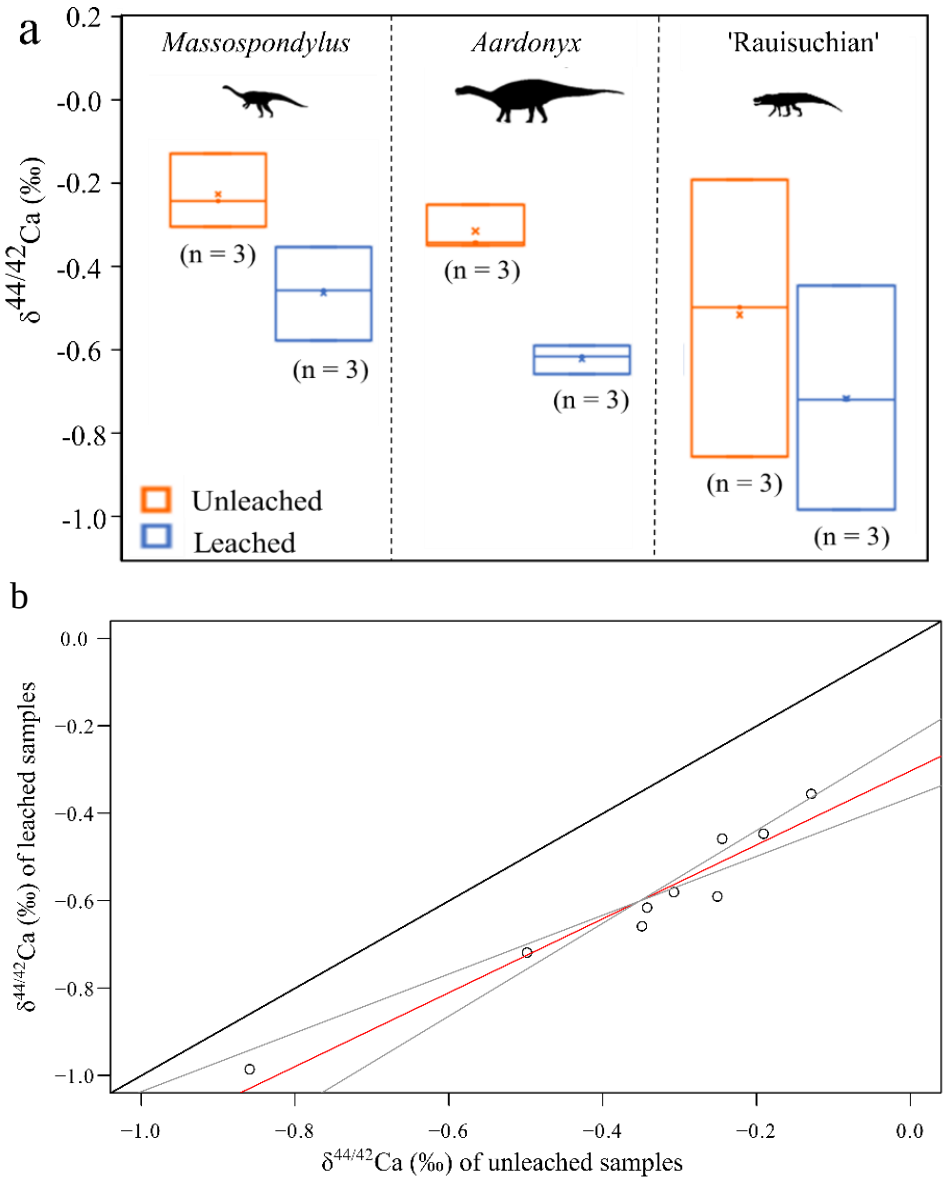


Figure 4.2: Elliot Formation tooth enamel samples analysed that were unleached or leached prior to ion-exchange chromatography. **(a)** A box plot showing the $\delta^{44/42}$Ca (‰) values of the *Massospondylus*, *Aardonyx and* 'rauisuchian' samples that were unleached and analysed (orange) and resampled, leached and analysed (blue). Three samples per taxa were analysed. Image source: prehistoric-wildlife.com;.Bordy *et al.* (2020) **(b)** An ordinary least squares (OLS) regression showing the relationship between the unleached (x-axis) vs leached (y-axis) $\delta^{44/42}$Ca (‰) values of each sample analysed. The OLS regression has a slope (red line) of 0.81 and $R^2 = 0.9337$. A slope of 1 is represented by the solid black line.

4.4.2. Effect of maturation on Ca-fractionation

The mean $\delta^{44/42}$Ca values for the different batches are as follows: Batch 1 of Day 1 (-0.43 ± 0.04 ‰ (2 s.e., n = 5)), Batch 2 of Day 1 (-0.38 ± 0.04 ‰ (2 s.e., n = 5)) and Batch 1 of Day 3 (-0.22 ± 0.03

‰ (2 s.e., n = 5)). The ranges for each of the batches are: Batch 1 of Day 1 (-0.62 ‰ to -0.26 ‰), Batch 2 of Day 1 (-0.52 ‰ to -0.19 ‰) and Batch 1 of Day 3 (-0.38 ‰ to -0.02 ‰). The samples run in Batch 1 on Day 1 have the lowest $\delta^{44/42}$Ca isotope values relative to the other batches (Fig. 4.3). Sample Ca3.3 is the only sample that has a slightly higher $\delta^{44/42}$Ca value of -0.44 ± 0.05 ‰ for Batch 1 Day 1 compared to the Batch 2 Day 2 $\delta^{44/42}$Ca value of -0.46 ± 0.05 ‰. Batch 2 of Day 1 has $\delta^{44/42}$Ca values that are slightly above Batch 1 Day 1 except for sample Ca3.3. All the Batch 1 Day 3 samples have the most $\delta^{44/42}$Ca-enriched values relative to the rest of the batches (Fig. 4.3).

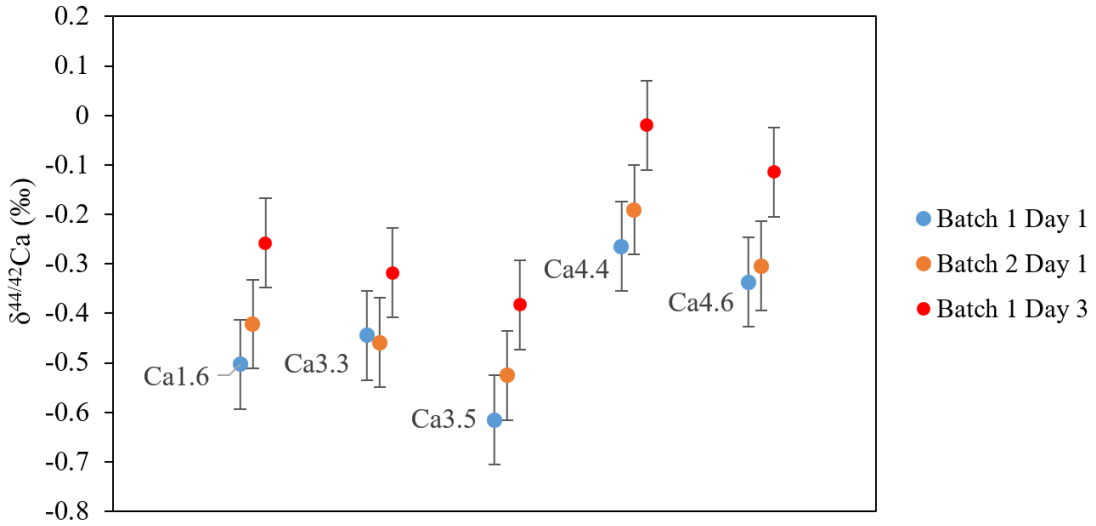


Figure 4.3: Effect of maturation on Ca-fractionation for samples Ca1.6, Ca3.3, Ca3.5, Ca4.4 and Ca4.6 were analysed on different days and represented by the different points. The colour of the points corresponds to the batch number. It should be noted that two batches were analysed on day 1 separated by 6 hours (see methods). The black lines represent the standard errors.

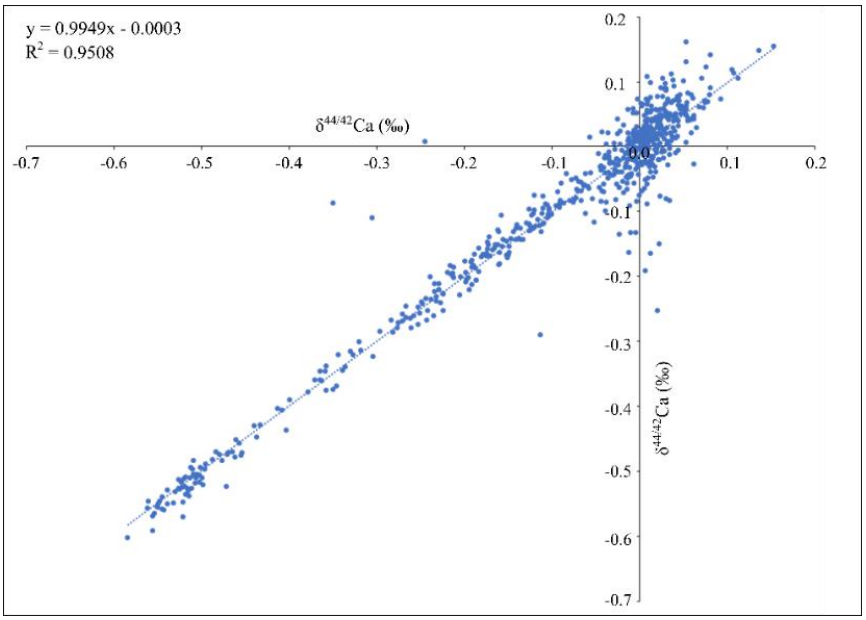


Figure 4.4: ICP Ca reference standard samples analysed for Ca isotope compositions. The ICP Ca samples are represented by the points (blue) with a trend line (blue) of 0.9949x – 0.0003.

4.5. Discussion

4.5.1. Sample leaching

The slight offset of approximately 0.05 ‰ on the reported NIST-SRM1486 standard $\delta^{44/42}$Ca values in this study relative to the mean literature value (Hassler *et al.,* 2018) indicates that the laboratory techniques followed are accurate and clean (Fig. 4.1). Any isotope variations cannot be attributed to the incorrect lab practices as the reference material $\delta^{44/42}$Ca values produced are repeatable and statistically within range to those stated in literature (Tacail *et al.,* 2015; Hassler *et al.,* 2018). Reference materials do not require leaching as they were unexposed to diagenetic influences and did not undergo fossilisation. The leached $\delta^{44/42}$Ca value for reference material plots among the other unleached values (Fig. 4.1) which is expected as these samples contain no exogenous Ca.

The unleached samples for all the examined taxa are consistently enriched in heavier $\delta^{44/42}$Ca values, which is consistent with the deposition of exogenous calcite that favours ^{44}Ca (Martin *et al.*, 2017). By leaching the samples during the sample preparation stage, the $\delta^{44/42}$Ca values of the leached samples are expected to be more $\delta^{44/42}$Ca-depleted as we are removing possible ^{44}Ca from exogenous calcite. There is an approximate $\delta^{44/42}$Ca mean shift of -0.25 ± 0.04 ‰ (2 s.e.) among samples with a broad range of $\delta^{44/42}$Ca values, presumed diets, body sizes, and stratigraphic positions (Fig 4.2a). *Massospondylus* and *Aardonyx* are presumed herbivores and our 'rauisuchian' sample consisted entirely of large carnivores (Yates *et al.*, 2010; Yates *et al.,* 2011; Tolchard *et al.,* 2019). All three of these taxa have varying body sizes as shown in the silhouettes in Fig. 4.2a. *Massospondylus* and *Aardonyx* are found in the upper Elliot Formation during the Early Jurassic epoch whereas 'rauisuchians' existed in the lower Elliot Formation during the Late Triassic (Knoll, 2004; Nesbitt *et al.*, 2013; McPhee *et al.*, 2017; Tolchard *et al.*, 2019; Bordy *et al.*, 2020). This suggests that the isotope shift observed is not influenced by the varying diets, body sizes or stratigraphic positions but likely a result of secondary processes such as diagenesis.

When comparing a simple linear regression of the leached and unleached values, the R^2 value of 0.9337 indicates that sample differences are statistically significant, and that the leached values are dependent on the unleached (Fig. 4.2b). Leached $\delta^{44/42}$Ca values for samples can be predicted using an equation from the regression model as leaching had an effect on almost all the fossil samples when comparing a simple linear regression of the leached and unleached values using OLS (Fig. 4.2b). Hereafter $\delta^{44/42}$Ca values discussed in this research have either been leached or corrected for diagenetic alteration using the regression equation: $y = 0.8171x \times -0.3135$ where x is represented by the unleached $\delta^{44/42}$Ca value.

These $\delta^{44/42}$Ca values are significantly different in all paired samples (Fig. 4.2) (Wilcoxon rank-sum test: *p*-value = 3.9×10^{-3}). The overall variance in $\delta^{44/42}$Ca values for *Aardonyx* and 'rauisuchian' is lower in the leached values indicating that leaching removes spurious variation caused by diagenetic alteration (Fig. 4.2a). This shows that biological processes are easier to analyse as the biological signal is stronger compared to the signal of diagenesis. The $\delta^{44/42}$Ca values shifted by different amounts as they experienced different amounts of diagenesis.

Obtaining and applying the leaching regression equation: $y = 0.8171x \times -0.3135$ to the unleached specimens allows direct comparison to values obtained from leached samples, effectively correcting for diagenetic biases (Appendix F). This would be useful for samples where there are small amounts of sample powder where there is a risk of sample loss if the sample has to be leached. There is a general shift observed when applying this equation and the corrected unleached samples remain in the relative position to the corrected unleached, but the $\delta^{44/42}$Ca values shift towards the negative (Appendix F).

The produced leached $\delta^{44/42}$Ca values are more in line with the dietary expectations for herbivores and carnivores as seen in Martin *et al.* (2018 and 2022). The herbivorous *Massospondylus* and *Aardonyx* are in the range of -0.66 ‰ to -0.36 ‰. This is in line with herbivorous extinct taxa analysed in Martin *et al.* (2022) and Hassler *et al.* (2018) as the $\delta^{44/42}$Ca values are for the herbivorous samples reported in the above-mentioned studies have a range in $\delta^{44/42}$Ca values from approximately -0.4 ‰. The carnivorous samples in Martin *et al.* (2022) and Hassler *et al.* (2018) have mean $\delta^{44/42}$Ca values of approximately -1.0 ‰. This is depleted relative to the carnivorous 'rauisuchians' in this study but it is also dependent on the food source. An offset of -0.3 ‰ for herbivorous to carnivorous diets is still observed in these specimens.

The unleached samples appear to have no difference among the dietary groups in their exogenous Ca content, meaning that even if the absolute values are incorrect, the relative position of the herbivores and carnivores in the spectrum of $\delta^{44/42}$Ca values are still informative for differentiating dietary preferences among the co-occurring fossil taxa. However, to obtain the accurate $\delta^{44/42}$Ca values, it is imperative to leach samples prior to sample digestion to remove any impurities.

The diagenetic alteration effect could reflect time since burial or localised effects of the Elliot Formation and its depositional and burial history. It is possible that younger Cretaceous specimens with the same burial conditions (e.g., humidity or precipitation) as Triassic specimens may not be as affected by diagenesis and would have a smaller leaching differential. The effects of diagenesis and testing leaching on samples that are different in age and were exposed to different burial conditions is a key area for further research. The findings in this research indicate that tooth

enamel, at least Jurassic or older in age, may be subject to diagenetic alteration in $\delta^{44/42}$Ca systems. Therefore, the appropriate corrections must be considered for such specimens.

4.5.2. Effect of maturation on Ca-fractionation

The $\delta^{44/42}$Ca values for these samples appeared to have fractionated and become more positive over time being in the 0.05 N HNO_3 solution (Fig. 4.3). The mean $\delta^{44/42}$Ca values and ranges gradually become more enriched when moving from Batch 1 of day 1 to Batch 1 of day 3. The $\delta^{44/42}$Ca values of all samples analysed in this way drift over time to more positive values, indicating fractionation within the sample tubes. This is not a true reflection of the initial $\delta^{44/42}$Ca values.

It is highly unlikely that fractionation could have occurred due to change in concentration of the 0.05 N HNO_3 acid as the beakers were kept in a temperature-controlled room and completely sealed using parafilm. The gradual change of the $\delta^{44/42}$Ca values are not reflective of instrumental drift as the ICP standard values remained consistent (Fig. 4.4). It may be possible that the sample had undergone kinetic fractionation as some of the sample was taken up by the machine while the rest was left in the beaker for a period of time (Schönbächler and Fehr, 2013).

This emphasises the importance of preparing and analysing samples within a short time period to avoid having samples in the loading medium for too long. If samples are to be re-analysed or have been prepared for mass spectrometry, it needs to be analysed as soon as possible so the most accurate $\delta^{44/42}$Ca values can be produced. For future work, it may be of interest to test the optimum period that a sample can be re-analysed before fractionation of the sample occurs. This can be done with analysing the sample at known time intervals.

4.6. Conclusion

Good lab practices and techniques are imperative for producing high-quality and accurate $\delta^{44/42}$Ca data. Factors like diagenesis and effects of sample ageing on Ca isotopic MC-ICPMS values can obscure true $\delta^{44/42}$Ca values. It is important to prepare, analyse and re-analyse samples within a shorter timeframe to avoid any sample fractionation. Diagenesis, while not widely considered a problem for samples of Cretaceous age or younger, clearly represents a strong source of biased error in Triassic–Jurassic aged samples of vertebrate teeth. Established leaching protocols, with the modifications suggested here, provide repeatable means of removing exogenous Ca and these leached samples then provide accurate $\delta^{44/42}$Ca results in-line with expectations for respective major dietary groups. Moreover, the relationship between the $\delta^{44/42}$Ca values in leached and

unleached samples is predictable, so that specimens that were unleached can be ‘corrected’ using a simple linear equation. Hereafter $\delta^{44/42}$Ca values discussed in this research have either been leached or corrected for diagenetic alteration using the regression equation: $y = 0.8171x \times -0.3135$ where x is represented by the unleached $\delta^{44/42}$Ca value.

From the data collected here, it is unclear whether the amount of exogenous Ca is a function of the age of a specimen (i.e., more time to accumulate exogenous Ca over additional millions of years) or unique to a particular formation or geological setting (e.g., the Elliot mudstone/sandstone complex is highly porous). Testing these effects are an important future direction for improving the Ca methodology.

5. Characterising the diverse palaeoecosystem of the Elliot Formation, South Africa, using Ca isotopes to trace diet.

5.1. Abstract

Trophic levels and diet of co-occurring taxa provide key insights into how ecosystems function. The different trophic structures allow us to understand biodiversity changes and the different ecological laws and principles that exist within an ecosystem, enabling comparisons of ancient and modern ecosystems using the same proxy.

In this chapter, we report the use of non-traditional Ca isotopes in deep time to infer palaeodietary aspects of dinosaurs and archosaurs, as well as provide an insight into the palaeodiets and palaeoecology of ancient animals in the Elliot Formation. Some of the taxa analysed lived in ecosystems ~ 210 Ma old but most of the taxa are from the upper Elliot Formation. It is possible that the different taxa occupied different palaeoenvironments with different palaeoecological issues than those of the lower or lower upper Elliot Formation. This analysis includes the oldest continental ecosystem yet analysed using these methods. Our study consists of a variety of specimens across a broad range of amniote lineages, ranging from: dinosaurs such as presumed herbivorous sauropodomorphs *Massospondylus and Aardonyx*, the presumed omnivorous ornithischian (*Lesothosaurus*), and the presumed carnivorous theropod *Megapnosaurus*; to cynodont therapsids (*Tritylodon, Pachygenelus and Scalenodontoides)*; to pseudosuchians such as the crocodylomorphs *Protosuchus* and *Orthosuchus* and earlier branching taxa ('rauisuchians' and poposauroids).

We found significant differences between $\delta^{44/42}$Ca values of large carnivorous pseudosuchians ('rauisuchians'; -0.45 ‰ to -1.17 ‰) and herbivorous sauropodomorph genera (-0.26 ‰ to -0.69 ‰). We also found that while some taxa had $\delta^{44/42}$Ca isotope values in-line with their presumed diets, other taxa had diverse diets. $\delta^{44/42}$Ca values in this study provide evidence for the possibility of crocodylomorph and the oldest theropod herbivory, as well as an omnivorous diet for a presumed herbivorous *Lesothosaurus*.

Our results highlight the role of non-traditional $\delta^{44/42}$Ca isotopes to understand trophic structures by distinguishing herbivores from carnivores in an ecosystem at least 210 million years old (Bordy *et al.*, 2020). This research shows potential for further insight into dietary niches, foraging habits, and metabolic processes in ancient ecosystems (Martin *et al.*, 2017).

5.2. Introduction

Energy transfer through trophic structure is a fundamental property of modern ecosystems (Owen-Smith, 1988). Comparing trophic webs can provide information about ecosystem function and resilience. Understanding these ecological factors in deep time, however, is challenging because of the nature of the fossil record. As a result, fundamental questions in palaeoecology remain unanswered, including: the nature of ecosystem change, particularly across mass extinction events; whether ecosystems functioned in similar ways in deep time; and how ecological factors influenced organismal diversity and evolution, e.g., via factors like niche partitioning and predator-prey body mass relationships (Nakazawa *et al.*, 2013; Kartzinel *et al.*, 2015).

Understanding trophic structures requires knowledge of food webs (Bakker, 1987). The recent development of non-traditional calcium isotopes ($\delta^{44/42}$Ca) provides distinct advantages for isotopic dietary reconstruction in palaeontology (Heuser *et al.*, 2011). Recent studies using $\delta^{44/42}$Ca have shown great promise for reconstructing food webs in modern and Cretaceous specimens (Martin *et al.*, 2018; Koutamanis *et al.*, 2021; Martin *et al.*, 2022; Nitzsche *et al.*, 2022). Recent reviews suggest that the isotopic fractionation of Ca is conserved within amniotes and across physiologies, making it useful for understanding the diets of phylogenetically disparate vertebrates within the same ecosystem (Hassler *et al.*, 2018; Martin *et al.*, 2017; Martin *et al.*, 2018).

Stable isotope systems provide an independent means of assessing feeding patterns in extinct animals. Traditional systems like carbon, oxygen and nitrogen are useful in assessing dietary data but can be affected by diagenetic biases or the requirement of large sample amounts in palaeontological analyses (Higgins, 2018).

Calcium (Ca) is abundant in bone and teeth and thus requires very small sample sizes from fossil specimens. The Ca found in tooth enamel is less susceptible to diagenesis due to the densely packed solid crystalline structure of the hydroxylapatite (Bocherens *et al.*, 1994), and Ca is a bio-essential element which displays isotopic fractionation along trophic chains and within and among plants and animals (Heuser *et al.*, 2011; Morgan *et al.*, 2012, Martin *et al.*, 2017). Plants have relatively high ^{44}Ca concentrations in their foliage as the heavier Ca isotope (^{44}Ca) moves from the soil to the plant and is deposited in the foliage (Hindshaw *et al.*, 2013). The lighter ^{42}Ca isotope, however, is concentrated in the roots and stems (Martin *et al.*, 2018). The ratio of $^{44/42}$Ca becomes progressively depleted in herbivores and then carnivores as physiological fractionation incorporates less and less ^{44}Ca into bones and teeth. The meat and bone consumed by carnivores are therefore typically depleted in ^{44}Ca (Martin *et al.*, 2022), due to biological fractionation in the body of their prey (Martin *et al.*, 2022; Morgan *et al.*, 2012). This means that in moving up the trophic pyramid, at least among terrestrial vertebrates, the expectation is to find decreasing ratios of $\delta^{44/42}$Ca.

Variation in $\delta^{44/42}$Ca is a potentially useful means of assessing ecological questions such as dietary range and trophic levels in extinct organisms where these ecological parameters cannot be directly observed (Martin *et al.*, 2022).

The application of stable Ca isotopes is still in its infancy, but recent studies of non-traditional calcium isotopes ($\delta^{44/42}$Ca) have shown their utility for understanding dietary preferences and reconstructing food webs in both modern and Cretaceous settings (i.e., 65 Ma) (Martin *et al.*, 2018; Martin *et al.*, 2022). Recent reviews suggest that the isotopic fractionation of Ca is conserved within amniotes and across physiologies, making it useful for understanding the diets of phylogenetically disparate vertebrates within the same ecosystem (Hassler *et al.*, 2018; Martin *et al.*, 2017; Martin *et al.*, 2018). This allows us to assess a broad range of ecological questions including dietary range and trophic level.

Ca isotopes have two distinct advantages over traditional stable isotopic systems like carbon, oxygen and nitrogen: 1) Ca requires a much smaller amount of sample powder, allowing study of unique or near-unique fossil taxa without destroying their morphology; 2) Ca in tooth enamel is not as susceptible to diagenesis due to its crystalline structure (Bocherens *et al.*, 1994; Martin *et al.*, 2018; Martin *et al.*, 2017). A major outstanding research question is whether the Ca isotopic method can be applied to terrestrial ecosystems in much deeper time, and if so whether the trophic structuring of those populations is in line with that observed in modern-day vertebrate assemblages.

The diverse vertebrate faunas of southern Africa's Elliot Formation (Stormberg Group, Karoo Supergroup) (Chapter 1, Fig. 1.1) provide an ideal natural laboratory for assessing the utility of $\delta^{44/42}$Ca in deep time and to understand palaeodietary dynamics of ancient vertebrates spanning the latest Triassic–earliest Jurassic interval (218–190 Ma) (Bordy *et al.*, 2020). This ecosystem is nearly three times older than the oldest Ca-characterised vertebrate terrestrial ecosystems to date (Hassler *et al.*, 2018; Martin *et al.*, 2022). The Elliot Formation strata are relatively well-dated and stratigraphically well-constrained. A variety of terrestrial vertebrates existed during this period in the Elliot Formation (e.g., Kitching and Raath, 1984; Knoll, 2004, Knoll, 2005, Viglietti *et al.*, 2020a and 2020b) ranging from: dinosaurs such as presumed herbivorous sauropodomorphs *Massospondylus and Aardonyx*, the presumed omnivorous ornithischian (*Lesothosaurus*), and the presumed carnivorous theropod *Megapnosaurus*; to cynodont therapsids (*Tritylodon, Pachygenelus and Scalenodontoides)*; to pseudosuchians such as the crocodylomorphs *Protosuchus* and *Orthosuchus* and earlier branching taxa ('rauisuchians' and poposauroids).

The diets of these extinct species have previously only been qualitatively inferred using coarse proxies such as dental morphology and phylogenetic relationships to evaluate feeding ecology (e.g., herbivore/carnivore) (Bakker, 1987; Barrett, 2005; Tolchard *et al.*, 2018). This has led to a

major gap in our knowledge due to the lack of quantifiable evidence for trophic relationships between taxa from the Elliot Formation. Here, we conduct the oldest non-traditional $\delta^{44/42}Ca$ analysis to date in a continental setting on terrestrial vertebrate ecosystems which contain a variety of co-occurring specimens from the Elliot Formation. This is to gain insight into trophic divisions of the Elliot Formation terrestrial vertebrates and characterise the diverse ecosystems by achieving an accurate reconstruction of major dietary preferences.

5.3. Methodology

We analysed the dentition from 69 individual specimens which included presumed herbivorous sauropodomorph dinosaurs (*Massospondylus* (n = 12), *Aardonyx* (n = 4) and *Pulanesaura* (n=2)), presumed herbivorous therapsids (*Tritylodon* (n = 9), *Pachygenelus* (n = 10) and *Scalenodontoides* (n = 2)) and presumed herbivorous ornithischian dinosaurs *Lesothosaurus* (n = 3) and *Heterodontosaurus (n = 1)*, through to presumed carnivorous crocodylomorphs (*Protosuchus* (n = 3), *Orthosuchus* (n = 1)), presumed carnivorous theropod dinosaurs *Megapnosaurus* (n = 6), and pseudosuchians of indeterminate phylogenetic affinity (n = 16) that represent presumed carnivorous rauisuchids and herbivorous poposauroids (Tolchard *et al.*, 2019). Most of the specimens were chosen as they once co-existed and have a variety of presumed diets such as herbivorous, carnivorous and insectivorous. For further details on each taxon, refer to Chapter 2 and Appendix G.

Microsampling of tooth enamel was performed using an in-house micro-drill with a 0.4 mm tungsten carbide drill bit to produce and collect approximately 400 µg of powder in the ultra-clean Wits Isotope Geoscience Laboratory (WIGL). After sampling, these specimens were returned to the collections at the Evolutionary Studies Institution (ESI). Heritage permission to work on the selected fossil specimens was obtained from the South African Heritage Resource Agency (SAHRA) (Permit ID: 2967 and 3210) (refer to Appendix G for all specimens sampled in this study).

To control for diagenetic alteration, samples were leached prior to digestion (using the methodology outlined in Chapter 4). Fifty-one tooth enamel powders were leached following the method stated in Chapter 4. The 18 samples that were not leached were corrected for diagenetic alteration using the regression equation: $y = 0.8171x \times -0.3135$ where x is represented by the unleached $\delta^{44/42}Ca$ value (see Chapter 4). Samples were dissolved and digested, and the subsequent Ca ion-exchange chromatography was performed in the WIGL following a modified method from Tacail *et al.* (2014) (using methodology outlined in Chapter 3 and see: Tables 3.5, 3.6, and 3.7).

The reference material NIST-SRM1486 (which has the most reliable reproduced isotopic composition in literature), and procedural blanks also separated and analysed alongside the fossil samples. Once the samples were dry after the ion-exchange chromatography, a drop of concentrated (14M) HNO_3 was added to each beaker to cover the sample. The samples were left to dry down on the hotplate at 90 °C. After the samples dried, the beakers were capped, sealed and carefully packaged to be transported to the ENS in Lyon, France.

$\delta^{44/42}$Ca isotope values for all samples were measured using a ThermoScientific Neptune Plus Multi Collector-Inductively Coupled Plasma Mass Spectrometer (MC-ICPMS) at École Normale Supérieure de Lyon (ENS; France). The mass spectrometry followed the same protocol as mentioned in Chapter 4 and Tacail *et al.* (2014). The in-house reference standard used for standard bracketing was the ICP Ca Lyon, a Specpure Ca plasma standard solution (Alfa Aesar), purified of strontium traces.

5.4. Results

In this study, the repeated measurements of the NIST-SRM1486 reference material produced $\delta^{44/42}$Ca values with an average of -0.96 ± 0.05 ‰ (2 s.e., n = 7) with an offset of approximately ± 0.05 ‰ compared to the mean literature value (Chapter 4, Fig. 4.1). The in-house reference standard, ICP Ca Lyon, analysed alongside these samples remained consistent (Chapter 4, Fig. 4.4). All the blanks for five chemistry sessions yielded a mean blank value of Ca of 40 ng.

5.4.1. Isotopic determination of palaeotrophic positions

The presumed herbivorous sauropodomorphs, *Massospondylus* and *Aardonyx*, have different $\delta^{44/42}$Ca values to the presumed carnivorous 'rauisuchians' (Fig 5.1). The herbivorous sauropodomorph genera range from -0.75 ‰ to -0.26 ‰ and the large carnivorous pseudosuchians 'rauisuchians' have a $\delta^{44/42}$Ca range of -1.17 ‰ to -0.45 ‰ (Table 5.1).

The presumed herbivorous sauropodomorphs in this study have different mean $\delta^{44/42}$Ca values (Fig. 5.2). *Massospondylus* has the highest $\delta^{44/42}$Ca values of the sauropodomorphs that range from -0.69 ‰ to -0.26 ‰ with a mean of -0.47 ± 0.06 ‰ (2 s.e.) (Table 5.1). The *Massospondylus* juvenile $\delta^{44/42}$Ca values are scattered whereas the adult samples plot closer together (Fig. 5.1). *Aardonyx* has the second highest $\delta^{44/42}$Ca values ranging from -0.66 ‰ to -0.51 ‰ with a mean of -0.59 ± 0.05 ‰ (2 s.e.). There is a lower variance within the $\delta^{44/42}$Ca values for these samples (Fig. 5.1).

Pulanesaura, the largest presumed herbivorous sauropodomorph in this study, has the lowest $\delta^{44/42}$Ca values with a range from -0.75 ‰ to -0.62 ‰ and a mean of -0.68 ± 0.04 ‰ (2 s.e.) (Fig. 5.2). The $\delta^{44/42}$Ca values for herbivorous sauropodomorphs overlap with the presumed herbivorous therapsids: *Scalenodontoides, Pachygenelus* and *Tritylodon* (Fig. 5.2). *Scalenodontoides* has the highest therapsid mean $\delta^{44/42}$Ca value of -0.49 ± 0.04 ‰ (2 s.e.) with a range of -0.54 ‰ to -0.44 ‰ in this study (Table 5.1). This is followed by *Pachygenelus* with a mean value of -0.53 ± 0.04 ‰ (2 s.e.) and a range of -0.54 ‰ to -0.44 ‰. *Pachygenelus* has the largest difference from *Tritylodon* and *Scalenodontoides* (Fig. 5.1). *Tritylodon* has the lowest $\delta^{44/42}$Ca values with a range from -0.87 ‰ and -0.56 ‰ and mean -0.68 ± 0.06 ‰ (2 s.e.) (Table 5.1). Among sauropodomorph and therapsid taxa, different species have varying $\delta^{44/42}$Ca values with means and variances that are statistically distinguishable.

Lesothosaurus has a $\delta^{44/42}$Ca mean value of -0.66 ± 0.08 ‰ (2 s.e.) whereas *Heterodontosaurus*, another ornithischian dinosaur, has a value of -0.49 ± 0.13 ‰ (2 s.e.) (Table 5.1). These dinosaurs from the same taxon have a mean $\delta^{44/42}$Ca difference of -0.17‰.

The presumed carnivorous *Megapnosaurus* has a range of -0.72 ‰ to -0.29 ‰ and a mean of -0.57 ± 0.06 ‰ (2 s.e.). This is higher than the $\delta^{44/42}$Ca values for 'rauisuchians' which have a range of -1.17 ‰ to -0.45 ‰ and a mean value of -0.81 ± 0.07 ‰ (2 s.e.). 'Rauisuchian' samples have the most $\delta^{44/42}$Ca-depleted values in this study system. This group also has the largest difference from the rest of the taxa analysed. These early branching pseudosuchians have vastly different $\delta^{44/42}$Ca values compared to the crocodylomorphs. *Orthosuchus* has a relatively high $\delta^{44/42}$Ca value of -0.54 ± 0.02 ‰ (2 s.e.) and *Protosuchus* has a range from -0.64 to -0.24 with an average of -0.43 ± 0.03 ‰ (2 s.e.).

Table 5.1: Summary of the mean, lowest and highest $\delta^{44/42}$ Ca values. The mean, lowest, highest, 25th percentile (Quartile 1) and 75th percentile (Quartile 3) $\delta^{44/42}$ Ca values for the taxa mentioned and selected in this study. 2 s.e.= 2 standard error from the values are represented in the $\delta^{44/42}$ Ca (‰) column.

Taxa	Genus	$\delta^{44/42}$Ca (‰)	2 s.e. (‰)	Presumed diet
Sauropodomorph	*Massospondylus* (n = 12)			Herbivore
	Mean	-0.4663	0.0550	
	Lowest	-0.6856	0.1149	
	Quartile 1 (25 percentile)	-0.5574	-	
	Quartile 3 (75 percentile)	-0.3965	-	
	Highest	-0.2571	0.0747	
	Aardonyx (n = 4)			
	Mean	-0.5930	0.0467	
	Lowest	-0.6587	0.0350	
	Quartile 1 (25 percentile)	-0.6269	-	
	Quartile 3 (75 percentile)	-0.5696	-	
	Highest	-0.5065	0.0428	
	Pulanesaura (n = 2)			
	Mean	-0.6817	0.04202	
	Lowest	-0.7479	0.0603	
	Quartile 1 (25 percentile)	-0.7148	-	
	Quartile 3 (75 percentile)	-0.6485	-	
	Highest	-0.6154	0.0238	
Crurotarsan	'Rauisuchian' (n = 16)			Carnivore
	Mean	-0.8083	0.0701	
	Lowest	-1.1744	0.0425	
	Quartile 1 (25 percentile)	-0.9160	-	
	Quartile 3 (75 percentile)	-0.6618	-	
	Highest	-0.4471	0.0977	
Crocodylomorpha	*Protosuchus* (n = 3)			Carnivore/Herbivore
	Mean	-0.4269	0.0309	
	Lowest	-0.6448	0.0351	
	Quartile 1 (25 percentile)	-0.5227	-	
	Quartile 3 (75 percentile)	-0.3179	-	
	Highest	-0.2353	0.0189	
	Orthosuchus (n = 1)			
	Value	-0.5425	0.0216	
Eucynodontia	*Trityllodon* (n = 9)			Herbivore
	Mean	-0.6775	0.0634	
	Lowest	-0.8650	0.0933	
	Quartile 1 (25 percentile)	-0.6882	-	

	Quartile 3 (75 percentile)	-0.6487	-	
	Highest	-0.5608	0.0471	
	Pachygenelus (n = 10)			
	Mean	-0.5296	0.0430	
	Lowest	-0.6534	0.0379	
	Quartile 1 (25 percentile)	-0.6395	-	
	Quartile 3 (75 percentile)	-0.4545	-	
	Highest	-0.3637	0.0171	
	Scalenodontoides (n = 2)			
	Mean	-0.4929	0.0357	
	Lowest	-0.5425	0.0216	
	Quartile 1 (25 percentile)	-0.5177	-	
	Quartile 3 (75 percentile)	-0.4680	-	
	Highest	-0.4432	0.0498	
Theropoda	*Megapnosaurus* (n = 6)			Carnivore/Herbivore
	Mean	-0.5684	0.0591	
	Lowest	-0.7173	0.0685	
	Quartile 1 (25 percentile)	-0.6507	-	
	Quartile 3 (75 percentile)	-0.5491	-	
	Highest	-0.2863	0.0284	
Ornithiscia	*Lesothosaurus* (n = 3)			Omnivore
	Mean	-0.6638	0.0795	
	Lowest	-0.6656	0.1039	
	Quartile 1 (25 percentile)	-0.6643	-	
	Quartile 3 (75 percentile)	-0.6630	-	
	Highest	-0.6629	0.0423	
	Heterodontosaurus (n = 1)			Herbivore
	Value	-0.4908	0.1276	
-	Reference material SRM1486 (n = 7)			-
	Mean	-0.9554	0.0451	
	Lowest	-1.0199	0.0260	
	Highest	-0.8686	0.0364	

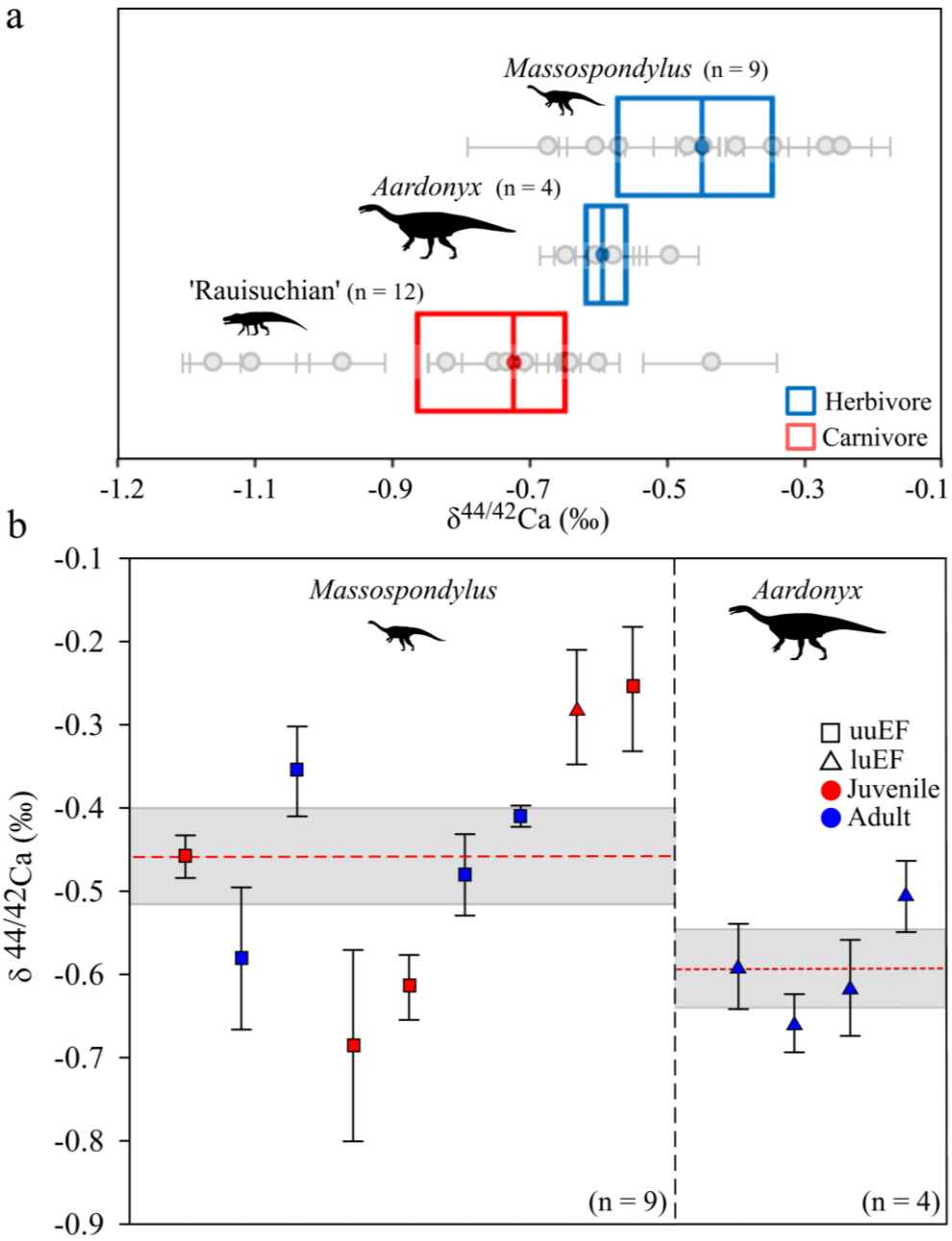


Figure 5.1: The $\delta^{44/42}$Ca (‰) difference between presumed Elliot Formation herbivores and carnivores. **(a)** The box plots, displaying Quartiles 1, 2, and 3, of the presumed herbivorous sauropodomorph genera namely: *Massospondylus* and *Aardonyx* are represented in blue and the presumed carnivorous 'rauisuchians' are represented in red. There is a distinct variation in the $\delta^{44/42}$Ca (‰) values between the herbivores and carnivores. Silhouettes of *Massospondylus*, *Aardonyx* and 'rauisuchian' scaled relative to the mass of the animals. This is showing the variation in morphology, size and stature. Image sources: prehistoric-wildlife.com. **(b)** $\delta^{44/42}$Ca (‰) values of sauropodomorph specimens analysed. The juvenile specimens of *Massospondylus* (red) and the lower upper Elliot Formation (luEF) (triangle) are indicated above. The rest of the specimens are upper upper Elliot Formation (uuEF) (square) and range from sub-adult to adult (blue).

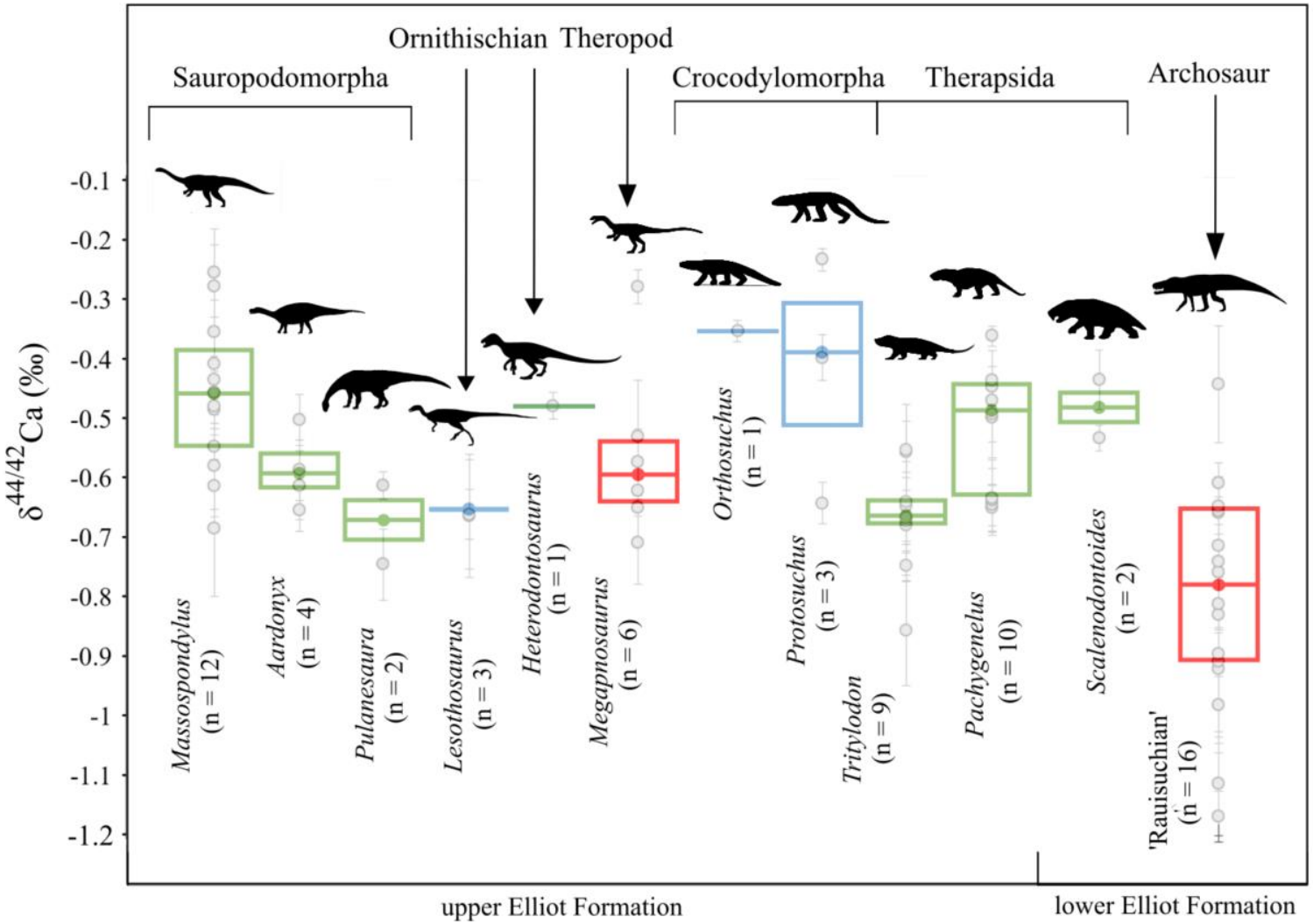


Figure 5.2: The $\delta^{44/42}$Ca (‰) difference between presumed herbivores, carnivores and omnivores. The box plots, displaying Quartiles 1, 2, and 3, of the co-occurring presumed herbivorous taxa represented in green, presumed carnivorous represented in red and the presumed omnivorous taxa represented in blue. Silhouettes are not to scale. Image sources: prehistoric-wildlife.com

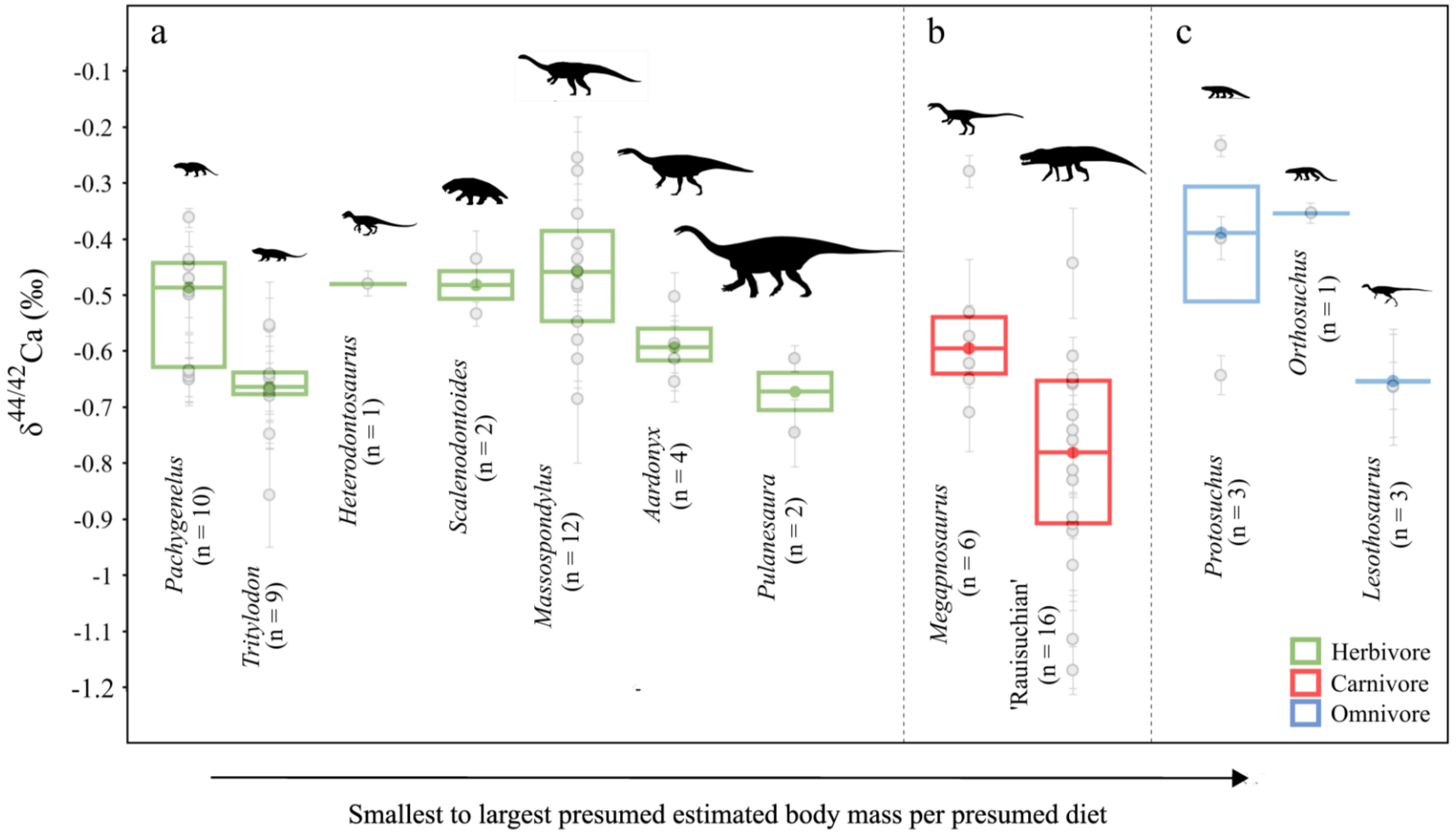


Figure 5.3: The $\delta^{44/42}$Ca (‰) difference between the $\delta^{44/42}$Ca values and the estimated body mass of the a) herbivores, b) carnivores and c) omnivores. The box plots, displaying Quartiles 1, 2, and 3, of the co-occurring presumed herbivorous taxa represented in green, presumed carnivorous represented in red and the presumed omnivorous taxa represented in blue. Image sources: prehistoric-wildlife.com

5.5. Discussion

In this study, the repeated measurements of the NIST-SRM1486 reference material produced values within the reported $\delta^{44/42}$Ca mean literature value of -1.00 ± 0.07 ‰ (Tacail *et al.*, 2015; Hassler *et al.*, 2018) value (Fig. 4.1). This indicates that the data produced are accurate and reproducible.

The in-house reference standard, ICP Ca Lyon, analysed alongside these samples remained consistent and produced a line with a gradient almost equal to one which shows that there was no instrumental biases or drifts. The data produced is accurate.

All blanks for five chemistry sessions yielded a mean value of Ca of 40 ng. This is almost 1000 times less than the Ca present in the samples (Hassler *et al.*, 2018).

5.5.1. Isotopic determination of palaeotrophic positions

A general overview of the $\delta^{44/42}$Ca data for the various presumed diets shows that $\delta^{44/42}$Ca values do vary for the different presumed diets. Presumed herbivorous sauropodomorpha and therapsida fall in the same range. These taxa plot relatively higher than the presumed carnivorous taxa, meaning they are relatively enriched in ^{44}Ca, consistent with expectations from the literature and theoretical isotopic fractionation gradients along trophic spectra. The presumed carnivorous *Megapnosaurus* and 'rauisuchian' plot relatively lower than the herbivores. Other taxa in the analysis, including *Lesothosaurus, Heterodontosaurus, Protosuchus* and *Orthosuchus* plot between presumed herbivores and carnivores, perhaps indicating a more varied diet.

The presumed carnivorous 'rauisuchian' specimens show depleted $\delta^{44/42}$Ca isotope values ($\bar{x}$ = -0.81± 0.07 ‰; n = 16) (Table 5.1) in contrast to herbivorous sympatric sauropodomorphs, *Massospondylus* and *Aardonyx*, which have enriched $\delta^{44/42}$Ca values ranging between -0.26 ‰ to -0.69 ‰ (n = 13). These differences are significant (Wilcoxon rank-sum test: *p*-value = 9.8×10^{-4}). These values indicate that $\delta^{44/42}$Ca analysis can be used to determine conspicuous dietary differences as far back in time as the Triassic–Jurassic period. These differences are consistent with hypotheses from tooth morphology and cranial shape that have long hypothesised herbivorous and carnivorous diets for these species.

Massospondylus, Aardonyx, Pulanesaura and *Lesothosaurus* are presumed to be herbivorous primary consumers within their ecosystem and the presumed carnivorous 'rauisuchian' equivalent can be considered the secondary consumer feeding on these herbivores. The suggested size (Tolchard *et al.*, 2019; Botha-Brink and Smith, 2011) for 'rauisuchians' could presumably rank them as the top predators of their palaeoecosystem within the lower Elliot Formation with their possible prey being

similar to the presumed herbivorous sauropodomorphs and ornithischian dinosauria: *Massospondylus, Aardonyx* and *Lesothosaurus* (Fig. 5.4).

The $\delta^{44/42}$Ca range seen between the large carnivorous pseudosuchians 'rauisuchians' and herbivorous sauropodomorph genera closely resemble $\delta^{44/42}$Ca values for modern taxa with herbivorous and carnivorous diets with carnivore-herbivore offsets of approximately 0.3 ‰ (Martin *et al.*, 2018) (Fig. 5.1). This arises as fractionation occurs within the body resulting in bone, blood and organs being depleted in ^{44}Ca (lowering $\delta^{44/42}$Ca values) compared to the food source (Heuser *et al.*, 2011; Morgan *et al.*, 2012; Hassler *et al.*, 2021). The absolute $\delta^{44/42}$Ca values seen for the modern ecosystem in a study by Martin *et al.* (2018) differ from the values obtained here for Elliot Formation palaeoecosystems. However, there are overlapping $\delta^{44/42}$Ca ranges for herbivorous and carnivorous samples in $\delta^{44/42}$Ca studies of other palaeoecosystems such as the Cretaceous and Palaeogene in Hassler *et al.* (2018) and Martin *et al.* (2022). The relative positions and magnitude of the offset between herbivores and carnivores seen in modern and ancient ecosystems using $\delta^{44/42}$Ca isotopes are the same as those displayed in this study. In a study by Martin *et al.* (2018), herbivorous Bovidae samples were relatively $\delta^{44/42}$Ca-enriched compared to the carnivorous Felidae samples, indicating a depletion of ^{44}Ca when moving through the trophic levels. The relative positioning of the taxa is, therefore, more important for determining trophic level compared to the absolute value when analysing extinct ecosystems. In Martin *et al.* (2018), the same taxa were analysed and compared from the Turkana Basin and Tsavo (Kenya). The same taxa from each locality produced different absolute values but had the same relative positioning between the two groups. The Ca isotopic differences between 'rauisuchians' and sauropodomorphs in this study allows us to fingerprint the differences between carnivores and herbivores within this ancient ecosystem. Irrespective of timeframes (i.e., within the formation and between the Triassic-Jurassic and present day), there are differences between carnivores and herbivores.

To control for isotopic variation through time, data was also collected from *Massospondylus* specimens from their full stratigraphic range across the upper Elliot Formation. The lack of correlation between stratigraphic height and $\delta^{44/42}$Ca values of the *Massospondylus* specimens suggests that temporal/stratigraphic or spatial/lithological differences are unlikely to yield predictable biases in $\delta^{44/42}$Ca results (Fig. 5.1b). This suggests that comparisons of $\delta^{44/42}$Ca values across ecosystems, even at great temporal distances, is feasible.

Referring to Fig. 5.1a, the juvenile *Massospondylus* samples display a larger variance compared to the adult samples. This may indicate that juvenile *Massospondylus* had a more diverse diet and ate a variety of foods compared to adult *Massospondylus*, which had a more restricted diet. This feeding behaviour is similar to extant crocodilians such as juvenile *Crocodylus niloticus*. A study by Hutton (1987) highlights the diverse diet of juvenile *Crocodylus niloticus* which includes insects, fish, birds

and other prey whereas the adult *Crocodylus niloticus* have a less diverse range of large-bodied prey. The young smaller size *Crocodylus niloticus* had a larger variety of prey in its gut compared to the large adult crocodiles with a more restricted diet (Hutton, 1987). Tooth replacement rates for dinosaurs such as *Massospondylus* are inferred to be comparatively higher than those of contemporaneous therapsids. Therefore, it is more likely that the signal from teeth in dinosaurs captures dietary transitions between juveniles and adults (Gow *et al.,* 1990). The *Aardonyx* samples have a smaller variance as the $\delta^{44/42}$Ca values plot closer to each other (Fig. 5.1b). This may indicate that *Aardonyx* had a more restricted diet and did not eat a large variety of vegetation. This may, additionally, reflect the restricted diet of adult *Aardonyx* specimens as there were no available juvenile specimens of *Aardonyx* in the analysis.

The presumed herbivorous sauropodomorpha, therapsida and the ornithischian *Heterodontosaurus,* fall within the same range and have relatively enriched $\delta^{44/42}$Ca values. *Heterodontosaurus* has sharp canines and premaxillary beak suggesting possible omnivory (Crompton and Attridge, 1986; Sciscio *et al.,* 2017; Radermacher *et al.,* 2021), but the relatively enriched $\delta^{44/42}$Ca value plots in the range of the herbivorous specimens (Fig. 5.2) suggesting that *Heterodontosaurus* could just be herbivorous and used posterior maxillary and dentary teeth showing clear occlusal dental wear to possible grind tough plant material (Norman *et al*., 2011).

The ‘rauisuchian’ samples have the most $\delta^{44/42}$Ca-depleted values relative to the other taxa (Fig. 5.2) The ‘rauisuchian’ $\delta^{44/42}$ Ca values are also widespread (Fig. 5.2) as the lower precision of taxonomic identification of the carnivorous ‘rauisuchian’ teeth undoubtedly contributes to the higher observed variance of the $\delta^{44/42}$ Ca values.

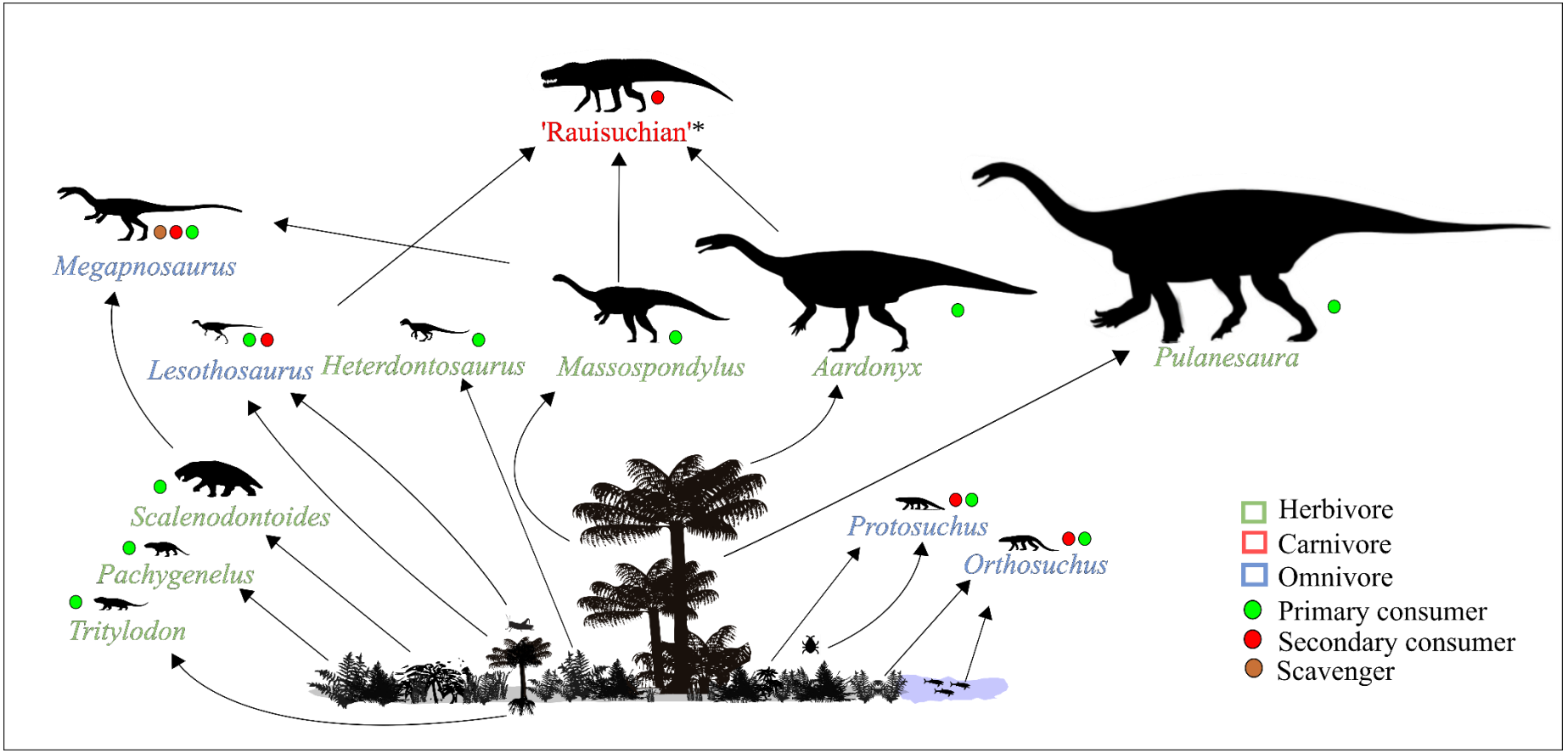


Figure 5.4: Hypothetical Elliot Formation food web using the $\delta^{44/42}$Ca (‰) values. The dietary preferences are suggested based on the $\delta^{44/42}$Ca (‰) values obtained in this study. *uEF carnivore such as *Dracovenator* that could not be analysed. Silhouettes of all taxa are scaled relative to the mass of the animals. Image sources: prehistoric-wildlife.com

5.5.2. Resource partitioning in sympatric herbivores

We also observe isotopic differences between co-occurring herbivorous taxa (Fig. 5.3). *Massospondylus, Aardonyx* and *Pulanesaura* were co-existing, presumed herbivorous sauropodomorphs that may have filled different niches, but little information is available on resource partitioning between these species. The $\delta^{44/42}$Ca values reported are in line with isotopic signatures of herbivory as seen in Cretaceous and Palaeogene studies by Martin *et al.* (2022) and Hassler *et al.* (2018). The mean $\delta^{44/42}$Ca value differences for *Massospondylus* (-0.47 ± 0.06 ‰), *Aardonyx* (-0.59 ± 0.05 ‰) and *Pulanesaura* (-0.68 ± 0.04 ‰) may be due to preferential consumption of different vegetative resources by differing sauropodomorph species - a phenomenon also observed in extant herbivorous taxa and in Cretaceous herbivores (Hassler *et al.*, 2018).

The size differences between *Massospondylus, Aardonyx* and *Pulanesaura,* differences in their gross anatomy, and potential postural differences (Yates *et al.*, 2010, McPhee *et al.*, 2018, Chapelle *et al.*, 2021) are possibly correlated with different foraging strategies (Gee, 2011). In living herbivores, differing $\delta^{44/42}$Ca values are present in differing foraging strategies such as browsing and grazing (Martin *et al.*, 2018). For example, the ± 450 kg body mass, bipedal posture, long flexible neck, and narrow snout of *Massospondylus* may reflect selective browsing of high-quality forage similar to modern-day kudu (Owen-Smith, 1988; Chapelle *et al.*, 2021). In contrast, the more robust body form, broader skull, and ±1 tonne body mass of *Aardonyx* may reflect bulk browsing of lower-quality vegetation to fulfil their metabolic demand similar to a rhinoceros (Yates *et al.*, 2010; Owen-Smith, 1988; Yates and Barrett, 2010). *Pulanesaura* could be compared to a modern-day bull elephant in size and was a bulk browser feeding on lower-quality food similar to *Aardonyx* (Owen-Smith, 1988; Yates *et al.*, 2010; McPhee *et al.*, 2015). The larger the body size, the more low-quality food has to be consumed to ensure the dietary requirements are met compared to a relatively smaller body size which may consume high quality food and only less is required to meet dietary requirements (Owen-Smith, 1988). This predictable relationship between herbivore body size and fodder in living animals therefore may have been in place even in Triassic herbivore communities. If so, we could predict that isotopic values from the largest herbivores in the system, such as *Ledumahadi*, could show further variation to those analysed in this study (McPhee *et al.*, 2018).

Although the herbivores measured have significantly different $\delta^{44/42}$Ca values, it is unlikely that size alone is a driver of these differences. Within *Massospondylus,* specimens measured ranged in inferred body mass from 100 kg to 500 kg (Chapelle *et al.*, 2021). The $\delta^{44/42}$Ca values of these specimens display no relation the with inferred body mass (Fig. 5.1a). Moreover, these specimens had lower intraspecific variance than the interspecific variance observed between size classes (Fig.

5.1a). The stature and the size of the selected ancient animals are vastly different and could influence what they ate or how much they consumed. It can be inferred that the $\delta^{44/42}$Ca values are not affected by physiological size differences within the body but are more likely to reflect isotopic composition of what was being consumed by these ancient animals.

The phenomenon of resource partitioning can also be seen in the therapsid samples analysed in this study. Karoo-aged therapsids, mammal-like reptiles, such as *Tritylodon, Pachygenelus* and *Scalenodontoides* are presumed to be herbivorous and fall in-line with other presumed herbivorous sauropodomorphs (Kemp, 2006; Muchlinkski, 2020). In addition to the herbivorous diet, *Scalenodontoides* and the co-occurring *Tritylodon* and *Pachygenelus* have notable isotopic differences between them (Fig. 5.2). This may be attributed to the different niches these therapsids may have filled with varying diets and the concentration of the different Ca isotopes from different food sources.

These species have conspicuous differences in tooth morphology, for example the precise occlusion of the molariforms of *Tritylodon,* suggesting that they were eating different parts of Mesozoic plants. Differing dentition allows for more specialised diets as the dental morphology influences the type of resource that can be consumed e.g., Lions have large canines to tear through meat whereas cows have large flat teeth for grinding (Martin *et al.,* 2018). These differences may be attributed to ways these species could have processed the consumed food such as metabolic influences, it could also be the consumption of different resources by the various therapsids. This is observed in extant and Cretaceous herbivorous taxa (Martin *et al.,* 2018; Martin *et al.,* 2022). Varying morphological characteristics such as body size, and dental morphology and complexity can influence the type of the vegetation consumed by the different therapsids (Ruta *et al.,* 2013). There has been no definite evidence of niche partitioning, but this could possibly be a proxy which could indicate varying feeding behaviours.

We specifically see a variation between *Tritylodon* and *Pachygenelus* with different ranging $\delta^{44/42}$Ca values and a mean difference of -0.15 ‰ (Fig. 5.2). *Tritylodon* has more $\delta^{44/42}$Ca-depleted values compared to *Pachygenelus.* These two taxa are from the same formation, the upper Elliot formation (Bonaparte and Crompton, 2018; Ruta *et al.,* 2013), but are presumed to have fulfilled different niches and fed on different foliage due to their differing dentition. *Tritylodon* is presumed to have massive cheek muscles with teeth for grinding and is presumed to have fed on vegetation like stems and roots and tubers as it had complex cheek teeth (Owen, 1884) whereas *Pachygenelus* has less specialised dentition (Gow, 2001). Stems and roots of plants are more $\delta^{44/42}$Ca-depleted relative to the foliage as the roots are more enriched in ^{42}Ca (Hindshaw *et al.,* 2013). *Tritylodon* is a more specialised herbivore that broke down hard foods like roots in its oral cavity based on the

precise dental occlusion of the upper and lower postcanines (Smith and Kitching, 1997; Gow *et al.*, 1990). The $\delta^{44/42}$Ca values for *Pachygenelus* are more enriched and would correlate with plant foliage by having more ^{44}Ca compared to the roots consumed by *Tritylodon* (Bonaparte and Crompton, 2017; Hindshaw *et al.*, 2013).

Scalenodontoides, also presumed to be herbivorous, falls within the range of *Pachygenelus* but both of these taxa differ stratigraphically as *Scalenodontoides* is found in the lower Elliot Formation (Ruta *et al.*, 2013, Viglietti *et al.*, 2020a). The sizes of *Scalenodontoides* and *Pachygenelus* are vastly different and could influence what they ate or how much they consumed. The size of *Pachygenelus* is comparable to a modern rabbit and the *Scalenodontoides* size is comparable to a modern lion (Abdala *et al.*, 2007; Bonaparte and Crompton, 2018). This size difference could infer different herbivorous diets with the same $\delta^{44/42}$Ca values (Crompton and Ellenberger, 1957).

We can infer that the $\delta^{44/42}$Ca values are not affected by these differences within the body but are more likely to reflect isotopic composition of what was being consumed by these ancient animals. While the body mass order for the therapsids from smallest to large is *Pachygenelus*, *Tritylodon* and *Scalenodontoides*, there is no body size and $\delta^{44/42}$Ca value patterns observed (Fig. 5.3). However, these species have more specialised morphologies which would have an influence on their diets. *Tritylodon* has the most $\delta^{44/42}$Ca-depleted values which correlates with the presumed tuber diet (Hindshaw *et al.*, 2013). Tubers and the roots of plants are the most $\delta^{44/42}$Ca-depleted part of the plant (Hindshaw *et al.*, 2013). *Tritylodon* has large incisors and robust forelimbs suited for burrowing and digging up roots, similarly to modern moles (Gaetano *et al.*, 2017). Whereas *Scalenodontoides* and *Pachygenelus* have similar dentition, but vary in size, which could have influenced the quality and amount of food consumed.

Pachygenelus also has the largest variance in $\delta^{44/42}$Ca isotopes compared to *Tritylodon* and *Scalendontoides* (Fig. 5.2). As seen in the *Massospondylus* $\delta^{44/42}$Ca values for different fossil specimens, the *Pachygenelus* fossil specimens that were sampled also varied in size suggesting interspecies variation within *Pachygenelus*. The younger *Pachygenelus* specimens, which are smaller in size, consumed a diet that was more $\delta^{44/42}$Ca-enriched compared to the larger adult specimens.

5.5.3. Differing $\delta^{44/42}$Ca values for presumed diets

Lesothosaurus and *Heterodontosaurus* are ornithischian dinosaurs with similar body sizes that co-existed but the $\delta^{44/42}$Ca difference between samples are -0.17 ‰. *Lesothosaurus* has more $\delta^{44/42}$Ca-

depleted values relative to *Heterodontosaurus* (Table 5.1). *Heterodontosaurus* falls in the herbivory range which indicates a herbivorous diet whereas *Lesothosaurus* is more $\delta^{44/42}$Ca-depleted and could have a mixed omnivorous diet. *Lesothosaurus* is presumed to have fed on shoots and fructifications (Norman and Weishampel, 1991) but the $\delta^{44/42}$Ca values for this specimen is relatively negative compared to the presumed herbivorous sauropodomorphs that it existed alongside (Fig. 5.2). This could potentially be due to a variation in the diet of *Lesothosaurus* where the shoots and fruitifications may have been relatively depleted in ^{44}Ca. While it may be common for shoots and stems to have relatively depleted $\delta^{44/42}$Ca values, this is not typically seen in fruits (Hindshaw *et al.,* 2013). The relatively negative $\delta^{44/42}$Ca values could possibly suggest that *Lesothosaurus* may be omnivorous. According to Barrett (2000), it is possible that *Lesothosaurus* were opportunistic omnivores if they were to successfully survive the drier climate periods. These ancient animals could have feed on small prey during this period (Barret, 2000) which would influence the relatively negative $\delta^{44/42}$Ca values represented for *Lesothosaurus* (Fig. 6.1).

'Rauisuchians' may have preyed on megaherbivores similar to *Massospondylus* and *Aardonyx* (Fig. 5.4), but the presumed carnivorous *Megapnosaurus* was much smaller in size (Munyikwa and Raath, 1999; Bordy *et al.,* 2021), making it more difficult to prey on these large herbivorous animals. Instead, these small theropods may have functioned as scavengers within their palaeoecosystem (Fig. 5.4). While 'rauisuchians' could have fed on the organs, blood and bone bringing down their $\delta^{44/42}$Ca values, the relatively enriched $\delta^{44/42}$Ca value for *Megapnosaurus* (Fig. 5.2) could indicate that this theropod may have fed solely on the muscle tissue of their prey (Morgan *et al.,* 2012). Bone material of these megaherbivores would have been too large for *Megapnosaurus* to crush and is likely that hypercarnivores could have eaten bone leading to more $\delta^{44/42}$Ca-depleted values as seen in 'rauisuchians'. In a study by Tutken *et al.* (2018), the theropod *Allosaurus*, has $\delta^{44/42}$Ca values in-line with the analysed herbivorous sauropodomorph suggesting that the theropod consumed more of the meat and less bone material. Blood and tissue are relatively enriched in ^{44}Ca which would put *Megapnosaurus* relatively more positive than 'rauisuchians' as bone is relatively depleted in ^{44}Ca (Morgan *et al.,* 2012, Martin *et al.,* 2018). It is possible that the animals consumed by *Megapnosaurus*, their Ca source, could have had relatively positive $\delta^{44/42}$Ca values which is now shown by the high $\delta^{44/42}$Ca value of -0.57 ± 0.06 ‰ (Table 5.1) (Tutken *et al.,* 2018).

When studying the other species that existed alongside *Megapnosaurus,* it is possible that they did not directly feed on therapsids like *Scalenodontoides* as this animal was much larger in size but could have scavenged on *Scalenodontoides*. *Tritylodon* can also be ruled out as the $\delta^{44/42}$Ca values are lower than *Megapnosaurus* which does not correlate with the movement of $\delta^{44/42}$Ca isotopes

from prey to consumer. *Pachygenelus* could be a potential food source for *Megapnosaurus* as *Pachygenelus* has slightly higher $\delta^{44/42}$Ca values than *Megapnosaurus* and is a smaller animal (Fig. 5.3). Elliot Formation crocodylomorpha could be potential prey for *Megapnosaurus*, as *Orthosuchus* and *Protosuchus* are smaller in size and have relatively higher $\delta^{44/42}$Ca values than *Megapnosaurus.* If these crocodylomorphs were to be consumed by *Orthosuchus* and *Protosuchus*, fractionation along the food chain would result to the current *Megapnosaurus* $\delta^{44/42}$Ca range as the consumer has a relatively ^{42}Ca-depleted value to the food source (Martin *et al.*, 2018).

The relatively positive $\delta^{44/42}$Ca value for *Megapnosaurus* may also suggest the possibility of theropod herbivory in *Megapnosaurus* as there are multiple instances of herbivory evolving in theropods (e.g., *Oviraptorosauria* and *Therizinosauria*) (Fig. 5.3) (Barrett, 2014). This would suggest that *Megapnosaurus* could be one of the oldest theropods to have an herbivorous diet (Barrett, 2014). However, the herbivorous theropod lineages have distinct modifications of the dental structure that are not present in *Megapnosaurus.*

The $\delta^{44/42}$Ca values obtained *for Orthosuchus* and *Protosuchus* are higher than expected for a typical carnivorous diet like the 'rauisuchians' in this study or, for example, *Tyrannosaurus rex* (Martin *et al.*, 2022) (Fig. 5.2). *Protosuchus* is presumed to be carnivorous and to have fed on small prey due to dental morphological characteristics such as serrated teeth (Irmis *et al.*, 2013). In a study by Tutken *et al.* (2018), insectivores are seen to have relatively enriched $\delta^{44/42}$Ca values compared to other carnivores. *Protosuchus* is seen to have $\delta^{44/42}$Ca values that are relatively enriched compared to the other carnivorous Karoo archosaurs, 'rauisuchians', analysed in this study. While these $\delta^{44/42}$Ca values could be representative of an insectivorous diet, it is possible that these values could represent herbivory in the diet of these crocodylomorphs (Melstrom and Irmis, 2019; Dollman and Choiniere, 2022). This is due to the $\delta^{44/42}$Ca values for *Protosuchus* within the same range as the $\delta^{44/42}$Ca values for the herbivorous sauropodomorphs, *Massospondylus* and *Aardonyx* (Fig. 5.2). The complexity of the dentition and comparatively robust construction of the palate in *Protosuchus* would suggest herbivory (Dollman and Choiniere, 2022) There is a possibility that *Protosuchus* was herbivorous as herbivory is hypothesised to have evolved multiple times in crocodyliforms and first occurred in protosuchids (Benson and Godoy, 2019).

Protosuchus and *Orthosuchus* have a $\delta^{44/42}$Ca difference of -0.12 ‰. The relatively $\delta^{44/42}$Ca-enriched values of *Orthosuchus* could suggest an herbivorous diet (Fig. 5.2) but the different dentition may imply a different diet from herbivory. *Orthosuchus* could also have a been a piscivore, as the posterior end of the maxilla is edentulous, a feature commonly seen in piscivores (Nash, 1968). Piscivory is a common dietary mode amongst extant crocodylomorpha, and Elliot ecosystems likely had an abundance of fish (Cloudsley-Thompson, 2005; Sciscio *et al.*, 2020). While *Orthosuchus* was terrestrial, there is a possibility that this animal was transitioning and

adapting to being aquatic and fed on fish (Buffetaut, 1979). The $\delta^{44/42}$Ca value of *Orthosuchus* (-0.54‰) is not the same as the absolute values seen in Hassler *et al.* (2018) for piscivorous Crocodylomorpha and Spinosauridae with mean $\delta^{44/42}$Ca values of approximately -1.0 ‰ and -1.35 respectively. This could be due to different $\delta^{44/42}$Ca values in the food source.

5.6. Conclusion

Our results reveal the utility of Ca isotopes in distinguishing trophic level within palaeoecosystems as old as those preserved in the rich Karoo sequence. $\delta^{44/42}$Ca isotopes can be used to understand ancient population dynamics and dietary behaviour in palaeoecosystems. Developing isotopic proxies and metrics that can contribute to the understanding of ancient population dynamics and dietary behaviour, is a critical endeavour for advancing palaeontological analysis of past ecosystems. It can be complimentary to other proxies along with overcoming the shortcomings of poor preservation. $\delta^{44/42}$Ca isotope variability can assist in characterizing palaeoecosystems, such as those found in the rich Karoo, by identifying the different trophic levels that once existed. We can identify the dietary differences between herbivores, carnivores and omnivores as well as infer the differences between different herbivorous species from the same lineages, opening the possibility of studying niche partitioning and dietary preference among therapsid species. This contributes to the morphological diversity of the fossils, which indicates that there were therapsids of different body size that co-existed and had adapted to fill different niches. These differences were transferable through time within the formation.

The data in this study provide evidence that Ca isotopes are also useful across ecosystems older in age preserving highly conserved and comparable relative enrichment values across this time frame. This can be used to gain insight into trophic divisions such as herbivore-carnivore of Elliot Formation vertebrates.

Testing important ecological principles in temporally constrained formations allows us to understand the historical nature of biodiversity changes and the different laws that govern biological life forms on Earth. Being able to determine dietary dynamic factors such as palaeodiet and palaeotrophic range will enable the development and improvement of palaeoecological analysis. Ultimately, these isotopic tools can be used to understand dynamics within ancient ecosystems and their response to environmental stress (e.g., droughts, mass extinctions).

6. Sex determination of *Crocodylus niloticus* using Ca isotopes.

6.1. Abstract

Calcium is a vital nutrient in the reproductive physiology of animals that lay eggs or experience lactation (Dacke *et al.*, 2015). The fluctuating levels of Ca during these periods of reproduction can influence $\delta^{44/42}$Ca values present in the body as seen in lactating mothers (Tacail *et al*., 2017). This chapter focuses on further expanding the application and utility of the non-traditional $\delta^{44/42}$Ca isotope method to determine sex of modern crocodilians, specifically *Crocodylus niloticus.* The selected samples were from a controlled environment (e.g., diet) with known sex. If $\delta^{44/42}$Ca could be used to determine sex, the study would be extended to dinosaurs and other extinct animals. Each juvenile specimen was sampled once to obtain an overall $\delta^{44/42}$Ca value, and the adult specimen was sampled along the cross section for any $\delta^{44/42}$Ca variance during tooth formation. Here we show the $\delta^{44/42}$Ca values of male and female juvenile *Crocodylus niloticus* and an adult female *Crocodylus niloticus.* The juvenile *Crocodylus niloticus* female samples yield mean $\delta^{44/42}$Ca values of -0.93 ± 0.02 ‰ (n = 4) whereas the juvenile male samples yield mean $\delta^{44/42}$Ca values of -0.92 ± 0.02 ‰ (n = 5). The $\delta^{44/42}$Ca ranges for the *Crocodylus niloticus* juvenile male and female overlap as females have a $\delta^{44/42}$Ca range of -1.14 ‰ to -0.82 ‰ and males $\delta^{44/42}$Ca range from -1.09 ‰ to -0.81 ‰. There are no conspicuous $\delta^{44/42}$Ca variations observed for the juvenile samples. The female adult samples did not have much variation in $\delta^{44/42}$Ca values throughout the dentine ring cross section of the tooth. Crocodile's teeth are constantly being replaced and a relatively new tooth that may have formed out of the breeding and/or nesting season may not have varying $\delta^{44/42}$Ca values for females. It is possible that the non-traditional $\delta^{44/42}$Ca isotope method may not function as a proxy for determining sex as there is no isotopic differences observed for the different sexes of the same species.

6.2. Introduction

Many living tetrapod groups display large phenotypic differences between sexes including weight differences (e.g., male vs. female rhinos); elaborate display features (e.g., bovid horns) or height differences (e.g. tallest male elephant is the most attractive and dominant) (Moczek and Emlen, 2000; Petrie *et al*., 1991; Senter, 2007). Presumably, these phenotypic differences were also present in extinct tetrapod groups (Erickson *et al*., 2005). However, determining the sex of extinct animals is challenging and the best methods currently rely on large sample sizes and may require destructive methods such as osteohistology (Chapman *et al.*, 1997; Chinsamy, 1990). Such

methods have provided some interesting insights in palaeobiology, such as sexual display of feathers that have evolved at least 125 million years ago in the most primitive birds, for example *Confuciusornis sanctus* (Chinsamy *et al*., 2013). The presence of a medullary bone has also been suggested as a proxy for the female sex in birds (Chinsamy and Barrett, 1997). *Confuciusornis sanctus* was found to have medullary bone tissue which separated the males with spectacular tails and females with no tails (Chinsamy *et al.*, 2013). Suitable sex-determination metrics that can accommodate small sample sizes and minimise specimen destruction would be advantageous and contribute to a variety of topics and long-standing debates. For example, *Triceratops* and *Torosaurus* possibly being two separate dinosaur lineages or the same dinosaur lineage but differ due to evolution is an ongoing taxonomical debate (Longrich and Field, 2012). Another debate is lambeosaurines possibly being male dimorphs to the female hadrosaurines as the crest found on the lambeosaurine may be a male dimorphic feature (Chapman *et al.*, 1997).

Sex determination in ancient animals would be helpful in providing a better understanding of population dynamics and the potential roles the different sexes played within their groups (Chinsamy and Barrett, 1997). It may also indicate dominant sexual attributes in different dinosaurs as well as sexual anatomical differences within the dinosaurs (Erickson *et al.*, 2005). Sex determination can provide further insight into the evolution of sexual selection and dinosaur reproductivity (Mallon, 2017; Chinsamy and Barrett, 1997). An example is the neck elongation in Sauropoda as males with longer necks could have been more dominant compared to other males and would have a higher success rate in finding a mate (Senter, 2007).

The small sample size for the different fossil groups decreases the reliability of the results as there are not many specimens to contradict or support the theories presented (Chapman *et al.*, 1997). One of the proxies suggested for sex determination is the presence of a medullary bone in dinosaurs (Chinsamy and Barrett, 1997). The medullary bone and medullary cavity are found in female birds during ovulation (Kerschnitzki *et al.*, 2014). The medullary bone stores the minerals required for the formation of calcareous-rich eggshells (Kerschnitzki *et al.*, 2014). There is no current evidence that this bone exists in extant reptiles such as alligators and crocodiles, which implies that there is no definite evidence that a medullary bone existed in non-avian theropods or if it can be used for sexual determination (Schweitzer *et al.*, 2007). Also, the possibility of a medullary bone existing in a *Tyrannosaurus rex* (T.rex) does not yield reliable results as this is based on one specimen which is not sufficient evidence (Erickson *et al.*, 2005; Brusatte *et al.*, 2010). Another proxy suggested to identify the sex of a T.rex is a larger pelvic structure for females to allow eggs to pass through (Larson and Frey, 1992). The large distance between the ischial and first tail chevron shown in Fig. 6.1 below exists within the broad pelvic structure of the dinosaurs and crocodiles (Fischman, 1993).

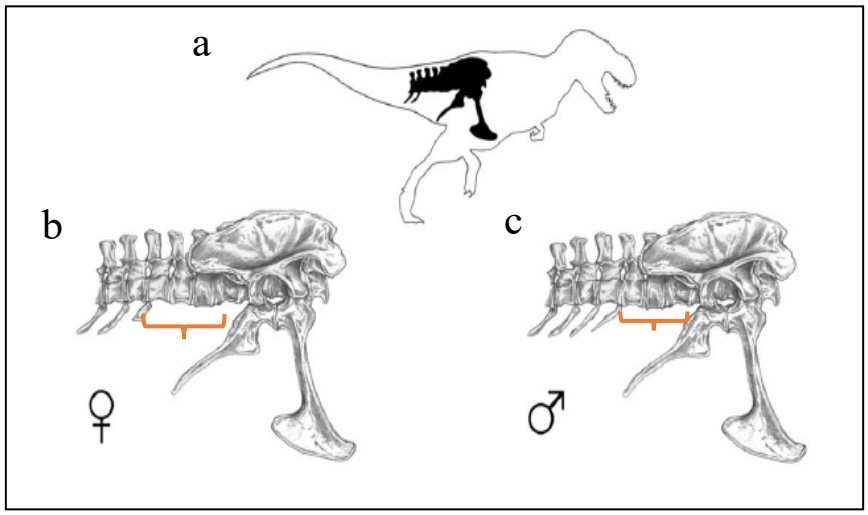


Figure 6.1: (a) Showing the position of the chevrons and pelvic bones in a *Tyrannosaurus rex.* **(b)** Female *Tyrannosaurus rex* caudal vertebrae and pelvic bones. Highlighted area indicating distance between first chevron and ischial **(c)** Male *Tyrannosaurus rex* caudal vertebrae and pelvic bones. Highlighted area indicating distance between first chevron and ischial. (Erickson *et al.*, 2005).

Modern crocodiles are the existing examples of Dinosauria as they are highly similar to Archosauria, non-avian dinosaurs (Erickson *et al.*, 2005; Brazaitis and Watanabe, 2011). Female crocodiles are said to have a larger gap between the ischial and the first chevron as well as the first chevron is shorter in females compared to males as shown in Fig. 6.2 below. Males have a longer first chevron to attach penile retractor muscles (Fischman, 1993; Erickson *et al.*, 2005).

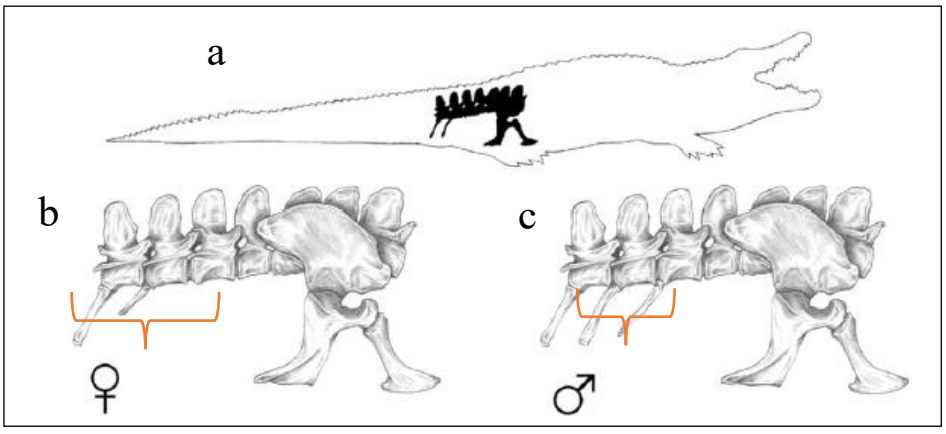


Figure 6.2: (a) Showing the position of the chevrons and pelvic bones in an *Alligator mississipiensis.* **(b)** Female *Alligator mississipiensis* caudal vertebrae and pelvic bones. Highlighted in orange indicates the distance between first chevron and ischial **(c)** Male *Alligator mississipiensis* caudal vertebrae and pelvic bones. Highlighted in orange shows the distance between first chevron and ischial. (Erickson *et al.*, 2005).

A study conducted by Erickson *et al.* (2005) focused on sex determination using the first chevron based on the various stages of the embryos of *Alligator mississipiensis* (Fig. 6.3). The variation between the males and females using chevron morphology was disproved by Erickson *et al.* (2005) as the males and females did not have definite differences in the position and size of the first chevron. This suggests that this is an inaccurate method for sex determination.

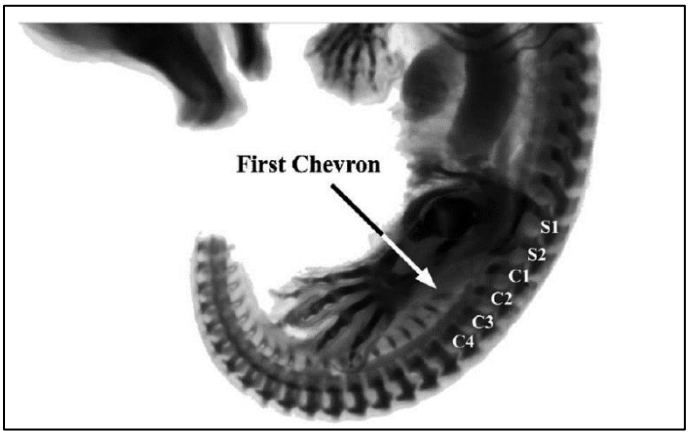


Figure 6.3: An embryo of an *Alligator mississipiensis* on day 26 in the egg (Erickson *et al*., 2005).

Anatomical features, such as horns, have been used as indicators for sexual dimorphism as can be seen in *Agujaceratops.* This dinosaur had horn cores positioned on the supraorbital with varying lengths and horn curvature which is suggested as a proxy for sex as shown below in Fig. 6.4 (Switek, 2012). It is suggested that females had shorter, more curved horns and males had longer horns as a predatory defence mechanism and courtship aid. The skull development of the fossil indicates age and sexual maturity (Lehman, 1990). Unfortunately, there is no definite evidence that the females have shorter curved horns and the males have longer horns which makes this study and proxy unreliable.

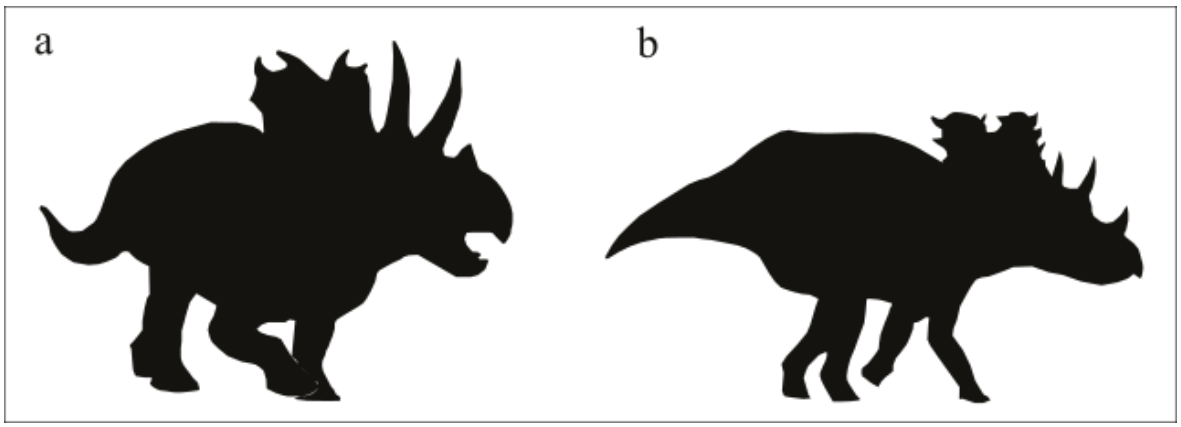


Figure 6.4: (a) Male *Agujaceratops* **(b)** Female *Agujaceratops*. Silhouettes modified from images on Dinosaurfact.net (2007).

Despite the proposed sex proxies, currently the only definite evidence that indicates the sex of fossils is the presence of eggs found within the pelvic cavity (Erickson *et al.*, 2005). A pair of oviraptorid eggs were found within the body cavity of a dinosaur in China (Fig. 6.5) (Erickson *et al.*, 2005). This is extremely rare and uncommon. If no eggs are present, it does not immediately imply that the dinosaur is male, but it may not have reached sexual maturation or was not pregnant at the time (Mallon, 2017). Hence there is a clear paucity of definite factors or metrics that can be widely used to determine sex in these extinct animals.

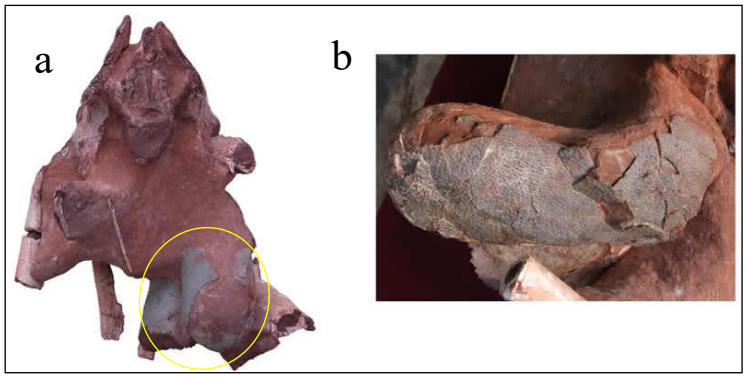


Figure 6.5: (a) Pair of eggs highlighted by the yellow circle attached to fossilised pelvis **(b)** Eggshell texture preserved (Images adapted from Cheng, 2005).

Ca is a bio-essential element in the body (Martin *et al.*, 2017). Females fractionate Ca differently when experiencing reproductive processes such as lactation or laying eggs (Tacail *et al.*, 2017). In lactating females, the body produces more ^{42}Ca as this is lighter isotopes moves through the mammary epithelium easier compared to heavier Ca isotopes (Tacail *et al.*, 2017). A study by Dacke *et al.* (2015) discussed the osteoderms in mature female alligators containing mature ova had a higher density compared to a nested mature female. This indicates the high production of Ca in the body required to lay eggs. In a study by Skulan and DePaolo (1999), the alligator eggshells were enriched in the light ^{40}Ca isotope over the heavier ^{44}Ca isotope. Eggshells, like breast milk, appear to utilise the lighter isotope from the producer's body (Skulan and DePaolo, 1999). These reproductive processes perturb the Ca levels in females and could influence the $\delta^{44/42}Ca$ values whereas the males do not experience these processes and could, therefore, have different $\delta^{44/42}Ca$ values (Martin *et al.*, 2017).

The purpose of this chapter is to determine if non-traditional $\delta^{44/42}Ca$ isotopes, as used in previous human lactation studies (Tacail *et al.*, 2017), can be utilised for sex determination in other animal systems such as modern egg-laying crocodiles, *Crocodylus niloticus.* And if so, can it be extended to dinosaurs and other extinct animals. Previous studies on humans have shown that Ca can be used

as a marker for sex determination, but can it be used to determine sex in dinosaur fossils such as *Massospondylus carinatus, Aardonyx celestae, Pulanesaura eocollum* and *Megapnosaurus rhodesiensis*? Isotope analyses of bone and teeth could provide a sex proxy or metric for extinct tetrapods as it has been shown to differentiate between the sexes of several extant animals (Jaouen *et al*., 2012; Tacail *et al*., 2017; Hassler *et al.*, 2021).

For ground-truthing, the modern animal study system used is modern crocodilians, particularly *Crocodylus niloticus.* This system was selected because of the readily available study specimens of known sex, the ease of sampling as it is easier to get teeth as crocodiles generate approximately eighty teeth per year and there is the presumed metabolic similarity to extinct reptilian outgroups such as dinosaurs (Pooley and Gans, 1961; Brazaitis and Watanabe, 2011). Crocodiles share a common ancestor with birds (and thus dinosaurs) that diverged about 250 Ma and have the slowest molecular rate change in vertebrates and least likely to differ in DNA from dinosaurs (Gee, 1998; Mohan, 2014).

6.3. Methodology

We analysed the dentition of 10 individual *Crocodylus niloticus* specimens being a mature female (n = 1), juvenile males (n = 5) and juvenile females (n = 4) (Table 6.1). The crocodile teeth samples were collected from an accredited crocodile farm as samples required a controlled environment where environmental variables are limited (e.g., different ecosystem with different resources). The crocodiles must be born in captivity and background information such as sex, age and diet are recorded. The specimens were kept in the ESI collection.

Table 6.1: *Crocodylus niloticus* specimens analysed in this study.

Female		Male	
Sample number	Age	Sample number	Age
Female E	42-years-old	Male 2 sample 2	2-3 years old
Female C sample 3	2-3 years old	Male 3 sample 1	
Female 17 sample 2		Male 5 sample 2	
Female 21 sample 3		Male 6 sample 2	
Female 28 sample 1		Male 7 sample 1	

Following sample collection, the samples were cleaned by placing the tooth in a jar of isopropanol and putting it in an ultrasonic bath for 2 mins to remove any impurities. Once this was done, the teeth were placed into a jar of Milli-Q and were ultrasonicated for 2 mins. The isopropanol and Milli-Q in the jars were discarded and replaced between washes. The samples were then wiped down. The adult female tooth was cut longitudinal to expose the enamel and dentine rings.

To prepare for microdrilling, the tooth samples were gently cleaned with ethanol and photographed. Microsampling of the tooth enamel of the juvenile specimens (Fig. 6.6a) was performed using a handheld 8200 Dremel microdrill with a 0.4 mm tungsten carbide bit and the adult tooth specimen was sampled using a MicroMill with a tungsten carbide drill bit (Fig. 6.6b) at École Normale Supérieure de Lyon (ENS; France). Ethanol was used to clean drill bits, the Dremel and surrounding workspace before and after drilling each sample.

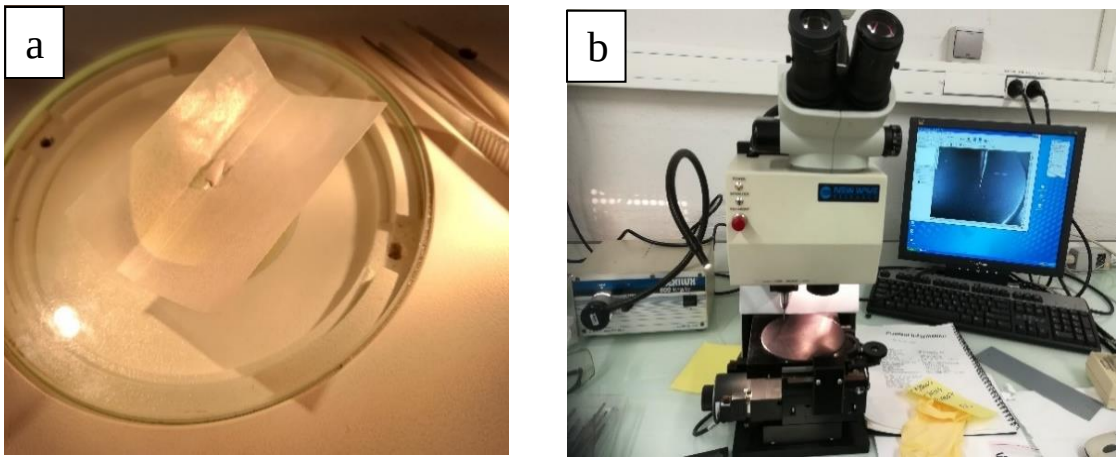


Figure 6.6: Sampling of *Crocodylus niloticus* teeth. **(a)** A juvenile tooth prepared for microsampling using the handheld Dremel. **(b)** The MicroMill used to sample the adult tooth (Female E).

Specimen Female E, the mature adult *Crocodylus niloticus*, was sampled longitudinally in nine spots creating a transect across the tooth (Fig. 6.7). This was done to sample the dentine rings of the tooth in order to determine if there were Ca patterns or cycles varying along the teeth as the tooth formed. The male and female juvenile specimens were sampled once to identify any possible $\delta^{44/42}$Ca isotope variations between the different sexes.

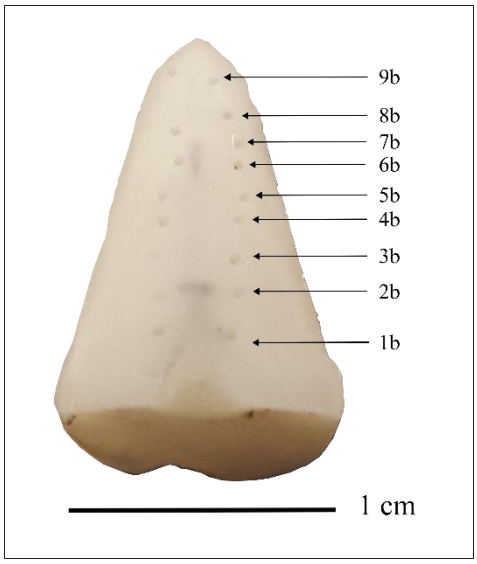


Figure 6.7: Specimen Female E with the labels indicating the 9 sample spots 1b to 9b from the bottom of the tooth to the top of the crown.

Once the microsampling was complete, the sample powders were weighed using a high-precision Mettler microbalance scale to ensure the acquired amount of ~400 µg was obtained. The sample powders were then transferred to polypropylene beakers to start the digestion process as mentioned in Chapter 3. Ion-exchange chromatography was performed on the tooth powder at the ENS following the modified method from Tacail *et al.* (2014) as mentioned in Table 3.6 and 3.7 of Chapter 3. The $\delta^{44/42}$Ca isotope values for all samples were measured using a ThermoScientific Neptune Plus MC-ICPMS at the ENS (Tacail *et al.*, 2014).

6.4. Results

The adult female samples have $\delta^{44/42}$Ca values ranging between -1.12 ‰ to -0.90 ‰ as shown in Fig. 6.7a. The juvenile female samples have a $\delta^{44/42}$Ca range of -1.14 ‰ to -0.82 ‰ while the juvenile male samples have a range of -1.09 ‰ to -0.81 ‰. The juvenile female samples yield a mean $\delta^{44/42}$Ca value of -0.93 ± 0.02 ‰ (n = 5) whereas the male samples yield a mean $\delta^{44/42}$Ca value of -0.92 ± 0.02 ‰ (n = 5) (Fig. 6.7b).

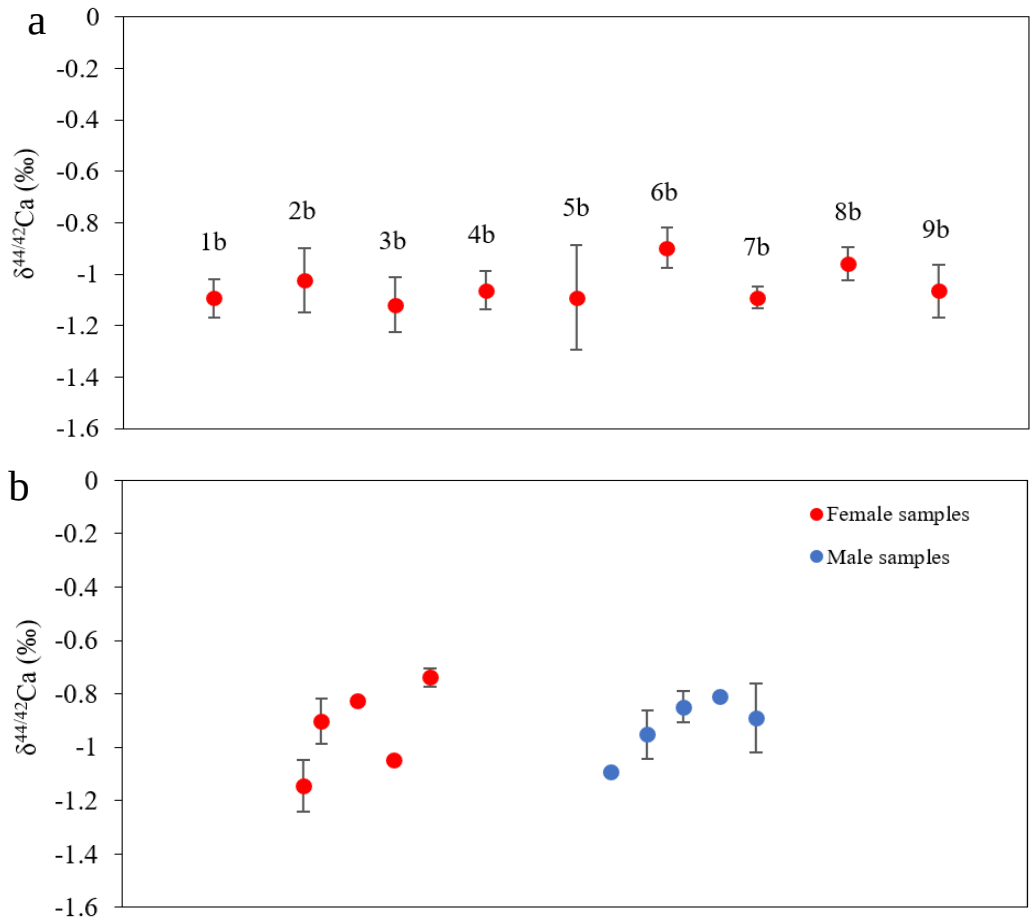


Figure 6.8: The $\delta^{44/42}$Ca (‰) difference between female and male *Crocodylus niloticus*. The scatter plots (red and blue points) display the $\delta^{44/42}$Ca (‰) values with the standard error (black lines) **(a)** The consecutive cross section sampling points are in the same range for Female E. **(b)** The male and female juvenile *Crocodylus niloticus* samples have $\delta^{44/42}$Ca (‰) values in the same range.

6.5. Discussion

The results produced in this chapter are accurate as the multiple measurements analysed from the adult female tooth, Female E, do not have any erratic variations (Fig. 6.8a). This can be indicative of instrumental accuracy and error of repeated measurements can be ruled out as there is no source of any relative $\delta^{44/42}$Ca value variations. The lack of relative $\delta^{44/42}$Ca variations show that there is no instrumental drift.

The multiple samples analysed from the adult female tooth specimen, Female E, displayed no distinct variations in the $\delta^{44/42}$Ca isotope values for the different rings analysed (Fig 6.8a). It is possible that the tooth may have been relatively new and could only be used as a geochemical marker for a short period of time of the specimen's life as crocodiles constantly replace teeth and can grow a new tooth in one to two months (Poole, 1960). If the tooth was there for a short period

of time, it may have not captured any isotope variations if there were no ova being produced or laying of eggs during the time of tooth formation (Dacke *et al.,* 2015). Crocodile's teeth are constantly being replaced and a relatively new tooth that may have formed out of the breeding and/or nesting season may not have varying $\delta^{44/42}$Ca values for females. The hard structure of tooth enamel may also make it difficult to record any fluctuations if a tooth has formed prior to breeding and/or nesting season (Hassler *et al.,* 2021). While the process of lactation in humans and sheep affect $\delta^{44/42}$Ca values, teeth may not be a successful marker for sex determination as this may need an 'active' marker that may only appear during the occurrence of lactation or egg laying (e.g. breast milk) (Tacail *et al.,* 2017; Reynard *et al.,* 2010).

The juvenile samples do not display any fluctuations or $\delta^{44/42}$Ca isotope differences for the different sexes (Fig. 6.8b). The male and female samples have $\delta^{44/42}$Ca values and ranges that overlap. It is possible that these samples did not reach sexual maturity, typically reached at 19 years old and, therefore, have not experienced any Ca fluctuations in the body resulting in any variations recorded during tooth formation (Cott, 1960; Warner *et al.,* 2016). It could also be that the fractionation of $\delta^{44/42}$Ca isotopes in the teeth does not differ for males and females. It is possible that Ca variations may only be observed in the osteoderms of females when containing ova (Dacke *et al.,* 2015).

Tracing $\delta^{44/42}$Ca isotope values in animals like crocodiles for sexing may be challenging compared to other lifestyle factors such as diet because the teeth are constantly being replaced. Experiments could be conducted during breeding and nesting season, to possibly identify any isotope differences between a pregnant or nesting female crocodile versus a male crocodile.

In terms of extending this technique to extinct fauna, a test could be conducted on a fossil that has dentary material and a gut cavity containing eggs. $\delta^{44/42}$Ca isotope analysis could be carried out on the tooth of the individual, eggshells as well as other individuals of the same species to identify any possible $\delta^{44/42}$Ca isotope differences.

6.6. Conclusion

Our results show that the non-traditional $\delta^{44/42}$Ca isotope method may not function as a successful proxy for sex determination as there were no $\delta^{44/42}$Ca isotopic differences observed for the different sexes of the same species. This study encountered limiting factors such as sample size from the same species, tooth replacement and reproductive age and processes. This pilot study could be further expanded by exploring the use of $\delta^{44/42}$Ca values of *Crocodylus niloticus* during the different stages of egg production and nesting. There is the potential to expand sample size to a variety of ages as well as to analyse osteoderms alongside teeth to further understand Ca

concentrations and fluctuations (Dacke *et al.*, 2015). It is possible that the $\delta^{44/42}$Ca values may not be reflective of the reproductive physiology but rather an inference from the surrounding environments and/or the diet.

7. Generalised Conclusion

This Ph.D. research highlights the methodology and applications of non-traditional $\delta^{44/42}$Ca isotopes. We can now separate ions more efficiently and ensure high-quality and reliable results are produced as seen in Chapter 3. The optimisation of the method allows for a quicker chemistry and enhanced throughput of samples. This is achieved by using columns with a wider diameter which allows acid to pass through the columns at a faster rate without compromising the ion separation procedure.

When conducting ion-exchange chromatography, it is important to ensure that the best lab practices and techniques are conducted to ensure high-quality data. Chapter 4 highlights the importance of leaching samples and controlling for diagenetic biases in samples as old as those from the Triassic–Jurassic period. We can control for diagenetic biases through leaching samples as old as those from the Triassic–Jurassic period. Leaching is an effective mean of removing secondary Ca precipitates and can allow corrections of unleached samples when attaining a good level of reliability and consistency. It is important to leach samples and avoid any producing biased results and that can lead to false $\delta^{44/42}$Ca absolute values. Another important lab practice is to ensure that samples are prepared and analysed in a timely manner to avoid sample ageing on Ca after ion-exchange chromatography and before mass spectrometry. Not considering these practices can produce incorrect $\delta^{44/42}$Ca values.

Chapter 5 reveals the application of $\delta^{44/42}$Ca isotopes for palaeodietary preferences in terrestrial ecosystems that are as deep in time as the Triassic-Jurassic period. $\delta^{44/42}$Ca isotopes can be used alongside other dietary proxies to characterise and conduct palaeoecological analysis. This allows for better understanding of population dynamics, dietary preferences and behaviours and trophic divisions of ancient animals. It is possible to identify herbivores, *Massospondylus* and *Aardonyx,* and carnivores, 'rauisuchians', and to further identify and differentiate the trophic levels that existed in the extinct Elliot ecosystem. Based on the $\delta^{44/42}$Ca values produced in this study, herbivorous animals that existed in the Elliot Formation are *Massospondylus, Aardonyx, Pulanesaura, Heterodontosaurus, Tritylodon, Scalenodontoides* and *Pachygenelus.* The carnivorous animals in the ecosystems were *Megapnosaurus* and 'rauisuchians'. Animals like *Lesothosaurus, Orthosuchus* and *Protosuchus* had more diverse diets such as omnivory and/or piscivory.

Resource partitioning within taxa could also be suggested by varying $\delta^{44/42}$Ca values between the same lineages. The difference between the $\delta^{44/42}$Ca values could contribute to the morphological diversity of the fossils. This is seen in the sauropodomorphs, *Massospondylus* and *Aardonyx,* as

well as in therapsids, *Tritylodon, Scalenodontoides* and *Pachygenelus,* where different body sizes co-existed and adapted to fill different niches.

Chapter 6 further tests the application of $\delta^{44/42}$Ca isotopes in reproductive physiology as Ca is an essential element in this process. Results produced in this study shows that there is no difference in the $\delta^{44/42}$Ca values between the different sexes of the same species. Further research can be done to understand the various stages and sexual maturity of modern taxa such as *Crocodylus niloticus.* Analysis can be done on the various stages such as juvenile, sexual maturity, breeding, ova prior to nesting and then in the nesting period. This will track the cycle of $\delta^{44/42}$Ca isotopes during these periods and compare it to that of male *Crocodylus niloticus.*

In summary, the research presented in this PhD has made a valuable contribution to further understanding the diverse palaeoecosystems of the Elliot Formation and the advancement of non-traditional $\delta^{44/42}$Ca isotopes in palaeoecological analysis.

8. Reference list

Abdala, F., Damiani, R., Yates, A. and Neveling, J. (2007). A non-mammaliaform cynodont from Upper Triassic of South Africa: a therapsid Lazarus taxon. *Palaeontologia Africana*, **42**, 17-23.

Albarède, F. (2015). Metal stable isotopes in the human body: a tribute of geochemistry to medicine. *Elements*, **11**, 265-269.

Apaldetti, C., Martinez, R.N., Cerda, I.A., Pol, D. and Alcober, O. (2018). An early trend towards gigantism in Triassic sauropodomorph dinosaurs. *Nature Ecology and Evolution*, **2**, 1227–1232.

Apaldetii, C., Pol. D., Ezcurra, M. D. and Martínez, R.N. (2021). Sauropodomorph evolution across the Triassic–Jurassic boundary: body size, locomotion, and their influence on morphological disparity. *Scientific Reports*, **11**, p.22534.

Bakker, R. T. (1987). Dinosaur feeding behaviour and the origin of flowering plants. *Nature*, **274**, 661-663.

Balter, V., Saliege, J. F., Bocherens, H. and Person, A. (2002). Evidence of Physico-chemical and isotopic modifications in archaeological bones during controlled acid etching. *Archaeometry*, **44**, 329-336.

Baron, M. G., Norman, D. B. and Barrett, P. M (2017). A new hypothesis of dinosaur relationships and early dinosaur evolution. *Nature*, **543**, 501-506.

Barrett P. M. (2000). Prosauropod dinosaurs and iguanas: speculations on the diets of extinct reptiles. In: Sues H-D, ed. Evolution of herbivory in terrestrial vertebrates: perspectives from the fossil record. Cambridge: Cambridge University Press, 4278.

Barrett, P. M. (2005). The diet of ostrich dinosaurs (Theropoda: Ornithomimosauria). *Palaeontology*, **48**, 347–358.

Barrett, P. M. (2014). Paleobiology of Herbivorous Dinosaurs. Annual Review of Earth and Planetary Science, **42**, 207-230.

Barrett, P. M., Butler, R. J., Yates, A. M., Baron, M. G. and Choiniere, J. N. (2016). New specimens of the basal ornithischian dinosaur *Lesothosaurus diagnosticus* Galton, 1978 from the Early Jurassic of South Africa, *Palaeontologia africana*, **50**, 48-63.

Battail, B (2005). Late Triassic traversodontids (Synapsida: Cynodontia) in southern Africa. *Palaeontologica Africana*, **41**, 67-80.

Benson, R. B. J. (2018). Dinosaur Macroevolution and Macroecology. *Annual Review of Ecology, Evolution, and Systematics*, **49**, 379-408.

Benson, R. B. J. and Godoy, P. L. (2019). Evolution: Much on the Menu for Ancient Crocs. *Current Biology Dispatches*, **29**, R683-R704.

Benton, M. J. (2007). *The Dinosauria.* University of California Press, US, 861pp.

Best, M. (2002). *Igneous and Metamorphic Petrology 2nd Edition.* Blackwell Publishing, UK, 729pp.

Bocherens, H., Brinkman, D. B., Dauphin, Y. and Mariotti, A. (1994). Microstructural and geochemical investigations on late Cretaceous archosaur teeth from Alberta, Canada. *Canadian Journal of Earth Sciences*, **31**, 783–792.

Bonaparte, J. F. and Crompton, A. W. (2018). Origin and relationships of the Ictidosauria to non-mammalian cynodonts and mammals, *Historical Biology,* **30**, 174-182.

Bordy, E., Abrahams, M., Sharman, G. R., Viglietti, P. A., Benson, R. B. J., McPhee, B. W., Barrett, P. M., Sciscio, L., Condon, D., Mundil, R., Rademan, Z., Jinnah, Z., Clark, J. M., Suarez, C. A., Chapelle, K. E. J. and Choiniere, J. N. (2020). A chronostratigraphic framework for the upper Stormberg Group: Implications for the Triassic-Jurassic boundary in southern Africa. *Earth-Science Reviews,* **203**, 1-24.

Bordy, E. M. (2021). Darting towards Storm Shelter: A minute dinosaur trackway from southern Africa. *South African Journal of Science,* **117**, 1-11.

Botha, J., Lee-Thorp, J. and Sponheimer, M. (2004). An Examination of Triassic Cynodont Tooth Enamel Chemistry Using Fourier Transform Infrared Spectroscopy. *Calcified Tissue International*, **74**, 162-169.

Botha, J., Choiniere, J.N. and Benson, R.B. (2022). Rapid growth preceded gigantism in sauropodomorph evolution. *Current Biology*, **32**, 4501-4507.

Botha-Brink, J. and Smith, R. M. H. (2011). Osteohistology of the Triassic archosauromorphs Prolacerta, Proterosuchus, Euparkeria, and Erythrosuchus from the Karoo Basin of South Africa. *Journal of Vertebrate Paleontology,* **31**, 1238-1254.

Brazaitis, P. and Watanabe, M. E. (2011). Crocodilian behavior: a window to dinosaur behavior. *Historical Biology*, **23**, 73-90.

Bristowe, A. and Raath, M. A. (2004). A juvenile coelophysoid skull from the Early Jurassic of Zimbabwe, and the synonymy of *Coelophysis* and *Syntarsus. Palaeontologia Africana*, **40**, 31-41.

Brusatte, S. L., Norell M. A., Carr, T. D., Erickson, G. M., Hutchinson, J. R., Balanoff, A. M., Bever, G. S., Choiniere, J. N., Makovicky, P. J. and Xu, X. (2010). Tyrannosaur Paleobiology: New Research on Ancient Exemplar Organisms. *Science*, **329**, 1481-1485.

Buffetaut, E. (1979). The Evolution of the Crocodilians. *Scientific American,* **241**, 130-145.

Butler, R. J., Porro, L. B. and Norman, D. B. (2008). A juvenile skull of the primitive ornithischian dinosaur *Heterodontosaurus tucki* from the 'Stormberg' of Southern Africa, *Journal of Vertebrate Palaeontology*, **28**, 702-711.

Button, D. J., Porro, L. B., Lautenschlager, S., Jones, M. E. H. and Barrett, P. M. (2023). Multiple pathways to herbivory underpinned deep divergences in ornithischian evolution. *Current Biology*, **33**, 557-565.

Cabreira, S. F., Kellner, A. W. A., Dias-da-Silva, S., da Silva, R. L., Bronzati, M., Marsola, J. C.

A., Müller, R. T., Bittencourt, J. S., Batista, B. J., Raugust, T., Carriho, R., Brodt, A. and Langer, M. C. (2016). A Unique Late Triassic Dinosauromorph Assemblage Reveals Dinosaur Ancestral Anatomy and Diet. *Current Biology*, **26**, 3090-3095.

Catuneanu, O., Wopfner, H., Eriksson, P. G., Cairncross, B., Rubidge, B. S., Smith, R. M. H. and Hancox, P. J., (2005). The Karoo basins of south-central Africa. *Journal of African Earth Sciences*, **43**, 211-253.

Cloudsley-Thompson, J.L. (2005). *Ecology and behaviour of Mesozoic reptiles*. Springer Science & Business Media, New York, 219pp.

Chapelle, K. E. J., Botha, J. and Choiniere, J. N. (2021). Extreme growth plasticity in the early branching sauropodomorph *Massospondylus carinatus. Biology Letters*, **17**, 1-6.

Chapelle, K. E. J. and Choiniere, J. N. (2018). A revised cranial description of *Massospondylus carinatus* Owen (Dinosauria: Sauropodomorpha) based on computed tomographic scans and a review of cranial characters for basal Sauropodomorpha. *PeerJ*, 1-84.

Chapman, R. E., Weishampel, D. B., Hunt, G. and Rasskin-Gutman, D. (1997). Sexual dimorphism in dinosaurs. *Dinofest International Proceedings*, 83-93.

Cheng, Y. (2005). Dinosaur eggs found whole in mother's belly. *New Scientist.* Available from: https://www.newscientist.com/article/dn7267-dinosaur-eggs-found-whole-in-mothers-belly/ (Accessed 04 April 2018).

Chinsamy, A. (1990). Physiological implications of the bone histology of Syntarsus Rhodesiensis (Saurischia: Therapoda). *Palaeontologia africana*, **27**, 77-82.

Chinsamy, A. and Barrett, P. M. (1997). Sex and old bones? *Journey of Vertebrate Paleontology*, **17**, 450-450.

Chinsamy, A., Chiappe, L. M., Marugán-Lobón, J., Chunlig, G. and Fengjiao, Z. (2013). Gender identification of the Mesozoic bird *Confuciusornis sanctus*. Nature communications, **4**, 1-5.

Close, R. A., Friedman, M., Lloyd, G. T. and Benson, R. B. J. (2015). Evidence for a Mid-Jurassic Adaptive Radiation in Mammals. *Current Biology*, **25**, 2137-2142.

Cott, H. B. (1960). Scientific results of an inquiry into the ecology and economic status of the Nile Crocodile (*Crocodilus niloticus*) in Uganda and Northern Rhodesia. *The Zoological Society of London*, **29**, 213-340.

Crompton, A. W. (1963). On the lower jaw of *Diarthrognathus* and the origin of the mammalian lower jaw. *Journal of Zoology*, **4**, 697-749.

Crompton, A. W. and Attridge, J. (1986). Masticatory apparatus of the larger herbivores during Late Triassic and Early Jurassic times. *The Beginning of the Age of the Dinosaurs*, pp.223-236.

Crompton, A. W. and Ellenberger, F. (1957). On a new cynodont from the Molteno beds and the origin of the Tritylodontids. *Annals of the South African museum*, **44**, 1-14.

Cuéllar-Cruz, M. and Moreno, A (2019). The Role of Calcium and Strontium as the Most Dominant Elements during Combinations of Different Alkaline Earth Metals in the Synthesis of Crystalline Silica-Carbonate Biomorphs. *Crystals*, **9**, 1-19.

Dacke, C. G., Elsey, R. M., Trosclair III, P. L., Sugiyama, T., Nevarez, J. G. and Schweitzer, M. H. (2015). Alligator osteoderms as a source of labile calcium for eggshell formation. *Journal of Zoology*, **297**, 255-264.

Dinosaur.net. (2007). Agujaceratops pictures and facts. *The Dinosaur Database*. Available from: http://dinosaurpictures.org/Agujaceratops-pictures (Accessed 01 April 2018).

Dodat, P.J., Tacail, T., Albalat, E., Gomez-Olivencia, A., Couture-Veschambre, A., Holliday, T., Madeline, S., Martin, J., Rmoultilova, R., Maureille, B, and Balter, V. (2020). Isotopic calcium biogeochemistry of MIS 5 fossil vertebrate bones: application to the study of the dietary reconstruction of Regourdou 1 Neandertal fossil. *Journal of Human Evolution*, **151**, 1-11.

Dollman, K. and Choiniere, J. N. (2022). Palate evolution in early-branching crocodylomorphs: Implications for homology, systematics, and ecomorphology. *The Anatomical Record*, **305**, 2766-2790.

Dollman, K. N., Viglietti, P. A. and Choiniere, J. N. (2019). A new specimen of *Orthosuchus stormbergi* (Nash 1968) and a review of the distribution of Southern African Lower Jurassic crocodylomorphs, *Historical Biology*, **31**, 653-664.

Enax, J., Fabritius, H. O., Rack, A., Prymak, O., Rabbe, D. and Epple, M. (2013). Characterization of crocodile teeth: Correlation of composition, microstructure, and hardness. *Journal of Structual Biology*, **184**, 155-163.

Erickson, G. M., Lappin, A. K. and Larson, P. (2005). Androgynous rex – The utility of chevrons for determining the sex of crocodilians and non-avian dinosaurs. *Zoology*, **108**, 277-286.

Farkaš, J. (2018). *Calcium Isotopes. I*n: White, W.M. (eds) Encyclopedia of Geochemistry. Encyclopedia of Earth Sciences Series. Springer, New York, 181-186 pp.

Fastovsky, D. E. (2000). Dinosaur architectural adaptations for a gymnosperm-dominated world. In: Gastaldo, R. A. and DiMichele, W. A. (eds.). Phanerozic Terrestrial Ecosystems. *Paleontological Society Papers*, **6**, 183–207.

Fischman, J. (1993). To Sex a T. rex. *Science*, **262**, 846-846.

Fisher, D. C. (1981). Crocodilian scatology, microvertebrate concentrations, and enamel-less teeth. *Paleobiology*, **7**, 262-275.

Fox, C. P., Whiteside, J. H., Olsen, P. E., Cui, X., Summons, R. E., Idiz, E. and Grice, K. (2022). Two-pronged kill mechanism at the end-Triassic mass extinction. *Geology*, **50**, 448-453.

Gaetano, L. C., Abdala, F. and Govender, R. (2017). The postcranial skeleton of the Lower Jurassic Tritylodon longaevus from Southern Africa. *Ameghiniana*, **54**, 1–35.

Gee, H. (1998). Birds and dinosaurs- the debate is over. *Nature*, **10**, 1-5.

Gee, C. T. (2011). *Biology of the sauropod dinosaurs: understanding the life of giants*. Indiana University Press, Bloomington, 34-56pp.

Gow, C. E. (2001). A partial skeleton of the tritheledontid *Pachygenelus* (Therapsida: Cynodontia). *Palaeontologia africana*, **37**, 93-97.

Gow, C. E. and Hancox, P. J. (1993). First complete skull of the Late Triassic *Scalenodontoides* (reptilia cynodontia) from Southern Africa, *New Mexico Museum of Natureal History & Science Bulletin*, **3**, 161-168.

Gow, C. E., Kitching, J. W. and Raath, M. A. (1990). Skulls of the prosauropod dinosaur *Massospondylus Carinatus* Owen in the collections of the Bernard Price Institute for palaeontological research. *Palaeontologia Africana,* **27**, 45-58.

Hassler, A., Martin, J. E., Amiot, R., Tacail, T., Arnaud Godet, F., Allain, R. and Balter, V. (2018). Calcium isotopes offer clues on resource partitioning among Cretaceous predatory dinosaurs. *Proceedings of the Royal Society Biology,* **285**, 1-8.

Hassler, A., Martin, J. E., Ferchaud, S., Grivault, D., Le Goff, S., Albalat, E., Hernandez, J, Tacail, T and Balter, V. (2021). Lactation and gestation controls on calcium isotopic compositions in a mammalian model. *Metallomics*, **13**, 1-14.

Hassler, A., Martin, J. E., Merceron, G., Garel, M. and Balter, V. (2021). Calcium isotopic variability of cervid bioapatite and implications for mammalian physiology and diet. *Palaeogeography, Palaeoclimatology, Palaeoecology,* **573**, 1-14.

Hautmann, M. (2012). Effect of end-Triassic CO_2 maximum on carbonate sedimentation and marine mass extinction. *Facies,* **50,** 257-261.

Heuser, A., Tutken, T., Gussone, N. and Galer, S. J. G. (2011). Calcium isotopes in fossil bones and teeth – Diagenetic versus biogenic origin. *Geochimica et Cosmochimica Acta*, **75**, 3419-3433.

Higgins, P. (2018). *Methods in Paleoecology*: *Reconstructing Cenozoic Terrestrial Environments and Ecological Communities.* Springer International Publishing AG, New York, 410pp.

Hindshaw, R. S., Reynolds, B. C., Wiederhold, J. G., Kiczka, M., Kretzschmar, R. and Bourdon, B. (2013). Calcium isotope fractionation in alpine plants. *Biogeochemistry*, **112**, 373-388.

Hoefs, J. (2015). *Stable Isotope Geochemistry*. Springer, New York, 389pp.

Hoppert, M. (2011). Metalloenzymes. In: Reitner J., Thiel V. (eds) Encyclopedia of Geobiology. Encyclopedia of Earth Sciences Series. Springer, Dordrecht.

Hull, P. (2015). Life in the Aftermath of Mass Extinctions. *Current Biology,* **25**, 941-952.

Hutton, J. M. (1987). Growth and Feeding Ecology of the Nile Crocodile Crocodylus niloticus at Ngezi, Zimbabwe. *Journal of Animal Ecology,* **56**, 25-38.

Irmis, R. B. (2010). Evaluating hypotheses for the early diversification of dinosaurs. *Earth and Environmental Science Transactions of the Royal Society of Edinburgh*, **101**, 397-426.

Irmis, R. B., Nesbitt, S. J. and Sues, H.D. (2013). Early Crocodylomorpha. *Anatomy, Phylogeny and Palaeobiology of Early Archosaurs and their Kin*. Geological Society, London, Special Publications, **379**, 275–302.

Jaouen, K., Balter, V., Herrscher, E., Lamboux, A., Telouk, P. and Albarède, F. (2012). Fe and Cu Isotopes in Archeological Human Bones and the Their Relationship to Sex. *American Journal of Physical Anthropology,* **148**, 334-340.

Jaouen, K., Balter, V., Herrscher, E., Lamboux, A., Telouk, P., Universite, D. L. and Lyon, I. (2012). *Fe and Cu Stable Isotopes in Archeological Human Bones and Their Relationship to Sex*. **340**, 334–340.

Kartzinel, T. R., Chen, P. A., Coverdale, T. C., Erickson, D. L., John Kress, W., Kuzmina, M. L., Rubenstein, D. I., Wang, W. and Pringle, R. M. (2015). DNA metabarcoding illuminates dietary niche partitioning by African large herbivores. *Proceedings of the National Academy of Sciences of the United States of America*, **112**, 8019-8024.

Kemp, T. S. (2006). The origin and early radiation of the therapsid mammal-like reptiles: a palaeobiological hypothesis. *Journal of Evolutionary Biology*, **19**, 1231-1247.

Kerschnitzki, M., Zandr, T. Zaslansky, P. Fratzl, P., Shahar, R. and Wagermaier, W. (2014). Rapid alterations of avian medullary bone material during the daily egg-laying cycle. *Bone*, **69**, 109-117.

Kitching, J. W. and Raath, M. A. (1984). Fossils from the Elliot and Clarens Formations (Karoo sequence) of the Northeastern Cape, Orange Free State and Lesotho, and a suggested biozonation based on tetrapods. *Palaeontologia Africana*, **25**, 111-125.

Knoll, F. (2004). Review of the tetrapod fauna of the "Lower Stormberg Group" of the main Karoo Basin (southern Africa): implication for the age of Lower Elliot Formation. *Bulletin de la Société géologique de France*, **175**, 73-83.

Knoll, F. (2005). The tetrapod fauna of the Upper Elliot and Clarens formations in the main Karoo Basin (South Africa and Lesotho). *Bulletin de la Société géologique de France*, **176**, 81-91.

Knudson, K. J., Williams, H. M., Buikstra, J., Tomczak, P. D., Gordon, G. W. and Anbar, A. D. (2010). Introducing $\delta^{88/86}$Sr analysis in archaeology: a demonstration of the utility of strontium isotope fractionation in paleodietary studies. *Journal of Archaeological Science*, **37**, 2352-2364.

Koutamanis, D., Roberts, G.L. and Dosseto, A. (2021). Inter-and intra-individual variability of calcium and strontium isotopes in modern Tasmanian wombats. *Palaeogeography, Palaeoclimatology, Palaeoecology*, **574**, 1-13.

Kovács, E. B., Ruhl, M., Demény, A., Fórizs, I., Hegyi, I., Horváth-Kostka, Z. R., Móricz, F, Vallner, Z. and Pálfy, J. (2020). Mercury anomalies and carbon isotope excursions in the western Tethyan Csővár section support the link between CAMP volcanism and the end-Triassic extinction. *Global and Planetary Change*, **194**, 1-17.

Kutty, T. S., Chatterjee, S., Galton, P. M. and Upchurch, P. (2007). Basal sauropodomorphs (dinosauria: saurischia) from the Lower Jurassic of India: Their anatomy and relationships. *Journal of Palaeontology*, **81**, 1218-1240.

Larson, P. L. and Frey, E. (1992). Sexual dimorphism in the abundant Upper Cretaceous theropod, Tyrannosaurus rex. *Journal of Vertebrate Paleontology*, **12**, 38.

Lehman, T. M. (1990). The ceratopsian subfamily Chasmosaurinae: sexual dimorphism and systematics. In: Carpenter, K., Currie, P. J. (Eds.), Dinosaur Systematics: Approaches and Perspectives. Cambridge University Press, Cambridge, pp. 211-229.

Lillywhite, H. B. (2014). *How Snakes Work. Structure, Function, and Behavior of the World's*

Snakes. Oxford University Press, New York, 227pp.

Longrich, N. R. and Field, D. J. (2012). Torosaurus is not Triceratops: Ontogeny in Chasmosaurine Ceratopsids as a Case Study in Dinosaur Taxonomy. *PlOS ONE*, **7**, 1-10.

Lucas, J., Lucas, P., Le Mercier, T., Rollat, A. and Davenport, W. (2015). Rare Earths. *Elsevier,* 370pp.

Maclaren, J. A., Anderson, P. S. L., Barrett, P. M. and Rayfield, E. J. (2017). Herbivorous dinosaur jaw disparity and its relationship to extrinsic evolutionary drivers. *Paleobiology*, **43**, 15–33.

Makin, D. F., Chamaillé-Jammes, S. and Shrader, A. M. (2017). Herbivores employ a suite of antipredator behaviours to minimize risk from ambush and cursorial predators. *Animal Behaviour*, **127**, 225-231.

Mallon, J. C. (2017). Recognizing sexual dimorphism in the fossil record: lessons from nonavian dinosaurs. *Paleobiology*, **3**, 495-507.

Mannion, P. D. (2009). Review and analysis of African sauropodomorph dinosaur diversity. *Palaeontologica Africana*, **44**, 108-111.

Martin, J. E., Tacail, T. and Balter, V. (2017). Non-traditional isotope perspectives in vertebrate palaeobiology. *Palaeontology*, **60**, 1-18.

Martin, J. E., Tacail, T., Cerling, T. E. and Balter, V. (2018). Calcium isotopes in enamel of modern and Plio-Pleistocene East African mammals. *Earth and Planetary Science Letters*, **503**, 227-235.

Martin, J. E., Hassler, A., Montagnac, G., Therrien, F. and Balter, V. (2022). The stability of dinosaur communities before the Cretaceous-Paleogene (K-Pg) boundary: A perspective from southern Alberta using calcium isotopes as a dietary proxy. *GSA Bulletin 2022*, 1-13.

McCarthy, T. and Rubidge, B. (2005). *Earth and Life.* Struik Nature, South Africa, 333pp.

McPhee, B. W., Benson, R. B. J., Botha-Brink, J., Bordy, E. M. and Choiniere, J. N. (2018). A Giant Dinosaur from the Earliest Jurassic of South Africa and the Transition to Quadrupedality in Early Sauropodomorphs. *Current Biology*, **28**, 3143-3151.

McPhee, B. W., Bonnan, M. F., Yates, A. M., Neveling, J. and Choiniere, J. N. (2015). A new basal sauropod from the pre-Toarcian Jurassic of South Africa: evidence of niche-partitioning at the sauropodomorph-sauropod boundary? *Scientific reports*, **5**¸ 1-12.

McPhee, B. W., Bordy, E. M., Sciscio, L. and Choiniere, J. N. (2017). The sauropodomorph biostratigraphy of the Elliot Formation of southern Africa: Tracking the evolution of Sauropodomorpha across the Triassic–Jurassic boundary. *Acta Palaeontologica Polonica*, **62**, 441-465.

McPhee, B. W. and Choiniere, J. N. (2016). A hyper-robust sauropodomorph dinosaur ilium from the Upper Triassic-Lower Jurassic Elliot Formation of South Africa: Implications for the functional diversity of basal Sauropodomorph. *Journal of African Earth Sciences*, **123**, 177-184.

Melstrom, K. and Irmis, R. B. (2019). Repeared Evolution of Herbivorous Crocodyliforms during the Age of Dinosaurs. *Current Biology Report*, **29**, 2389-2395.

Moczek, A. P. and Emlen, D. J. (2000). Male horn dimorphism in the scarab beetle, *Onthophagus taurus*: do alternative reproductive tactics favour alternative phenotypes? *Animal Behaviour*, **59**, 459-466.

Mohan, G. (2014). When it comes to DNA, crocodiles and birds flock together. *Los Angeles Times.* Available from: http://www.latimes.com/science/sciencenow/la-sci-sn-crocodile-bird-genome-20141212-story.html (Accessed 05 May 2018).

Morgan, J. L. L., Skulan, J. L., Gordon, G. W., Romaniello, S. J., Smith, S. M. and Anbar, A. D. (2012). Rapidly assessing changes in bone material balance using natural stable calcium isotopes. *Proceedings of the National Academy of Sciences of the United States of America*., **109**, 9989-9994.

Muchlinski, M. N., Wible, J. R., Corfe, I., Sullivan, M. and Grant, R. A. (2020). Good Vibrations: the evolution of whisking in small mammals. Anat Rec (Hoboken), **1**, 89-99.

Mujal, E., Foth, C., Maxwell, E. E., Seegis, D. and Schoch, R. R. (2022). Feeding habits of the Middle Triassic pseudosuchian *Batrachotomus kupferzellensis* from Germany and palaeoecological implications for archosaurs. *Palaeontology*, **65**, 1-31.

Müller, R. T. and Garcia, M. S. (2020). A paraphyletic 'Silesauridae' as an alternative hypothesis for the initial radiation of ornithischian dinosaurs. *Biology Letters*, **16**, 1-5.

Munyikwa, D. and Raath, M. A. (1999). Further material of the Ceratosaurian dinosaur *Syntarsus* from the Elliot Formation (Early Jurassic) of South Africa, *Palaeontologia Africana*, **35**, 55-59.

Nakazawa, T., Ohba, S. and Ushio, M. (2013). Predator–prey body size relationships when predators can consume prey larger than themselves. *Biology Letters*, **9**, 1-5.

Nash, D. (1968). A crocodile from the Upper Triassic of Lesotho. *Journal of Zoology London*, **156**, 163-179.

Nesbitt, S. J., Brusatte, S. L., Desojo, J. B., Liparini, A., De Franca, M. A. G., Weinbaum, J. C. and Gower, D. J. (2013). Rauisuchia. *Geological Society London Special Publications*, **379**, 241-274.

Nitzsche, K.N., Wakaki, S., Yamashita, K., Shin, K.C., Kato, Y., Kamauchi, H. and Tayasu, I., (2022). Calcium and strontium stable isotopes reveal similar behaviors of essential Ca and nonessential Sr in stream food webs. *Ecosphere*, **13**, p.e3921.

Norman, D. B., Crompton, A. W., Butler, R. J., Porro, L. B. and Charig, A. J. (2011). The Lower Jurassic ornithischian dinosaur *Heterodontosaurus tucki* Crompton & Charig, 1962: cranial anatomy, functional morphology, taxonomy, and relationships. *Zoological Journal of the Linnean Society*, **163**, 182-276.

Norman, D. B. and Weishampel, D. B. (1991). Feeding mechanisms in some small herbivorous dinosaurs: processes and patterns. In Rayner MV, Wootton RJ, eds. Biomechanics in evolution. Cambridge: Cambridge University Press, 161-182.

Owen, R. (1884). On the Skull and Dentition of a Triassic Mammal (*Tritylodon longaevus*, Owen) from South Africa. *Quarterly Journal of the Geological Society*, **40**, 146-152.

Owen-Smith, R. N. (1988). Megaherbivores- The influence of very large body size on ecology. Cambridge University Press, New York, 369.

Owen-Smith, N., Martin, J. and Yoganand, K. (2015). Spatially nested niche partitioning between syntopic grazers at foraging arena scale within overlapping home ranges. *Ecosphere,* **6**, 1-17.

Petrie, M., Halliday, T. and Sanders, C. (1991). Peahens prefer peacocks with elaborate trains. *Animals Behaviour,* **41**, 323-331.

Poole, D. F. G. (1960). Notes on tooth replacement in the Nile crocodile *Crocodylus niloticus. Proceedings of the Zoological Society of London,* **136**, 131-140.

Pooley, A. C. and Gans, C. (1976). The Nile Crocodile. *Scientific American,* **234**, 114-125.

Popowics, T. E. and Fortelius, M. (1997). On the cutting edge: Tooth blade sharpnessin herbivorous and faunivorous mammals. *Annales Zoologici Fennici,* **34**, 73-88.

Porro, L. B., Butler, R. J., Barrett, P. M., Moore-Fay, S. and Abel, R. L. (2011). New heterodontosaurid specimens from the Lower Jurassic of southern Africa and the early ornithischian dinosaur radiation. *Earth and Environmental Science Transactions of the Royal Society of Edinburgh,* **101**, 351-366.

Raath, M. A. (1969). A new coelurosaurian dinosaur from the Forest Sandstone of Rhodesia. *National Museums of Southern Rhodesia, Arnoldia,* **4**, 1-25.

Radermacher, V. J., Fernandez, V., Schachner, E. R., Butler, R. J., Bordy, E. M., Hudgins, M. N., de Klerk, W. J., Chapelle, K. E. J. and Choiniere, J. N. (2021). A new *Heterodontosaurus* specimen elucidates the unique ventilatory macroevolution of ornithischian dinosaurs. *Evolutionary Biology,* **10**, 1-39.

Rauhut O.W., Fechner R. E., Remes K. R. and Reis K.A. (2011). How to get big in the Mesozoic: the evolution of the sauropodomorph body plan. Biology of the sauropod dinosaurs: Understanding the life of giants. Indiana University Press, 119-49.

Reynard, L. M., Henderson, G. M. and Hedges, R. E. M. (2010). Calcium isotope ratios in animal and human bone. *Geochimica et Cosmochimica,* **74**, 3735-3750.

Reynard, L. M., Henderson, G. M. and Hedges, R. E. M. (2011). Calcium isotopes in archaeological bones and their relationship to dairy consumption. *Journal of Archaeological Science,* **38**, 657-664.

Reynard, B. and Balter, V. (2014). Trace elements and their isotopes in bones and teeth: Diet, environments, diagenesis, and dating of archeological and paleontological samples. *Palaeogeography, Palaeoclimatology, Palaeoecology,* **416**, 4-16.

Roopnarine, P. D. and Angielczyk, K. D. (2015). Community stability and selective extinction during the Permian-Triassic mass extinction. *Palaeoecology,* **350**, 90-93.

Russell, W. A., Papanastassiou, D. A. and Tombrello, T. A. (1978). Ca isotope fractionation on the Earth and other solar system materials. *Geochim. et Cosmochim. Acta.,* **42**, 107.

Ruta, M., Botha-Brink, J., Mitchell, S. A. and Benton, M. J. (2013). The radiation of cynodonts and the ground plan of mammalian morphological diversity. *Proceedings of the Royal Society Biology,* **280**, 1-10.

Salgado, L., Canudo, J. I., Garrido, A. C., Moreno-Azanza, M., Martinez, L. C. A., Coria, R. A. and Gasca, J. M. (2017). A new primitive Neornithischian dinosaur from the Jurassic of Patagonia with gut contents. *Nature Scientific Reports*, **7**, 1-10.

Sanders, P. M. (1997). Teeth and jaws. *Encyclopedia of dinosaurs*, pp.717-725.

Schoepfer, S. D., Algeo, T. J., van de Schootbrugge, B. and Whiteside, J. H. (2022). The Triassic-Jurassic transition – A review of environmental change at the dawn of modern life. *Earth-Science Reviews*, **232**, 104099.

Schönbächler, M. and Fehr, M. A. (2013). Basics of Ion Exchange Chromatography for Selected Geological Applications. Treatise on Geochemistry 2nd Edition, 124-144.

Sciscio, L. and Bordy, E. M. (2016). Palaeoclimatic conditions in the Late Triassic-Early Jurassic of southern Africa: A geochemical assessment of the Elliot Formation. *Journal of African Earth Sciences*, **119**, 102–119.

Sciscio, L., Bordy, E. M. and Head, H. V. (2020). A Late Triassic aquatic community: *Undichna*-like and related swimming traces from a freshwater pond in the lower Elliot Formation of South Africa. *Journal of African Earth Sciences*, **172**, 1-27.

Sciscio, L., Knoll, F., Bordy, E. M., de Kock, M. O. and Redelstorff, R. (2017). Digital reconstruction of the mandible of an adult *Lesothosaurus diagnosticus* with insight into the tooth replacement process and diet, *PeerJ*, **3054**, 1-20.

Schweitzer, M. H., Elsey, R. M., Dacke, C. G., Horner, J. R. and Lamm, E. T. (2007). Do egg-laying crocodilian (*Alligator mississipiensis*) archosaurs form medullary bone? **40**, 1152-1158.

Senter, P. (2007). Necks for sex: sexual selection as an explanation for sauropod dinosaur neck elongation. *Journal of Zoology*, **271**, 45-53.

Sereno, P. C. (2012). Taxonomy, morphology, masticatory function and phylogeny of heterodontosaurid dinosaurs. *Zookeys*, **226**, 1-225.

Skulan, J. and DePaolo, D. J. (1999). Calcium isotope fractionation between soft and mineralized tissues as a monitor of calcium use in vertebrates. *Proceedings of the National Academy of Sciences of the United States of America*, **96**, 13709-13713.

Skulan, J., DePaolo, D. J. and Owens, T. L. (1997). Biological control of calicum isotopic abundances in the global calcium cycle. *Geochimica et Cosmochimica Acta*, **61**, 2505-2510.

Smith, R. and Kitching, J. (1997). Sedimentology and vertebrate taphonomy of the *Tritylodon* Acme Zone: a reworked palaeosol in the Lower Jurassic Elliot Formation, Karoo Supergroup, South Africa. *Palaeogeography, Palaeoclimatology, Palaeoecology*, **131**, 29-50.

Switek, B. (2012). A is for Agujaceratops. Smithsonian.com. Available from: https://www.smithsonianmag.com/science-nature/a-is-for-agujaceratops-73226937/ (Accessed 04 April 2018).

Tacail, T., Albalat, E., Telouk, P. and Balter, V. (2014). A simplified protocol for measurement of Ca isotopes in biological samples. *Journal of Analytical Atomic Spectrometry*, **29**, 529–535.

Tacail, T., Télouk, P. and Balter, V. (2015). Precise analysis of calcium stable isotope variations in biological apatites using laser ablation MC-ICPMS. *Journal of Analytical Atomic Spectrometry.,* **31**, 152-162.

Tacail, T., Thivichon-Prince, B., Martin, J. E., Charles, C., Viriot, L. and Balter, V. (2017). Assessing human weaning practices with calcium isotopes in tooth enamel. *Proceedings of the National Academy of Sciences of the United States of America*., **114**, 6268-6273.

Tacail, T., Le Houedec, S. and Skulan, J. L. (2020). New frontiers in calcium stable isotope geochemistry: Perspectives in present and past vertebrate biology. *Chemical Geology*, **537**, 1-13.

Tolchard, F., Nesbitt, S. J., Desojo, J. B., Viglietti, P., Butler, R. J. and Choiniere, J, N. (2019). 'Rauisuchian' material from the lower Elliot Formation of South Africa and Lesotho: Implications for Late Triassic biogeography and biostratigraphy. *Journal of African Earth Sciences,* **160**, 1-13.

Tutken, T., Hellmund, M. and Galer, S. J. G. (2018). Diet and trophic level reconstruction of extinct avian and non-avian dinosaurs using Ca isotopes.

Warner, J. K., Combrink, X., Calverley, P., Champion, G. and Downs, C. T. (2016). Morphometrics, sex ratio, sexual size dimorphism, biomass, and population size of the Nile crocodile (*Crocodylus niloticus*) at its southern range limit in KwaZulu Natal, South Africa. *Zoomorphology,* **135**, 511-521.

Wink, C. S., Elsey, R. M. and Hill, E. M. (1987). Changes in Femoral Robusticity and Porosity During the Reproductive Cycle of the Female Alligator (*Alligator mississippiensis*). *Journal of Morphology,* **193**, 317-321.

Viglietti, P.A., McPhee, B. W., Bordy, E. M., Sciscio, L., Barrett, P. M., Benson R. B. J., Wills, S., Chapelle, Tolchard, F. and Choiniere, J. N. (2020). Biostratigraphy of the *Scalenodontoides* Assemblage Zone (Stormberg Group, Karoo Supergroup), South Africa. *South African Journal of Geology,* **123**, 239-248.

Viglietti, P.A., McPhee, B. W., Bordy, E. M., Sciscio, L., Barrett, P. M., Benson R. B. J., Wills, S., Chapelle, K. E. J., Dollman, K. N., Mdekazi, C. and Choiniere, J. N. (2020). Biostratigraphy of the *Massospondylus* Assemblage Zone (Stormberg Group, Karoo Supergroup), South Africa. *South African Journal of Geology,* **123**, 249-262.

Yates, A. M. and Barrett, P. M. (2010). *Massospondylus carinatus* Owen 1854 (Dinosauria: Sauropodomorpha) from the Lower Jurassic of South Africa: Proposed conservation of usage by designation of neotype. *Palaeontologia africana.,* **45**, 7-10.

Yates, A. M., Bonnan, M. F., Neveling, J., Chinsamy, A. and Blackbeard, M. G. (2010). A new transitional sauropodomorph dinosaur from the Early Jurassic of South Africa and the evolution of sauropod feeding and quadrupedalism. *Proceedings of the Royal Society,* **277**, 787-794.

Yates, A. M., Bonnan, M. F. and Neveling, J. (2011). A new basal sauropodomorph dinosaur from the Early Jurassic of South Africa. *Journal of Vertebrate Palaeontology,* **31**, 610-625.

Zanno, L. E. and Makovicky, P. J. (2011). Herbivorous ecomorphology and specialization patterns in theropod dinosaur evolution. *Proceedings of the National Academy of Sciences of the United States of America*., **108**, 232-237.

Appendix

Appendix A

BIOLOGY LETTERS

Tracing diet in Mesozoic archosaurs and dinosaurs of the Elliot Formation, South Africa using Ca isotopes

Journal:	*Biology Letters*
Manuscript ID	Draft
Article Type:	Research
Date Submitted by the Author:	n/a
Complete List of Authors:	Davechand, Priyanka; University of the Witwatersrand Johannesburg, School of Geosciences Hassler, A. Bybee, Grant; University of the Witwatersrand Johannesburg School of Geosciences Choiniere, Jonah; University of the Witwatersrand Johannesburg, Evolutionary Studies Institute Martin, Jeremy Pochat-Cottilloux, Yohan; ENS de Lyon Balter, Vincent
Subject:	Palaeontology < BIOLOGY, Ecosystem < BIOLOGY
Categories:	Palaeontology
Keywords:	diet, Mesozoic, archosaurs, dinosaurs, Ca isotopes, fossils

SCHOLARONE™
Manuscripts

Author-supplied statements

Relevant information will appear here if provided.

Ethics

Does your article include research that required ethical approval or permits?:
Yes

Statement (if applicable):
Heritage permission to work on the selected fossil specimens was obtained from the South African Heritage Resource Agency (SAHRA) (Permit ID: 3210).

Data

It is a condition of publication that data, code and materials supporting your paper are made publicly available. Does your paper present new data?:
Yes

Statement (if applicable):
The data is provided in the supplementary material uploaded.

Conflict of interest

I/We declare we have no competing interests

Statement (if applicable):
CUST_STATE_CONFLICT :No data available.

For Review Only

Tracing diet in Mesozoic archosaurs and dinosaurs of the Elliot Formation, South Africa using Ca isotopes

P. DAVECHAND[1], A. HASSLER[2], G.M. BYBEE[1], J.N. CHOINIERE[1], J.E. MARTIN[2], Y. POCHAT-COTTILLOUX[2], V. BALTER[2]

[1]Univ. of the Witwatersrand; 831772@students.wits.ac.za, grant.bybee@wits.ac.za, jonah.choiniere@wits.ac.za
[2]Univ. Lyon 1, ENS de Lyon; auguste.hassler@ens-lyon.fr, jeremy.martin@ens-lyon.fr, yohan.pochat-cottilloux@univ-lyon1.fr, vincent.balter@ens-lyon.fr

Abstract:

Inferring the diets of extinct animals is challenging. Direct dietary evidence such as gut contents is rare, necessitating the use of proxy data, e.g. dental morphology. The nature of these proxies limits their application to trophic difference reconstruction in ancient ecosystems, such as predator-prey relationships, leaving fundamental feeding ecology questions unanswered.

Stable isotope studies address these shortcomings but traditional methods using carbon and oxygen are susceptible to diagenetic biases during fossil preservation and require large amounts of material. Studies show that non-traditional calcium (Ca) isotopes are useful for understanding dietary preferences in modern and Cretaceous settings and require minimally invasive sample amounts.

Here we report the use of Ca isotopes in deeper time to infer palaeodiet aspects of dinosaurs and archosaurs in the Elliot Formation (Karoo Supergroup, South Africa). We find significant differences between $\delta^{44/42}$Ca values of large carnivorous pseudosuchians ('rauisuchians'; -0.45 ‰ to -1.17 ‰) and co-occurring herbivorous sauropodomorph genera (-0.26 ‰ to -0.69 ‰).

Our results highlight the role of non-traditional $\delta^{44/42}$Ca isotopes to understand trophic structures by distinguishing herbivores from carnivores in an ecosystem at least 210 million years old. This research shows potential for further insight into dietary niches, foraging habits, and metabolic processes in ancient ecosystems.

For Review Only

Calcium (Ca) is a bio-essential element with stable isotopes that fractionate along the trophic chain and within and among plants and animals[1,2,3]. Plants have relatively high ^{44}Ca concentrations in their foliage[4]. The ratio of $^{44/42}Ca$ becomes progressively depleted in herbivores and then carnivores as physiological fractionation incorporates less and less ^{44}Ca into bones and teeth. The meat and bone consumed by carnivores are depleted in ^{44}Ca[1], due to fractionation in the body of their prey[2,3]. The variation in $^{44/42}Ca$ is therefore a potentially useful means of assessing ecological questions such as dietary range and trophic levels in extinct organisms where these ecological parameters cannot be directly observe[1].

The study of stable Ca isotopes is still in its infancy, but recent studies have shown their utility for understanding dietary preferences and reconstructing food webs in both modern[5] and Cretaceous settings (i.e., 65 mya[1]). Ca isotopes have distinct advantages over traditional stable isotopic systems like carbon, oxygen and nitrogen, as calcium requires a much smaller amount of sample powder and is not as susceptible to diagenesis[5,6]. A major outstanding research question is whether the Ca isotopic method can be applied to terrestrial ecosystems in much deeper time.

The diverse vertebrate faunas of southern Africa's Elliot Formation (Stormberg Group, Karoo Supergroup) (Fig. 1) are an ideal natural laboratory for assessing the utility of $\delta^{44/42}Ca$ in deep time. These strata contain vertebrate fossils spanning the latest Triassic–earliest Jurassic interval (218–190 Ma[7]), nearly three times the age of the oldest Ca-characterised terrestrial ecosystem to date[1,8]. The diets of these extinct species have previously only been qualitatively inferred using coarse proxies such as dental morphology and phylogenetic relationships to evaluate feeding ecology (e.g., herbivore/carnivore)[9]. This has led to a major gap in our knowledge due to the lack of quantifiable evidence for trophic relationships between taxa from the Elliot Formation, leaving many fundamental questions about feeding ecology unanswered. Here, we conduct the oldest non-traditional $\delta^{44/42}Ca$ analysis to date in a continental setting on co-existing presumed herbivorous sauropodomorphs and presumed carnivorous 'rauisuchian' specimens to gain insight into trophic divisions of Elliot Formation vertebrates and achieve an accurate reconstruction of major dietary preferences.

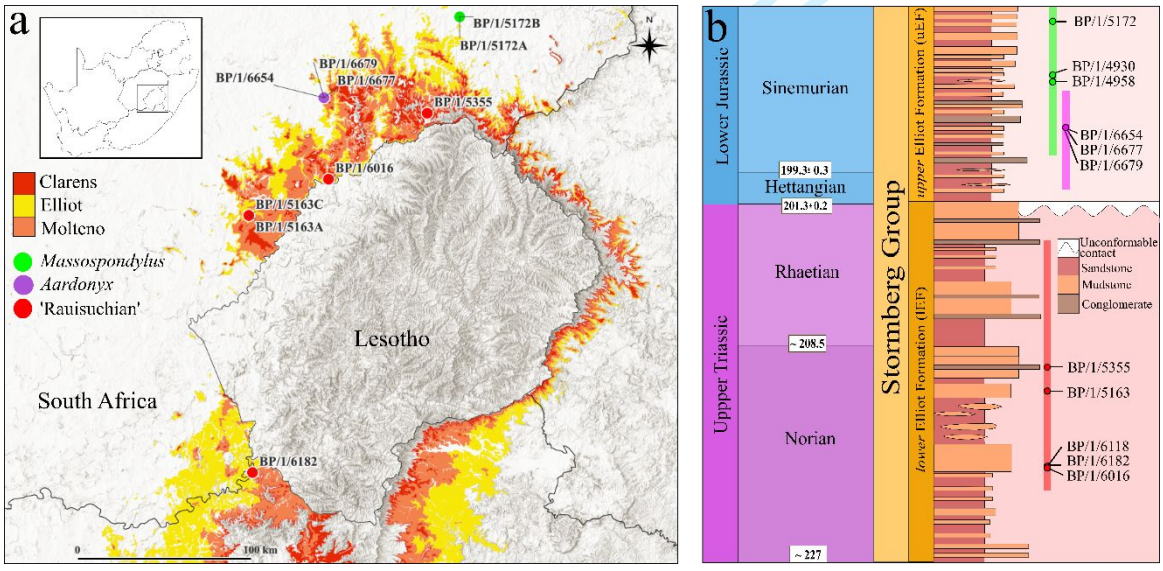


Fig. 1| Locality map and stratigraphic section of the sauropodomorph and 'rauisuchian' fossils. (a) A distribution map showing the geological overview and fossil distribution within

the Karoo Supergroup **(b)** A schematic stratigraphic section of the Stormberg Group (Karoo Supergroup), from approximately 227 to 190.8 myo, modified after Bordy *et al.,* 2020[7] showing the position of each fossil. Specimens with poor provenance are not shown above.

We analysed the dentition from 25 individual specimens, including the herbivorous sauropodomorphs *Massospondylus* (n= 9), *Aardonyx* (n= 4) and carnivorous pseudosuchians of indeterminate phylogenetic affinity (n= 12) that represent rauisuchids and poposauroids[10]. Heritage permission to work on the selected fossil specimens was obtained from the South African Heritage Resource Agency (SAHRA) (Permit ID: 3210).

Microsampling of tooth enamel was performed using an inhouse micro-drill with a 0.4 mm tungsten carbide drill bit to produce and collect approximately 400 µg of powder in the ultra-clean Wits Isotope Geoscience Laboratory (WIGL).

To control for diagenetic alteration, samples were leached prior to digestion. Samples were dissolved and digested, and the subsequent Ca ion-exchange chromatography was performed in the WIGL following a modified method from Tacail *et al.,* 2014[11] (see Supplementary Methods for details). $\delta^{44/42}$Ca isotope values for all samples were measured using a ThermoScientific Neptune Plus Multi Collector-Inductively Coupled Plasma Mass Spectrometer (MC-ICPMS) at École Normale Supérieure de Lyon (ENS; France). Repeated measurements of the NIST-SRM1486 (bone meal) reference material produced values within the reported $\delta^{44/42}$Ca mean literature value of -1.00 ± 0.07 ‰[12, 8] value (Supplementary Fig. 1). The NIST-SRM1486 in this study has an average of -0.96 ± 0.05 ‰ (2 s.e., n = 7) with an offset of approximately 0.05 ‰ compared to the mean literature value. The in-house reference standard used was the ICP Ca Lyon, a Specpure Ca plasma standard solution (Alfa Aesar), purified of strontium traces used for standard bracketing (Supplementary Fig. 2). The mean blank value of Ca for five chemistry sessions was 40 ng.

Isotopic determination of palaeotrophic position

Presumed carnivorous 'rauisuchian' specimens show depleted $\delta^{44/42}$Ca isotope values ($\bar{x}$ = -0.78 ± 0.06 ‰; n = 12; see Supplementary Table 1) in contrast to herbivorous sauropodomorphs which have enriched $\delta^{44/42}$Ca values ranging between -0.26 ‰ to -0.69 ‰ (n = 13). (Fig 3a). These differences are significant (Wilcoxon rank-sum test: *p*-value = 9.8×10^{-4}) and closely resemble $\delta^{44/42}$Ca values for modern trophic chains which display carnivore-herbivore offsets of approximately 0.3 ‰[5]. This arises as fractionation occurs within the body resulting to bone, blood and organs being depleted in ^{44}Ca (lowering $\delta^{44/42}$Ca values) compared to the food source[2,3,13]. Lower precision of taxonomic identification of the carnivorous 'rauisuchian' teeth undoubtedly contributes to the higher observed variance of the $\delta^{44/42}$ Ca values ranging from -0.45 ‰ to -1.17 ‰.

For Review Only

Table 1| Summary of the mean, lowest and highest $\delta^{44/42}$ Ca values

Taxa	Genus	δ44/42Ca	2 s.e.	Presumed diet
Sauropodomorph	*Massospondylus* (n = 9)			Herbivore
	Mean	-0.4581	0.0582	
	Lowest	-0.6856	0.1149	
	Quartile 1 (25 percentile)	-0.5809	-	
	Quartile 3 (75 percentile)	-0.3561	-	
	Highest	-0.2571	0.0747	
	Aardonyx (n = 4)			
	Mean	-0.5930	0.0467	
	Lowest	-0.6587	0.0350	
	Quartile 1 (25 percentile)	-0.6269	-	
	Quartile 3 (75 percentile)	-0.5696	-	
	Highest	-0.5065	0.0428	
Crurotarsan	'Rauisuchian' (n = 12)			Carnivore
	Mean	-0.7813	0.0645	
	Lowest	-1.1744	0.0425	
	Quartile 1 (25 percentile)	-0.8720	-	
	Quartile 3 (75 percentile)	-0.6579	-	
	Highest	-0.4471	0.0977	
-	Standard SRM1486 (n = 7)			-
	Mean	-0.9554	0.0451	
	Lowest	-1.0199	0.0260	
	Highest	-0.8686	0.0364	

The mean, lowest, highest, 25th percentile (Quartile 1) and 75th percentile (Quartile 3) $\delta^{44/42}$ Ca values for the *Massospondylus, Aardonyx* and 'Rauisuchian' selected samples. 2 s.e.= 2 standard error from the values are represented in the $\delta^{44/42}$ Ca (‰) column.

To control for isotopic variation through time, we collected data from *Massospondylus* specimens from their full stratigraphic range across the upper Elliot Formation. The lack of correlation between stratigraphic height and $\delta^{44/42}$Ca values of the *Massospondylus* specimens suggests that temporal/stratigraphic or spatial/lithological differences are unlikely to yield predictable biases in $\delta^{44/42}$Ca results. The Ca isotopic differences between 'rauisuchians' and sauropodomorphs in this study allows us to fingerprint the differences between carnivores and herbivores within this ancient ecosystem. This suggests that comparisons of $\delta^{44/42}$Ca values across ecosystems, even at great temporal distances, is feasible.

We also observe isotopic differences between co-occuring herbivorous taxa (Fig. 2). *Massospondylus* and *Aardonyx* were co-existing, presumed herbivorous sauropodomorphs that may have filled different niches, but little information is available on resource partitioning between these species. The $\delta^{44/42}$Ca values reported are in line with isotopic signatures of herbivory. *Massospondylus* specimens have a $\delta^{44/42}$Ca mean value of -0.46 ± 0.06 ‰ (n = 9) and *Aardonyx* has a $\delta^{44/42}$Ca mean value of -0.59 ± 0.05 ‰ (n=4) (Fig. 2b). This difference may be due to preferential consumption of different vegetative resources by differing sauropodomorph species – a phenomenon also observed in extant herbivorous taxa and that was identified in Cretaceous herbivores[1].

For Review Only

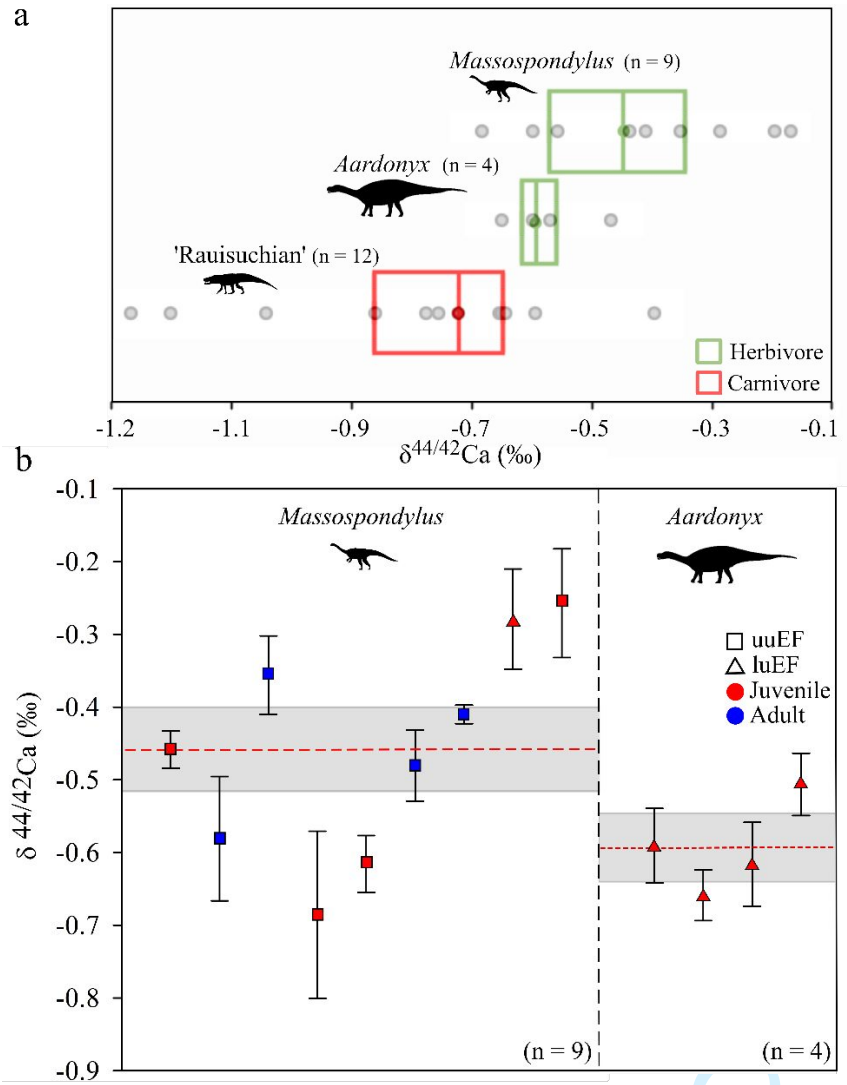


Fig. 2| The $\delta^{44/42}$Ca (‰) difference between presumed herbivores and carnivores. (a) The box plots, displaying Quartiles 1, 2, and 3, of the co-occurring presumed herbivorous sauropodomorph genera namely: *Massospondylus* and *Aardonyx* are represented in green and the presumed carnivorous 'rauisuchians' are represented in red. There is a distinct variation in the $\delta^{44/42}$Ca (‰) values between the herbivores and carnivores. Silhouettes of *Massospondylus*, *Aardonyx* and 'rauisuchian' scaled relative to the mass of the animals. This is showing the variation in morphology, size and stature[14,15]. **(b)** $\delta^{44/42}$Ca (‰) values of sauropodomorph specimens analysed. The juvenile specimens (red) and the lower upper Elliot Formation (luEF) (triangle) are indicated above. The rest of the specimens are upper upper Elliot Formation (uuEF) (square) and range from sub-adult to adult (blue).

The size difference between *Massospondylus* and *Aardonyx,* differences in their gross anatomy, and potential postural differences[16] are possibly correlated with different foraging strategies[17]. In living herbivores, differing $\delta^{44/42}$Ca values are present in differing foraging strategies such as browsing and grazing[5]. For example, the ±450 kg body mass, bipedal posture, long flexible neck, and narrow snout of *Massospondylus* may reflect selective browsing of high-quality forage similar to modern-day kudu[18]. In contrast, the more robust body form, broader skull, and ±1 tonne body mass of *Aardonyx* may reflect bulk browsing of lower-quality vegetation to fulfill their metabolic demand similar to a rhinoceros[16,18,19].

Our results reveal the utility of Ca isotopes in distinguishing trophic level within palaeoecosystems as old as those preserved in the rich Karoo sequence. Developing isotopic proxies and metrics that can contribute to the understanding of ancient population dynamics and dietary behaviour, is a critical endeavour for advancing palaeontological analysis of past ecosystems. The data in this study provide evidence that Ca isotopes are also useful across ecosystems older in age, preserving highly conserved and comparable relative enrichment values across this time frame to gain insight into trophic divisions such as herbivore-carnivore, of Elliot Formation vertebrates.

References

[1] Martin, J. E., Hassler, A., Montagnac, G., Therrien, F. and Balter, V. (2022). The stability of dinosaur communities before the Cretaceous-Paleogene (K-Pg) boundary: A perspective from southern Alberta using calcium isotopes as a dietary proxy. *GSA Bulletin 2022,* 1-13. (https://doi.org/10.1130/B36222.1)

[2] Heuser, A., Tutken, T., Gussone, N. and Galer, S. J. G. (2011). Calcium isotopes in fossil bones and teeth – Diagenetic versus biogenic origin. *Geochimica et Cosmochimica Acta,* **75**, 3419-3433. (https://doi.org/10.1016/j.gca.2011.03.032)

[3] Morgan, J. L. L., Skulan, J. L., Gordon, G. W., Romaniello, S. J., Smith, S. M. and Anbar, A. D. (2012). Rapidly assessing changes in bone mineral balance using natural stable calcium isotopes. *PNAS,* **109**, 9989-9994. (www.pnas.org/cgi/doi/10.1073/pnas.1119587109)

[4] Hindshaw, R. S., Reynolds, B. C., Wiederhold, J. G., Kiczka, M., Kretzschmar, R. and Bourdon, B. (2013). Calcium isotope fractionation in alpine plants. *Biogeochemistry*, **112**, 373-388. (https://doi.org/10.1007/s10533-012-9732-1)

[5] Martin, J. E., Tacail, T., Cerling, T. E. and Balter, V. (2018). Calcium isotopes in enamel of modern and Plio-Pleistocene East African mammals. *Earth and Planetary Science Letters,* **503**, 227-235. (https://doi.org/10.1016/j.epsl.2018.09.026)

[6] Martin, J. E., Tacail, T. and Balter, V. (2017). Non-traditional isotope perspectives in vertebrate palaeobiology. *Palaeontology*, 1-18. (https://doi.org/10.1111/pala.12300)

[7] Bordy, E., Abrahams, M., Sharman, G. R., Viglietti, P. A., Benson, R. B. J., McPhee, B. W., Barrett, P. M., Sciscio, L., Condon, D., Mundil, R., Rademan, Z., Jinnah, Z., Clark, J. M., Suarez, C. A., Chapelle, K. E. J. and Choiniere, J. N. (2020). A chronostratigraphic framework for the upper

Review Only

Stormberg Group: Implications for the Triassic-Jurassic boundary in southern Africa. *Earth-Science Reviews,* **203**, 1-24. (https://doi.org/10.1016/j.earscirev.2020.103120)

[8] Hassler, A., Martin, J. E., Amiot, R., Tacail, T., Arnaud Godet, F., Allain, R. and Balter, V. (2018). Calcium isotopes offer clues on resource partitioning among Cretaceous predatory dinosaurs. *Proc. R. Soc. B.,* **285**, 1-8. (http://dx.doi.org/10.1098/rspb.2018.0197)

[9] Bakker, R. T. (1987). Dinosaur feeding behaviour and the origin of flowering plants. *Nature,* **274**, 661-663.

[10] Tolchard, F., Nesbitt, S. J., Desojo, J. B., Viglietti, P., Butler, R. J. and Choiniere, J, N. (2019). 'Rauisuchian' material from the lower Elliot Formation of South Africa and Lesotho: Implications for Late Triassic biogeography and biostratigraphy. *Journal of African Earth Sciences*, **160**, 1-13. (https://doi.org/10.1016/j.jafrearsci.2019.103610)

[11] Tacail, T., Albalat, E., Télouk, P. and Balter, V. (2014). A simplified protocol for measurements of Ca isotopes in biological samples. *J. Anal. At. Spectrom.,* **26**, 529-535. (https://doi.org/10.1039/c3ja50337b)

[12] Tacail, T., Télouk, P. and Balter, V. (2015). Precise analysis of calcium stable isotope variations in biological apatites using laser ablation MC-ICPMS. *Journal of Analytical Atomic Spectrom.,* **31**, 152-162. (https://doi.org/10.1039/c5ja00239g)

[13] Hassler, A., Martin, J. E., Ferchaud, S., Grivault, D., Le Goff, S., Albalat, E., Hernandez, J, Tacail, T and Balter, V. (2021). Lactation and gestation controls on calcium isotopic compositions in a mammalian model. *Metallomics*, **13**, 1-14. (https://doi.org/10.1093/mtomcs/mfab019)

[14] prehistoric-wildlife (2011). *Aardonyx,* http://www.prehistoric-wildlife.com/species/a/aardonyx.html (Accessed 10 November 2021).

[15] prehistoric-wildlife (2011). *Massospondylus,* http://www.prehistoric-wildlife.com/species/m/massospondylus.html (Accessed 10 November 2021).

[16] Yates, A. M., Bonnan, M. F., Neveling, J., Chinsamy, A. and Blackbeard, M. G. (2010). A new transitional sauropodomorph dinosaur from the Early Jurassic of South Africa and the evolution of sauropod feeding and quadrupedalism. *Proceedings of the Royal Society,* **277**, 787-794. (https://doi.org/10.1098/rspb.2009.1440)

For Review Only

[17] Gee, C. T. (2011). *Biology of the sauropod dinosaurs: understanding the life of giants*. Indiana University Press, Bloomington, 34-56pp.

[18] Owen-Smith, R. N. (1988). Megaherbivores- The influence of very large body size on ecology. Cambridge University Press, New York, 369.

[19] Yates, A. M. and Barrett, P. M. (2010). *Massospondylus carinatus* Owen 1854 (Dinosauria: Sauropodomorpha) from the Lower Jurassic of South Africa: Proposed conservation of usage by designation of neotype. *Palaeont. Afr.,* **45**, 7-10.

Acknowledgements

We would like to thank Linda Iaccheri and Kimberley Beaton (Wits Isotope Geoscience Laboratory) for the assistance and guidance of the ion-exchange chromatography. We thank Simon Wills for the GIS components of this research. We also thank Bernhard Zipfel and Sifelani Jirah, collections managers, for providing access to specimens and specimen records in their care at the Evolutionary Studies Institute, South Africa.

Funding

We would like to express our gratitude and acknowledge the support of the following funding sources: DST-NRF Centre of Excellence in Palaeosciences (CoE-Pal) from 2019 to 2021, GENUS 2022 to present, Geological Society of South Africa (GSSA) Research Education and Investment (REI) Fund in 2019, Palaeontological Scientific Trust (PAST) in 2018. Opinions expressed and conclusions arrived at, are those of the author and are not necessarily to be attributed to the funding sources acknowledged.

For Review Only

Appendix B

Received: 1 March 2020 | Revised: 2 April 2020 | Accepted: 2 April 2020

DOI: 10.1002/rcm.8806

PROTOCOL

Rapid Communications in Mass Spectrometry WILEY

Absence of temperature effect on elution profiles on anionic and cationic ion-exchange resins from 4°C to 28°C

Aline Lamboux[1] | Auguste Hassler[1] | Priyanka Davechand[2] | Vincent Balter[1]

[1]Univ Lyon, ENSL, Univ Lyon 1, CNRS UMR 5276, LGL-TPE, F-69007 Lyon, France

[2]School of Geoscience, University of the Witwatersrand, 1 Jan Smuts Avenue, Johannesburg, 2000, South Africa

Correspondence
V. Balter, Univ Lyon, ENSL, Univ Lyon 1, CNRS UMR 5276, LGL-TPE, F-69007 Lyon, France
Email: vincent.balter@ens-lyon.fr

Rationale: In labs devoted to the geochemistry of non-traditional isotopes, chemical elution is necessary to purify the element of interest. Elution is always performed in over-pressured and air-conditioned clean rooms. We took advantage of an air-conditioning failure in our lab during summer 2018 to study the effect of temperature on the characteristics of the elution profiles of ion-exchange resins.

Methods: We performed the ion-exchange separation of copper, iron and zinc on macroporous anionic AG MP-1 resin and that of calcium on cationic AG 50W-X12 resin, at 28°C, prior to the measurement of their isotopic ratios by mass spectrometry. We further performed these experiments in a clean hood in a cold room at 4°C. The elution curves were processed on biological standards, i.e. bovine liver (SRM-1577c), fetal bovine serum (FBS), bone meal (SRM-1486) and the seawater IAPSO standard.

Results: The elution profiles of major elements for each matrix, and those of copper, iron, zinc and calcium, were compared with those classically achieved at 20°C in air-conditioned conditions. The results show that the elution profiles preserve their characteristics whatever the temperature, suggesting that partitioning coefficients between resin and solution are thermo-independent in the range of temperature from 4°C to 28°C.

Conclusions: If generalized to other matrices, notably inorganic, and to other elements, notably the extreme case of the separation of Rare Earth Elements, the present results suggest that clean labs may not have to be air-conditioned. This would reduce installation and operating costs and have a positive effect on the environment, paving the way for the development of a "green geochemistry".

1 | INTRODUCTION

The measurement of metal stable isotope ratios is of wide interest in many fields, from cosmochemistry (e.g.,[1–3]), endogenous geochemistry (e.g.,[4–6]), environmental geochemistry,[7–9] paleoenvironments,[10–12] to plant biology[13–15] and animal biology.[16–18] Recent advances have even been achieved in the field of medicine.[19–21] Whatever the application, a preliminary step consisting of the separation of the element of interest from the matrix is necessary prior to the mass spectrometric analyses of metal isotope ratios. This step is classically achieved by means of ion-exchange chromatography. The principle is based on electrostatic interactions between a stationary phase displaying ionic functional groups with a mobile phase containing analyte ions with the opposite charge. The stationary phase can thus be anionic or cationic. Resins containing anionic or cationic functional groups were developed in the frame of the Manhattan project for the separation and purification of strategic metals to study their nuclear properties. Series of articles describing the protocol for eluting metals were first published in the 1950s by Spedding et al for cationic resins[22] and Kraus and Moore for anionic resins.[23] These protocols have evolved since then with the commercialization of new resins, and today methods even exist for the fully automated separation of

 © 2020 John Wiley & Sons, Ltd.

metals (e.g.,[24,25]). Whatever the type of the resin (anionic or cationic) and given the reversible exchange reaction between two ions A and B between a resin R and the solution S, the equilibrium is:

$$A_R + B_S \rightleftharpoons A_S + B_R$$

and applying the mass action law gives:

$$K^{\ominus}_{A/B} = \frac{|A|_S \times |B|_R}{|A|_R \times |B|_S}$$

where $K^{\ominus}_{A/B}$ is the equilibrium constant and |A| and |B| the activity of A and B in the resin and the solution. As for all equilibrium constants, $K^{\ominus}_{A/B}$ is related to the standard change of the Gibbs free energy of the reaction ($\Delta G^{\ominus}$) in kJ:

$$\Delta G^{\ominus} = -RT\ln K^{\ominus}_{A/B}$$

where R is the universal gas constant and T the absolute temperature in °K. The value of $K^{\ominus}_{A/B}$ varies as a function of temperature. Conventionally, ion-exchange chromatography is carried out in air-conditioned clean rooms kept at a constant temperature, usually set between 17°C and 20°C.

In a cleanroom, the temperature is regulated with an air-conditioning unit, which is often part of a heating, ventilating and air-conditioning (HVAC) system. HVAC thus provides both over-pressured and temperature-conditioned air in a single unit, but these can be regulated by two independent units. Cleanrooms are isolated from outdoor contaminations by venting filtered air that eventually goes through an additional hood air filter to protect the workplace.

In July 2018, we experienced a HVAC breakdown at the cleanroom of the Laboratoire de Géologie de Lyon that lasted several weeks during a period of heat-wave. The temperature rapidly rose in the cleanroom and stabilized around 28°C. Most users then stopped working, but we took advantage of the situation to test the influence of the temperature on the $K^{\ominus}$ values between metals and cationic and anionic resins. We executed the classical elution protocols and looked for changes in the elution profiles relative to those calibrated at 20°C. We then repeated the procedure at 4°C in a cold room. We performed the elution protocols at 28°C and 4°C for the separation of Cu, Fe, and Zn on AG MP-1 macroporous anionic resin following Maréchal et al[26] and for the separation of Ca on AG 50W-X12 cationic resin following Tacail et al.[27] We constructed the elution curves for standards that are routinely used in the lab and for which we have fairly good experience at 20°C, i.e. the SRM-1577c "bovine liver" international reference material and fetal bovine liver (FBS) for the separation of Cu, Fe and Zn, and the SRM-1486 "bone meal" and IAPSO seawater international reference materials for the separation of Mg and Ca. In all cases, we also monitored the elution profiles of the associated major elements.

2 | EXPERIMENTAL

2.1 | Reagents and digestion

Ultrapure water (resistivity 18.2 MΩ cm) was produced using a Millipore Synergy system (Merck, Darmstadt, Germany). Concentrated technical grade HCl and HNO_3 (Carlo Erba Reagents, Milan, Italy) were distilled at low temperature in PFA equipment (Savillex, Eden Prairie, MN, USA). Hydrogen peroxide (H_2O_2, 30%) Suprapur was purchased from Merck. Macroporous anion-exchange resin AG MP-1 (100–200 mesh) and cation-exchange resin AG 50W-X12 (200–400 mesh) were purchased from BioRad Laboratories (Hercules, CA, USA). About 160 mg of FBS (lot number 014 M3399; Sigma–Aldrich, St Louis, MO, USA), 50 mg of SRM-1577c from the National Institute of Standards and Technology (NIST, Gaithersburg, MD, USA), 200 µg of SRM-1486 (NIST) and 50 µL of reference seawater provided by The International Association for the Physical Sciences of the Oceans (IAPSO) were digested using 3 mL concentrated distilled HNO_3 for 24 h. The vials were heated at 110°C for 3 days, then allowed to cool to room temperature. About 0.5 mL of Suprapur H_2O_2 (30%) was then added to the cooled down samples. After 2 h at room temperature, the vials were heated at 110°C on a hotplate for 2 days. The solutions were then evaporated to dryness and dissolved in 6 M HCl, evaporated again and taken up for chemical separation.

2.2 | Elutions on anionic resin

The FBS and SRM-1577c standards were redissolved in 3.2 mL and 4 mL of 7 M HCl + H_2O_2 0.001%, respectively. Chemical separation was then implemented according to the method of Maréchal et al[26]: 1 mL of sample was loaded on a quartz column containing 1.6 mL of AG MP-1 resin previously rinsed with 0.5 N HNO_3 and conditioned with 7 mL 7 M HCl + H_2O_2 0.001%. The matrix was eluted with 10 mL 7 M HCl + H_2O_2 0.001%. Copper was eluted with 20 mL 7 M HCl + H_2O_2 0.001%; Fe was eluted with 10 mL 2 M HCl + H_2O_2 0.001%; and, finally, Zn was eluted with 10 mL 0.5 M HNO_3. The eluted fraction was collected in a 2-mL aliquot, evaporated and taken up in 0.5 M HNO_3. The elution of S, Mg, Na, K, P and Ca was monitored in addition to that of Cu, Fe and Zn.

2.3 | Elutions on cationic resin

The SRM-1486 and the IAPSO standards were redissolved in 200 µL 0.4 M HCl. Chemical separation was then implemented according to the method of Tacail et al[27]: 10 µL and 50 µL of sample for SRM-1486 and IAPSO were loaded, respectively, on a column containing 210 µL of AG 50W-X12 resin previously rinsed with 6 mL 6 M HCl and conditioned with 3 mL 0.4 M HCl. The matrix was eluted with 13 mL 0.4 M HCl. Mg was then eluted with 3.5 mL 1 M HCl and

finally Ca and Sr were eluted with 2 mL 6 M HCl. The eluted fraction was collected in a 1-mL aliquot, evaporated and taken up in 0.5 M HNO_3. The elution of Mg, S, Na, P and Sr was monitored in addition to that of Ca.

2.4 | Instrumentation and measurement protocols

Single-element standard solutions from SCP Science (Québec, Canada) were used for the quantification of Ca, S, Mg, Na, K, P, Fe, Cu, Zn and Sr. Scandium and In solutions from SCP Science were used for the internal standard calibration to correct for oxide interferences and instrumental drift. All measurements were performed at the Laboratoire de Géologie de Lyon. The concentrations of Cu, Fe and Zn were measured using inductively coupled plasma mass spectrometry (ICP-MS) (7500CX; Agilent, Santa Clara, CA, USA). The concentrations of Ca, S, Mg, Na, K, P and Sr were measured using inductively coupled plasma atomic emission spectrometry (ICP-AES) (iCAP 7000 Series instrument; Thermo Fisher Scientific, Waltham, MA, USA). The concentrations were calculated using calibration curves based on multi-elemental solutions. The multi-elemental solutions were also used to monitor and correct the instrumental drift over the analytical session. The validity and reproducibility of major and trace element concentrations are estimated to be better than 10% (±2 sd) based on repeated measurements of the international reference materials as unknown samples.

3 | RESULTS

3.1 | Elutions on anionic resin

The concentrations of Na, K, S, Ca, Mg and P, which are major elements in the matrices of the bovine liver SRM-1577c and the fetal bovine liver FBS standards, were determined along with the Fe, Cu and Zn concentrations. Elution curves for these two standards at 4°C, 20°C and 28°C are presented in Figures 1A–1C for SRM 1577c and in Figures 2A–2C for FBS. The first 10 mL of 7 M HCl + H_2O_2 0.001% are used to discard elements present in the matrix: Na, K, S, Ca, Mg and P are totally discarded in this fraction, while Cu, Fe and Zn are still retained on the resin.

For SRM-1577c, 96.5%, 98.8%, and 99.3% of Cu are eluted with the next 20 mL of 7 M HCl + H_2O_2 0.001% at 4°C, 20°C and 28°C, respectively. Fe is further eluted at 92.7%, 86.9% and 95.5% with the next 10 mL of 2 M HCl + H_2O_2 0.001% at 4°C, 20°C and 28°C, respectively. Finally, 96.6%, 98.6% and 99.4% of Zn are eluted with 10 mL 0.5 M HNO_3 at 4°C, 20°C and 28°C, respectively.

For FBS, 92.6%, 100% and 100% of Cu are eluted with the next 20 mL of 7 M HCl + H_2O_2 0.001% at 4°C, 20°C and 28°C, respectively. Fe is further eluted at 84.6%, 93.1% and 83.6% with the next 10 mL of 2 M HCl + H_2O_2 0.001% at 4°C, 20°C and 28°C, respectively. Finally, 93.1%, 92.4% and 99.5% of Zn are eluted with 10 mL 0.5 M HNO_3 at 4°C, 20°C and 28°C, respectively.

It is noteworthy that some proportion of Fe is eluted along with the Zn fraction: representing 6.7%, 7.7% and 3.1% of Fe for SRM-1577c at 4°C, 20°C and 28°C, respectively, and 9.2%, 6.9% and 15.2% for FBS at 4°C, 20°C and 28°C, respectively.

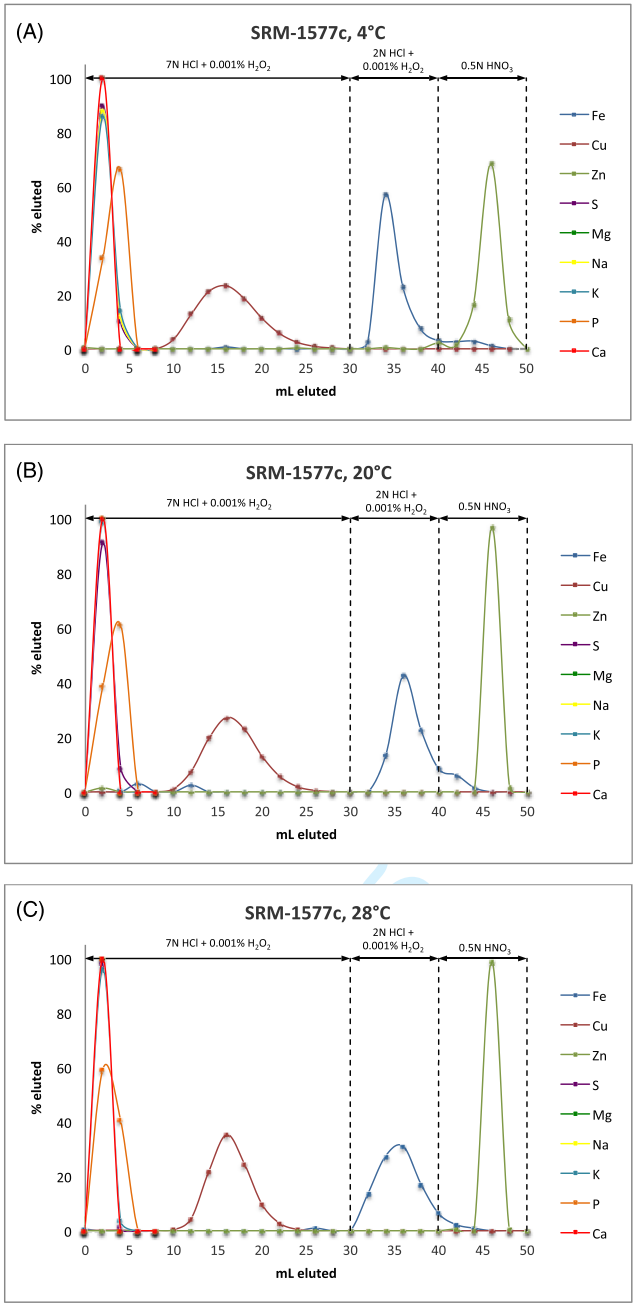


FIGURE 1 Elution of matrix elements P, K, Na, Mg, S, Ca and Cu, Fe and Zn from the SRM-1577c bovine liver standard on the macroporous anionic AG MP-1 resin at A, 4°C; B, 20°C; and C, 28°C. Uncertainty on centration measurement is ~ ±5% [Color figure can be viewed at wileyonlinelibrary.com]

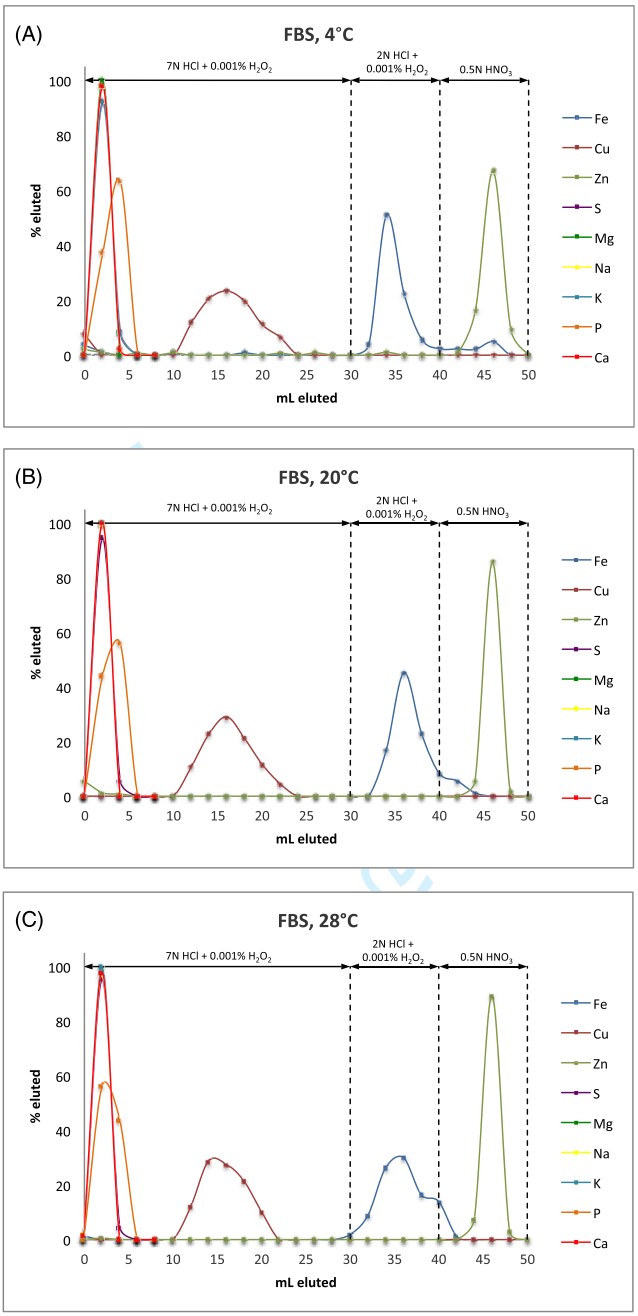


FIGURE 2 Elution of matrix elements P, K, Na, Mg, S, Ca and Cu, Fe and Zn from the FBS standard on the macroporous anionic AG MP-1 resin at A, 4°C; B, 20°C; and C, 28°C. Uncertainty on centration measurement is ~ ±5% [Color figure can be viewed at wileyonlinelibrary.com]

3.2 | Elutions on cationic resin

The concentrations of P, Mg and Na, which are major elements in the matrix of the bone meal SRM-1486 standard, were determined along with Ca concentrations. Elution curves for the SRM-1486 standard at 4°C, 20°C and 28°C are presented in Figures 3A–3C. The concentrations of Na, S and Mg, which are major elements in the matrix of the seawater IAPSO standard, were determined along with Ca and Sr concentrations. Elution curves for the IAPSO standard at 4°C, 20°C and 28°C are presented in Figures 4A–4C.

The first 13 mL of 0.4 M HCl are used to discard elements present in the matrix. The results show that Na, P and S are totally discarded. For both standards, Mg is completely eluted with 3.5 mL 1 M HCl at 4°C, 20°C and 28°C. For SRM-1486, Ca is completely eluted with 2.5 mL 6 M HCl at 4°C, 20°C and 28°C. For IAPSO, Ca and Sr are both completely eluted with 2.5 mL 6 M HCl at 4°C, 20°C and 28°C.

4 | DISCUSSION

The present results suggest some minor modifications to the protocol of Maréchal et al.[26] The elements of interest are mostly eluted as described by these authors for all temperatures. However, if all the matrix elements are always completely eluted with the first 6 mL 7 M HCl + H_2O_2 0.001%, Cu begins to be eluted at the eighth mL of 7 M HCl + H_2O_2 0.001%. To overcome any possible Cu loss, we suggest collecting the Cu fraction with 22 mL 7 M HCl + H_2O_2 0.001% after discarding the first 8 mL of 7 M HCl + H_2O_2 0.001% containing the matrix. Regarding Fe, a significant proportion is always retained on the resin and is eluted along with Zn in 0.5 M HNO_3. To obtain a better Fe extraction yield, the initial 10 mL volume of 2 M HCl + H_2O_2 0.001% should be extended to 15 mL.

Overall, the results show that the elution profiles for major and trace elements in various matrices, either on cationic or anionic resins, remain identical whatever the temperature between 4°C and 28°C. This suggests that the thermo-dependence of the partitioning coefficients $K^{\ominus}$ for most the elements and cationic and anionic resins is not high enough in this range of temperature to be measured.

For a given element, the $K^{\ominus}$ values are generally higher in anionic than in cationic resins. A comparison of $K^{\ominus}$ values for cationic and anionic resins is given as an example in Table 1. Over a suite of elements including Cu, Zn, Cd, Fe, Ga, In, Th and U, only Th exhibits $K^{\ominus}$ values higher in the AG MP-50 cationic resin than in the AG MP-1 and AG 1-X8 anionic resins. Some $K^{\ominus}$ values for anionic resins are so high that this kind of resin is sometimes said to be a "stick non-stick" resin. In these conditions, it is tempting to posit that anionic resins do not exhibit any apparent sensitivity to temperature, but the results of the study of Kraus and Raridon show that this is not the case.[30] Using the pre-loaded column technique, i.e. the resin is equilibrated with the ion whose adsorption is to be studied prior to being uniformly loaded in the column, these authors showed that the $K^{\ominus}$ values for Zn and Ga decreased with temperature increasing from 25°C to 150°C. These authors also published results for cationic resins showing that $K^{\ominus}$ values increase (Be, La, Co, Zn, Eu^{3+}) or decrease (Na, K, Ba, Rb, Cs) with increasing temperature from 2°C to 145°C.[31] The thermo-dependence of the $K^{\ominus}$ values was therefore established, but no generalized thermodynamic laws have been proposed between the various ion-exchange reactions. Some elements, such as Ba, even exhibit a curved thermo-dependence relationship.[31] The absence of a

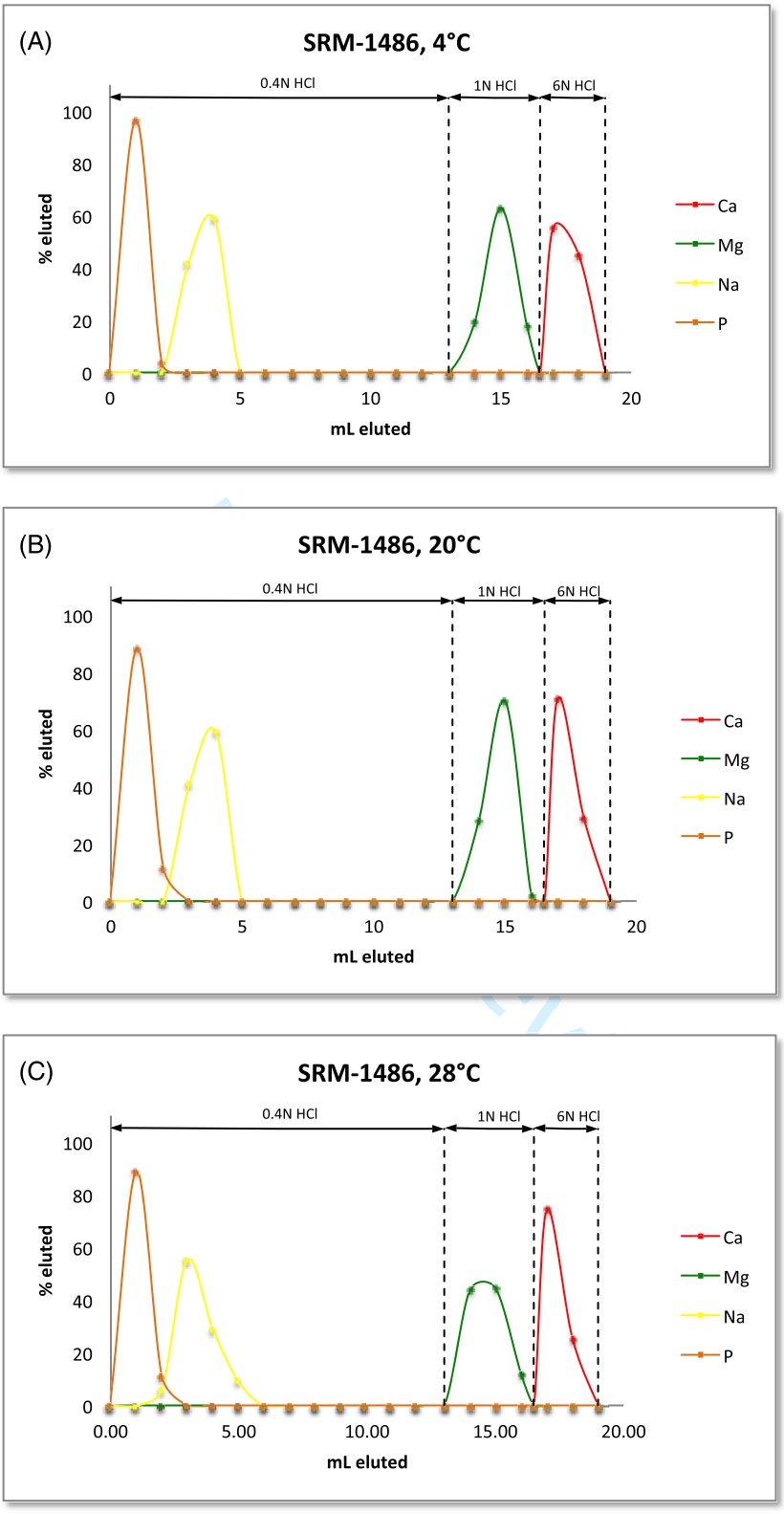


FIGURE 3 Elution of matrix elements P, Na and Mg and Ca from the SRM-1486 bone meal standard on the cationic AG 50W-X12 resin at A, 4°C; B, 20°C; and C, 28°C. Uncertainty on centration measurement is ~ ±5% [Color figure can be viewed at wileyonlinelibrary.com]

clear correlation between temperature and ion-exchange equilibria on cationic resins using the pre-loaded column technique is reinforced by results obtained using batch experiments.[32–34]

Theoretically, the varying temperature should have an effect not only on the value of the equilibrium constant, but also on the kinetic rate constant, i.e. with higher temperature, to a certain limit, increasing kinetics and therefore the separation factor. Note that the kinetics is also affected by the degree of crosslinking of the resin, with higher crosslinking decreasing kinetics. There have been fewer studies aimed at manipulating temperatures to improve separation factors on cationic resins than those dedicated to evaluating the thermo-dependence of ion-exchange equilibria. The separation of Rare Earth

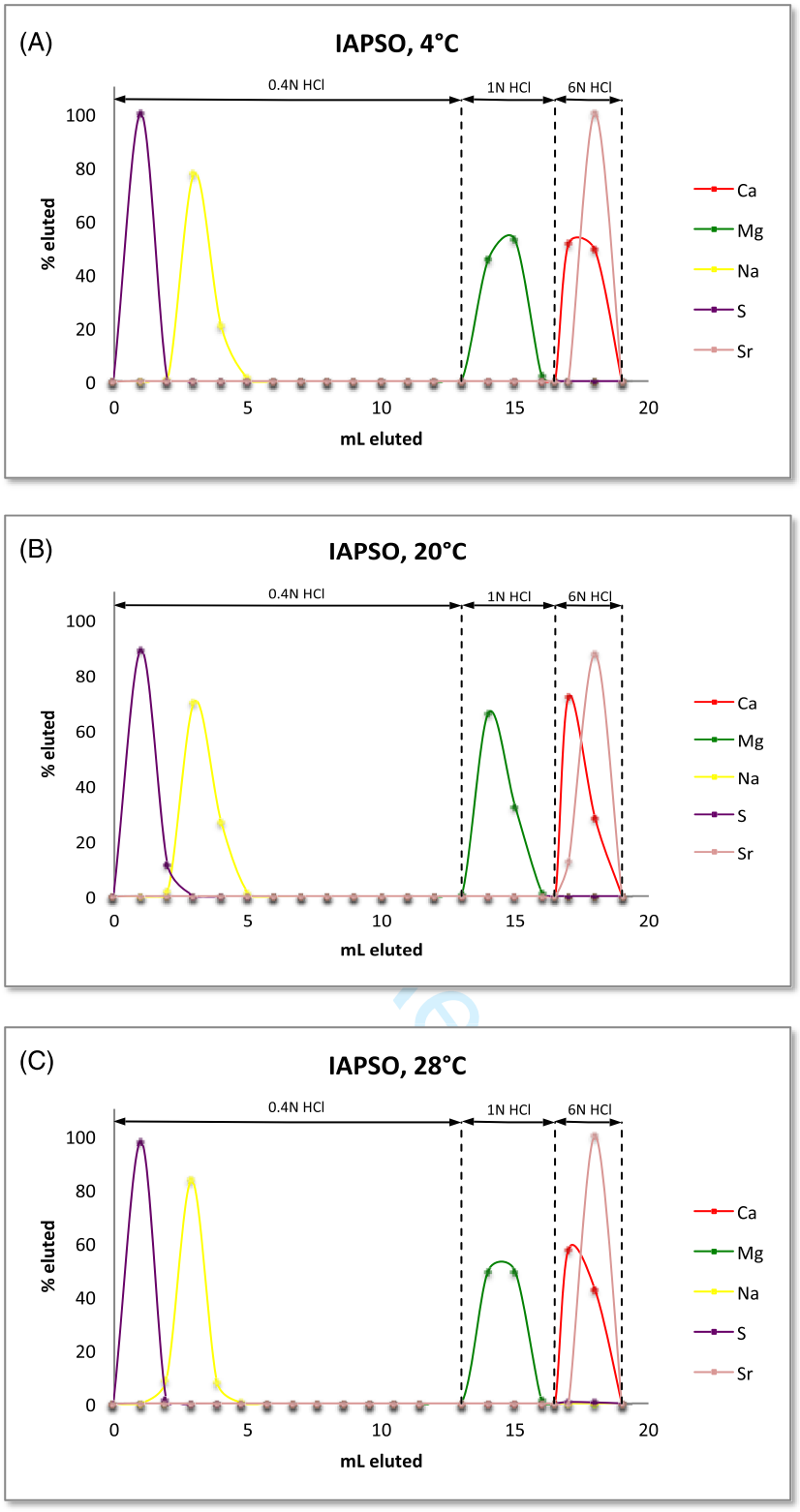


FIGURE 4 Elution of matrix elements P, Na and Mg and Ca from the IAPSO seawater standard on the cationic AG 50W-X12 resin at A, 4°C; B, 20°C; and C, 28°C. Uncertainty on centration measurement is ~ ±5% [Color figure can be viewed at wileyonlinelibrary.com]

Elements (REEs) has long been a focus of ion chromatography development, and the effects of temperature on the REE separation factors have been tested on several occasions. Glass[35] tested the influence of eluting Eu, Cm, Am and Pm on AG 50W-X12 at 87°C instead at room temperature, and found that the elution peaks appeared more rapidly and were less separated, suggesting that temperature improves kinetics and has a negative effect on the separation factor. Conversely, Strelow and Gricius[36] found a strong positive effect on the separation factor between La and Th on AG 50W-X8 at 50°C compared with room temperature, implying that the temperature effect on the separation factor is element-dependent.

TABLE 1 Comparison of $K^{\ominus}$ values for some elements on cationic and anionic resins in various HCl molarity

	Cationic resin AG MP-50[a]			Anionic resin AG MP-1[b]			Anionic resin AG 1-X8[b]		
	1 M	3 M	5 M	1 M	3 M	5 M	1 M	3 M	5 M
Cu(II)	27.7	1.9	<1		13.2	27.2		4	13.1
Zn	19.7	1.8	<1	412	830	416		554	276
Cd	2.1	<1	<1	986	989	473		626	269
Fe(III)	87	2.2	0.7		19.6	158		35.6	340
Ga	110	5	1.9		18.6	1020		24.3	1780
In	1.4	<1	<1		17.4	29.2		20.1	19.4
Th	104	1810	285		4.1	4.5		1.7	1
U(VI)	68	12.1	5.2		33.2	234		21.1	111

[a]Values from Strelow.[28]
[b]Values from van der Walt et al.[29]

Here, we found no effect of the temperature on the elution profiles of ten elements for four different types of matrices (i.e. serum, bone, liver and seawater). Our results are therefore divergent from the conclusions reached from the above literature references. Some allowances must be made that could reconcile these two apparently contradictory outcomes. First, our results are representative of a very narrow range of temperature, i.e. from 4°C to up 28°C, while those mentioned above can reach 200°C, with the first temperature point above room temperature, usually at 45–50°C. Second, our results were obtained on real samples while those mentioned above were obtained using synthetic solutions. In the former case, competition of the elements for adsorption on the functional groups is certainly important, and possibly attenuates any potential temperature effects.

The installation and the maintenance of HVAC in a clean lab represent a significant cost, but the impact on the environment also has to be considered. Nowadays the clean lab impact on the environment is a critical issue that must be taken into account, and reducing this impact is the goal of green chemistry. Originally, the principles of green chemistry were established through twelve rules by Anastas.[37] More recently, Gałuszka et al[38] extended the use of twelve hallmarks to green analytical chemistry. In all cases, the methodological developments of green chemistry involve not only reducing the samples, reagents and waste volumes production, but also minimizing the use of energy consumption, while keeping analytical performances unchanged. This represents the sixth of the twelfth principles of green chemistry proposed by Anastas "*Design for Energy Efficiency. Energy requirements of chemical processes should be recognized for their environmental and economic impacts and should be minimized. If possible, synthetic methods should be conducted at ambient temperature and pressure*".[37] Because our study shows that elution curves for 12 major and trace elements are not affected by temperature in a range compatible with natural seasonal variations, this suggests that air conditioning might not be necessary in clean labs used to perform ion-exchange chromatographic experiments. It does mean that air-conditioning is not important for comfortable working conditions. The present results should be challenged by further studies on other matrices and elements.

5 | CONCLUSIONS

For the ten monitored elements (S, Mg, Na, K, P, Ca, Cu, Fe, Zn and Sr), our results show no sizeable change in the elution pattern on both cationic and anionic resins as a function of the temperature. This suggests that partitioning coefficients between resin and solution are thermo-independent in the range of temperature from 4°C to 28°C, typical of seasonal variations. To complete the present study elution profiles of other elements and on other matrices should be performed, but the present results already suggest that clean labs may not need to be air-conditioned which represents, to our knowledge, the first proposition for the development of green geochemistry.

ORCID

Vincent Balter https://orcid.org/0000-0002-9236-4834

REFERENCES

1. Moynier F, Blichert-Toft J, Telouk P, Luck J-M, Albarède F. Comparative stable isotope geochemistry of Ni, Cu, Zn, and Fe in chondrites and iron meteorites. *Geochim Cosmochim Acta*. 2007;71 (17):4365-4379.
2. Tian Z, Chen H, Fegley B Jr, et al. Potassium isotopic compositions of howardite-eucrite-diogenite meteorites. *Geochim Cosmochim Acta*, 2019; 266, 611-632.
3. Teng F-Z, Li W-Y, Ke S, et al. Magnesium isotopic composition of the earth and chondrites. *Geochim Cosmochim Acta*. 2010;77:4150-4166.
4. Larson PB, Maher K, Ramos FC, Chang Z, Gaspar M, Meinert LD. Copper isotope ratios in magmatic and hydrothermal ore-forming environments. *Chem Geol*. 2003;201:337-350.
5. Teng F-Z, Wadhwa M, Helz RT. Investigation of magnesium isotope fractionation during basalt differentiation: Implications for a chondritic composition of the terrestrial mantle. *Earth Planet Sci Lett*. 2007;261:84-92.

6. Chen H, Savage PS, Teng F-Z, Helz RT, Moynier F. Zinc isotope fractionation during magmatic differentiation and the isotopic composition of the bulk Earth. *Earth Planet Sci Lett*. 2013;369–370:34-42.
7. Cloquet C, Carignan J, Libourel G, Sterckeman T, Perdrix E. Tracing source pollution in soils using cadmium and lead isotopes. *Environ Sci Technol*. 2006;40(8):2525-2530.
8. Feng X, Foucher D, Hintelmann H, Yan H, He T, Qiu G. Tracing mercury contamination sources in sediments using mercury isotope compositions. *Environ Sci Technol*. 2010;44(9):3363-3368.
9. Aucour A-M, Bedell J-P, Queyron M, Tholé R, Lamboux A, Sarret G. Zn speciation and stable isotope fractionation in a contaminated urban wetland soil–*Typha latifolia* system. *Environ Sci Technol*. 2017;51(15):8350-8358.
10. Xu L, Lehmann B, Mao J, et al. Mo isotope and trace element patterns of lower Cambrian black shales in South China: Multi-proxy constraints on the paleoenvironment. *Chem Geol*. 2012;318:45-59.
11. Saenger C, Wang Z. Magnesium isotope fractionation in biogenic and abiogenic carbonates: Implications for paleoenvironmental proxies. *Quat Sci Rev*. 2014;90:1-21.
12. Brazier J-M, Suan G, Tacail T, et al. Calcium isotope evidence for dramatic increase of continental weathering during the Toarcian oceanic anoxic event (early Jurassic). *Earth Planet Sci Lett*. 2015;411:164-176.
13. Moynier F, Pichat S, Pons M-L, Fike D, Balter V, Albarède F. Isotopic fractionation and transport mechanisms of Zn in plants. *Chem Geol*. 2009;267:125-130.
14. Bolou-Bi EB, Poszwa A, Leyval C, Vigier N. Experimental determination of magnesium isotope fractionation during higher plant growth. *Geochim Cosmochim Acta*. 2010;74:2523-2537.
15. Schmitt A-D, Cobert F, Bourgeade P, et al. Calcium isotope fractionation during plant growth under a limited nutrient supply. *Geochim Cosmochim Acta*. 2013;110:70-83.
16. Martin JE, Vance D, Balter V. Magnesium stable isotope ecology using mammal tooth enamel. *Proc Natl Acad Sci*. 2015; 112:(2), 430-435.
17. Martin JE, Tacail T, Cerling TE, Balter V. Calcium isotopes in enamel of modern and Plio-Pleistocene east African mammals. *Earth Planet Sci Lett*. 2018;503:227-235.
18. Sauzéat L, Laurençon A, Balter V. Metallome evolution in ageing *C. elegans* and a copper stable isotope perspective. *Metallomics*. 2018;10(3):496-503.
19. Bondanese VP, Lamboux A, Simon M, et al. Hypoxia induces copper stable isotope fractionation in hepatocellular carcinoma, in a HIF-independent manner. *Metallomics*. 2018;8:1177-1184.
20. Albarède F, Télouk P, Balter V. Medical applications of isotope metallomics. Measurements, theories and applications of non-traditional stable isotopes. *Rev Mineral Geochem*. 2017;82:851-885.
21. Sauzéat L, Bernard E, Perret-Liaudet A, et al. Isotopic evidence for disrupted copper metabolism in amyotrophic lateral sclerosis. *iScience*. 2018;6:264-271.
22. Spedding FH, Voigt AF, Gladrow EM, Sleight NR. The separation of rare earths by ion exchange. I. Cerium and yttrium. *J Am Chem Soc*. 1947;69(11):2777-2781.
23. Kraus KA, Moore GE. Anion exchange studies. I. Separation of zirconium and niobium in HCl-HF mixtures. *J Am Chem Soc*. 1951;73:9-13.
24. Ireland TJ, Tissot FLH, Yokochi R, Dauphas N. Teflon-HPLC: A novel chromatographic system for application to isotope geochemistry and other industries. *Chem Geol*. 2013;357:203-214.
25. Romaniello SJ, Field MP, Smith HB, Gordon GW, Kim MH, Anbar AD. Fully automated chromatographic purification of Sr and Ca for isotopic analysis. *J Anal At Spectrom*. 2015;30:1906-1912.
26. Maréchal CN, Télouk P, Albarède F. Precise analysis of copper and zinc isotopic compositions by plasma-source mass spectrometry. *Chem Geol*. 1999;156:251-273.
27. Tacail T, Albalat E, Télouk P, Balter V. A simplified protocol for measurement of Ca isotopes in biological samples. *J Anal At Spectrom*. 2014;29:529-535.
28. Strelow FEW. Distribution coefficients and ion exchange behavior of 46 elements with a macroreticular cation exchange resin in hydrochloric acid. *Anal Chem*. 1984;56:1053-1056.
29. van der Walt TN, Strelow FWE, Verheij R. The influence of crosslinkage on the distribution coefficients and anion exchange behaviour of some elements in hydrochloric acid. *Solvent Extr Ion Exc*. 1985;3:732-740.
30. Kraus KA, Raridon RJ. Anion exchange studies. XXXI. Adsorption of Zn(II) and Ga(III) from HCl solutions in the temperature range 25 to 150°C. *J Am Chem Soc*. 1960;82:3271-3276.
31. Kraus KA, Raridon RJ. Temperature dependence of some cation exchange equilibria in the range 0 to 200°. *J Phys Chem*. 1959;63:1901-1907.
32. Bonner OD, Smith LL. The effect of temperature on ion-exchange equilibria. I. the sodium–hydrogen and cupric–hydrogen exchanges. *J Phys Chem*. 1957;61:1614-1617.
33. Bonner OD, Pruett RR. The effect of temperature on ion exchange equilibria. II. The ammonium-hydrogen and thallous-hydrogen exchanges. *J Phys Chem*. 1959;63:1417-1420.
34. Bonner OD, Pruett RR. The effect of temperature on ion exchange equilibria. III. Exchanges involving some divalent ions. *J Phys Chem*. 1959;63:1420-1423.
35. Glass RA. Chelating agents applied to ion-exchange separations of americium and curium. *J Am Chem Soc*. 1955;77:807-809.
36. Strelow FWE, Gricius AJ. Separation of thorium from lanthanum and other elements by cation-exchange chromatography at elevated temperatures. *Anal Chem*. 1972;44(11):1898-1900.
37. Anastas PT. Green chemistry and the role of analytical methodology development. *Crit Rev Anal Chem*. 1999;29:167-175.
38. Gałuszka A, Migaszewski Z, Namieśnik J. The 12 principles of green analytical chemistry and the SIGNIFICANCE mnemonic of green analytical practices. *TrAC Trends Anal Chem*. 2013;50:78-84.

How to cite this article: Lamboux A, Hassler A, Davechand P, Balter V. Absence of temperature effect on elution profiles on anionic and cationic ion-exchange resins from 4°C to 28°C. *Rapid Commun Mass Spectrom*. 2020;34:e8806. https://doi.org/10.1002/rcm.8806

Appendix C

Chemical Geology 606 (2022) 121000

Contents lists available at ScienceDirect

Chemical Geology

journal homepage: www.elsevier.com/locate/chemgeo

Simultaneous analysis of stable and radiogenic strontium isotopes in reference materials, plants and modern tooth enamel

Danaé Guiserix [a,*], Emmanuelle Albalat [a], Henriette Ueckermann [b], Priyanka Davechand [c], Linda M. Iaccheri [c], Grant Bybee [c], Shaw Badenhorst [d], Vincent Balter [a]

[a] CNRS UMR 5276, LGLTPE, Univ. Lyon, ENS de Lyon, Univ. Lyon 1, 46 Allée d'Italie, 69342 Lyon Cedex 07, France
[b] Department of Geology, University of Johannesburg, Auckland Park 2006, South Africa
[c] School of Geosciences, University of the Witwatersrand, 1 Jan Smuts Avenue, Braamfontein, Johannesburg 2000, South Africa
[d] Evolutionary Studies Institute, University of the Witwatersrand, Private Bag 3, Wits 2050, South Africa

ARTICLE INFO

Editor: Karen Johannesson

Keywords:
Non-traditional isotopes
Stable strontium isotopes
Radiogenic strontium isotopes
Trophic chain
Weaning

ABSTRACT

Radiogenic strontium isotopes ($^{87}Sr/^{86}Sr$) are a useful tool in forensics, ecology, bioarcheology and paleoanthropology allowing investigation of present and past migration and landscape use. The measurement of the $^{87}Sr/^{86}Sr$ ratio traditionally assumes a constant stable ($^{88}Sr/^{86}Sr$) isotope ratio. However, some studies indicate that these stable Sr isotopes may display mass-dependent fractionation, suggesting that the $^{88}Sr/^{86}Sr$ ratio may fingerprint previously unknown dietary and physiological information. Here we present a survey of the variability of $\delta^{88}Sr$ values, along with the $^{87}Sr/^{86}Sr$ ratios, in fourteen reference materials of geological and biological origin using MC-ICPMS. The measurements employ a simple sample-standard bracketing method and zirconium external correction. Comparisons with double-spiked $\delta^{88}Sr$ TIMS analyses show a very good agreement (0.014 ‰; n = 10). We then applied this method to explore the fractionation of the $^{88}Sr/^{86}Sr$ ratio in tooth enamel of mammals from two modern food-chains (Kruger National Park and Western Cape, South Africa), and from modern South African chacma baboon populations. Clear differences in the $\delta^{88}Sr$ values are observed between plants and teeth of herbivores (~ −0.26 ‰; n = 5), but the distinction between herbivores and carnivores requires further investigation. Variations between tooth enamel of young and adult baboons suggests that the $\delta^{88}Sr$ is a promising indicator of weaning behaviors. Our method implementation and preliminary results highlight the importance of coupled radiogenic and stable Sr isotope determination in extant and extinct vertebrates.

1. Introduction

There are four naturally occurring strontium (Sr) isotopes, all of which are stable (^{84}Sr, ^{86}Sr, ^{88}Sr, ^{87}Sr), but one, ^{87}Sr, is the radiogenic product of the β-decay radioactivity of rubidium-87 (^{87}Rb; half-life = 48.8 Ga). Given that the atomic properties of Sr are similar to those of calcium (Ca), Sr is incorporated into the body as a Ca substitute, undergoing discrimination processes that lower the Sr/Ca ratio during metabolic processes involving Ca (Balter, 2004). Multi-collector inductively-coupled plasma mass spectrometers (MC-ICPMS) and thermal ionization mass spectrometers (TIMS), which are routinely used for the measurements of the $^{87}Sr/^{86}Sr$ ratio, induce an instrumental mass-bias during measurement that needs to be corrected, thus the true $^{86}Sr/^{88}Sr$ ratio is traditionally set at 0.1194 to correct the mass-bias on the $^{87}Sr/^{86}Sr$ ratio. The $^{87}Sr/^{86}Sr$ ratio in the body of an animal records that of the soil/substrate on which the animal lives (Price et al., 2002; Lazzerini et al., 2021). By measuring the $^{87}Sr/^{86}Sr$ ratio in tissues forming at different periods of life, such as bone and tooth enamel, or within tooth enamel using laser ablation, it is possible to reconstruct the mobility and range of the animal, with reference to the Sr isotope ratio of the substrate (Knudson et al., 2004; Sillen and Balter, 2018).

However, with the improvement of MC-ICPMS precision in the last twenty years, variations of the $^{88}Sr/^{86}Sr$ ratio have been increasingly scrutinized in geological materials since the first measurement of that ratio in seawater (Fietzke and Eisenhauer, 2006). Variations of this ratio relative to the international standard NIST SRM-987 are expressed as $\delta^{88/86}Sr_{SRM987}$, defined as following:

$$\delta^{88/86}Sr_{SRM987} = \left(\frac{{}^{88}Sr/{}^{86}Sr_{\text{sample}}}{{}^{88}Sr/{}^{86}Sr_{\text{NIST SRM987}}} - 1 \right) \times 1000$$

* Corresponding author.
E-mail address: danae.guiserix@ens-lyon.fr (D. Guiserix).

https://doi.org/10.1016/j.chemgeo.2022.121000
Received 10 March 2022; Received in revised form 25 May 2022; Accepted 22 June 2022
Available online 25 June 2022
0009-2541/© 2022 Elsevier B.V. All rights reserved.

The classical and shorter notation $\delta^{88}Sr$ will be used in the following text. There is only scarce data concerning the $\delta^{88}Sr$ value in biological materials. Recent studies suggest that stable Sr isotopes in bone and tooth enamel may be a good indicator of paleodietary range and trophic level (Knudson et al., 2010; Lewis et al., 2017; Brazier et al., 2020). Indeed, ^{86}Sr seems to be preferentially incorporated into biological system compared to ^{88}Sr. Analyses of plants show preferred uptake of ^{86}Sr relative to ^{88}Sr in the nutrient pathways leading to lighter isotopic signatures in leaves than in roots and soil (de Souza et al., 2010; Liu et al., 2016; Guibourdenche et al., 2020). Up trophic chains, the Sr isotope fractionation remains poorly studied, but it is already noticeable that all $\delta^{88}Sr$ values in plants are positive (de Souza et al., 2010; Liu et al., 2016; Hajj et al., 2017; Brazier et al., 2020), while all $\delta^{88}Sr$ values in terrestrial animals are negative (Knudson et al., 2010; Lewis et al., 2017; Brazier et al., 2020), relative to the SRM-987 standard. In a controlled feeding study on pigs, a shift of −0.32 ‰ from diet to dental enamel has been observed (Lewis et al., 2017), consistent with the plant data. Different methods have been developed in order to overcome instrumental mass bias during measurements of the $^{88}Sr/^{86}Sr$ and $^{87}Sr/^{86}Sr$ ratios. Analyses with a TIMS use a $^{84}Sr/^{86}Sr$ double spike to correct for the instrumental mass bias (Krabbenhöft et al., 2009; Neymark et al., 2014; Charlier et al., 2017; Lewis et al., 2017; Brazier et al., 2020) and is the method of reference to achieve the best precision (between 0.01 and 0.02 ‰ (Brazier et al., 2020)). Measurement method using a MC-ICPMS includes sample-standard bracketing method (SSB) (Fietzke and Eisenhauer, 2006; Ma et al., 2013) and correction using a zirconium (Zr) internal standard (Ohno and Hirata, 2007; Liu et al., 2012, 2016, 2017; Xu et al., 2020). Both methods can be used simultaneously (Irrgeher et al., 2013; Liu et al., 2017; Argentino et al., 2021).

A combination of these two methods is used in the present study and we test the procedure on fourteen reference materials with various mineral and biological matrices. The robustness and accuracy of this method was assessed in different laboratories. In South Africa sample preparation was done at the Wits Isotope Geoscience Laboratory (WIGL, University of the Witwatersrand, Johannesburg, South Africa), while the analytical measurements were done at the University of Johannesburg (UJ, Johannesburg, South Africa). Further work was achieved at the Laboratoire de géologie de Lyon (LGLTPE, Ecole Normale Supérieure de Lyon, France). In addition to the reference materials, we also measured the $^{88}Sr/^{86}Sr$ and $^{87}Sr/^{86}Sr$ ratios in animal and plant samples from extant ecosystems in South Africa to provide a first overview of the Sr stable isotope systematics in modern ecosystems and to challenge the possible use as a paleodietary indicator.

2. Material and methods

2.1. Reference material description

Eleven reference materials with known $^{88}Sr/^{86}Sr$ and $^{87}Sr/^{86}Sr$ ratios (biological matrix: SRM-1400, SRM-1486, BCR-380R, BCR-383 and SRM-1570a; geological matrix: JC-p1, UB-N, BHVO-2, BCR-1, and GS-N; seawater: IAPSO) and three reference materials with unknown $^{88}Sr/^{86}Sr$ and $^{87}Sr/^{86}Sr$ ratios (geological matrix: Granite GA, NBS-120c and SRM-915b) were analyzed in both labs. The descriptions of the standards are provided in Table 1. Reference material aliquots were weighed to reach around 5 μg of Sr.

2.2. Sample description

We also measure $^{88}Sr/^{86}Sr$ and $^{87}Sr/^{86}Sr$ ratios in two sets of modern samples. The first set of samples are from tooth enamel collected from modern chacma baboon (*Papio ursinus*) skulls provided by the Ditsong National Museum of Natural History (Pretoria, South Africa). Teeth were extracted from sixteen skulls of chacma baboons from a reserve in Calitzdorp (Western Cape, South Africa). Details for baboons and the geographical context are available in a previous study (Brand, 1994).

Table 1
Description of the reference materials analyzed in this study.

Reference material	Description	Sr ($\mu g.g^{-1}$)
Animal		
BCR-380R	Whole milk powder	2.72
NIST SRM 1400	Cow bone ash powder	249
NIST SRM 1486	Cow bone meal powder	264
Vegetal		
BCR-383	Green bean powder	5.26
NIST SRM 1570a	Spinach powder	55
Carbonate		
JC-p1	Coral powder (*Porites* sp.)	6896
NIST SRM 915b	Calcium carbonate	150
Sea water		
IAPSO	North Atlantic sea water	7.9
Crustal and mantle rocks		
UB-N	Serpentinite powder	9
BHVO-2	Basalt powder	389
BCR-1	Basalt powder	330
GS-N	Granite powder	570
Granite GA	Granite powder	310
NIST NBS 120c	Phosphate rock powder	840

The list of sampled individuals is presented in Table S1. The first molar of the upper jaw was sampled in 4 adults (over 6 years old) and 3 sub-adults (around 3 years old). Deciduous teeth (milk incisor, molar and canine) from 8 sub-adult baboons and the third molar from an adult were also sampled. All the teeth were washed with distilled water before drilling and the surfaces were cleaned with an abrasive drill bit. Sampling was located in the mesio- or distobuccal cusps of the teeth, and drilled using a bit diameter of 0.8 mm. Only the enamel was sampled to avoid contamination with dentine. Between 5 and 10 mg of powder was recovered. This set of material has been analyzed at UJ, using the WIGL-UJ method. The second set of samples consists in tooth enamel of herbivores and carnivores from the Kruger National Park (KNP) and Western Cape (WC), in South Africa. Details for sex, age and geographical context of these specimens are given in Table S2. The teeth were cleaned with distilled water before sampling. Plant residues trapped in the dentition of herbivorous mammals were also collected. The samples were stored at the Ditsong National Museum of Natural History (Pretoria, South Africa). They were prepared and analyzed at the LGLTPE, using the LGLTPE-2 analytical method. Around 5 mg of enamel powder was sampled, and the same quantity was taken from plant residues.

2.3. Sample digestion

2.3.1. WIGL

All sample preparation procedures were carried out in a Class 100 clean room under laminar flow hoods. Organics present in biological samples were removed via an oxidative digestion procedure. Thus 2 mL of concentrated HNO_3 (14 M) and 0.5 mL of H_2O_2 (30%) were added to SRM-1400 and SRM-1486, but also to evaporated IAPSO and baboon tooth enamel. Beakers were then left on a hotplate for three days at 110 °C. They were opened at regular 10 min intervals during the first hours to allow degassing. The BHVO-2 standard was dissolved using 2 mL of concentrated HNO_3 (14 M) and 1 mL concentrated HF. The closed beakers were left on a hotplate (110 °C) for 48 h. After complete dissolution all the samples were dried down and subsequently taken up with 1 mL of HNO_3 (3 M).

2.3.2. LGLTPE

Sample preparation procedures at the LGLTPE were carried out in a

Table 2
Ion exchange protocols for the chromatographic separation of Sr.

Lab	WIGL	LGLTPE
Wash	4 mL 0.5 M HNO_3	4 mL 0.5 M HNO_3
Conditioning	2.5 mL 3 M HNO_3	2.5 mL 3 M HNO_3
Load sample	1 mL 3 M HNO_3	1 mL 3 M HNO_3
Matrix elution	2.5 mL 3 M HNO_3	3.5 mL 3 M HNO_3
Sr elution	16 mL 0.5 M HNO_3	7 mL 0.005 M HNO_3

clean room under laminar flow hoods. All the acids used were purified twice by sub-boiling distillation. As at the WIGL, 4 mL concentrated HNO_3 (15 M) and 1 mL H_2O_2 (30%) were added to standards containing organics (i.e., BCR-383, BCR-380R, SRM-1486, SRM-1400 and SRM-1570a), but also to IAPSO and JC-p1, and closed beakers were left on a hotplate (110 °C) for 48 h. They were unscrewed regularly to allow degassing. Tooth enamel samples and plant residues from the KNP and WC were dissolved using the same protocol. The SRM-915b and NBS-120c standards were dissolved in 1 mL concentrated HNO_3 (15 M) and centrifuged to remove potential silicate particles. All rock samples (i.e., UB-N, BHVO-2, BCR-1, GS-N and Granite GA) were digested using 2 mL concentrated HNO_3 (15 M) and 1 mL concentrated HF. Closed beakers were left on the hotplate (110 °C) for 48 h and evaporated to dryness, taken up with 6 N HCl and a few drops of $HClO_4$ and evaporated on a hotplate (120 °C) to eliminate fluorides. This last step was repeated until all fluorides were dissolved. After, digestion all the samples were dried down and redissolved in 1 mL of 3 M HNO_3.

2.4. Sample preparation and instrumentation

2.4.1. WIGL

Isotopic measurements of Sr in biological and geological samples require the separation of Sr from the matrix with a special attention to avoid any isobaric interference with ^{87}Rb and Zr contamination. Strontium must be recovered quantitatively after the chromatographic separation to ensure the absence of any chemical isotopic mass fractionation during matrix and Sr elutions. The column chemistry protocol set up at WIGL was inspired by that of Tacail et al. (Tacail et al., 2014) and De Muynck et al. (De Muynck et al., 2009). Both protocols use the Sr spec™ resin (TrisKem International). 300 µL of Sr spec™ resin is loaded into 2 mL polypropylene columns. The elution protocol is given in Table 2. The resin is discarded after a single use.

2.4.2. UJ

The isotopic analyses were performed on a Nu Plasma II (Nu Instrument) MC-ICPMS at UJ. The SRM-987 was used as the isotopic reference standard for Sr. On the day of the analysis session, samples and standards were diluted with 0.05 M HNO_3 to reach a concentration of 500 µg.L^{-1}, leading to a typical intensity of 8 V in the H1 collector (^{88}Sr). A high purity Zr solution (Alfa Aesar, 1000 ppm) was diluted and added to the standard and sample solutions at 500 µg.L^{-1}. The true ratio of ^{91}Zr/^{90}Zr is 0.218126 according to the commission on isotopic abundances IUPAC (Meija et al., 2016). Measurements were carried out in static mode and a single measurement consisted of one block of 40 cycles with an integration time of 10 s. Daily calibration was performed to optimize operating conditions for maximum Sr and Zr signal stability, which was monitored with repeated measurements on SRM-987. The instrument settings are given in Table 3.

2.4.2.1. Interference correction. Krypton (Kr) contamination of argon (Ar) gas may interfere with ^{86}Sr. Measurement background was determined at the start of each measurement session by analyzing a 0.05 M HNO_3 laboratory blank. The on-peak background intensities were subtracted from the measurement signals during measurement, correcting for possible Kr interference.

To calculate the ^{87}Sr/^{86}Sr values, the isobaric interference of ^{87}Rb on ^{87}Sr was corrected following the equation:

$$^{87}Rb = Meas\left(^{85}Rb\right) \times Ref\left(^{87}Rb/^{85}Rb\right) \times \left(\frac{M(^{87}Rb)}{M(^{85}Rb)}\right)^{Fract_{Sr}} \quad (1)$$

$$^{87}Sr = Meas\left(^{87}Sr\right) - ^{87}Rb \quad (2)$$

With *Meas(^{85}Rb)* and *Meas(^{87}Sr)* being the measured intensity at mass 85 and 87, respectively, and *M(^{87}Rb)* and *M(^{85}Rb)* corresponding to Rb isotopic masses. *Ref(^{87}Rb/^{85}Rb)* is the natural abundance ratio extracted from the latest IUPAC report (0.3856, (Meija et al., 2016)). $Fract_{Sr}$ is the fractionation factor defined as in Eq. (3) that can be used to correct for Rb interferences as long as the Rb concentration in the sample is small (Ehrlich et al., 2001). The average measured intensity of mass 85 in the samples was 2*10^{-05} V, which is negligible compared to the intensity measured on mass 87 (0.7 V).

2.4.2.2. Normalization of ^{87}Sr/^{86}Sr ratio. The ^{87}Sr/^{86}Sr ratio was obtained according to classic calculations (Marisa Almeida and D. Vasconcelos, 2001). The instrumental mass bias is evaluated by the

Table 3
Instrument settings and data acquisition parameters for MC-ICP-MS analysis, and main differences between the three measurement methods.

Method	UJ	LGLTPE-1	LGLTPE-2
Element (+internal standard)	Sr(+Zr)	Sr(+Zr)	Sr(+Zr)
MC-ICP-MS	Nu Plasma II	Nu Plasma 500	Nu Plasma 500
RF power (W)	1300	1350	1350
Plasma condition	wet, cyclonic spray chamber	idem	idem
Coolant Ar flow (*L. min*$^{-1}$)	13.00	13.00	13.5
Auxiliary Ar flow (*L. min*$^{-1}$)	0.80	1.46	1.80
Nebulizer Ar flow (*L. min*$^{-1}$)	34.50	37.9	35.1
Mass resolution	300	300	300
Cup configuration	H6: ^{91}Zr; H5: ^{90}Zr H1: ^{88}Sr; L1: ^{87}Sr L3: ^{86}Sr; L5: ^{85}Rb L6: ^{83}Kr; L7: ^{82}Kr	H6: ^{91}Zr; H5: ^{90}Zr H2: ^{88}Sr; Ax: ^{87}Sr L2: ^{86}Sr; L3: ^{85}Rb L4: ^{84}Sr; L5: ^{83}Kr	H6: ^{92}Zr; H5: ^{91}Zr H4: ^{90}Zr; Ax: ^{88}Sr L2: ^{87}Sr; L3: ^{86}Sr L4: ^{85}Rb; L5: ^{84}Sr
Sensitivity	^{88}Sr 0.5 ppm: 8 V	^{88}Sr 0.3 ppm: 8 V	^{88}Sr 0.3 ppm: 8 V
Integration time (s)	10	10	10
Cycles	40	40	20
Isotope ratio used for mass bias correction of ^{88}Sr/^{86}Sr	^{91}Zr/^{90}Zr	^{91}Zr/^{90}Zr	^{92}Zr/^{90}Zr and ^{91}Zr/^{90}Zr
Baselines	On-peak zero	Deflected beam	On-peak zero
Blank signal	2.7*10^{-3} V	3.5*10^{-3} V	3.5*10^{-3} V
Kr interference correction	None	Yes	None
Rb interference correction	Yes	Yes	Yes

fractionation factor $Fract_{Sr}$, calculated using Russel's exponential law (Russell et al., 1978):

$$Fract_{Sr} = \frac{Ln\left(\frac{True\left(^{86}Sr/^{88}Sr\right)}{Meas\left(^{86}Sr/^{88}Sr\right)}\right)}{Ln\left(\frac{M(^{86}Sr)}{M(^{88}Sr)}\right)} \quad (3)$$

$M(^{88}Sr)$ and $M(^{86}Sr)$ correspond to Sr isotopic masses and $True\ (^{86}Sr/^{88}Sr)$ equals 0.1194 (Meija et al., 2016). This fractionation factor can then be used to normalize the $^{87}Sr/^{86}Sr$ ratio:

$$Norm\left(^{87}Sr/^{86}Sr\right) = Meas\left(^{87}Sr/^{86}Sr\right) \times \left(\frac{M(^{87}Sr)}{M(^{86}Sr)}\right)^{Fract_{Sr}} \quad (4)$$

However, the mass bias may change during the analytical session. Thus, a sample-standard bracketing method (SSB) was applied to take these variations into account, using the equation:

$$\left(^{87}Sr/^{86}Sr\right)_{sample} = Norm\left(^{87}Sr/^{86}Sr\right)_{sample} \times \frac{Ref\left(^{87}Sr/^{86}Sr\right)_{SRM987} \times 2}{Norm\left(^{87}Sr/^{86}Sr\right)_{stdA} + Norm\left(^{87}Sr/^{86}Sr\right)_{stdB}} \quad (5)$$

With $Norm(^{87}Sr/^{86}Sr)_{std}$ being the measured and normalized $^{87}Sr/^{86}Sr$ ratios of the previous (A) and following (B) standards. $Ref\ (^{87}Sr/^{86}Sr)_{SRM987}$ is the "true" $^{87}Sr/^{86}Sr$ value of the NIST SRM-987, set at 0.71024. Although NIST certifies the SRM-987 reference material $^{87}Sr/^{86}Sr$ value at 0.71034 ± 0.00026, previous studies have rather been measuring and using a value of 0.71024, which falls inside the uncertainties of the certified value. This difference may be explained using 0.1194 as the true $^{86}Sr/^{88}Sr$, instead of the true value of this standard (0.119352). For the sake of comparison with other studies (e.g. Weber et al., 2018; Brazier et al., 2020), it was decided to use in the present study a SRM-987 $^{87}Sr/^{86}Sr$ value of 0.71024 as the bracketing standard value.

As the measurement method proposed here allows the measurements of the stable $^{88}Sr/^{86}Sr$ ratio corrected from the mass bias and the normalized radiogenic $^{87}Sr/^{86}Sr$ ratio simultaneously, it is possible to use the Zr-corrected $^{86}Sr/^{88}Sr$ ratio of a sample to normalize its $^{87}Sr/^{86}Sr$ ratio. However, the $^{87}Sr/^{86}Sr$ value in a biological sample obtained after normalization to a constant $^{86}Sr/^{88}Sr$ ratio of 0.1194 can solely correspond to the initial $^{87}Sr/^{86}Sr$ ratio i.e., that of the substrate, which depends ultimately on ^{87}Rb radioactive disintegration. This constitutes the methodological ground on which are based provenance and mobility studies. Taking these considerations into account and for the sake of comparison with previous work, in this study we decided to present only the $^{87}Sr/^{86}Sr$ ratio normalized with a constant $^{86}Sr/^{88}Sr$ ratio of 0.1194. A comparison of those two corrections through three analytical sessions can be found in Figs. S1 (Supplementary material) showing, as expected, a strong correlation with a 1:1 slope.

2.4.2.3. Correction of the $^{88}Sr/^{86}Sr$ ratio. Given that Zr and Sr have very similar masses, instrumental mass fractionation does not vary independently for both elements (Maréchal et al., 1999). Therefore, the Zr fractionation factor can then be used to correct $^{88}Sr/^{86}Sr$ using Russel's exponential law (Russell et al., 1978). The measured $^{91}Zr/^{90}Zr$ ratio is used to calculate the fractionation factor of the instrument ($Fract_{Zr}$) using the equation:

$$Fract_{Zr} = \frac{Ln\left(\frac{True\left(^{91}Zr/^{90}Zr\right)}{Meas\left(^{91}Zr/^{90}Zr\right)}\right)}{Ln\left(\frac{M(^{91}Zr)}{M(^{90}Zr)}\right)} \quad (6)$$

With $M(^{91}Zr)$ and $M(^{90}Zr)$ corresponding to Zr isotopes isotopic masses. The stable isotopic composition of Sr is then corrected using the equation:

$$Corr\left(^{88}Sr/^{86}Sr\right) = Meas\left(^{88}Sr/^{86}Sr\right) \times \left(\frac{M(^{88}Sr)}{M(^{86}Sr)}\right)^{Fract_{Zr}} \quad (7)$$

We also apply the sample-standard bracketing method (SSB) to correct for the instrumental mass-bias variations during the measurement session. The sample $\delta^{88}Sr$ value is calculated using the $^{88}Sr/^{86}Sr$ ratio averaged from the previous (A) and the following (B) standard:

$$\delta^{88}Sr = \left(\frac{Corr\left(^{88}Sr/^{86}Sr\right)_{sample} \times 2}{Corr\left(^{88}Sr/^{86}Sr\right)_{stdA} + Corr\left(^{88}Sr/^{86}Sr\right)_{stdB}} - 1\right) \times 1000 \quad (8)$$

This standard must have known Sr isotopic composition. Special care was given to closely match the concentration between the bracketing standard (SRM-987) and the samples (Ma et al., 2013; Liu et al., 2016). The co-variation between Sr and Zr can be observed in Figs. S2 and S3, showing the drift of the non-corrected $^{92}Zr/^{90}Zr$ and $^{88}Sr/^{86}Sr$ ratios in SRM-987 through an analytical session.

2.4.3. LGLTPE

Strontium was isolated from the matrix using a protocol similar to that set-up at WIGL with identical resin volume and size column, however the acid molarity for the Sr elution was slightly modified to reduce acid consumption. As shown in Table 2, Sr is eluted with 7 mL of 0.005 M HNO_3. A small aliquot (15 µL) was saved before and after the elution protocol for the quantitative determination of Sr and other trace element concentrations.

The measurement of Sr, Rb and Zr concentrations was performed on a quadrupole ICPMS (Thermo Scientific, iCap-Q) using the ^{85}Rb, ^{88}Sr and ^{90}Zr masses. Aliquots were diluted in 5 mL of 0.5 M HNO_3 with 2 µg.L^{-1} rhodium (Rh) as an internal standard. Strontium recovery from the chromatographic separation was found to be $95.5 \pm 6\%$ (2SD, $n = 24$), suggesting quantitative yields and therefore absence of any mass-dependent fractionation. The low amount of Sr in procedural blanks (between 1 and 4 ng) was typically 0.04% of total Sr in the samples. After the chromatographic separation of Sr, the Sr/Zr ratio was >100 on average.

Isotopic analyses were performed on a Nu Plasma 500 MC-ICP-MS (Nu Instruments). On the day of the measurement session, samples and standards were diluted with 0.05 M HNO_3 to reach a Sr concentration corresponding to an intensity of 8 V in the H2 collector (^{88}Sr) (usually 250 or 300 µg.L^{-1}). The solutions were then doped with a high purity Zr solution (Alfa Aesar) to reach a $^{90}Zr/^{88}Sr$ close to unity. Measurements were carried out in static, multi collection mode and one single measurement consisted in one block of 40 cycles with an

integration time of 10 s. Electronic zero by ESA deflection were subtracted online on each measurement. Krypton possible contribution was monitored by measuring the intensity at mass 83 (^{83}Kr) and subtracting its influence on mass 86:

$$^{86}Kr = Meas\left(^{83}Kr\right) \times Ref\left(^{86}Kr/^{83}Kr\right) \quad (9)$$

$$^{86}Sr = Meas\left(^{86}Sr\right) - {}^{86}Kr \quad (10)$$

With $M(^{86}Kr)$ and $M(^{83}Kr)$ corresponding to Kr isotopic masses. $Ref\ (^{86}Kr/^{83}Kr)$ (1.50) is the ratio of Kr isotopes natural abundances extracted from the latest IUPAC report (Meija et al., 2016). The isobaric interference of ^{87}Rb on ^{87}Sr was corrected using Eqs. (1) and (2). The typical intensity on mass 85 (^{85}Rb) for the samples was $2*10^{-4}$ V which is low enough to use the correction, with a measured intensity of 0.7 V on mass 87. The ^{87}Sr/^{86}Sr ratio was normalized using Eqs. (3) and (4) and the instrumental induced mass-bias on ^{88}Sr/^{86}Sr was corrected using Eqs. (6) and (7). SSB was also applied using Eq. (8). This analytical method is indicated as LGLTPE-1.

A second analytical method was tested at LGLTPE, indicated as LGLTPE-2 in Table 3. This method used an on-peak baseline measurement with 10 s integration time prior to each measurement session using a 0.05 M HNO_3 blank. The measured intensities were then subtracted on line during the analytical sequence for all the samples and standards. Thus, the Kr correction became unnecessary and Eqs. (9) and (10) were not used. The collector configuration of the LGLTPE-2 method (Table 3) allowed the measurement of both ^{91}Zr/^{90}Zr and ^{92}Zr/^{90}Zr ratios. Thus the ^{88}Sr/^{86}Sr ratio could be corrected for mass bias using the ^{91}Zr/^{90}Zr and ^{92}Zr/^{90}Zr ratios with Eqs. (6) and (7), using $True(^{92}Zr/^{90}Zr)$ of 0.333243 (Meija et al., 2016). It was observed by Liu and collaborators that best fit occurred between the mass bias affecting ^{92}Zr/^{90}Zr and ^{88}Sr/^{86}Sr ratios, compared to that affecting ^{91}Zr/^{90}Zr (Liu et al., 2012). These authors also find a better precision when using the ^{92}Zr/^{90}Zr ratio. In the present study, both corrections were compared. Measurements giving δ^{88}Sr values with differences higher than 0.05 ‰ between the two corrections were not considered. The samples δ^{88}Sr values given here with the LGLTPE-2 method are the δ^{88}Sr values corrected with the ^{92}Zr/^{90}Zr ratio. SSB was also applied using Eq. (8). Specificities of each method are summarized in Table 3.

2.5. U (k = 2) expanded uncertainties

The measurement uncertainties in this work regarding certified reference materials are given as expanded uncertainties (U) to compare with other studies. The measurement uncertainties were calculated by multiplying the combined uncertainty $u_c(y)$ of isotopic ratios by a coverage factor k such that $U = ku_c(y)$. Here $k = 2$, which corresponds to a level of confidence of 95%. The calculation of the combined uncertainty $u_c(y)$ of a δ value involves the uncertainties of the isotopic ratios of the sample and those of the bracketing standards. The full description of the calculation is presented in Sullivan et al. (Sullivan et al., 2020), and the final equation is given here for a symbolic rA/a isotope ratio:

$$u^2\left(r^{A/a}\right) = \left(\frac{1}{r^{A/a}_{std}}\right)^2 \times u^2\left(r^{A/a}_{std}\right) + \left(-\frac{r^{A/a}_{spl}}{\left(r^{A/a}_{std}\right)^2}\right)^2 \times u^2\left(r^{A/a}_{spl}\right) \quad (11)$$

With *std* and *spl* corresponding to the standard and the sample, respectively, and $u(r)$ the standard uncertainty for the measured ratio, which can be estimated by using the standard deviation calculated from the different blocks corresponding to one block of measurement.

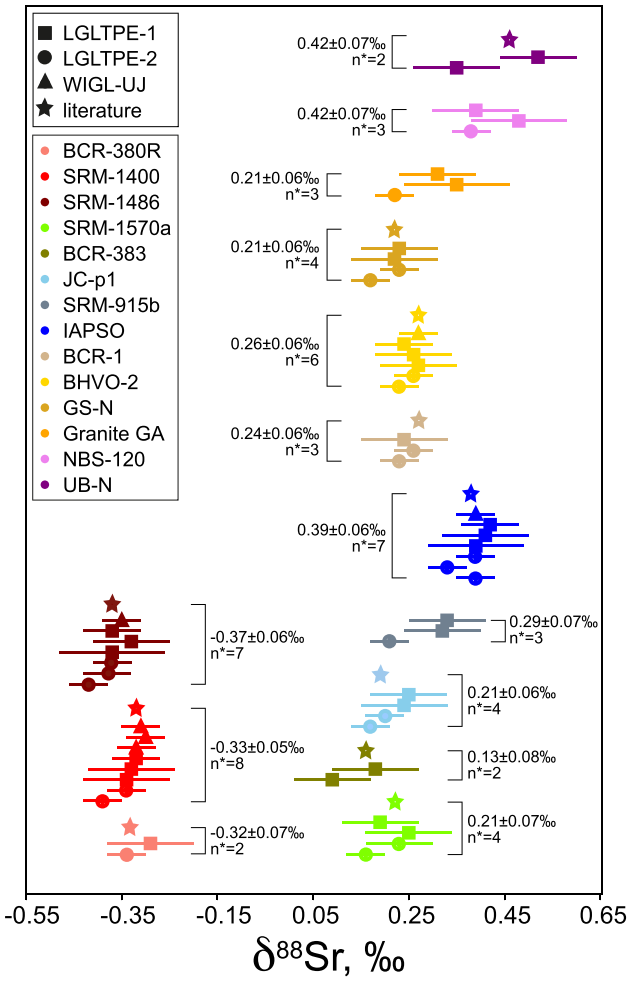


Fig. 1. δ^{88}Sr values for the reference materials measured in the WIGL-UJ and in the LGLTPE; Error associated to the mean value is the mean of U (k = 2) for each aliquot digested and processed according to the chromatographic procedure. The n* value corresponds to the number of these aliquots. A mean of literature values is presented, all references used for the compilation are presented in Table S2.

3. Results

3.1. Reference materials

Sample-standard bracketing and the Sr correction methods described produced an ^{87}Sr/^{86}Sr ratio for SRM-987 of 0.71023 ± 0,00003 (U, k = 2, n = 47) at UJ, 0.71037 ±0.00005 (U, k = 2, n = 152) for LGLTPE-1 and 0.71026 ± 0.00004 (U, k = 2, n = 284) for LGLTPE-2 (note again that the commonly used ^{87}Sr/^{86}Sr value is 0.71024 ± 0.00026 (McArthur et al., 2001; Weber et al., 2018; Brazier et al., 2020), while the certified value is 0.71034 ± 0.00026). Using the sample-standard bracketing and Zr correction methods, the corresponding SRM-987 δ^{88}Sr values are −0.003 ± 0.039 ‰ (U, k = 2, n = 47) at UJ, 0.001 ± 0.094 ‰ (U, k = 2, n = 152) for LGLTPE-1 and -0.001 ± 0.039 ‰ (U, k = 2, n = 284) for LGLTPE-2. The δ^{88}Sr results for the SRM-987 are summarized in Fig. S4. The analytical uncertainties in the LGLTPE show a clear improvement when using the LGLTPE-2 method. All the uncertainties are comparable with those measured by TIMS i.e. between 0.026 and 0.074 ‰, U, k = 2 (Brazier et al., 2020).

The δ^{88}Sr values of the fourteen reference materials are presented in Fig. 1 and compared with the literature values in Table S3. All literature values used for compilation are presented in Table S4. For the sake of

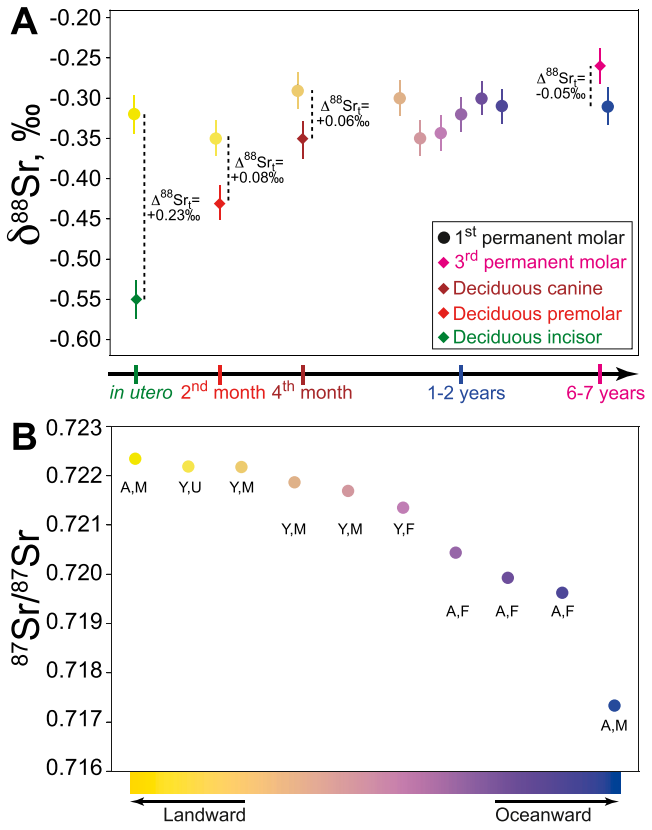


Fig. 2. A $\delta^{88}Sr$ results of the set of various teeth from the baboon skulls with their erupting order (note that for specimen with both deciduous tooth and 1st permanent molar analyzed, the result for the 1st permanent molar is not presented according to the timeline). Error bars are the 2SD calculated from repeated measurements of the SRM1400 during the same analytical session (0.02 ‰; 2SD; n = 4); $\Delta^{88}Sr_t$ is defined for a given specimen as the difference between $\delta^{88}Sr$ value in the first molar and $\delta^{88}Sr$ value in another tooth. B $^{87}Sr/^{86}Sr$ results for 10 baboon specimens; A = adult, Y = young, F = female, M = male, U = unknown sex; The color gradient for1st molars identifies individuals in panel 2A and 2B.

visibility, only some of them are presented in Table S3.

For all standards except UB-N, the results from WIGL-UJ, LGLTPE-1 and LGLTPE-2 are identical within uncertainties. There is a good accuracy with literature values, even for less studied materials such as SRM-1400, SRM-1486, BCR-380R, BCR-383, SRM-1570a, BCR-1 and GS-N. The U (k = 2) uncertainties calculated in the present study range between 0.04 and 0.09 ‰. The measured values for UB-N are highly variable, and this variability can be found in the literature, as Brazier et al. (Brazier et al., 2020) and Ma et al. (Ma et al., 2013) are each finding different $\delta^{88}Sr$ values (0.389 ‰ and 0.539 ‰ respectively), suggesting that UB-N is a heterogeneous material.

Radiogenic Sr results for the fourteen reference materials are presented and compared to literature values in Table S5 and all literature values used for compilation are presented in Table S4. For all samples, the results of the present study are in good agreement with referenced values. The expanded uncertainty U (k = 2) on the $^{87}Sr/^{86}Sr$ ratio ranges between $3*10^{-5}$ and $6*10^{-5}$, which is slightly higher than that achieved by TIMS ($2*10^{-5}$, (Brazier et al., 2020)).

3.2. Tooth enamel samples

The $\delta^{88}Sr$ values and $^{87}Sr/^{86}Sr$ ratios of baboon teeth are given in Table S1. All the samples from baboon teeth were analyzed only once, using the WIGL-UJ method. The mean $\delta^{88}Sr$ value for all first molars of

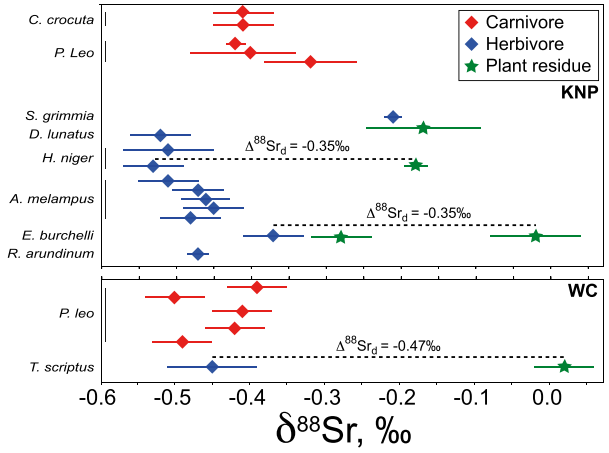


Fig. 3. $\delta^{88}Sr$ values for carnivores, herbivores and plants in KNP and WC; A dashed line links teeth and associated plant residues; The corresponding Sr isotope fractionation value ($\Delta^{88}Sr_d$) is given; Errors bars are 2SD calculated on repeated measurements of the same sample.

adult baboons is −0.31 ‰. Males (−0.30 ± 0.01 ‰, 2SD, n = 2) and females (−0.31 ± 0.02 ‰, 2SD, n = 3) have similar $\delta^{88}Sr$ values. The mean $\delta^{88}Sr$ value of all the first molars (adult and young specimens) is −0.32 ± 0.06 ‰ (2SD, n = 10). The three deciduous teeth $\delta^{88}Sr$ values are −0.55 ‰ (deciduous incisor), −0.43 ‰ (deciduous premolar), and −0.35 ‰ (deciduous canine). These are significantly lower than first molars $\delta^{88}Sr$ of both adult and young specimens. The third molar has a $\delta^{88}Sr$ value of −0.26 ‰, which is significantly higher than first molars and deciduous teeth. These results are shown in Fig. 2A according to the tooth eruption order in baboon life. The $^{87}Sr/^{86}Sr$ values for the ten baboon specimens are presented in Fig. 2B There appears to be three significantly different clusters of specimens. Six specimens with high $^{87}Sr/^{86}Sr$ values (0.722 to 0.721), three adult females with low values (0.719) and one adult male with a very low value (0.716).

The $\delta^{88}Sr$ values and $^{87}Sr/^{86}Sr$ ratios of KNP and WC animals are given in Table S2 and shown in Fig. 3 according to species. They were all obtained using the LGLTPE-2 method. The $\delta^{88}Sr$ values range from −0.52 to −0.21 ‰ in enamel and from −0.28 to −0.02 ‰ in plant. At KNP, the mean $\delta^{88}Sr$ value for herbivores is −0.45 ± 0.17 ‰ (2SD, n = 11) and is −0.39 ± 0.07 ‰ (2SD, n = 5) for carnivores. At WC, there is one herbivorous specimen only (*Tragelaphus scriptus*) and its $\delta^{88}Sr$ value is −0.45 ‰, indistinguishable from the mean $\delta^{88}Sr$ value of *Panthera Leo*, which is −0.44 ± 0.10 ‰ (2SD, n = 5). The $^{87}Sr/^{86}Sr$ ratios range from 0.707 to 0.760 at KNP and from 0.709 to 0.730 at WC and are consistent with previous results (Balter et al., 2008). This variation range is important and can be explained by the complex geological context of these regions (Schutte, 1986; Shone and Booth, 2005).

4. Discussion

4.1. Strontium isotopes in reference materials

Despite small differences between the WIGL-UJ, LGLTPE-1 and LGLTPE-2 methods, notably in the chromatographic separation of Sr (Table 2) and the instrumental settings (Table 3), the $\delta^{88}Sr$ values of reference materials show excellent reproducibility between methods and very good accuracy when compared with literature values. This suggest that the overall protocol is robust, however several observations can be made for some analytical procedures. Consistent with the literature (Liu et al., 2012; Xu et al., 2020), the LGLTPE-2 method using the $^{92}Zr/^{90}Zr$ ratio to correct the instrumental mass bias on $^{88}Sr/^{86}Sr$ shows an enhanced accuracy with literature results (mean accuracy of 0.013 ‰ compared to (Krabbenhöft et al., 2009; Ma et al., 2013; Liu et al., 2017; Brazier et al., 2020)), than the LGLTPE-1 using $^{91}Zr/^{90}Zr$ ratio (mean

accuracy of 0.018 ‰ compared to (Krabbenhöft et al., 2009; Ma et al., 2013; Liu et al., 2017; Brazier et al., 2020)). The precision and accuracy at UJ (mean 2SD of 0.02 ‰, and mean accuracy of 0.015 ‰ compared to (Ma et al., 2013; Brazier et al., 2020)) are comparable to those achieved using LGLTPE-2 (mean 2SD of 0.04 ‰, and mean accuracy of 0.013 ‰), showing the importance of the on-peak baseline measurement with systematic blank subtraction. This was not done using LGLTPE-1 and clearly improves the precision of the results and lower the instrumental uncertainties (U(k = 2) = 0.09 ‰ for LGLTPE-1 vs U(k = 2) = 0.04 ‰ for LGLTPE-2 and UJ). The present results agree very well with the literature, which highlights a clear offset towards ^{88}Sr-depleted biological materials originating from animals (Brazier et al., 2020). To the best of our knowledge, three reference materials studied here had not been analyzed for strontium isotopes. The SRM-915b is a calcium carbonate standard used in analyses of Ca stable isotopes. It has been measured in three different aliquots, and the mean of its ^{87}Sr/^{86}Sr ratio is 0.70800 ± 0.00005 (2SD, n = 3). The mean δ^{88}Sr value is 0.33 ± 0.01 ‰ (2SD, n = 2) using the LGLTPE-1 method and 0.21 ‰ using the LGLTPE-2 method. Further measurements are needed to resolve this discrepancy, but we emphasize that the LGLTPE-2 mean is most probably closer to the true value. The NBS-120c is a phosphorite rock, which has been measured in three different aliquots yielding a mean ^{87}Sr/^{86}Sr ratio of 0.70885 ± 0.00005 (2SD, n = 3) and a mean δ^{88}Sr value of 0.41 ± 0.06 ‰ (2SD, n = 3). Once again, the dispersion between LGLTPE-1 and LGLTPE-2 is quite high. It must be noted that this material shows the highest δ^{88}Sr value measured in this study. It may be linked with its phosphate nature. Granite GA is a geochemical reference sample of granite material. It has been measured in three different aliquots, yielding a mean ^{87}Sr/^{86}Sr value of 0.71376 ± 0.00005 (2SD, n = 3). The mean δ^{88}Sr value measured using LGLTPE-1 is 0.33 ± 0.04 ‰ (2SD, n = 2) and the one measured using LGLTPE-2 is 0.22 ± 0.03 ‰. Further measurements are needed to choose between these two values, but the LGLTPE-2 mean is most probably closer to the actual value. As the measurement method is shown to be reliable using reference materials, it is possible to interpret the results obtained on biological material such as plant and tooth enamel.

4.2. Intra-individual variations of enamel Sr isotopes

The study of different tooth types in modern baboons allows evaluation of the extent of intra-individual variations of the δ^{88}Sr value. Of note is that all the baboon teeth have negative δ^{88}Sr values, in accordance with available data for bone and teeth (Knudson et al., 2010; Romaniello et al., 2015; Lewis et al., 2017; Brazier et al., 2020). Discussion on the possible use of the δ^{88}Sr value as a dietary proxy is challenging for baboons because there is a lack of isotopic data for possible dietary sources, which could be numerous as these are omnivorous animals (Hamilton III et al., 1978; Codron et al., 2006; Johnson et al., 2013). The most obvious pattern is a clear difference between the δ^{88}Sr value of milk and permanent teeth, the latter being ^{88}Sr-enriched compared to the former. This indicates a difference of diet between baboons older than six years old and baboons younger than four. The most likely explanation is that young baboons consume breast milk in various but decreasing amounts during their first years. It is known that the Sr/Ca ratio is much lower in breast milk than in other non-milk foods (Sillen and Smith, 1984; Mays, 2003; Humphrey et al., 2008; Nava et al., 2020). This difference between milk and non-milk food is explained by bio-purification processes, discriminating Sr against Ca in the mother's body. For instance, Ca is preferentially transferred across the mammary gland during lactation, whereas the circulation of Sr is passively constrained by the concentration gradient (Tsutaya and Yoneda, 2015). This process is known to also induce a mass-dependent fractionation of Ca isotopes, where milk is ^{44}Ca-depleted. The resulting negative $\delta^{44/42}$Ca signature and lower Sr/Ca ratio is found in human deciduous teeth and yields information about lactation period and weaning processes in modern and ancient human population (Tacail et al., 2017, 2019; Li et al., 2020).

The present δ^{88}Sr results suggest that Sr isotopes may also undergo mass-fractionation through mammary glands leading to a ^{88}Sr-depleted breast milk, compared to non-milk food and can trace the intensity of breast feeding and duration of the weaning process. Defining $\Delta^{88}Sr_t$ for one individual as the difference between the δ^{88}Sr value in the first molar and another tooth, shows decreasing values with increasing age at tooth eruption (Fig. 2A). Providing that milk has a low δ^{88}Sr value, this suggests the declining contribution of milk in baboon's diet as the animal ages. More precisely, during the first two-to-three months of life, young baboons are mostly breastfed and start to include non-milk food after the fourth month, while continuing to consume mother's milk to some extent. After the first year, baboons seem to shift to a milk-free adult diet. These dietary histories are consistent with known weaning processes of baboons (Rhine et al., 1985; Humphrey et al., 2008).

The ^{87}Sr/^{86}Sr ratios have been measured in the first molars and are distributed according to three groups (Fig. 2B) that should represent distinct bedrock types of the WC region. The ^{87}Sr/^{86}Sr ratios measured in enamel are consistent with the variability of the bioavailable ^{87}Sr/^{86}Sr ratios of plants measured in this area. In this region, the plant ^{87}Sr/^{86}Sr value gradually increases from 0.7087 to 0.7242 over 100 km between the coast and the land (Copeland et al., 2016). The baboons ^{87}Sr/^{86}Sr values thus indicate that the specimens were not living altogether at the same place when their first molars were forming. The baboons analyzed here originated from two different troops that were killed during hunting for population control in the Calitzdorp area (Brand, 1994). Chacma baboons are known to form sub-troops seasonally (Anderson, 1981), which are composed of a majority of adult females and young baboons (Anderson, 1981; Busse, 1984; Henzi et al., 1999). While it is not possible to reallocate baboon individuals in one or the other troop, our results however suggest that the ^{87}Sr/^{86}Sr ratio in enamel can help to reconstitute sub-trooping recruitment strategies in living primates.

4.3. Inter-individual variations of enamel Sr isotopes

For individuals found with plant residues, a $\Delta^{88}Sr_d$ can be defined as the difference between δ^{88}Sr value of the animal and that of the plant (Fig. 3). TM16661-PR and TM16690-PR are plant residues from teeth of specimens that were not analyzed in this study. The $\Delta^{88}Sr_d$ is always negative, indicating that the δ^{88}Sr values of herbivores tooth enamel is ^{88}Sr-depleted relative to plants, consistent with a feeding study performed on pigs (Lewis et al., 2017). These authors found a $\Delta^{88}Sr_d$ value of −0.32 ± 0.06 ‰, close to the average of −0.26 ‰ calculated here. Our results exhibit a much higher dispersion of the $\Delta^{88}Sr_d$ values, which can be explained by the natural, and therefore uncontrolled, context of the study. A Wilcoxson rank test was performed on all the δ^{88}Sr dataset of KNP to compare results for herbivores and carnivores. The P-value obtained is 0.03 suggesting that the differences between herbivores and carnivores can be considered significant. Thus, the $\Delta^{88}Sr_d$ values can also be calculated from enamel of carnivores to herbivores, and are, strikingly, not negative. At KNP, the $\Delta^{88}Sr_d$ value is 0.06 ‰, but it reaches 0.08 ‰ when one possible herbivore outlier (*Sylvicapra grimmia*) is excluded. Indeed, *Sylvicapra grimmia* presents the highest δ^{88}Sr and ^{87}Sr/^{86}Sr values (respectively −0.21 ‰ and 0.760) in the KNP dataset, which suggests a location effect. *Equus burchelli* also presents a higher δ^{88}Sr value than the other herbivores and represents the only pure grazer in the herbivore set, so different metabolisms may play a role in δ^{88}Sr differences. In the WC, the $\Delta^{88}Sr_d$ value is 0.01 ‰, but it is a less robust measure due to the presence of only one herbivore. The pattern of the Sr stable isotopes fractionation from plants to carnivores resembles that of Zn, for which the δ^{66}Zn value first strongly increases from plants to herbivores and then decreases to carnivores (Jaouen et al., 2013). The systematics of Sr stable isotope fractionation up mammal trophic chain thus requires further investigations to understand the origin of the observed isotopic variability before validating the δ^{88}Sr value as a robust

proxy of past diet and trophic position.

4.4. Further perspectives for combined stable and radiogenic Sr analyses

The present study emphasizes the interest and feasibility of analyzing the $\delta^{88}Sr$ and $^{87}Sr/^{86}Sr$ values simultaneously. Cost and duration of measurement is the same as when analyzing one or the other independently using MC-ICP-MS. The Sr chromatographic separation for 24 samples takes a day only, and with the whole SSB procedure, one sample can be analyzed in 45 min. The simplicity of the methodology will surely encourage more studies using stable and radiogenic Sr isotopes for (paleo)ecological and geological purposes.

Other non-traditional stable isotopes are already fulfilling the role of dietary/weaning tracer, such as $\delta^{44/42}Ca$ (Martin et al., 2018; Tacail et al., 2019, 2020, 2021), and $\delta^{66/64}Zn$ (Jaouen et al., 2013, 2016, 2020; Bourgon et al., 2020) measured in the mineral phase (hydroxyapatite) of bone and teeth. So far, the original $\delta^{44/42}Ca$ and $\delta^{66/64}Zn$ signatures are shown to be preserved in tooth enamel hydroxyapatite, (Martin et al., 2015; Hassler et al., 2018; Bourgon et al., 2020). As presented here, the combined $\delta^{88}Sr$ and $^{87}Sr/^{86}Sr$ analyses in animal and vegetal tissues provide information about diet and localization, and thus may enable an extended reconstruction of life history. Further work is needed to assess the preservation of the biological signature of Sr isotopes in fossil bone and tooth enamel. More studies are also needed to decipher the behavior of Sr through metabolic processes such as digestion or milk production, because metabolism may override the Sr dietary isotopic signature. The $\delta^{88}Sr$ value could represent a metabolic signature of the studied taxa. Results of stable Sr isotopes have been recently obtained by Nitzsche et al. in invertebrates of a stream food web (Nitzsche et al., 2022). The $\delta^{88}Sr$ value seems to discriminate different feeding behaviors and might be a dietary tracer in aquatic as well as terrestrial ecosystems.

The perspectives of $\delta^{88}Sr$ and $^{87}Sr/^{86}Sr$ combined analyses are not restricted to paleo(ecological) studies. A temperature dependent Sr isotope fractionation occurs between water and biologically mineralized carbonates. A 0.033‰/°C thermodependency is reported for natural coral samples (*Pavona clavus*) (Fietzke and Eisenhauer, 2006) and a similar value of 0.026 ‰/°C has been determined for another coral species (*Lophelia pertusa*) (Rüggeberg et al., 2008). A preliminary study shows that there might be a similar thermo-dependent process of fractionation for stable Sr isotopes in coccolithophore species (Stevenson et al., 2014). These studies suggest that the $\delta^{88}Sr$ value in carbonates could be used as a paleothermometer to reconstruct ancient ocean temperatures along with the $^{87}Sr/^{86}Sr$ value that could be used as a time calibration tool (Veizer et al., 1999).

Considering the differences between silicate-dominated (Bulk silicate Earth $\delta^{88}Sr$ value estimated as 0.29 ‰ (Ma et al., 2013)) and carbonate-dominated systems (Marine carbonates $\delta^{88}Sr$ value between 0.10 and 0.20 ‰ (Krabbenhöft et al., 2010)), the measurement of $\delta^{88}Sr$ could be an added value to that of $^{87}Sr/^{86}Sr$ for studying weathering processes. There is a preferential leaching of heavy Sr isotopes into the hydrosphere during silicate weathering, but a preferential leaching of light Sr isotope preferential leaching of heavy strontium during primary formed carbonate weathering (Chao et al., 2015). The river $\delta^{88}Sr$ value is therefore different whether it is carbonate- or silicate-dominated and this helps to identify the weathering processes that occurred before the water reached the river. The concomitant analysis of the $^{87}Sr/^{86}Sr$ value could give additional constrains on the provenance of the weathered material.

5. Conclusion

The measurement of Sr stable isotopes by MC-ICPMS using combined sample-standard bracketing and Zr correction is shown to be a robust and easy method. The method permits the simultaneous measurement of the stable $^{88}Sr/^{86}Sr$ and radiogenic $^{87}Sr/^{86}Sr$ ratios. This method has been implemented and evaluated in different laboratories and yields accurate and reproducible results on a wide variety of reference materials. Preliminary results on tooth enamel samples show that the $\delta^{88}Sr$ value is a potential indicator of weaning practices. Encouraging results show that enamel $\delta^{88}Sr$ values potentially discriminate herbivores from carnivores, but this necessitates further studies to understand the source of isotopic heterogeneity. Generally, more data is necessary to better understand the effect of physiology on Sr isotopes and to extend the use of the $\delta^{88}Sr$ values as a companion of $\delta^{44/42}Ca$ in biomedical studies.

Declaration of Competing Interest

There are no conflicts of interest to declare.

Acknowledgements

Many thanks are due to the Ditsong National Museum of Natural History (Pretoria, South Africa), for providing access to the samples. We would like to thank Clément P. Bataille, and an anonymous reviewer for their helpful comments that helped improve the clarity of the paper.

Appendix A. Supplementary data

Supplementary materials are available for this article and include Tables S1, S2, S3, S4, S5, and Figs. S1, S2 and S3. Supplementary data to this article can be found online at https://doi.org/10.1016/j.chemgeo.2022.121000.

References

Anderson, C.M., 1981. Subtrooping in a chacma baboon (Papio ursinus) population. Primates 22, 445–458.
Argentino, C., Lugli, F., Cipriani, A., Panieri, G., 2021. Testing miniaturized extraction chromatography protocols for combined 87Sr/86Sr and δ88/86Sr analyses of pore water by MC-ICP-MS. Limnol. Oceanogr. Methods 19, 431–440.
Balter, V., 2004. Allometric constraints on Sr/ca and Ba/ca partitioning in terrestrial mammalian trophic chains. Oecologia 139, 83–88.
Balter, V., Telouk, P., Reynard, B., Braga, J., Thackeray, F., Albarède, F., 2008. Analysis of coupled Sr/ca and 87Sr/86Sr variations in enamel using laser-ablation tandem quadrupole-multicollector ICPMS. Geochim. Cosmochim. Acta 72, 3980–3990.
Bourgon, N., Jaouen, K., Bacon, A.-M., Jochum, K.P., Dufour, E., Duringer, P., Ponche, J.-L., Joannes-Boyau, R., Boesch, Q., Antoine, P.-O., others, 2020. Zinc isotopes in late Pleistocene fossil teeth from a Southeast Asian cave setting preserve paleodietary information. Proc. Natl. Acad. Sci. 117, 4675–4681.
Brand, D., 1994. Weight growth of chacma baboons in the southern Cape province, South Africa. Rev. Zool. Afr. 108, 71–75.
Brazier, J.-M., Schmitt, A.-D., Pelt, E., Lemarchand, D., Gangloff, S., Tacail, T., Balter, V., 2020. Determination of radiogenic 87Sr/86Sr and stable δ88/86SrSRM987 isotope values of thirteen mineral, vegetal and animal reference materials by DS-TIMS. Geostand. Geoanal. Res. 44 (2), 331–348. https://doi.org/10.1111/ggr.12308.
Busse, C.D., 1984. Spatial structure of chacma baboon groups. Int. J. Primatol. 5, 247–261.
Chao, H.-C., You, C.-F., Liu, H.-C., Chung, C.-H., 2015. Evidence for stable Sr isotope fractionation by silicate weathering in a small sedimentary watershed in southwestern Taiwan. Geochim. Cosmochim. Acta 165, 324–341.
Charlier, B., Parkinson, I., Burton, K., Grady, M., Wilson, C., Smith, E., 2017. Stable strontium isotopic heterogeneity in the solar system from double-spike data. Geochem. Perspect. Lett. 4, 35–40.
Codron, D., Lee-Thorp, J.A., Sponheimer, M., de Ruiter, D., Codron, J., 2006. Inter-and intrahabitat dietary variability of chacma baboons (Papio ursinus) in South African savannas based on fecal δ13C, δ15N, and% N. Am. J. Phys. Anthropol. Off. Publ. Am. Assoc. Phys. Anthropol. 129, 204–214.
Copeland, S.R., Cawthra, H.C., Fisher, E.C., Lee-Thorp, J.A., Cowling, R.M., Le Roux, P.J., Hodgkins, J., Marean, C.W., 2016. Strontium isotope investigation of ungulate movement patterns on the Pleistocene Paleo-Agulhas plain of the Greater Cape floristic region, South Africa. Quat. Sci. Rev. 141, 65–84.
De Muynck, D., Huelga-Suarez, G., Van Heghe, L., Degryse, P., Vanhaecke, F., 2009. Systematic evaluation of a strontium-specific extraction chromatographic resin for obtaining a purified Sr fraction with quantitative recovery from complex and Ca-rich matrices. J. Anal. At. Spectrom. 24, 1498–1510.
Ehrlich, S., Gavrieli, I., Dor, L.-B., Halicz, L., 2001. Direct high-precision measurements of the 87Sr/86Sr isotope ratio in natural water, carbonates and related materials by multiple collector inductively coupled plasma mass spectrometry (MC-ICP-MS). J. Anal. At. Spectrom. 16, 1389–1392.
Fietzke, J., Eisenhauer, A., 2006. Determination of temperature-dependent stable strontium isotope (88Sr/86Sr) fractionation via bracketing standard MC-ICP-MS. Geochem. Geophys. Geosyst. 7.

Guibourdenche, L., Stevenson, R., Pedneault, K., Poirier, A., Widory, D., 2020. Characterizing nutrient pathways in Quebec (Canada) vineyards: Insight from stable and radiogenic strontium isotopes. Chem. Geol. 532, 119375.
Hajj, F., Poszwa, A., Bouchez, J., Guérold, F., 2017. Radiogenic and "stable" strontium isotopes in provenance studies: a review and first results on archaeological wood from shipwrecks. J. Archaeol. Sci. 86, 24–49.
Hamilton III, W.J., Buskirk, R.E., Buskirk, W.H., 1978. Omnivory and utilization of food resources by chacma baboons, Papio ursinus. Am. Nat. 112, 911–924.
Hassler, A., Martin, J.E., Amiot, R., Tacail, T., Godet, F.A., Allain, R., Balter, V., 2018. Calcium isotopes offer clues on resource partitioning among cretaceous predatory dinosaurs. Proc. R. Soc. B Biol. Sci. 285, 20180197.
Henzi, S., Weingrill, T., Barrett, L., 1999. Male behaviour and the evolutionary ecology of chacma baboons. South Afr. J. Sci. 95, 240–242.
Humphrey, L.T., Dirks, W., Dean, M.C., Jeffries, T.E., 2008. Tracking dietary transitions in weanling baboons (Papio hamadryas anubis) using strontium/calcium ratios in enamel. Folia Primatol. (Basel) 79, 197–212.
Irrgeher, J., Prohaska, T., Sturgeon, R.E., Mester, Z., Yang, L., 2013. Determination of strontium isotope amount ratios in biological tissues using MC-ICPMS. Anal. Methods 5, 1687–1694.
Jaouen, K., Pons, M.-L., Balter, V., 2013. Iron, copper and zinc isotopic fractionation up mammal trophic chains. Earth Planet. Sci. Lett. 374, 164–172.
Jaouen, K., Beasley, M., Schoeninger, M., Hublin, J.-J., Richards, M.P., 2016. Zinc isotope ratios of bones and teeth as new dietary indicators: results from a modern food web (Koobi Fora, Kenya). Sci. Rep. 6, 26281.
Jaouen, K., Trost, M., Bourgon, N., Colleter, R., Le Cabec, A., Tütken, T., Elias, Oliveira R., Pons, M.L., Méjean, P., Steinbrenner, S., others, 2020. Zinc isotope variations in archeological human teeth (Lapa do Santo, Brazil) reveal dietary transitions in childhood and no contamination from gloves. PLoS One 15, e0232379.
Johnson, C.A., Raubenheimer, D., Rothman, J.M., Clarke, D., Swedell, L., 2013. 30 days in the life: daily nutrient balancing in a wild chacma baboon. PLoS One 8.
Knudson, K.J., Price, T.D., Buikstra, J.E., Blom, D.E., 2004. The use of strontium isotope analysis to investigate Tiwanaku migration and mortuary ritual in Bolivia and Peru. Archaeometry 46, 5–18.
Knudson, K.J., Williams, H.M., Buikstra, J.E., Tomczak, P.D., Gordon, G.W., Anbar, A.D., 2010. Introducing δ88/86Sr analysis in archaeology: a demonstration of the utility of strontium isotope fractionation in paleodietary studies. J. Archaeol. Sci. 37, 2352–2364.
Krabbenhöft, A., Fietzke, J., Eisenhauer, A., Liebetrau, V., Böhm, F., Vollstaedt, H., 2009. Determination of radiogenic and stable strontium isotope ratios (87 Sr/86 Sr; δ 88/86 Sr) by thermal ionization mass spectrometry applying an 87 Sr/84 Sr double spike. J. Anal. At. Spectrom. 24, 1267–1271.
Krabbenhöft, A., Eisenhauer, A., Böhm, F., Vollstaedt, H., Fietzke, J., Liebetrau, V., Augustin, N., Peucker-Ehrenbrink, B., Müller, M., Horn, C., others, 2010. Constraining the marine strontium budget with natural strontium isotope fractionations (87Sr/86Sr, δ88/86Sr) of carbonates, hydrothermal solutions and river waters. Geochim. Cosmochim. Acta 74, 4097–4109.
Lazzerini, N., Balter, V., Coulon, A., Tacail, T., Marchina, C., Lemoine, M., Bayarkhuu, N., Turbat, T., Lepetz, S., Zazzo, A., 2021. Monthly mobility inferred from isoscapes and laser ablation strontium isotope ratios in caprine tooth enamel. Sci. Rep. 11, 2277.
Lewis, J., Pike, A., Coath, C., Evershed, R., 2017. Strontium concentration, radiogenic (87Sr/86Sr) and stable (δ 88Sr) strontium isotope systematics in a controlled feeding study. STAR Sci. Technol. Archaeol. Res. 3, 45–57.
Li, Q., Nava, A., Reynard, L.M., Thirlwall, M., Bondioli, L., Müller, W., 2020. Spatially-resolved Ca isotopic and trace element variations in human deciduous teeth record diet and physiological change. Environ. Archaeol. 1–10.
Liu, H.-C., You, C.-F., Huang, K.-F., Chung, C.-H., 2012. Precise determination of triple Sr isotopes (δ87Sr and δ88Sr) using MC-ICP-MS. Talanta 88, 338–344.
Liu, H.-C., Chung, C.-H., You, C.-F., Chiang, Y.-H., 2016. Determination of 87 Sr/86 Sr and δ 88/86 Sr ratios in plant materials using MC-ICP-MS. Anal. Bioanal. Chem. 408, 387–397.
Liu, H.-C., You, C.-F., Zhou, H., Huang, K.-F., Chung, C.-H., Huang, W.-J., Tang, J., 2017. Effect of calcite precipitation on stable strontium isotopic compositions: insights from riverine and pool waters in a karst cave. Chem. Geol. 456, 85–97.
Ma, J., Wei, G., Liu, Y., Ren, Z., Xu, Y., Yang, Y., 2013. Precise measurement of stable (δ 88/86 Sr) and radiogenic (87 Sr/86 Sr) strontium isotope ratios in geological standard reference materials using MC-ICP-MS. Chin. Sci. Bull. 58, 3111–3118.
Maréchal, C.N., Télouk, P., Albarède, F., 1999. Precise analysis of copper and zinc isotopic compositions by plasma-source mass spectrometry. Chem. Geol. 156, 251–273.
Marisa Almeida, C., D. Vasconcelos, M.T.S., 2001. ICP-MS determination of strontium isotope ratio in wine in order to be used as a fingerprint of its regional origin. J. Anal. At. Spectrom. 16, 607–611.
Martin, J.E., Tacail, T., Adnet, S., Girard, C., Balter, V., 2015. Calcium isotopes reveal the trophic position of extant and fossil elasmobranchs. Chem. Geol. 415, 118–125.
Martin, J.E., Tacail, T., Cerling, T.E., Balter, V., 2018. Calcium isotopes in enamel of modern and Plio-Pleistocene East African mammals. Earth Planet. Sci. Lett. 503, 227–235. https://doi.org/10.1016/j.epsl.2018.09.026. ISSN 0012-821X.
Mays, S., 2003. Bone strontium: calcium ratios and duration of breastfeeding in a Mediaeval skeletal population. J. Archaeol. Sci. 30, 731–741.
McArthur, J.M., Howarth, R.J., Bailey, T.R., 2001. Strontium isotope stratigraphy: LOWESS version 3: best fit to the marine Sr-isotope curve for 0–509 Ma and accompanying look-up table for deriving numerical age. J. Geol. 109, 155–170. https://doi.org/10.1086/319243.
Meija, J., Coplen, T.B., Berglund, M., Brand, W.A., De Bièvre, P., Gröning, M., Holden, N. E., Irrgeher, J., Loss, R.D., Walczyk, T., others, 2016. Atomic weights of the elements 2013 (IUPAC Technical Report). Pure Appl. Chem. 88, 265–291.
Nava, A., Lugli, F., Romandini, M., Badino, F., Evans, D., Helbling, A.H., Oxilia, G., Arrighi, S., Bortolini, E., Delpiano, D., Duches, R., Figus, C., Livraghi, A., Marciani, G., Silvestrini, S., Cipriani, A., Giovanardi, T., Pini, R., Tuniz, C., Bernardini, F., Dori, I., Coppa, A., Cristiani, E., Dean, C., Bondioli, L., Peresani, M., Müller, W., Benazzi, S., 2020. Early life of Neanderthals. Proc. Natl. Acad. Sci. 117, 28719–28726.
Neymark, L.A., Premo, W.R., Mel'nikov, N.N., Emsbo, P., 2014. Precise determination of δ 88 Sr in rocks, minerals, and waters by double-spike TIMS: a powerful tool in the study of geological, hydrological and biological processes. J. Anal. At. Spectrom. 29, 65–75.
Nitzsche, K.N., Wakaki, S., Yamashita, K., Shin, K.-C., Kato, Y., Kamauchi, H., Tayasu, I., 2022. Calcium and strontium stable isotopes reveal similar behaviors of essential Ca and nonessential Sr in stream food webs. Ecosphere 13, e3921.
Ohno, T., Hirata, T., 2007. Simultaneous determination of mass-dependent isotopic fractionation and radiogenic isotope variation of strontium in geochemical samples by multiple collector-ICP-mass spectrometry. Anal. Sci. 23, 1275–1280.
Price, T.D., Burton, J.H., Bentley, R.A., 2002. The characterization of biologically available strontium isotope ratios for the study of prehistoric migration. Archaeometry 44, 117–135.
Rhine, R., Norton, G., Wynn, G., Wynn, R., 1985. Weaning of free-ranging infant baboons (Papio cynocephalus) as indicated by one-zero and instantaneous sampling of feeding. Int. J. Primatol. 6, 491.
Romaniello, S., Field, M., Smith, H., Gordon, G., Kim, M., Anbar, A., 2015. Fully automated chromatographic purification of Sr and Ca for isotopic analysis. J. Anal. At. Spectrom. 30, 1906–1912.
Rüggeberg, A., Fietzke, J., Liebetrau, V., Eisenhauer, A., Dullo, W.-C., Freiwald, A., 2008. Stable strontium isotopes (δ88/86Sr) in cold-water corals—a new proxy for reconstruction of intermediate ocean water temperatures. Earth Planet. Sci. Lett. 269, 570–575.
Russell, W., Papanastassiou, D., Tombrello, T., 1978. Ca isotope fractionation on the Earth and other solar system materials. Geochim. Cosmochim. Acta 42, 1075–1090.
Schutte, I., 1986. The general geology of the Kruger National Park. Koedoe Afr. Prot. Area Conserv. Sci. 29, 13–37. https://doi.org/10.4102/koedoe.v29i1.517.
Shone, R.W., Booth, P.W.K., 2005. The Cape Basin, South Africa: a review. J. Afr. Earth Sci. 43, 196–210.
Sillen, A., Smith, P., 1984. Weaning patterns are reflected in strontium-calcium ratios of juvenile skeletons. J. Archaeol. Sci. 11, 237–245.
Sillen, A., Balter, V., 2018. Strontium isotopic aspects of *Paranthropus robustus* teeth; implications for habitat, residence, and growth. J. Human Evol. 114, 118–130. https://doi.org/10.1016/j.jhevol.2017.09.009. ISSN 0047-2484.
de Souza, G.F., Reynolds, B.C., Kiczka, M., Bourdon, B., 2010. Evidence for mass-dependent isotopic fractionation of strontium in a glaciated granitic watershed. Geochim. Cosmochim. Acta 74, 2596–2614.
Stevenson, E.I., Hermoso, M., Rickaby, R.E., Tyler, J.J., Minoletti, F., Parkinson, I.J., Mokadem, F., Burton, K.W., 2014. Controls on stable strontium isotope fractionation in coccolithophores with implications for the marine Sr cycle. Geochim. Cosmochim. Acta 128, 225–235.
Sullivan, K., Layton-Matthews, D., Leybourne, M., Kidder, J., Mester, Z., Yang, L., 2020. Copper Isotopic analysis in geological and biological reference materials by MC-ICP-MS. Geostand. Geoanal. Res. 44, 349–362.
Tacail, T., Albalat, E., Télouk, P., Balter, V., 2014. A simplified protocol for measurement of Ca isotopes in biological samples. J. Anal. At. Spectrom. 29, 529–535.
Tacail, T., Martin, J.E., Herrscher, E., Albalat, E., Verna, C., Ramirez-Rozzi, F., Clark, G., Valentin, F., Balter, V., 2021. Quantifying the evolution of animal dairy intake in humans using calcium isotopes. Quat. Sci. Rev. 256 (106843) https://doi.org/10.1016/j.quascirev.2021.106843. ISSN 0277-3791.
Tacail, T., Thivichon-Prince, B., Martin, J.E., Charles, C., Viriot, L., Balter, V., 2017. Assessing human weaning practices with calcium isotopes in tooth enamel. Proc. Natl. Acad. Sci. 114, 6268–6273.
Tacail, T., Le Houedec, S., Skulan, J.L., 2020. New frontiers in calcium stable isotope geochemistry: perspectives in present and past vertebrate biology. Chem. Geol. 537 (119471) https://doi.org/10.1016/j.chemgeo.2020.119471. ISSN 0009-2541.
Tacail, T., Martin, J.E., Arnaud-Godet, F., Thackeray, J.F., Cerling, T.E., Braga, J., Balter, V., 2019. Calcium isotopic patterns in enamel reflect different nursing behaviors among South African early hominins. Sci. Adv. 5, eaax3250.
Tsutaya, T., Yoneda, M., 2015. Reconstruction of breastfeeding and weaning practices using stable isotope and trace element analyses: a review. Am. J. Phys. Anthropol. 156, 2–21.
Veizer, J., Ala, D., Azmy, K., Bruckschen, P., Buhl, D., Bruhn, F., Carden, G.A.F., Diener, A., Ebneth, S., Godderis, Y., Jasper, T., Korte, C., Pawellek, F., Podlaha, O.G., Strauss, H., 1999. 87Sr/86Sr, δ13C and δ18O evolution of Phanerozoic seawater. Chem. Geol. 161, 59–88.
Weber, M., Lugli, F., Jochum, K.P., Cipriani, A., Scholz, D., 2018. Calcium carbonate and phosphate reference materials for monitoring bulk and microanalytical determination of Sr isotopes. Geostand. Geoanal. Res. 42, 77–89.
Xu, J., Yang, S., Yang, Y., Liu, Y., Xie, X., Spectroscopy, A., 2020. Precise determination of stable strontium isotopic compositions by MC-ICP-MS. At. Spectrosc. Norwalk Conn. 41, 64–73.

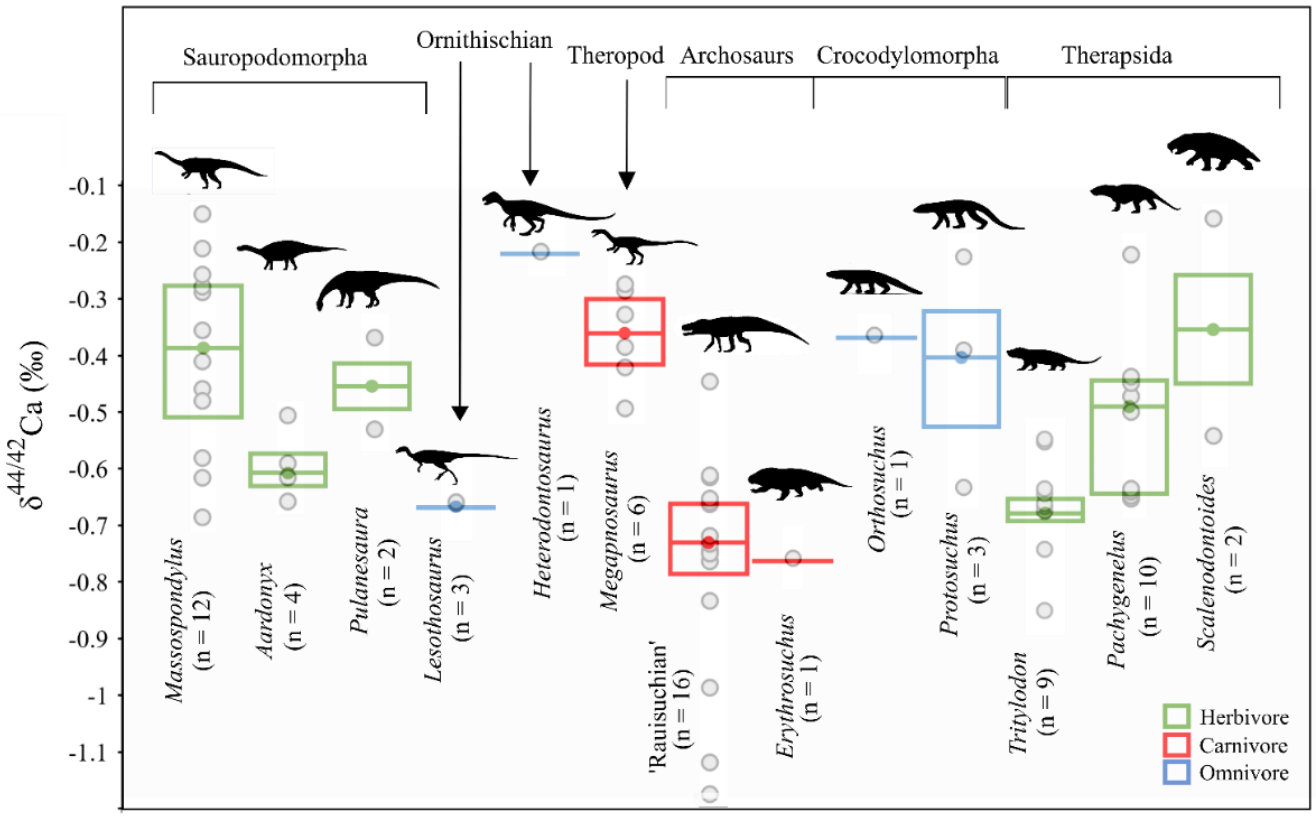
Appendix D: The literature and calibration $\delta^{44/42}Ca$ values for the reference materials, NIST-SRM1400 and NIST-SRM1486.

Sample	Literature value		$\delta^{44/42}Ca$ (‰)	2 s.e. (‰)	Reference
	Mean	± values			
SRM1400Ca	-1.00	0.10	-1.15	0.10	Hassler *et al.*, 2018
00rCa			-1.11	0.15	
00r2Ca			-1.06	0.24	
86rCa	-1.00	0.07	-1.01	0.20	Tacail *et al.*, 2015
86r2Ca			-0.95	0.21	

Appendix E: The ppm values for Ca^{44} (KED), Ca^{44} (STD), Ca^{48} (STD) and Sr^{88} (KED) collected at different concentrations (ppb) for a calibration 8 (yield test).

		44Ca (KED)	44Ca (STD)	48Ca (STD)	88Sr (KED)
		Y (ppm)	Y (ppm)	Y (ppm)	Y (ppm)
	wash	70538.18898	1771243.055	-125625.6627	1335.275052
	Blk	0.000123159	0.005596228	-0.000599292	1.41497E-06
	std 10ppb	0.011730709	0.023065609	0.007389705	0.009904451
	std 30ppb	0.030999469	0.038357834	0.027189104	0.029431591
	std 50ppb	0.05073657	0.05188486	0.055423309	0.049194323
	std 75ppb	0.075602035	0.074824065	0.074361636	0.074772846
	std 100ppb	0.098722103	0.095390362	0.098886591	0.100768311
	wash	11261.33763	691134.0862	-30984.86334	234.3411752
	BLANK	4.683354946	35.04061707	1.609620284	0.103330707
Ca after chem	Y2.1C	18750.32452	123266.8242	9060.152279	0.308959476
Sr after chem	Y2.1S	318.734799	1250.522113	57.38693662	168.7689226
Before chem	Y2.2	22362.55063	145983.8509	9296.426573	231.2218398
EL digest	Y2.3	35645.6471	252130.871	12051.74281	363.8309943
Sr after chem	Y2.1S	318.734799	1250.522113	57.38693662	168.7689226
EL digest	Y2.3	35645.6471	252130.871	12051.74281	363.8309943

Appendix F: The $\delta^{44/42}$Ca (‰) difference between presumed herbivores, carnivores and omnivores. The box plots, displaying Quartiles 1, 2, and 3, of the co-occurring presumed herbivorous taxa represented in green, presumed carnivorous represented in red and the presumed omnivorous taxa represented in blue. Silhouettes are not to scale. Image sources: prehistoricwildlife.com



Appendix G: The data collected for all the fossil specimens analysed.

Superorder	Taxon	no.	Object code	Chem sample no.	Genus	Species	Presumed diet	Enamel	Dentine/ discarded	Additional info
Dinosauria	Sauropodomorph	1	BP/1/4930	A1.1	*Massospondylus*	*carinatus*	Herbivore	x		
		2	BP/1/4958	A1.2	*Massospondylus*	*carinatus*	Herbivore	x		juvenile
		3	BP/1/5231	A1.3	*Massospondylus*	*sp.*	Herbivore	x		juvenile
		4	BP/1/4376	A1.4	*Massospondylus*	*carinatus*	Herbivore	x		juvenile
		5	BP/1/7123	A3.7	*Massospondylus*		Herbivore	x		
		6	BP/1/8571	A6.1	*Massospondylus*		Herbivore	x		
		7	BP/1/5241	Ca5.3	*Massospondylus*	*carinatus*	Herbivore	x		sub-adult
		8	BP/1/8242	A6.4	*Massospondylus*		Herbivore	x		juvenile
		9	BP/1/5172B	A3.6	*Massospondylus*		Herbivore	x		
		10	BP/1/6161	Ca4.7	*Massospondylus*	*sp.*	Herbivore	x		juvenile
		11	BP/1/8468	A7.7	*Massospondylus*		Herbivore	x		
		12	BP/1/5172A	A3.5	*Massospondylus*		Herbivore	x		
		13	BP/1/6679	A1.5	*Aardonyx*	*celestae*	Herbivore	x		
		14	BP/1/6677	A1.6	*Aardonyx*	*celestae*	Herbivore	x		
		15	BP/1/6654	A1.7	*Aardonyx*	*celestae*	Herbivore	x		
		16	BP/1/8238	Ca5.5	*Aardonyx*	*celestae*	Herbivore	x		
		17	BP/1/6678	Ca2.2	*Aardonyx*	*celestae*	Herbivore		x	
		18	BP/1/6766	Ca5.4	*Aardonyx*	*celestae*	Herbivore		x	
		19	BP/1/6204	Ca5.7	*Pulanesaura*	*eocollum*	Herbivore	x		

		20	BP/1/6207	Ca6.3	*Pulanesaura*	*eocollum*	Herbivore	x		
	Ornithischia	21	BP/1/4881	A5.1	*Lesothosaurus*	*sp.*	Omnivore	x		
		22	BP/1/5010	A6.5	*Lesothosaurus*	*sp.*	Omnivore	x		
		23	BP/1/5330	A5.2	*Lesothosaurus*	*sp.*	Omnivore	x		
		24	BP/1/5253	Ca2.6	*Heterodontosaurid*	*Lycorhinus angustidens*	Herbivore	x		
	Theropoda	25		Ca2.4	*Megapnosaurus*	*sp.*	Carnivore	x		
		26	BP/1/6608	Ca1.6	*Megapnosaurus*	*sp.*	Carnivore	x		
		27	BP/1/6504	Ca1.4	*Megapnosaurus*	*sp.*	Carnivore	x		
		28	BP/1/6894	Ca1.5	*Megapnosaurus*	*sp.*	Carnivore	x		
		29	BP/1/5350	Ca5.6	*Megapnosaurus*	*rhodesiensis*	Carnivore	x		
		30	BP/1/6598	Ca1.3	*Megapnosaurus*	*sp.*	Carnivore	x		
Archosauria	Crurotarsan	31	BP/1/6016	A2.1	Rauisuchian	sp.	Carnivore	x		
		32	BP/1/5163A	A2.2	Rauisuchid	sp.	Carnivore	x		
		33	BP/1/5163C	A2.3	Rauisuchid	sp.	Carnivore	x		
		34	BP/1/8574	A4.7	Rauisuchian	sp.	Carnivore	x		
		35	BP/1/5355	A5.4	Rauisuchian	sp.	Carnivore	x		
		36	BP/1/5730	A4.4	Rauisuchian	sp.	Carnivore	x		
		37	BP/1/5283	A4.3	Rauisuchian	sp.	Carnivore	x		
		38	BP/1/6182	A4.1	Rauisuchid	sp.	Carnivore	x		
		39	BP/1/8671(B)	A8.1	Rauisuchian	sp.	Carnivore	x		
		40	BP/1/8671(A)	A5.7	Rauisuchian	sp.	Carnivore	x		

		41	BP/1/8573	A7.2	Rauisuchian	sp.	Carnivore	x		
		42	BP/1/7910	Ca3.1	Rauisuchian	sp.	Carnivore	x		
		43	BP/1/5163F	Ca3.7	Rauisuchid	sp.	Carnivore	x		
		44	BP/1/5163E	Ca3.6	Rauisuchid	sp.	Carnivore	x		
		45	BP/1/5163D	Ca3.5	Rauisuchid	sp.	Carnivore	x		
		46	BP/1/6118	A4.2	Rauisuchid	Sp.	Carnivore	x		
		47	BP/1/5163B	Ca3.3	Rauisuchid	sp.	Carnivore		x	
		48	BP/1/5302	Ca4.1	Rauisuchid/Polonosuchid	sp.	Carnivore		x	
		49	BP/1/8235	Ca4.6	Rauisuchian	sp.	Carnivore		x	
		50	BP/1/8120	Ca6.5	Rauisuchid/Polonosuchid	sp.	Carnivore		x	
		51	BP/1/2094	A7.4	*Erythrosuchus*		Carnivore	x		
	Crocodylomorpha	52	BP/1/7979	Ca4.5	*Orthosuchus*		Carnivore	x		
		53	BP/1/4382	A4.6	*Protosuchus*	*sp.*	Omnivore	x		
		54	BP/1/5290	Ca6.1	*Protosuchus*	*haughtoni*	Omnivore	x		
		55	BP/1/4770	Ca6.2	*Protosuchus*	*haughtoni*	Omnivore	x		
Therapsida	Eucynodontia	56	BP/1/5269	A5.5	*Tritylodon*	*longaevus*	Herbivore	x		
		57	BP/1/8580	A4.5	*Tritylodon*	*longaevus*	Herbivore	x		
		58	BP/1/4781	A3.3	*Tritylodon*	*longaevus*	Herbivore	x		
		59	BP/1/4745	A2.6	*Tritylodon*	*longaevus*	Herbivore	x		

		60	BP/1/5166	A3.1	*Tritylodon*	*longaevus*	Herbivore	x		
		61	BP/1/4878	A2.7	*Tritylodon*	*longaevus*	Herbivore	x		
		62	BP/1/5289	A2.5	*Tritylodon*	*longaevus*	Herbivore	x		
		63	BP/1/5168a	A3.4	*Tritylodon*	*longaevus*	Herbivore	x		
		64	BP/1/5167	A3.2	*Tritylodon*	*longaevus*	Herbivore	x		
		65	BP/1/4741	A5.6	*Pachygenelus*	*monus*	Herbivore	x		
		66	BP/1/5109	A6.6	*Pachygenelus*	*monus*	Herbivore	x		
		67	BP/1/4761	A5.3	*Pachygenelus*	*monus*	Herbivore	x		
		68	BP/1/5162	A7.3	*Pachygenelus*	*monus*	Herbivore	x		
		69	BP/1/5110?	A7.6	*Pachygenelus*	*monus*	Herbivore	x		
		70	BP/1/5292	A6.3	*Pachygenelus*	*monus*	Herbivore	x		
		71	BP/1/5110	A6.7	*Pachygenelus*	*monus*	Herbivore	x		
		72	BP/1/8119	A6.2	*Pachygenelus*	*monus*	Herbivore	x		
		73	BP/1/4381	Ca6.4	*Pachygenelus*	*monus*	Herbivore	x		
		74	BP/1/5691	Ca6.7	*Pachygenelus*	*monus*	Herbivore	x		
		75	BP/1/8388	A7.1	*Scalenodontoides*	*macrodontes*	Herbivore	x		
		76	BP/1/5395		*Scalenodontoides*	*macrodontes*	Herbivore	x		
Reference material		77	SRM1486	A1.8						
		78	SRM1486	A3.8						
		79	SRM1486	A5.8						
		80	SRM1486	A6.8						
		81	SRM1486	A7.8						

	82	SRM1486	86 Pr1						
	83	SRM1486	86 Pr2						

no.	Chem sample no. 2021 and 2019	Genus	Leached $\delta^{44/42}$Ca (‰)	2 s.e. (‰)	Chem sample no. 2019	Unleached $\delta^{44/42}$Ca (‰)	2 s.e. (‰)	Adjusted with regression equation (‰)
1	A1.1	*Massospondylus*	-0.458530613	0.025670758	Ca5.1	-0.2446644	0.030612817	
2	A1.2	*Massospondylus*	-0.580869753	0.085462614	Ca2.3	-0.3074352	0.027905294	
3	A1.3	*Massospondylus*	-0.356079031	0.053929229	Ca4.3	-0.1289259	0.035761468	
4	A1.4	*Massospondylus*			Ca5.2	-0.2110171	0.022996965	-0.485922098
5	A3.7	*Massospondylus*	-0.685641714	0.11489316	-	-	-	
6	A6.1	*Massospondylus*	-0.615654004	0.039086568	-	-	-	
7	Ca5.3	*Massospondylus*			Ca5.3	-0.2889099	0.031208857	-0.549568253
8	A6.4	*Massospondylus*	-0.480392478	0.048883009	-	-	-	
9	A3.6	*Massospondylus*	-0.409962321	0.012748275	-	-	-	
10	Ca4.7	*Massospondylus*			Ca4.7	-0.1505605	0.081831772	-0.436523011
11	A7.7	*Massospondylus*	-0.278916668	0.068789463	-	-		
12	A3.5	*Massospondylus*	-0.257109102	0.074678816	-	-		
13	A1.5	*Aardonyx*	-0.590607973	0.051236354	Ca1.1	-0.2508887	0.008835295	
14	A1.6	*Aardonyx*	-0.658683683	0.034955248	Ca1.2	-0.3489842	0.040406119	
15	A1.7	*Aardonyx*	-0.616270574	0.057680056	Ca2.1	-0.3423011	0.002295604	
16	Ca5.5	*Aardonyx*	-0.506481419	0.042766606	-	-	-	

17	Ca2.2	*Aardonyx*		-	Ca2.2	-0.3956103	0.125203995	
18	Ca5.4	*Aardonyx*		-	Ca5.4	-0.2616191	0.064369201	
19	Ca5.7	*Pulanesaura*		-	Ca5.7	-0.5316413	0.060258173	-0.747904071
20	Ca6.3	*Pulanesaura*		-	Ca6.3	-0.3694815	0.023777519	-0.615403342
21	A5.1	*Lesothosaurus*	-0.665571795	0.103942792				
22	A6.5	*Lesothosaurus*	-0.662995555	0.092166331				
23	A5.2	*Lesothosaurus*	-0.662944755	0.042291584				
24	Ca2.6	*Heterodontosaurid*			Ca2.6	-0.2170248	0.127615254	-0.490830925
25	Ca2.4				Ca2.4	-0.4941733	0.068542744	-0.717288999
26	Ca1.6				Ca1.6	-0.4215042	0.014433216	-0.657911091
27	Ca1.4				Ca1.4	-0.386139	0.091620694	-0.629014137
28	Ca1.5				Ca1.5	-0.3280033	0.056555835	-0.581511472
29	Ca5.6	*Megapnosaurus*	-0.286307677	0.028363422				
30	Ca1.3				Ca1.3	-0.2750973	0.095107874	-0.538281989
31	A2.1	Rauisuchian	-0.4470552	0.0976753	Ca4.4	-0.1909434	0.082529777	
32	A2.2	Rauisuchid	-0.986083295	0.064623767	Ca3.2	-0.8589744	0.011392956	
33	A2.3	Rauisuchid	-0.719020266	0.117303301	Ca3.4	-0.4984119	0.105520024	
34	A4.7	Rauisuchian	-1.174374868	0.042458079	-	-	-	
35	A5.4		-1.118446379	0.087752638	-	-	-	
36	A4.4		-0.833953288	0.025029645	-	-	-	
37	A4.3	Rauisuchian	-0.763270921	0.092868511	-	-	-	
38	A4.1	Rauisuchid	-0.662604593	0.054881283	-	-	-	
39	A8.1	Rauisuchian	-0.659328896	0.0228526	-	-	-	

40	A5.7	Rauisuchian	-0.653462748	0.046029908	-	-	-	
41	A7.2	Rauisuchian	-0.745766621	0.088130715	-	-	-	
42	Ca3.1	Rauisuchian			Ca3.1	-0.7503416	0.112712933	-0.92660409
43	Ca3.7	Rauisuchid			Ca3.7	-0.7329753	0.155190684	-0.912414127
44	Ca3.6	Rauisuchid			Ca3.6	-0.719121	0.036777342	-0.901093799
45	Ca3.5	Rauisuchid			Ca3.5	-0.6154698	0.044134578	-0.816400355
46	A4.2		-0.612570361	0.033964999	-	-	-	
47	Ca3.3	Rauisuchid		-	Ca3.3	-0.4816236	0.093591333	
48	Ca4.1	Rauisuchid/Polonosuchid		-	Ca4.1	-0.4411423	0.027940191	
49	Ca4.6	Rauisuchian		-	Ca4.6	-0.337059	0.002838944	
50	Ca6.5	Rauisuchid/Polonosuchid		-	Ca6.5	-0.2798133	0.036530556	
51	A7.4	*Erythrosuchus*	-0.758646185	0.045232056	-			
52	Ca4.5	*Orthosuchus*	-0.365009578	0.104894915	-			
53	A4.6	*Protosuchus*	-0.644829295	0.035125918	-			
54	Ca6.1	*Protosuchus*	-0.400488178	0.038725771				
55	Ca6.2	*Protosuchus*	-0.235301973	0.018884766				
56	A5.5	*Tritylodon*	-0.86500517	0.093316925	-			
57	A4.5	*Tritylodon*	-0.756667051	0.026039125				
58	A3.3	*Tritylodon*	-0.68817824	0.032653727				
59	A2.6	*Tritylodon*	-0.680583874	0.099823216				
60	A3.1	*Tritylodon*	-0.675013895	0.045673238				
61	A2.7	*Tritylodon*	-0.656961884	0.058783877				

62	A2.5	*Tritylodon*	-0.648655228	0.086143815				
63	A3.4	*Tritylodon*	-0.565143271	0.080951916				
64	A3.2	*Tritylodon*	-0.56084653	0.047062457				
65	A5.6	*Pachygenelus*	-0.653360209	0.037914731	-			
66	A6.6	*Pachygenelus*	-0.648046708	0.034927238				
67	A5.3	*Pachygenelus*	-0.640678988	0.053790739				
68	A7.3	*Pachygenelus*	-0.636159562	0.06307854				
69	A7.6	*Pachygenelus*	-0.500445492	0.069018082				
70	A6.3	*Pachygenelus*	-0.472084755	0.025728209				
71	A6.7	*Pachygenelus*	-0.448600672	0.032765389				
72	A6.2	*Pachygenelus*	-0.437904037	0.049666159				
73	Ca6.4	*Pachygenelus*			Ca6.4	-0.2225046	0.046272838	-0.495308532
74	Ca6.7	*Pachygenelus*			Ca6.7	-0.0614262	0.017084048	-0.363691328
75	A7.1	*Scalenodontoides*	-0.542498336	0.021611521				
76		*Scalenodontoides*			Ca1.7	-0.1587557	0.049757578	-0.44321929
77	A1.8		-0.985	0.0425				
78	A3.8				-	-0.8685821	0.036392144	
79	A5.8				-	-1.0007987	0.025362332	
80	A6.8				-	-0.9386324	0.082386084	
81	A7.8				-	-0.8953309	0.065727402	
82	86 Pr1				86 Pr1	-1.0199351	0.025993114	
83	86 Pr2				86 Pr2	-0.9794693	0.037021891	